Identification of the genetic alterations in prostate cancer metastases

Elzbieta Stankiewicz

Submitted in partial fulfilment of the requirements of the Degree of Doctor of Philosophy

Supervisor: Dr Yong-Jie Lu and Prof D. Berney

Molecular Oncology and Imaging

Barts Cancer Institute

Queen Mary University of London

John Vane Science Centre

Charterhouse Square

London EC1M 6BQ

STATEMENT OF ORIGINALITY

I, Elzbieta Stankiewicz, confirm that the research included within this thesis is my own work or that where it has been carried out in collaboration with, or supported by others, that this is duly acknowledged below and my contribution indicated.

Mrs Tracy Chaplin provided help with the hybridisation, staining and scanning of Affymetrix SNP array. Dr. Xueying Mao helped me with SNP data analysis and FISH methodology. Dr. Marc Yeste-Velasco helped me with generation of stable 22RV1 shFBXL4 cells.

I attest that I have exercised reasonable care to ensure that the work is original, and does not to the best of my knowledge break any UK law, infringe any third party's copyright or other Intellectual Property Right, or contain any confidential material.

I accept that the College has the right to use plagiarism detection software to check the electronic version of the thesis.

I confirm that this thesis has not been previously submitted for the award of a degree by this or any other university.

Signature: Elzbieta Stankewicz

Date: 30.06.16

ACKNOWLEDGEMENTS

I would like to thank my supervisors, Dr. Yong-Jie Lu and Prof Dan Berney for giving me the opportunity to do this PhD and for all their support, patience and guidance without which I would not be able to complete my dissertation.

I would also like to thank all my colleagues in Barts Cancer Institute that advised, helped and supported me through my PhD.

This work was supported by the ORCHID charity.

Abstract

Prostate cancer (PCa) is the most common cancer among men in Western developed countries. While the majority of PCa diagnosed by PSA screening are indolent, advanced and metastatic disease has a significant mortality and morbidity. Bone metastases are extremely common in PCa and identification of bone metastasis associated genes may provide insights into PCa progression and assist in finding new drug targets. However, the genetic study of bone metastases is very limited due to the difficulty of sampling.

We performed genome-wide analysis of six fresh frozen PCa bone metastases. We found several alterations commonly present in advanced PCa, including gains at: 1q32.1, broad gains of 8q (*MYC, NCOA2*), 9q33.2-34.3, 11q13.1-14.1 (*CCND1*), 12q24.23-24.31, 16p13.3, 16p12.1-11.2 and Xq12-13.1 (*AR*) as well as losses at: 5q11.1-22.1, 5q14.3-23.1, 6q14.1-22, 8p23.2-p21, 13q13.2-31.1 (*RB1*), 17p13.1-12 (*TP53*) and 18q11.1-22.3. Two cases also showed *PTEN* loss and one sample had deletion indicative of *TMPRSS2-ERG* fusion.

For downstream analysis we concentrated on *CCND1* oncogene at 11q13 and *FBXL4* at 6q16 as potential drivers of these genomic changes. Using fluorescence *in situ* hybridisation we found common *CCND1* gain and *FBXL4* loss in PCa bone metastases (54.5%, 12/22 and 47.8%, 11/23, respectively), much less frequent in primary tumours (7%, 10/142 and 13.8%, 20/145, respectively) and absent in BPH cases (0/55). The expression levels of cyclin D1 protein, coded by *CCND1* correlated with *CCND1* copy number gain ($p < 0.0001$) and were higher in metastatic tumours than in primary PCa ($p = 0.015$), confirming cyclin D1 involvement in advanced PCa.

Presence of *FBXL4* loss in early stage primary PCa strongly correlated with current PCa prognostic markers and with worse patient survival. Therefore, we propose that *FBXL4* may be a tumour suppressor gene in prostate, whose loss in early PCa could be indicative of more aggressive disease. Using *in vitro* experiments we demonstrated that FBXL4 regulates cells motility and invasion. We confirmed that ERLEC1, an ER lectin involved in ER stress response pathway is a degradation target of FBXL4. As activation of ER stress response pathway is linked to enhanced cell migration and invasion, loss of *FBXL4* could be one of the mechanisms by which cancer cells increase their efficiency to respond to stress and to escalate their metastatic potential through stabilisation of ERLEC1. Further studies of FBXL4 – ERLEC1 axis are necessary to establish how they contribute to PCa progression. This knowledge can potentially help to develop novel targeted therapies for aggressive disease harbouring FBXL4 abnormalities.

ABBREVIATIONS

ADT	Androgen deprivation therapy
AR	Androgen receptor
BAC	Bacterial artificial chromosomes
bp	Base pair
BPH	Benign prostatic hyperplasia
BSA	Bovine serum albumin
cDNA	Complementary deoxyribonucleic acid
CGH	Comparative genomic hybridisation
CIN	Chromosome instability
CAN	Copy number alteration
CNV	Copy number variation
CRL	Cullin-RING E3 ubiquitin ligases
CRPC	Castration resistant prostate cancer
DAPI	4,6-diamidino-2-phenylindole dihydrochloride
DEPC	Diethylpyrocarbonate, inactivates RNase enzymes
DHT	Dihydrotestosterone
DIG	Digoxigenin
DMEM	Eagle's minimal essential medium
DMSO	Dimethyl sulphoxide
DNA	Deoxyribonucleic acid
dNTP	Deoxyribonucleotide triphosphate
DRE	Digital rectal examination
DPX	Di-n-butyle phthalate in xylene
DTT	Dithiothreitol
EB	Tris/HCl
EMT	Epithelial-mesenchymal transition

ER	Endoplasmic reticulum
ERAD	Endoplasmic reticulum associated degradation
FAM	Carboxyfluorescein
FCS	Foetal Calf Serum
FFPE	Formalin-Fixed, Paraffin-Embedded
FISH	Fluorescence *in situ* hybridisation
GOLF	Genome Oriented Laboratory File system
GWAS	Genome-wide association study
H&E	Hematoxylin and eosin
HGPIN	High grade prostatic intraepithelial neoplasia
IF	Immunofluorescence
IHC	Immunohistochemistry
Kb	Kilobase
LB	Lysogeny broth
LNM	Lymph node metastasis
LOH	Loss of heterozygosity
MAD	Mitochondria associated degradation
mCRPC	Metastatic castration resistant prostate cancer
MIN/MSI	Microsatellite instability
mRNA	Messenger RNA
MOR	Minimal overlapping region
NaCl	Sodium chloride
PBS	Phosphate-buffered saline
PCa	Prostate cancer
PCR	Polymerase chain reaction
PIN	Prostatic intraepithelial neoplasia
PSA	Prostate-specific antigen

qPCR	Quantitative PCR
RNA	Ribonucleic acid
rpm	Revolutions per minutes
RPMI	Roswell Park Memorial Institute medium
SCF	Skp, Cullin, F-box containing ubiquitin ligases
shRNA	Small hairpin Ribonucleic Acid
siRNA	Small interfering Ribonucleic Acid
SNP	Single nucleotide polymorphism
SSC	Sodium chloride sodium citrate
TAPG	Transatlantic Prostate Group
TBE	Tris/Borate/EDTA
TE	Tris/EDTA
TMA	Tissue microarray
TNM	Staging System: T-primary tumour, N- number of involved lymph nodes, M-metastasis
TSG	Tumour suppressor gene
TURP	Transurethral resection of the prostate
UPR	Unfolded protein response
UTP	Uridine 5'-triphosphate
V	Volt
WB	Western blot

TABLE OF CONTENT

STATEMENT OF ORIGINALITY 2

ABBREVIATIONS 5

LIST OF TABLES 16

1 INTRODUCTION AND AIMS 20

1.1 PROSTATE CANCER 20

1.1.1 The prostate anatomy and origin of prostate cancer 20

1.1.2 Prostate cancer incidence, mortality and survival 21

1.1.3 Risk factors 22

1.1.4 Role of androgen in PCa 22

1.1.5 Prostate cancer screening using PSA 23

1.1.6 Gleason grading system 24

1.1.7 Staging of prostate cancer 26

1.1.8 PCa treatment 27

1.1.8.1 Localised low-risk indolent prostate cancer 28

1.1.8.2 High-risk prostate cancer 28

1.2 GENETIC ALTERATION IN PROSTATE CANCER 29

1.2.1 Genomic instability and cancer 29

1.2.2 Prostate cancer susceptibility genes 31

1.2.3 Somatic genetic changes in prostate cancer 33

1.3 METASTATIC PROSTATE CANCER 38

1.3.1 Mechanism of metastasis 38

1.3.2 Bone metastases 41

1.3.2.1 Normal bone physiology 42

1.3.2.2 Types of bone metastases 43

1.3.2.3 Model of osteolytic bone metastases 44

1.3.2.4 Model of osteoblastic bone metastases in prostate cancer 45

1.4 AIMS 48

2 MATERIAL AND METHODS 50

2.1 CLINICAL SAMPLES 50

2.2 CELL LINES AND CELL CULTURE 51

2.3 HEMATOXYLIN-EOSIN (H&E) STAINING 51

2.4 DNA EXTRACTION 51

2.4.1 Fresh frozen samples and cell lines 51

2.4.2 Simultaneous DNA and RNA extraction 52
2.4.3 FFPE samples 53
2.5 SAMPLE PREPARATION FOR SNP 6.0 ARRAY ANALYSIS 53
2.5.1 Restriction enzyme digestion 54
2.5.2 Ligation 54
2.5.3 PCR 55
2.5.4 PCR product purification 55
2.5.5 Fragmentation 56
2.5.6 Labelling 56
2.5.7 Hybridisation 57
2.5.8 Washing and Staining 58
2.5.9 Scanning 58
2.5.10 SNP array data analysis 59
2.6 FLUORESCENT *IN SITU* HYBRIDISATION (FISH) 59
2.6.1 FISH probe preparation 59
2.6.1.1 Bacterial artificial chromosome (BAC) DNA preparation 59
2.6.1.2 BAC DNA amplification, cleaning and labelling 60
2.6.2 Cell and tissue pre-treatment 61
2.6.3 Hybridisation and post-hybridisation washes 62
2.7 RNA EXPRESSION ANALYSIS 63
2.7.1 RNA extraction 63
2.7.2 Complementary DNA (cDNA) synthesis 64
2.7.3 Quantitative Polymerase Chain Reaction (qPCR) 64
2.8 PROTEIN ANALYSIS 66
2.8.1 Western blot (WB) 66
2.8.1.1 Protein extraction 66
2.8.1.2 Bradford assay 66
2.8.1.3 Sodium Dodecyl Sulphate-PolyacrylAmide Gel Electrophoresis (SDS-PAGE) and PVDF membrane transfer 67
2.8.1.4 Antibody incubation and protein detection 68
2.8.2 Immunochistochemistry (IHC) 71
2.8.2.1 Cell lines 71
2.8.2.2 FFPE tissue sections 72
2.8.3 Immunofluorescence (IF) 73
2.9 *FBXL4* GENE KNOCKDOWN 74
2.9.1 Gene knockdown with small interfering RNA (siRNA) 74
2.9.2 Gene knockdown with short hairpin RNA (shRNA) constructs 75
2.10 *FBXL4* CLONING 78

2.10.1 C-terminus Flag tag *FBXL4* construct preparation 78
2.10.2 DNA purification using Minelute Gel extraction Kit 80
2.10.3 Cloning of *FBXL4* construct into TOPO® TA vector 81
2.10.4 Transformation of Chemically Competent Cells 82
2.10.5 Plasmid purification with The Wizard® Plus Minipreps DNA Purification System 83
2.10.6 Restriction digestion of C-Flag *FBXL4* pCR™4-TOPO® TA vector and subcloning into pcDNA4/TO expression vector 83
2.10.7 Subcloning C-Flag *FBXL4* fragment into pcDNA4/TO expression vector 84
2.10.8 Large scale pcDNA4/TO expression vector with C-terminus Flag tag *FBXL4* construct amplification 86
2.11 TRANSIENT FBXL4 OVEREXPRESSION 87
2.12 PRODUCTION OF STABLY TRANSFECTED CELLS WITH C-FLAG *FBXL4* PLASMID DNA 88
2.12.1 Production of cells constitutively overexpressing *FBXL4* 88
2.12.2 Tetracycline - inducible system for FBXL4 overexpression 88
2.13 CELL VIABILITY ASSAY 89
2.14 CELL MIGRATION ASSAY 90
2.15 CELL INVASION 91
2.15.1 Matrigel invasion 91
2.15.2 Collagen invasion 91
2.15.2.1 Single cell collagen invasion assay through native collagen type-I matrice 91
2.15.2.2 Single cell invasion assay through collagen type-I/Matrigel matrix 92
3 GENOME-WIDE ALTERATIONS IN PCA BONE METASTASES 95
3.1 INTRODUCTION 95
3.2 RESULTS 95
3.2.1 Sample and SNP 6.0 array data quality control 95
3.2.2 Genomic copy number changes detected in PCa bone metastases 98
3.2.3 Confirmation of copy number changes in six fresh frozen bone metastases 108
3.3 DISCUSSION 109
3.3.1 The common regions with copy number changes with same chromosomal breakpoints 109
3.3.2 The common regions with copy number changes with different chromosomal breakpoints 111
3.3.3 Copy number confirmation at *CCND1* and *FBXL4* locus 113
4 ANALYSIS OF 11Q13 GAIN/ CCND1 GENE IN PCA 116
4.1 INTRODUCTION 116
4.1.1 The 11q13-14 gain and potential driver genes 116

4.1.2 Cellular function of *CCND1* product, cyclin D1 117
4.2 RESULTS 120
4.2.1 FISH analysis of 11q13/*CCND1* gain in larger cohort of metastatic and primary PCa samples 120
4.2.2 Cyclin D1 protein immunoexpression in FFPE PCa samples 121
4.2.3 Correlation between cyclin D1 expression and 11q13/*CCND1* copy number gain 125
4.2.4 Cyclin D1 transcripts expression in prostate samples 127
4.3 DISCUSSION 130
4.3.1 11q13/*CCND1* gain is more prevalent in metastatic than primary PCa 130
4.3.2 Cyclin D1 IHC staining intensity is stronger in bone metastases than in primary tumours 130
4.3.3 PCa samples with 11q13/*CCND1* gain show stronger cyclin D1 median staining intensity than cases with 11q13/*CCND1* neutral copy number 132
4.3.4 Cyclin D1a and cyclin D1b transcript levels do not correlate with PCa progression. 134
5 ANALYSIS OF 6Q16/*FBXL4* LOSS IN PCA 137
5.1 INTRODUCTION 137
5.2 RESULTS 138
5.2.1 FISH analysis of FFPE samples finds 6q16/*FBXL4* loss in half of PCa bone metastases and in a small subset of primary tumours 138
5.2.2 *FBXL4* copy number loss in conservatively managed localised PCa correlates with cancer progression 139
5.2.3 *FBXL4* expression 141
5.2.3.1 *FBXL4* RNA expression is reduced in PCa 141
5.2.3.2 *FBXL4* protein expression 143
5.2.3.2.1 Anti-FBXL4 antibody testing using inducible protein expression in HEK293 cells 143
5.2.3.2.2 FBXL4 overexpression is lost in PCa cell lines upon selection for stable clones 147
5.2.3.2.3 Anti-FBXL4 antibody testing using protein downregulation models 150
5.2.3.2.4 FBXL4 protein immunoexpression in FFPE PCa samples 153
5.3 DISCUSSION 155
5.3.1 *FBXL4* loss is more prevalent in metastatic PCa tumours and correlated with cancer progression and poor patient outcome 155
5.3.2 Challenges in assessing FBXL4 protein levels 157
5.3.3 FBXL4 protein expression is reduced in PCa cancer but do not correlate with FBXL4 copy number status 159
6 *FBXL4* FUNCTION IN PCA 162

6.1 INTRODUCTION 162
6.2 RESULTS 165
6.2.1 *FBXL4* knockdown leads to increased PCa cell migration and invasion without affecting cell viability 165
6.2.2 *FBXL4* overexpression leads to reduced cell migration 169
6.2.3 *FBXL4* co-localises with mitochondria 169
6.2.4 *FBXL4* does not regulate epithelial to mesenchymal transition (EMT) related proteins 170
6.2.5 ERLEC1 protein as a potential downstream target of FBXL4 171
6.2.5.1 Anti-ERLEC1 antibody validation 171
6.2.5.2 Relation between FBXL4 and ERLEC1 expression levels using *in vitro* cell line models 173
6.3 DISCUSSION 175
6.3.1 FBXL4 regulates cell migration and invasion without affecting proliferation. 175
6.3.2 ERLEC1 protein levels are regulated by FBXL4 179
7 FINAL DISCUSSION AND FUTURE PLANS 182
7.1 FINAL DISCUSSION 182
7.1.1 Genomic copy number changes in prostate cancer revealed by genome-wide analysis 182
7.1.2 11q13/*CCND1* copy number gain and cyclin D1 expression in PCa 183
7.1.3 Role of *FBXL4* loss in PCa 184
7.1.4 Conclusions 185
8 REFERENCES 188

LIST OF FIGURES

Figure 1 Different anatomical zones of prostate gland. 20

Figure 2 Progression pathway for prostate cancer. 21

Figure 3. Gleason score system. 26

Figure 4 The steps involved in tumour cells metastasis to the bone. 38

Figure 5 Classification of bone metastases. 43

Figure 6 The vicious cycle in osteolytic metastasis. 45

Figure 7. GIPZ lentiviral particles 76

Figure 8. pCR™4-TOPO® TA Vector map. 81

Figure 9. pcDNA4/TO vector map. 85

Figure 10. pcDNA6/TR vector map. 85

Figure 11. Protocol for single cell invasion through collagen. 92

Figure 12. Cancer purity in FFPE decalcified PCa bone metastases samples derived from the same patients as fresh frozen specimens. 96

Figure 13. Agarose gel electrophoresis based quality control steps during samples preparation for SNP 6 arrays. 97

Figure 14. Summary of all regions with copy number changes in 6 PCa bone metastases detected by SNP 6.0 array analysis. 100

Figure 15. Copy number loss at 6q present in six PCa bone metastases. 104

Figure 16. Copy number changes detected on chromosome 8 in PCa bone metastases. 105

Figure 17. Copy number gain on chromosome X at AR locus. 106

Figure 18. Copy number changes present on chromosome 11 in PCa bone metastases. 107

Figure 19 Copy number changes at chromosome 16. 108

Figure 20. Relative Copy number confirmation at 11q13 and 6q16 using qPCR. 109

Figure 21. *CCND1* location on chromosome 11q13. 117

Figure 22. Cyclin D1 function. 118

Figure 23. Difference in domain structure of cyclin D1 and D1b. 119

Figure 24. Representative FISH images of copy number changes at 11q13 in prostate samples. 121

Figure 25. Examples of cyclin D1 IHC in bone metastases. 122

Figure 26. Examples of cyclin D1 IHC in primary PCa and BPH. 124

Figure 27. Comparison of cyclin D1 immunoexpression in primary and metastatic PCa samples. 125

Figure 28. PCa with 11q13 gain show significantly stronger cyclin D1 immunoexpression and in more cell nuclei than cases with neutral copy number at *CCDN1* locus. 127

Figure 29. RNA expression of full length cyclin D1a and its alternative splice variant, cyclin D1b in prostate cell lines. 128

Figure 30. Cyclin D1 transcripts expression in prostate clinical samples by qPCR. ... 129

Figure 31. Cyclin d1 transcripts expression across prostate clinical samples by qPCR. 129

Figure 32. Representative FISH images of copy number changes at FBXL4 in prostate samples. 139

Figure 33. *FBXL4* loss is significantly associated with decreased PCa specific survival. 140

Figure 34 *FBXL4* expression levels in prostate clinical samples measured by q-RT-PCR. 142

Figure 35 *FBXL4* expression in prostate cell lines measured by qPCR. 143

Figure 36. Confirmation of FBXL4 RNA overexpression in HEK293 cells..... 144

Figure 37. Anti-FBXL4 antibodies specificity in HEK293 C-Flag FBXL4 overexpression system by WB..... 145

Figure 38. Confirmation of FBXL4 protein detection by IHC with anti-FBXL4 antibodies in HEK293 cells overexpressing FBXL4..... 146

Figure 39. PCa cell lines fail to stably express high levels of FBXL4 protein. 148

Figure 40. Lack of FBXL4 protein overexpression in stable PCa cell lines. 149

Figure 41. Stable cell populations retain FBXL4 expression vector. 149

Figure 42. FBXL4 knockdown in PCA cell lines..... 150

Figure 43. FBXL4 knockdown in PCa cell lines is undetectable at protein levels by WB. 151

Figure 44. Anti-FBXL4 antibody fails to detect FBXL4 downredulation by immunohistochemistry in 22RV1 cells..... 152

Figure 45. Examples of FBXL4 IHC in prostate clinical samples. 154

Figure 46. Comparison of FBXL4 immunoexpression in primary and metastatic PCa samples. 154

Figure 47. no significant difference in FBXL4 immunoexpression between PCas with and without *FBXL4* copy number loss. 155

Figure 48. The SKP1-CUL1-F-box (SCF) complex. 162

Figure 49. Three-dimensional structural modelling of FBXL4 protein. 163

Figure 50. The effect of *FBXL4* knockdown on PCa cells viability. 166

Figure 51. FBXL4 knockdown increases PCa cell migration. 167

Figure 52. *FBXL4* knockdown leads to increased PCa cell invasion. 167

Figure 53. FBXL4 knockdown increases 22RV1 cell migration/invasion on collagen/Matrigel 3D culture. 168

Figure 54. *FBXL4* overexpression leads to reduced HEK293 cell migration without affecting cells viability. 169

Figure 55. FBXL4 protein co-localises with mitochondria in HEK293 overexpressing FBXL4. 170

Figure 56. FBXL4 does not regulate EMT markers expression. 171

Figure 57. Anti-ERLEC1 antibody testing in HEK293 cells. 172

Figure 58. Anti-ERLEC1 antibody tested in FFPE clinical samples by IHC. 173

Figure 59. ERLEC1 protein is commonly expressed in prostate cell lines. 174

Figure 60. ERLEC1 protein expression in PCa cell lines with FBXL4 knockdown. 174

Figure 61. ERLEC1 protein expression in HEK293 cells overexpressing FBXL4. 175

LIST OF TABLES

Table 1 Risk stratification for men with localised prostate cancer. 27

Table 2 Somatic genetic changes in prostate cancer. 37

Table 3 Available patient and tumour information for fresh frozen PCa bone metastases. 50

Table 4 Restriction digestion mix preparation. 54

Table 5 Ligation mix preparation. 55

Table 6 PCR master mix preparation. 55

Table 7 Fragmentation reagent preparation. 56

Table 8 Labelling mix preparation. 57

Table 9 Hybridisation mixture preparation. 57

Table 10 Washing and staining process. 58

Table 11 BAC clones used for FISH probes preparation 63

Table 12 List of used TaqMan assays. 65

Table 13 qRT-PCR master mix. 65

Table 14 Standard qPCR program. 66

Table 15 Lysis buffer preparation. 66

Table 16 10% Resolving gel preparation. 68

Table 17 Stacking gel preparation. 68

Table 18 Primary and secondary antibodies used for western blot. 70

Table 19 Primary antibodies used for IHC/IF. 71

Table 20 Cell seeding densities for siRNA knockdown. 74

Table 21 List of siRNAs used for knockdown experiments. 74

Table 22. Optimisation of the number of transducing units (TU)/ viral particles per every cell in the well (MOI). 77

Table 23. PCR master mix. 78

Table 24. PCR cycling conditions. 79

Table 25. Primers for Sanger sequencing of full length C-flag *FBXL4.* 79

Table 26. PCR master mix. 80

Table 27. PCR cycling conditons. 80

Table 28. Adding polyA tail to C-Flag FBXL4 PCR product. 82

Table 29. Ligation mixture using TOPO® TA Cloning® Kit. 82

Table 30. Restriction digestion reaction mix. 84

Table 31. DNA ligation mix. 86

Table 32. C-Flag *FBXL4* pcDNA4/TO vector restriction digestion. 86

Table 33. Cell seeding densities for gene overexpression. 87

Table 34. Primers flanking flag region of C-Flag *FBXL4* pcDNA4/TO vector. 88

Table 35. 1 mg/ml collagen preparation. 92

Table 36. Collagen-matrigel matrix composition. 93

Table 37 Quality control of SNP array data generated for the PCa bone metastases. 98

Table 38 Common copy number changes with the same genomic breakpoints present in more than half of the PCa bone metastases. 101

Table 39. Copy number changes with different genomic breakpoints in PCa bone metastases. 102

Table 40 Frequency of CCND1 gain detected by FISH in primary and metastatic PCa 120

Table 41. Cyclin D1 expression on the background of genetic changes in *CCND1/RB/CDKN2A* and *TP53/CDKN1A* pathways 123

Table 42 Median and average cyclin D1 immunoexpression in primary PCa and bone metastases. 125

Table 43 Frequency of *FBXL4* loss detected by FISH in primary and metastatic PCa. 138

Table 44. Correlation of FBXL4 loss with Gleason scores and clinical stages. 140

Table 45. Multivariate analysis of clinicopathological parameters. 141

Table 46 Difference in *FBXL4* transcript expression between PCa bone metastases, primary tumours and BPH samples. 142

Table 47 Median and average FBXL4 immunoexpression in prostate clinical samples. 155

Table 48. PCa cell migration and invasion increases after FBXL4 knockdown. 168

CHAPTER 1

Introduction and Aims

1.1 Prostate cancer

1.1.1 The prostate anatomy and origin of prostate cancer

The prostate gland is size of a walnut. It surrounds the urethra just below the urinary bladder and can be felt during a rectal examination. Prostate produces and secretes fluid that nourishes and protects sperm [1]. Four basic anatomic regions can be distinguished in adult prostate (Figure 1). The transition zone surrounds the urethra and constitutes about 5-10% of the mass of the glandular prostate. Benign prostatic hyperplasia (BPH) develops here but also 10-15% of prostate cancers (PCa). The central zone accounts for 20-25% of the prostate, lies below the proximal urethral segment and contains the ejaculatory ducts. 15-20% of cancers develop in this zone. The peripheral zone includes 70-75% of the prostate and surround the central zone laterally, occupying the apical region of the prostate. Most PCa cases (about 70%) begin in the peripheral zone [2, 3]. PCa often presents as multicentric lesions located in different zones of the prostate and typically of different grades [4, 5].

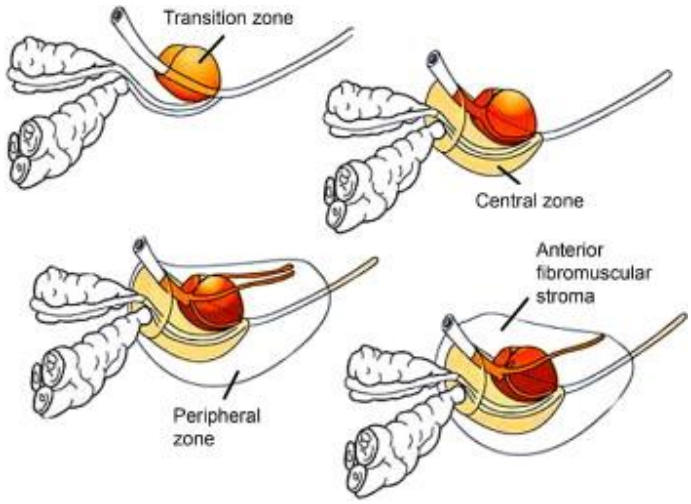

FIGURE 1 DIFFERENT ANATOMICAL ZONES OF PROSTATE GLAND. Adapted from Crawford *et al* [3].

Histologically, the normal prostate consists of glandular epithelium and fibromuscular stroma. The glandular epithelium is composed of two cell layers: the basal layer and the differentiated luminal secretory layer, with rare neuroendocrine cells distributed mostly in the basal layer. The luminal epithelial cells express characteristic markers such as cytokeratins 8 and 18, as well as high levels of androgen receptor (AR). Basal cells are located beneath the luminal epithelium, and express p63 and the high-molecular-weight

cytokeratins 5 and 14, but express AR at low or undetectable levels. Finally, neuroendocrine cells are rare cells of unknown function that express endocrine markers such as chromogranin A and synaptophysin, but are AR-negative [6]. PCa starts in the glandular epithelium and is classified as adenocarcinoma (Figure 2). The earliest precursor is prostatic intraepithelial neoplasia (PIN) and high-grade PIN (HGPIN) is associated with concurrent PCa [7-9].

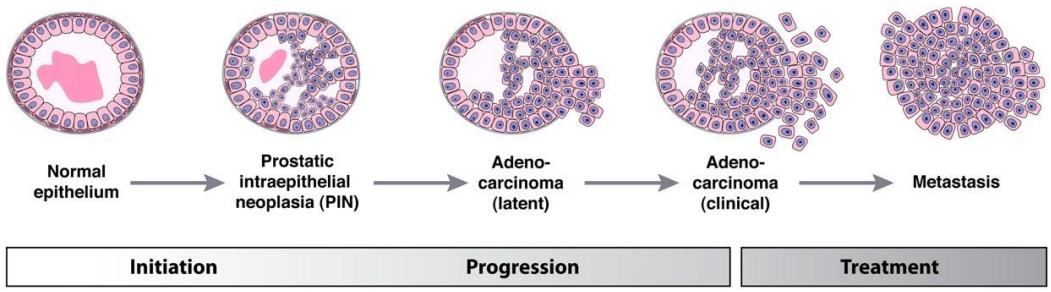

FIGURE 2 PROGRESSION PATHWAY FOR PROSTATE CANCER. Adapted from Shen *et al* [6].

1.1.2 Prostate cancer incidence, mortality and survival

PCa is the second most common cancer in men worldwide, accounting for 15% of the cancers diagnosed in men and is the fifth leading cause of death from cancer in men (6.6% of all cancer related-deaths in men) [10]. In western world, including Europe and North America, PCa is the most common male cancer and the second most frequent cause of cancer-related death [11, 12]. In the UK (2013) there are 47,300 new PCa cases a year (150 cases for every 100,000 males), accounting for 26% of all new cases of cancer in males, and 10,837 deaths from PCa (35 deaths for every 100,000 males), accounting for 13% of all cancer deaths in men [11]. PCa incidence varies more than 25-fold worldwide, with almost 70% of the cases occurring in more developed regions. The highest rates are observed in Australia/New Zealand, North America and in Europe while the lowest are found in Asian populations [10, 13, 14]. Much of the variation reflects differences in the use of prostate-specific antigen (PSA) testing, followed by diagnostic biopsy [10, 15].

PSA testing has a great effect on PCa incidence but lesser on mortality, as it often leads to detection of early stage PCa before clinical manifestation and without changing the actual time of death (discussed later) [15]. PCa mortality shows about 10 fold variation worldwide [10]. Mortality rates are generally high in black populations (Caribbean and

sub-Saharan Africa), very low in Asia and intermediate in the Americas and Oceania [11].

Survival from PCa strongly depends on the stage of the disease at diagnosis. In majority of cases, PCa develops progressively over many decades, which gives the opportunity for clinical therapeutic interventions e.g. strategies to prevent PCa or reduce the risk of developing the disease. Often PCa is an indolent, latent disease that will not result in clinical symptoms during the lifetime of an elderly patient. It is estimated from post-mortem data that around half of all men in their fifties have histological evidence of cancer in the prostate, which rises to 80% by age 80, but only 1 in 27 men (3.8%) will die from this disease [16, 17]. Consequently, men are more likely to die with PCa than from it, which should be considered when choosing the treatment [18]. However, there is a subset of PCas which are more aggressive, spreading into the seminal vesicles, bladder and rectum, and metastasizing to lymph nodes, bone, lung and other organs [19]. At present, there are no good prognostic markers to distinguish aggressive from indolent disease for early-diagnosed cancer [11]. In England in 2010-2011 five year PCa survival after diagnosis was about 85%, mostly due to the detection of latent, earlier, slow-growing tumours by PSA testing. However, if the disease is metastatic at presentation, five-year relative survival decreases to around 30%, which is in agreement with data from US [11, 12, 20].

1.1.3 Risk factors

The main risk factor for PCa is age and in the UK the highest incidence rates occur in men in their seventies [11]. A family history of PCa is one of the strongest risk factors for this disease. The inherited form represents only 9% of all PCas but accounts for a significant proportion (43%) of early-onset disease (disease onset - 55 years). The risk increases about two fold for men with a first-degree relative diagnosed with PCa at age 50. If more than one relative is affected, the individual's risk is four times the average [21, 22]. PCa incidence rates also differ between racial groups and are over 60% higher for black Americans than for white Americans while rates for Asian Americans are over 40% lower than for white Americans [12, 20]. This differences are due to genetic as well as environment factors and lifestyle choices, including diet [13, 23, 24].

1.1.4 Role of androgen in PCa

Androgens acting through AR are important in the development and maintenance of normal prostate (promote survival of the secretory epithelia and balance cell proliferation

and death) as well as in development and progression of PCa from early stage, through metastatic disease and hormonal resistance [9, 25]. Testosterone is the main circulating androgen in men. In the prostate and other organs, testosterone functions as a prohormone; it is converted to dihydrotestosterone (DHT) in the prostatic stromal and basal cells by 5α-reductase, an intracellular enzyme present in the prostate [3]. Inside the prostate cell, both testosterone and DHT bind to the cytoplasmic AR, stimulating the AR translocation to the nucleus where it binds to regulatory sequences of specific target genes, and activates their transcription promoting cell-cycle regulation, cell survival and lipogenesis [9]. This dependence of prostate cells on androgen for development, growth and survival is the base for treatment of locally advanced and metastatic cancer with androgen-deprivation therapy (ADT). However, patients inevitably progress and become resistant to ADT. Castration resistant PCa (CRPC) represents the final stage of the disease, with median survival of less than 2 years [26]. Despite systemic androgen depletion, CRPC continue to rely on AR signalling, which remains active and supports their survival and growth. Persistent activation of the AR signalling can occur through many mechanism such as AR amplification/overexpression, AR mutation or substitution including AR ligand binding domain mutation, AR splice variants, glucocorticoid receptor signalling or concentration of intratumoural androgens [27, 28].

1.1.5 Prostate cancer screening using PSA

Screening for PCa involves digital rectal examination (DRE) and blood test for PSA. PSA is a glycoprotein secreted by prostatic epithelial cells. It functions as a serine protease and is excreted in the ejaculate to liquefy semen. In normal conditions, PSA can be detected in blood at a low level. Disruption of normal prostatic architecture by cancer, benign enlargement, inflammation, or trauma can lead to elevated PSA serum levels. Patients with high PSA levels are sent for a prostate biopsy performed together with transrectal ultrasound, to provide a definitive diagnosis. However, serum PSA alone has low specificity and cannot reliably distinguish between BPH, prostatic infection or inflammation, and PCa, either low or high grade [29]. In US PCa screening with PSA using a threshold of 4.0 ng/ml results in about 75% of men with PSA levels of 4.0 to 10.0 ng/ml having unnecessary prostate biopsy as they do not have cancer [23, 30]. Introduction of annual PSA screening in US lead to dramatic increase in incidence of PCa but the vast majority of men are diagnosed with early stage localised disease in the absence of symptoms. Accounting for long natural history, PCa screening and subsequent treatment of early disease largely leads to unnecessary treatment of indolent cancers, as many patients will die with PCa rather than of the disease [29]. Recent meta-

analysis of randomised controlled trials on PCa screening showed that PCa screening did not significantly decrease prostate cancer-specific mortality in most of the trials but indeed led to overdiagnosis and overtreatment with adverse events such as infection, erectile dysfunction, and incontinence [31]. Two large landmark trials: the European Randomized Study of Screening for Prostate Cancer (ERSPC) [32, 33] and the US-based Prostate, Lung, Colorectal, and Ovarian (PLCO) Cancer Screening Trial [34] brought opposite results for PSA screeing impact on PCa patient mortality. The PLCO trial after 7-10 years follow up found 22% increase in PCa diagnosis but no significant reduction in mortality in screening group. However, this trial was criticised for poor design, with 70% contamination by PSA testing in the control group [35]. The ERSPC trial which used more strict criteria for patient selection concluded that PSA-based screening reduced the rate of death from PCa by 21% but indeed was associated with a high rate of overdiagnosis and overtreatment, with 781 men required to be invited for screening and 27 treated for PCa to prevent one PCa death [32, 33].

Regardless of problems with PSA testing reliability, currently they are no better prognostic biomarkers for PCa and PSA levels together with the Gleason score and TNM staging remain essential factors in stratification of risk for PCa progression. Additionally, PSA is used as a marker for detecting residual disease after treatment and tumour recurrence during follow-up. An undetectable level of PSA after radical prostatectomy or radiation therapy indicates the absence of recurrence [36].

1.1.6 Gleason grading system

PCa is commonly graded by the method described by Gleason, which assigns a score between 1 and 5 on the basis of the glandular architecture (lower scores indicate a well-differentiated glandular pattern) [37]. The Gleason score takes into account distinct patterns present in the same tumour, and is composed of the two most common patterns, ranging from 2 to 10 (Figure 3A). Gleason score is considered the most significant predictor of prognosis. It has been correlated to a number of clinical end points, including clinical stage, progression to metastatic disease and survival [38].

Over recent years Gleason score underwent several modifications. Gleason score 2 to 4 is nowadays not used on needle biopsy and Gleason score 5 is also avoided due to poor correlation with prostatectomy grade with almost all cases showing higher grade at resection [39]. It has been proposed that the virtual absence of Gleason score 2 to 4 in clinical practice makes it more appropriate from the purpose of prognosis and treatment

to state that the Gleason score ranges from 6 to 10 rather than from 2 to 10. This would mean that patients with a Gleason score 6 have the lowest grade tumour [40]. The most clinically relevant change over recent years was limitation of pattern 3 and widening the scope of pattern 4 carcinoma, which resulted in disease upgrading. The updated Gleason system produced a more homogeneous Gleason score 6, which now has an excellent prognosis (virtually 100% curable) when the disease is organ confined [40, 41]. On the contrary, Gleason score 7 (combination of grade 3 and 4) defines prognostically heterogeneous group of tumours, which can take different clinical courses, some staying indolent, others progressing to invasive and metastatic disease [42, 43]. Therefore, Gleason grade 7 is usually associated with a critical decision-making step in patient management and treatment choice. Identification of patients with a high risk of disease progression is one of the current challenges in the treatment of PCa [44].

For prognostic and therapeutic purposes Gleason grade is commonly grouped into three groups: 6, 7 and 8-10. Over the years, within the PCa with Gleason grade 7, numerous studies have demonstrated that patients with cancer of Gleason grade 4 + 3 have a worse prognosis than those with a score of 3 + 4, both in needle biopsies and radical prostatectomies [41]. Furthermore, patients with a Gleason grade 9-10 tumours had almost twice the risk of progression compared with Gleason grade 8. Therefore, classification of patients into low-, intermediate-, and high-risk categories based on a Gleason grade <7, 7, and >7 loses critical prognostic information and more accurate contemporary grading prognostic categories: 3 + 3, 3 + 4, 4 + 3, 8, and 9-10 were recently proposed [41, 45]. In 2016 the International Society of Urological Pathology (ISUP) has issued guidelines for the grading of PCa, recommending that Gleason scores ≤6, 3 + 4 = 7, 4 + 3 = 7, 8 and 9-10, respectively, be reported as five groups named: ISUP grades 1-5 (Figure 3B). This new grading system has been accepted by the World Health Organization for the 2016 edition of the genitourinary pathology blue book, as it can better predict patient outcome and facilitate patient communication [46-48].

Needle biopsy Gleason grade is routinely used to plan patient management and its accurate determination is crucial in deciding the best treatment [38]. However, there is a poor agreement between biopsy and prostatectomy Gleason score, with tendency of the score to be higher on prostatectomy, probably due to limited biopsy material and cancer heterogeneity [42, 49]. Failure of the biopsy specimen to accurately reflect the Gleason grade of the cancer has a key impact on patient treatment, leading to underestimation of the disease risk, and can compromise patient outcome [50].

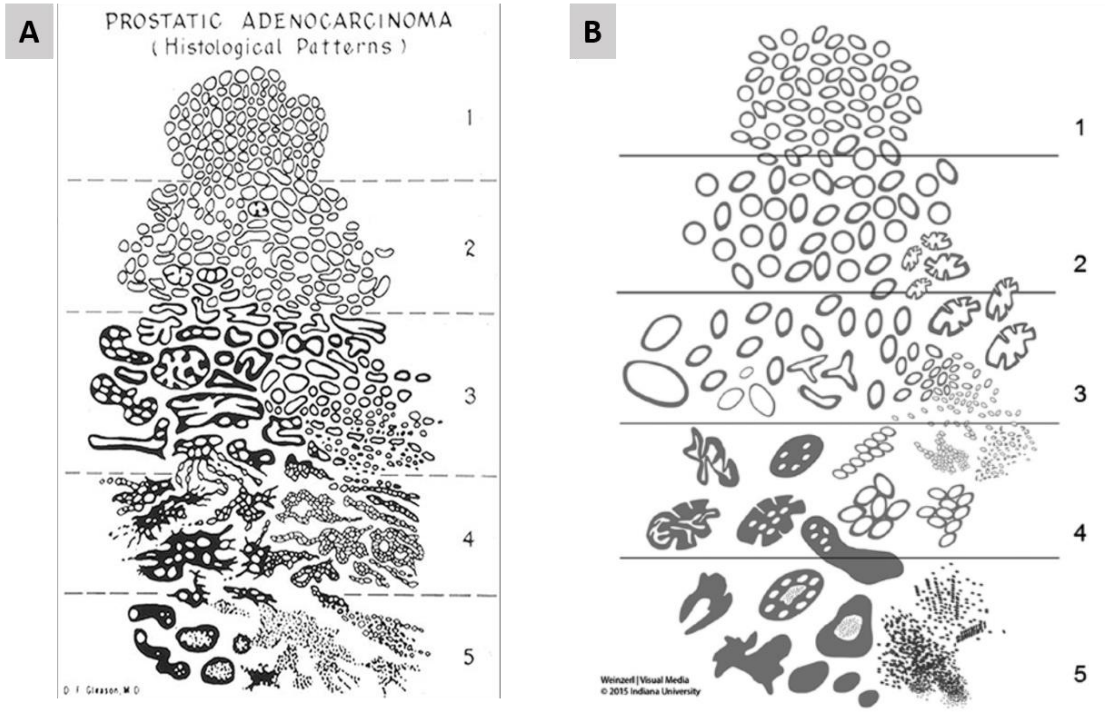

FIGURE 3. GLEASON SCORE SYSTEM. (A), In the original Gleason grading system a score between 1 and 5 is assigned to the prostate tissue based on the pattern of glandular architecture and two most common scores are combined together to give a final score from 2-10. (B), Recently modified Gleason score by ISUP simplifies grading into 5 groups: grade group 1: Gleason score ≤6; group 2: Gleason score 3 + 4 = 7; group 3: Gleason score 4 + 3 = 7; group 4: Gleason score 4 + 4 = 8, 3 + 5 = 8, 5 + 3 = 8; group 5: Gleason scores 9–10 [37, 48].

1.1.7 Staging of prostate cancer

Two types of staging can be distinguished for PCa. One is the clinical stage, which is an estimate of the spread of PCa at the time of diagnosis based on all information available before the first definitive treatment, including results of the physical exam (DRE), PSA tests, prostate biopsy, and any imaging tests performed.

Pathologic stage is performed after surgical resection of the primary tumour and is based on gross and microscopic examination of the prostatectomy specimen and dissected regional lymph nodes (if included) [51]. PCa pathologic stage follows the TNM staging system, which is the international standard for designating the extent of cancer and its prognosis. It takes into account the extent of the primary tumour (T category), whether the cancer has spread to nearby lymph nodes (N category) and absence or presence of distant metastasis (M category) [52].

Pathologic stage is crucial for determination of patient treatment and prognosis and is linked to patient survival and disease progression [53, 54]. Nonetheless, evaluation of tumour stage is to certain degree subjective and pathologists do not always agree on criteria to assess seminal vesicle invasion, extraprostatic invasion or the radical prostatectomy specimen margins, factors that are vital for subsequent patient treatment and prognosis [55-58].

1.1.8 PCa treatment

Introduction of PSA screening resulted in more frequent detection of small volume, low grade and organ confined PCas, which are diagnosed earlier in their course and are unlikely to ever become symptomatic during lifetime (indolent or clinically insignificant cancers). However, some of those tumours may progress quickly resulting in lethal disease. Therefore, it is extremely important to effectively predict the course of a newly diagnosed PCa and to distinguish between tumours that need immediate, invasive treatment with curative intent and indolent tumours that are unlikely to become symptomatic during the patient's lifetime [59, 60]. Nomograms to predict the outcome of disease treatments have been developed based on PSA, Gleason score and the TNM stage [59]. Currently (2016) clinical guidelines for PCa diagnosis and treatment (e.g. published by National Institute for Health and Clinical Excellence (NICE) https://www.nice.org.uk/guidance/qs91 and European Association of Urology (EAU) http://uroweb.org/guideline/prostate-cancer/) still categorise PCa into low, intermediate and high risk groups (Table 1) using regular Gleason score [61]. However ISUP-WHO 2014 grade grouping is expected to be gradually introduced into the standard pathology reporting (http://uroweb.org/guideline/prostate-cancer/).

TABLE 1 RISK STRATIFICATION FOR MEN WITH LOCALISED PROSTATE CANCER.

Risk stratification	PSA (ng/ ml)		Gleason score		Stage
Low risk	< 10	and	≤ 6	and	T1-T2a
Intermediate risk	10–20	or	7	or	T2b-T2c
High risk	> 20	or	8-10	or	T3-T4

1.1.8.1 Localised low-risk indolent prostate cancer

Management of low-risk indolent PCa focuses on avoiding patient overtreatment and increasing quality of life by minimizing treatment side effects. 'Watchful waiting' was commonly used in the 1970s and 1980s (the pre-PSA era) and was an approach that deferred treatment until the disease became symptomatic. It involved elderly patients with a relatively short life expectancy, whose cancer was likely to progress very slowly, with no symptoms and would not cause their death. Subsequently, this approach has evolved into 'active surveillance', where time is used as a prognostic test and curative therapy initiated when predetermined signs of progression become evident (a rise in PSA level or adverse findings on biopsy). Criteria to define cancer progression differ but mostly include PSA doubling time with a cutoff ranging between ≤2 and ≤4 years, Gleason score progression to ≥7 at rebiopsy (at intervals ranging from 1 to 4 years) and PSA progression >10 ng/mL, with PSA testing no more often than every 6 months [62, 63]. By these means, patients can avoid overtreatment without compromising their outcome [64] and are eligible for radical treatment if their disease progress [59, 60, 65]. Radical treatment includes radical prostatectomy and radiotherapy [61, 63].

1.1.8.2 High-risk prostate cancer

High-risk locally advanced PCa is treated with radical prostatectomy or combination of radiotherapy and androgen ablation. Androgen ablation involves androgen withdrawal by surgical castration (bilateral orchidectomy) or drug therapy with luteinising hormone-releasing hormone (LH-RH) analogues. Alternatively, the anti-androgens are administered alone or anti-androgens and castration are applied together, which is known as maximum androgen blockade or MAB [61]. ADT can give good short-term disease control. Initially, over 80% of patients positively respond to androgen ablation by dramatic reduction of prostate epithelial cells. However, after 1-2 years disease eventually progresses to hormone refractory state [9, 66, 67]. Secondary treatment for patients with progressive disease after androgen deprivation also concentrates on reduction of androgens and includes administration of a secondary antiandrogen, inhibition of adrenal androgen production, and further LH inhibition with progesterone or estrogenic agents. Secondary hormonal therapy also eventually fails and disease progresses to metastatic state [68].

Metastatic disease is common at the diagnosis and in the UK one in five men (20%) have metastases at diagnosis [69]. For many years standard treatment for patients with

metastatic PCa was ADT; however, most patients would eventually develop resistance leading to progression to metastatic castration resistant prostate cancer (mCRPC). For patients with mCRPC, docetaxel was the first agent to demonstrate a survival benefit (2-3 months in comparison to the standard chemotherapy) [70], and docetaxel plus prednisone became the new standard treatment for mCRPC. Vale *et al* [71] performed a meta-analysis of large randomised controlled trials combining docetaxel or bisphosphonates with standard of care in hormone-sensitive PCa patients. For metastatic (M1) disease they included results from three trials (CHAARTED [72], GETUG-15 [73], STAMPEDE [74]) representing 2992 (93%) of the 3206 patients enrolled in the relevant trials. They found an absolute 9% (95% CI 5–14) improvement in survival at 4 years in patients with docetaxel treatment, suggesting addition of docetaxel to standard of care should be considered standard treatment for men with M1 hormone-sensitive PCa who are starting treatment for the first time. For patients with locally advanced (M0) disease, failure-free survival was consistently prolonged with docetaxel (hazard ratio 0.70 (95% CI 0.61–0.81)) but not the patient survival (0.87 (0.69–1.09)), implying necessity for further studies of the effects of docetaxel on survival in the M0 disease. No evidence was found for improved survival with zoledronic acid in men with M1 or M0 disease.

For patients with mCRPC who had progressed after docetaxel chemotherapy, second-line therapies which improve overall survival include enzalutamide [75], abiraterone-prednisone [76] and cabazitaxel-prednisone [77]. The second-line taxane chemotherapy with cabazitaxel, seems to be effective also in patients who acquired resistance to AR axis-targeting agents, abiraterone and enzalutamide [78]. For patients with refractory disease, mainly palliative systemic or local therapy remains with options including radiotherapy to dominant sites of bone pain and treatment with bone-targeting agents [61, 79, 80].

1.2 Genetic alteration in prostate cancer

1.2.1 Genomic instability and cancer

Over a decade ago, six essential alterations in cell physiology that promote malignant transformation of normal human cells (hallmarks of cancer) have been proposed: self-sufficiency in growth signals, insensitivity to growth-inhibitory (antigrowth) signals, evasion of programmed cell death (apoptosis), limitless replicative potential, sustained angiogenesis, and tissue invasion and metastasis [81]. Constant progress in cancer research lead to emerging additional hallmarks, including the development of genomic

instability in cancer cells, inflammation, reprogramming of cellular energy metabolism in order to support continuous cell growth and proliferation, and active evasion by cancer cells from attack and elimination by immune cells [82].

Cancer is a complex disease, with multiple genes involved in its initiation, progression, invasion and metastasis. Most cancers show genomic instability, which can be described as an increased rate of alterations in the genome of tumour cells compared with normal cells. However, it is not clear at what stage of cancer development it arises and what is its molecular basis [83, 84]. Genomic instability exists at two distinct levels: nucleotide and chromosome.

Microsatellite instability (MSI; also known as MIN) is observed at the nucleotide level and manifests as small increases or decreases (''instability'') in the number of repeats in microsatellites (also known as *short tandem repeats*). Microsatellites are simple repeat sequences of 1 to 6 base pairs scattered throughout the genome and their repetitive nature makes them particularly prone to DNA replication slippage and replication errors [85]. Most of these errors are repaired by mismatch repair genes (e.g. *MLH1* and *MSH2*) and defects in these genes lead to microsatellite instability, resulting in high rate of mutations such as single nucleotide substitutions, duplications or deletions as well as deletions or insertions of few nucleotides [83, 86]. Single nucleotide changes can lead to modifications in subsequently translated amino acid sequence of the protein, resulting in amino acid change and/or different protein size (e.g. due to the creation of a premature stop codon). The deletion or insertion of one or two nucleotides within gene coding region causes a frameshift mutation resulting in the production of abnormal protein with an incorrect amino acid sequence that can be either longer or shorter than the normal protein. Defects in mismatch repair system dramatically increase mutation rates in affected cells, leading to accumulation of mutations in oncogenes and tumour-suppressor genes in the progeny of these cells, fuelling the process of oncogenesis through positive selection [84, 87, 88].

The most common form of genomic instability is observed at the chromosome level. Chromosomal instability (CIN) is defined as a persistently high rate of loss and gain of whole or part of chromosomes [84, 89]. Gain or loss of whole chromosomes leads to aneuploidy, while large-scale structural rearrangements of chromosomes result in deletions, duplications, inversions and unbalanced and balanced translocations. Frequent missegregation of chromosomes constantly shuffles gene dosage and increases the likelihood of emerging karyotypes that promote phenotypes associated

with advanced stage disease including invasion and growth in new microenvironments [90].

1.2.2 Prostate cancer susceptibility genes

Observation that PCa clusters within families suggested shared familial genetic risk factors for this disease [91]. Early studies of prostate susceptibility loci used family-based linkage analysis in an attempt to identify high-penetrance genetic variants that confer increased risk of developing PCa. The results of linkage studies provided several candidate chromosomal regions for PCa susceptibility loci (with subsequent search for candidate genes), including HPC1 region (1q24-25, harbouring *RNASEL*), PCAP (1q42-43), 8p22–23 (*MSR1*), 8q24, HPCX (Xq27-28), CAPB (1p36), HPC20 (20q13), HPC2 (17p11 with *ELAC2*), 16q23, 17q21 (*BRCA1*) and 13q12–13 (*BRCA2*) [92-95]. However, none of these regions have been convincingly replicated [96]. The extreme difficulty in finding consistent linkage results for highly penetrant genes across different studies indicated that multiple common genetic variants with small to moderate effect (penetrance) might be involved in prostate carcinogenesis [97].

Genome-wide association studies (GWAS) have recently emerged as a powerful tool to identify common genetic polymorphisms associated with cancer risk. GWASs are population-based case-control studies, which use high-resolution single-nucleotide polymorphisms (SNPs) array technology to search for association between common genetic variants (SNPs) and disease [98, 99]. GWASs have led to the identification of many loci that are potentially associated with PCa [95]. The most common region implicated in PCa susceptibility is located at 8q24 and is considered as gene desert. However, it contains regulatory elements involved in the tissue-specific transcriptional regulation of *MYC* expression, an oncogene which lies immediately downstream of that region. *MYC* is a well-known transcription factor essential to the regulation of cell proliferation and growth; is upregulated at both the mRNA and protein levels in aggressive PCa [100].

Linking genetic risk variants for PCa with potential biological functions is complicated by their large number. There are over 100 loci with thousands of surrogate SNPs in linkage disequilibrium [101, 102]. Most of variants are shared across populations, however some differences also exist [103-105]. Recent comprehensive analysis of data from 100 GWAS studies [97] revealed 250 PCa related SNPs mapped to 162 protein coding genes. 62 SNPs mapped to 41 genes had strong association with PCa ($p<10^{-8}$). Only ten of those

genes, including *EEFSEC, HNF1B, JAZF1, KLK3, MSMB, NUDT11, PDLIM5, POU5F1, RFX6,* and *TERT* contained multiple genetic variants with strong associations [97]. It is becoming clear now, that vast majority of PCa risk variants is located in regions outside of protein-coding exons, mainly among regulatory elements [101, 102, 106, 107]. Identification of the target gene of a regulatory element is challenging as regulatory elements can act over great distances [101]. Nonetheless, widespread disruption of ternary transcription factor–transcription factor–DNA complexes between AR, FOXA1 and HOXB13 has been detected, which may potentially alter the genomic binding landscape of AR [106]. FOXA1 and HOXB13 were recently indicated in reprogramming genomic AR binding from a normal epithelial binding profile to a tumorigenic binding profile [108]. Other transcription factors with frequently disrupted binding sites by PCa risk variants found in that study were ERG and CTCF [106]. Another study analysing 103 PCa risk variants also found transcription factors binding regions to be enriched for PCa risk variants, including AR, ERG, FOXA1, HOXB13 and CTCF binding regions [102]. Another genomic regions with potentially functional impact were CpG islands and regions for histone modifications.

Linkage studies of PCa aggressiveness have reported several risk variants linked to aggressive PCa, including: 5q14.3 (rs35148638, intronic to the RAS p21 protein activator 1, *RASA1*), 3q26.31 (rs78943174, intronic to the N-acetylated alpha-linked acidic dipeptidase-like2, *NAALADL2*) [109], 2q37.3 (rs2292884, in exon 9 of the melanophilin gene, MLPH), 12q13 (rs902774, in the type II keratin family cluster) [110], 17p12 (rs4054823, region with no known gene) [111], 22q13 (rs9623117, at trinucleotide repeat-containing gene 6b *TNRC6B*) [112] but these data have to be yet convincingly replicated.

The potential for false-positive results, lack of information on gene function, insensitivity to rare variants, requirement for large sample sizes, and possible biases due to case and control selection and genotyping errors, are important limitations of GWAS. Replication studies in independent cohorts are crucial to confirm associations of detected genetic variants with disease. Furthermore, the functional consequence of these replicated variants needs to be identified to accurately incorporate genetic predisposition into clinical decision making [113].

1.2.3 Somatic genetic changes in prostate cancer

Mutations are rare in PCa [114]. The most commonly mutated gene is *AR* with mutations occurring mostly in castration resistant PCa. Common, broadly mutated oncogenes such as *PIK3CA*, *KRAS* and *BRAF* are not commonly mutated in PCa. Mutations in TSGs like *TP53* and *PTEN* are also rare [115, 116] (Table 2). Exome sequencing identified novel recurrent gene mutations in PCa, including *SPOP, NCOA2, FOXA1* and *MED12*, with the *SPOP* gene being the most commonly mutated (6-15%) in primary PCa [115-118].

In contrast, the frequency of copy number alterations (CNAs) and genomic rearrangements is high in PCa, suggesting that the development and progression of PCa is primarily the result of an accumulation of larger-scale genomic aberrations, such as deletions, gains, and gene fusions [115, 119, 120]. Whole-genome sequencing shows that large numbers of chromosomal rearrangements are particularly common in early onset cases, many involving known cancer-associated genes (commonly including ETS genes) [117].

In recent years, many studies of genomic changes in PCa were published, mostly employing comparative genomic hybridisation (CGH) methods, single nucleotide polymorphism (SNP) arrays, and most recently next generatin sequencing (NGS). Sun *et al* [119] performed a combined analysis of all published CGH studies of PCa up to 2006 (41 CGH studies), including 659 localised, 225 advanced and 174 metastatic/recurrent tumours as well as 51 PCa cell lines and xenografts. Most commonly reported deleted region in PCa was chromosome 8p with the peak at 8p21.3 (34.1% tumours), followed by 13q21.31 (28%). Other commonly deleted regions were located at 6q14.1–21 (22.2%), 16q13–16q24.3 (17.85%), 18q12.1–23 (12.8%), 5q13.3–21.3 (13%), 2q21.2–22.3 (12.4%), and 10q23.1–25.3 (11.7%). Chromosome 8q was the most commonly gained region with peak gains at 8q22.2 (25.1% cancer samples), 8q24.13 (24.0%) and large gain at 8q21.3–24.3 (22.2%). The other commonly gained regions were: 7q11.21–32.3 (12.5%), Xq11.1–23 (10.8%), 17q24.1–25.3 (11.6%), and 3q23–26.33 (10.2%). More recent meta-analysis of PCa somatic copy number alterations from 11 aCGH and SNP microarray publications that included 563 primary, 161 advanced, 12 HGPIN and 110 matched benign samples generated very similar results with most common deletions at: 8p (8p23.3-p11.21, 61.8%), 13q123-q31.1 (52.9%), 16q11.2-q24.3 (52.3%), 6q12-q22.33 (46.7%), 5q11.2-q23.3 (42.9%), 17p13.3-p11.2 (37%), 10q23.2-q26.12 (36.3%), 18q12.1-q23 (32.8%), and 2q14.1-q24.2 (29.6%)

and common gains at 8q (8q11.21-q24.3, 31.9%), 16p13.3-p11.2 (26.3%), 7p22.3-q36.2 (24.8%), 3q13.33-q27.3 (18.7%) and 20q11.22-q13.33 (12.5%) [121].

Gene fusions are also reported in PCa. Tomlins *et al* [122] discovered recurrent gene fusions of the 5' untranslated region of the androgen-regulated gene, transmembrane protease serine 2 (*TMPRSS2*) to 3' exons of *ERG* or *ETV1* in PCa, subsequently leading to abnormally high expression of ERG or ETV1 protein. Since then, the same group and others confirmed fusion of *TMPRSS2* with *ERG* and other members of ETV family (*ETV1, ETV4, ETV5,* and *ELK4*) in about 50% of cancers, 16% of high-grade PIN lesions and sporadically in normal tissue adjacent to the tumour [123-126], suggesting that this rearrangement could be an early event that predisposes to clinical progression as it continues to be expressed in metastatic and castration-resistant disease. Transgenic mouse models showed that *TMPRSS2-ERG* fusion in combination with heterozygous *PTEN* loss accelerated PIN development but not progression to adenocarcinoma, suggesting that *TMPRSS2-ERG* fusion plays a role in initiation of prostatic neoplasia [127]. Several studies identified an association of the *TMPRSS2-ERG* fusion with higher Gleason score, higher stage, and more aggressive tumour behaviour [128-130]. Though, contradictory data also exists [131]. Recent studies suggest that expression of ERG rather than presence of fusion itself should be considered as PCa prognostic marker, however ERG RNA and/or protein analysis in PCa samples also gives inconsistent results, with reports either positively correlating ERG expression with high grade and stage tumours and shorter progression-free survival or presence of metastasis [132, 133] or linking high ERG IHC to better recurrence-free survival [134], lower Gleason score, better overall survival and longer free progression times to castration resistant disease [135]. Further studies are needed to evaluate prognostic value of this fusion in PCa.

To understand which of those genetic events occur early in PCa and which correlate with advanced high-risk disease, PCa progression models were developed, incorporating information from PCa animal models, aCGH studies, SNP arrays analysis and more recently, sequencing studies. Current PCa progression models generally indicate *NKX3.1* loss, the *TMPRSS2-ERG* translocation, and *SPOP* and *FOXA1* mutations as early events in PCa development. Subsequent loss or downregulation of TSGs such as *PTEN*, cyclin dependent kinase inhibitor p27 (*CDKN1B*), retinoblastoma (*RB1*) and *TP53* is considered to be responsible for early invasion PCa progression; with *TP53* mutations and *AR* mutations/amplifications specifically enriched in metastatic samples [116, 136-138]. AR pathway activation, often as a result of AR protein overexpression due to various genetic mechanisms (e.g. mutations, gene copy number gain or amplification),

is consistently involved in PCa progression to mCRPC and PCa treatment strategies are largely based on blockage of AR signalling [6, 115, 139-141]. Other genes like *MYC* and *NCOA2* (Table 2) were also implicated in prostate carcinogenesis [115].

The available whole-genome and gene expression profiling studies are increasingly used for molecular classification of PCa, aiming at identification of distinct genomic subclasses of PCa in order to help with risk stratification and possibly selection of management strategies. The PCas are commonly grouped, based on the identification of recurrent gene fusions consisting of androgen-regulated *TMPRSS2* gene and members of the ETS family of oncogenic transcription factors, in ETS-fusion positive and ETS-fusion negative subclasses [114, 117, 137, 142]. ETS-fusion positive tumours are enriched in mutations and deletions in *PTEN*, *TP53*, and deletions at 3p13, 16q and gain of 7q [116, 118, 143, 144]. In contrast, ETS-fusion negative tumours are positive for *SPOP* mutations, *CHD1* deletions, SPINK1 overexpression, as well as rare activating mutations in *RAF*, *RAS*, and *FGFR* genes [116-118, 122, 137, 145].

Classification of PCa based on gene expression analysis led to development of two commercially available gene panels aiming to help distinguish high-risk cancer from indolent disease at diagnosis. One of them (Prolaris®, Myriad Genetics, Salt Lake City, UT) measures Cell Cycle Progression score based on expression of 31 genes involved in cell cycle progression, and was proven highly prognostic, providing more information than either Gleason score or PSA [146, 147]. Another test (Oncotype Dx® Prostate Cancer Assay, Genomic Health, Redwood City, CA) utilises a 17 gene-expression-based signature, called the Genomic Prostate Score. Genes incorporated in the score represent multiple biological pathways, including stromal response, proliferation, cellular organization, basal epithelial, androgen signalling, and stress response [148]. Another genomic classifier test (Decipher, GenomeDx Biosciences, San Diego, CA, USA) was specifically developed to predicts early metastasis (within 5 years after surgery) in patients who underwent radical prostatectomy [149]. This test contains 22 RNA markers including a large number of non-coding RNA sequences and helps to better identify patients that require intensive multi-modal therapy.

Difficulty in assessment of the exact nature and sequence of genetic changes involved in PCa progression and association of specific genomic events with metastatic cancer comes from limited number of metastatic material available for study [139]. Majority of the PCa genomic studies have been performed on prostatectomy specimens, including studies of metastatic cancers. Not many genomic projects looked at somatic copy

number alterations specifically at PCa metastatic sites. Comparison between localised prostate tumours and tumours from metastatic sites (e.g. lymph nodes, liver, lung, adrenal, spleen, skin, bone) showed many common genetic changes like losses on 8p, 10q, 13q, and 16q and gains on 8q and Xq. However, tumours from metastatic sites had higher frequency of these changes and displayed additional rearrangements, suggesting that genomic changes accumulate with disease progression [150, 151]. Interestingly, an association of certain alterations within metastasis to specific distant sites has been proposed [151, 152]. Gains at 5q31.2–31.3, 5q35.2–35.3, 8p11.21, 11q13.2, and 16p13.3 were found more frequently in PCa liver metastases, while gains at 6p21.32–21.2 and 6p21.1 and loss at 22q12.1 were reported as common alterations for lymph node metastases [151]. Which genes within those regions are specifically involved in metastatic PCa and could be used as potential prognostic markers or treatment targets remains to be elucidated.

TABLE 2 SOMATIC GENETIC CHANGES IN PROSTATE CANCER.

Genetic change	Chromosomal region	Gene	Reference
Point mutations	17p13.1	*TP53*	[115, 116, 140, 153]
	Xq12	*AR*	[115, 140]
	1p36.2	*MTOR*	[153]
	13q12.3–13.2	*BRCA2*	[115]
	9p21	*CDKN2* (p16)	[154]
	10q23.31	*PTEN*	[116]
	3q26.32	*PIK3CA*	[116, 140]
	12p12-13.1	*CDKN1B* (p27)	[116]
	14q21.1	*FOXA1*	[116]
	Xq13.1	*MED12*	[116]
	17q21.33	*SPOP*	[116, 117]
	8q13.3	*NCOA2*	[115]
Deletion	10q23.31	*PTEN*	[115, 117, 121, 140, 153, 155-157]
	13q14.2	*RB1*	[115, 121, 140, 157-159]
	17p13.1	*TP53*	[115]
	12p12-13.1	*CDKN1B* (p27)	[160]
	9p21	*CDKN2* (p16)	[154]
	8p21.2	*NKX3.1*	[115, 161]
	13q12.3–13.2	*BRCA2*	[140]
Copy number gain/ amplification	8q24.21	*MYC*	[115, 140, 157, 162-164]
	8q13.3	*NCOA2*	[115, 164]
	8q24.2	*PSCA*	[163]
	Xq12	*AR*	[115, 140, 153, 165]
	7q35	*EZH2*	[115, 166]
	7q34	*BRAF*	[115]
	11q13.3	*CCND1* (cyclin D1)	[138, 167]
Gene fusion	21q22	*TMPRSS2-ERG*	[122, 168]

1.3 Metastatic prostate cancer

1.3.1 Mechanism of metastasis

Metastasis is the process in which cancer cells spread throughout the body, establishing new colonies in organs different from the one where the primary tumour originated. The ability to metastasize is a property of malignant tumours, and metastasis is the principal cause of death among cancer patients [169].

Metastasis is a complex, multistep process and involves angiogenesis, local invasion through the basement membrane (a hallmark characteristic of a metastatic cell), adhesion to vessel endothelium in the target organs, and extravasation into the tissue. Very few disseminated tumour cells will establish metastasis at distant organs and their success will depend on close collaboration with microenvironment (Figure 4) [170, 171].

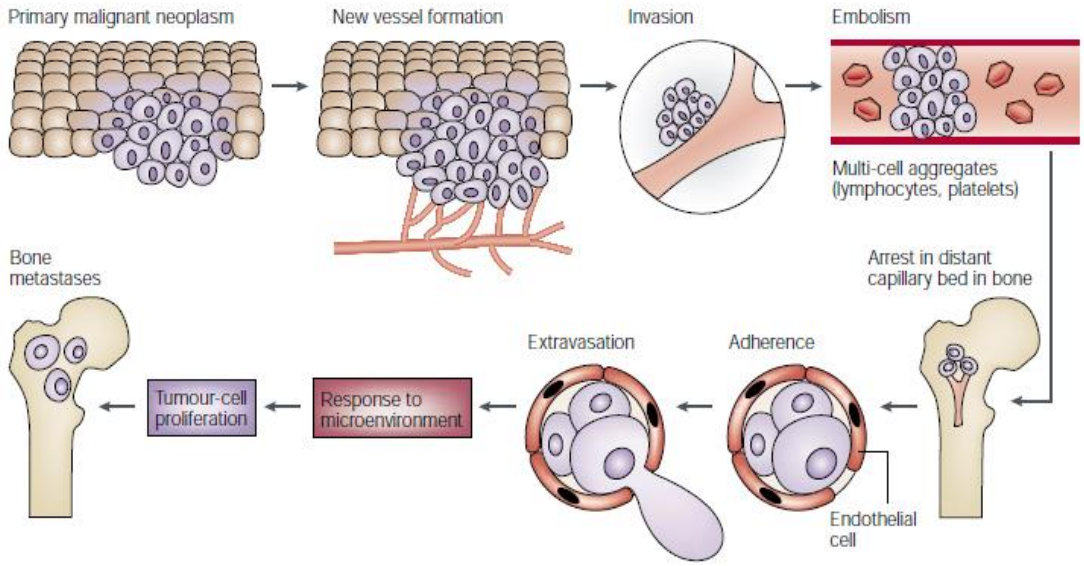

FIGURE 4 THE STEPS INVOLVED IN TUMOUR CELLS METASTASIS TO THE BONE. Adapted from Mundy *et al* [171].

At the early stage, tumour tends to spread to local lymph nodes through the lymphatic system. However, aggressive tumour cells eventually enter the bloodstream and reach distant tissues. Interestingly, different tumours have unique patterns of organ colonisation. It is not clear when primary tumour cells acquire metastatic capacity and why they spread to some organs but not others. Several theories have been proposed to answer those questions. Some models advocate acquisition of metastatic potential as

a late event in primary tumour progression. Darwinian or evolution models state that metastasis is a rare event which results from the selection of rare clones that emerge from a genetically heterogeneous and unstable population due to repeated cycles of mutation and clonal selection. Those individual cell clones over time would acquire novel genetic changes conferring a selective advantage within the primary tumour microenvironment but at the same time would randomly acquire key pro-metastatic mutations determining their accumulation in specific organs [169, 172]. Other models support early acquisition of metastatic potential by primary tumour cells. Pre-determination models state that a subset of the mutant alleles acquired by primary tumour cells early in tumourigenesis confers both: a selected replicative advantage and proclivity to metastasize later in tumourigenesis. Therefore, the tendency of a tumour to metastasize would be determined by the spectrum of mutations that progenitor cells acquire relatively early in tumourigenesis and then augmented by additional genetic changes at metastatic site [173]. Gene expression patterns of tumour cells at distant metastases seem to confirm both theories. A breast cancer study using *in vivo* selection described set of genes that marks and mediates breast cancer metastasis to the lungs [174]. Some of these genes provided growth advantages both in the primary tumour and in the lung microenvironment while others contribute to aggressive growth selectively in the lung. An expression signature was also suggested for breast cancer cells with osteolytic bone metastasis potential [175] where majority of highly overexpressed genes encoded cell membrane or secreted molecules relevant to the bone microenvironment. In that study, a parental MDA-MB-231 cell population already possessed previously reported poor-prognosis gene expression signature for primary breast cancer [173] and additionally expressed concrete set of bone metastasis genes, which gave it tissue-specific metastatic phenotype.

In 1889, Stephen Paget for the first time presented an explanation for the non-random patterns of cancer metastases. His ‘‘seed and soil’’ theory proposed that the metastatic sites contain factors that promote cancer cell growth similar to the tendency of seeds to grow in fertile soil [176]. Paget’s theory can therefore explain distant metastases that are organ-specific, such as metastases to the bone. Based on the Paget’s theory, circulating PCa cells would be able to establish bone metastases only if bone microenvironment was favourable for their growth [177, 178]. Contradictory theory was proposed by James Ewing and postulated that metastatic spread of cancer is determined purely by the vascular connections of the primary tumour; therefore cells released from a primary tumour will accumulate in the first highly vascularised organ that they encounter [176].

However, this theory can explain some of the metastases but not all and Paget's ''seed and soil'' theory is nowadays widely accepted.

Several mechanisms may be involved in selective establishment of distant metastases, including chemokine-receptor-mediated chemotaxis, the establishment of a metastatic niche, and a tumour cell genetic program that facilitates adaptation to a particular microenvironment. Tumour cells are known to express a variety of chemokine receptors, including C-X-C chemokine receptor type 4 (CXCR4) that serves as a receptor for C-X-C motif chemokine 12 (CXCL12, also known as stromal cell-derived factor-1, SDF-1) [179]. The CXCL12/CXCR4 pathway is involved in the retention and homing of endothelial (EPC) and hematopoietic progenitor cells (HPC) in the bone marrow microenvironment and lymphocyte trafficking. Functional CXCR4 is expressed on embryonic and tissue-committed stem cells, including proangiogenic cells and endothelial precursor cells. CXCL12 is constitutively expressed in many tissues and plays a role in the mobilisation and recruitment of CXCR4 expressing cells to the neoangiogenic niches [180]. CXCR4 is found on malignant epithelial cells and on cells from several hematopoietic malignancies which implies that the CXCL12/CXCR4 pathway may play a pivotal role in directing the metastasis of CXCR4 positive tumour cells to organs that express CXCL12 (e.g., lymph nodes, lungs, liver, or bones). Several CXCR4 positive cancers metastasize to the bones and lymph nodes in a CXCL12-dependent manner, including myeloma, acute and chronic leukaemia, breast, ovarian and prostate cancer [181]. PCa cell lines (PC3, DU145, LNCaP) express CXCR4 and they respond to CXCL12 treatment by migration across basement membrane monolayers and increased invasion [182]. Blocking CXCL12 binding with CXCR4 was shown to prevent the skeletal metastasis of PC3 cell line in nude mice [183] and blocking CXCR4 decreased the invasiveness of PC3 cells and reduced tumour spread with associated reduction in angiogenesis in *in vivo* orthotopic PCa model [184].

Homing to bone can also be caused by interaction between integrins on tumour cell surface and the supporting host stromal cells in bone (osteoclasts, new blood vessels, inflammatory cells, platelets and bone marrow stromal cells). The αvβ3 integrin interacts with bone-derived ostepontin (OPN), fibronectin and vitronectin, and expression of αvβ3 by breast and prostate cancer cells is associated with higher rates of bone metastasis, tumour-associated osteolysis and colonisation in bone [185]. Expression of integrins like α5β1, α2β1 and α4β1 (receptors for fibronectin, collagen I and vascular cell adhesion molecule 1 (VCAM1), respectively) by tumour cells has been implicated in the

interactions of leukaemia, myeloma, prostate and breast cancer cells with bone marrow stroma, and can result in enhanced colonisation and survival in bone [186].

It has been suggested that tumour cells can use their cytokine and chemokine repertoire to prepare the microenvironment of distant organs to receive disseminating cells. Tumour and associated stromal cell–derived chemokines can recruit endothelial and hematopoietic progenitor cells to the relevant organs prior to tumour cell arrival, which, together with tumour cell–derived deposition of fibronectin, appear to precondition the local microenvironment to form premetastatic niche. The exact mechanisms of premetastatic niche formation are still unclear and remain to be confirmed [187, 188]. The secretion of exosomes by tumour cells is also involved in the formation of pre-metastatic niches. Tumour-derived exosomes enhance vascular leakiness by inducing a pro-vasculogenic phenotype in bone marrow progenitor cells, “educating” the bone marrow to support tumour dissemination [189].

The ability of cells to establish themselves in the new host tissue microenvironment, so they can survive and proliferate, is the most important rate-limiting step in metastatic process [190]. Microenvironment of metastatic site not only provides fertile soil for tumour growth, but also influences cancer cells, triggering permanent genetic and phenotypic changes, conferring cancer cells selective growth and survival advantages. This influence is reciprocal as PCa cells can exhibit osteomimicry (bone cell-like properties) through expression of transcription factors (Runx2, MSX2), which are regulators of osteoblasts differentiation, leading to improved homing, adhesion, proliferation and survival in the bone microenvironment [191]. This reciprocal interaction between microenvironment and cancer cells may explain failure of gene expression studies of primary tumours to predict organ specific tropism of cancer cells. Furthermore, it also highlights necessity of development site – specific treatment, as bone directed therapy would be selective and effective only against bone metastasis but not against other metastatic sites or primary tumour [192].

1.3.2 Bone metastases

The most common metastatic site of PCa is bone: around 90% of patients dying from PCa have skeletal metastases. Less frequently PCa metastasize to lungs and kidney [193, 194]. Once tumours metastasize to bone, they are incurable and result in significant disease morbidity, causing pain, pathological fractures, nerve compression syndromes, and hypocalcaemia. Current treatments for metastatic disease are mainly palliative [193]

and therapies for mCRPC have shown only modest success, with prolonged survival measured in months [195]. Therefore, better understanding of bone metastases is needed in order to develop more efficient approaches and novel therapies to manage aggressive metastatic disease.

1.3.2.1 Normal bone physiology

Bone is made primarily of type I collagen (about 90% of the bone matrix proteins) that is mineralised with hydroxyapatite crystals. Collagen and most of the bone proteins are synthesised and secreted by bone forming cells, osteoblasts [196]. Osteoblast-mediated bone formation is balanced with osteoclast-mediated bone resorption in dynamic remodelling process in order to prevent accumulation of bone microdamage [170]. Osteoblasts are formed from mesenchymal stem cells in the bone marrow stroma, upon stimulation by bone morphogenic proteins (BMPs) and other bone matrix - derived factors such as transforming growth factor beta (TGF-β), insulin-like growth factor 1 and 2 (IGF-1 and IGF-2), or fibroblast growth factor (FGF) [196]. Osteoblasts produce the collagenous precursors of bone matrix (osteoid) and regulate bone mineralisation. They express bone regulatory factors, including parathyroid hormone (PTH) receptors, prostaglandins, estrogen, vitamin D3, and various cytokines [197]. Osteoclasts are large multinucleated cells differentiating from haematopoietic stem cells and responsible for dissolving both, the mineral and organic bone matrix. Osteoclast formation, activation and resorption are regulated by three members of the tumour necrosis factor (TNF) family of receptors and ligands: RANK (Receptor Activator of Nuclear Factor-kappa B), RANKL (RANK ligand) and OPG (osteoprotegerin) [196, 198, 199]. RANK is a surface receptor expressed on mature osteoclasts and their progenitors; it induces osteoclastogenesis and controls calcium metabolism. RANKL belongs to type II transmembrane proteins and is found on the surface of osteoblasts, bone stomal cells and in a soluble form within the bone microenvironment. In the presence of low levels of macrophage colony-stimulating factor (M-CSF) RANKL binds to its receptor RANK which leads to the differentiation of osteoclast progenitors and limits apoptosis of mature osteoclasts. Other molecules, including PTH, parathyroid hormone related protein (PTHrP) 1, 25-dihydroxyvitamin D, TNF, interleukin 1 (IL-1) and IL-11 can also induce osteoclastogenesis. OPG is secreted by the osteoblasts and stromal cells and acts as a soluble decoy receptor for RANKL. OPG competes with RANK for RANKL; therefore, it prevents the RANKL–RANK interaction on the osteoclast cell membrane. Binding of OPG to RANKL inhibits osteoclastogenesis leading to cessation of bone resorption [170, 198, 199].

1.3.2.2 Types of bone metastases

Bone metastases are classified as osteolytic, osteoblastic (osteosclerotic) or mixed lesions (Figure 5). Osteolytic metastases are typical for breast cancer, where tumour cells stimulate the activity of bone-resorbing osteoclasts, leading to enhanced bone destruction. Histologically, tumour cells reside in the bone marrow and are surrounded by bone degrading osteoclasts. Ultimately, osteolytic lesions lead to complete destruction of the bone wall allowing tumour cells to infiltrate the surrounding tissues. These osteolytic areas are very prone to fracture even in the absence of traumas. Osteoblastic metastases are common in PCa and are caused by cancer-derived factors that stimulate the differentiation and activity of bone-forming osteoblasts, thus leading to increased bone formation. Histologically, tumour cells are located within bone marrow and are surrounded by a high number of osteoblasts that form poor quality woven bone anchored at the surface of pre-existing trabeculae of the patient and tend to fill the marrow cavity without extension in the soft tissues. This confinement to the marrow spaces makes osteoblastic metastases progress more slowly than osteolytic lesions [200]. Bone resorption and formation are almost always coupled, often leading to the development of mixed lesions [191].

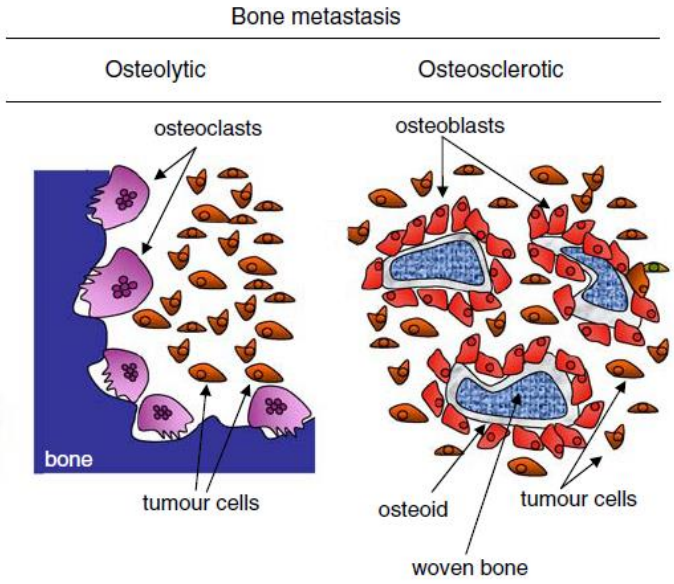

FIGURE 5 CLASSIFICATION OF BONE METASTASES. Left: osteolytic bone metastases display high number of osteoclasts which resorb the mineralised matrix and destroy the bone. Right: osteosclerotic bone metastases contain numerous osteoblasts, which form new bone within bone marrow occluding the medullary cavity. Adapted from Clezardin *et al* [191].

1.3.2.3 Model of osteolytic bone metastases

Model of bone metastases has been developed for breast cancer by Guise *et al* [201]. Breast cancer cells produce PTHrP, which induces osteoclastogenesis, and its high expression is specific to the bone metastatic niche. 90% of breast cancer bone metastases were found to express PTHrP, compared to only 17% at non-bone sites and 60% of the primary tumours [202]. Contradicting results for the relation between PTHrP expression in primary tumours and bone metastases lead to the conclusion that the bone microenvironment itself induces cancer cells to express PTHrP rather than cancer cells that metastasize to the bone have an intrinsically higher PTHrP expression [203, 204]. In bone marrow, PTHrP expressed by cancer cells binds to parathyroid hormone receptor 1 (PTHR1) on osteoblasts and causes osteoblastic expression of RANKL and M‑CSF, with a decrease in expression of OPG. RANKL then interacts with RANK expressed on hematopoietic osteoclast precursors, inducing their differentiation into mature osteoclasts. Osteoclasts degrade the bone, leading to release of bone-stored IGF-1 and TGF-β. IGF-1 stimulates breast cancer cell growth while TGF-β further stimulates production of PTHrP by cancer cells, resulting in a 'vicious cycle' of increased osteoclastic bone resorption (Figure 6). Breast cancer cells also produce multiple cytokines, including IL-6, IL-11, prostaglandin E2, M-CSF, and tumour necrosis factor alpha (TNF-α), which act to promote bone metastases by inducing osteoclastogenesis and suppressing osteoblasts [170, 197, 201, 205, 206].

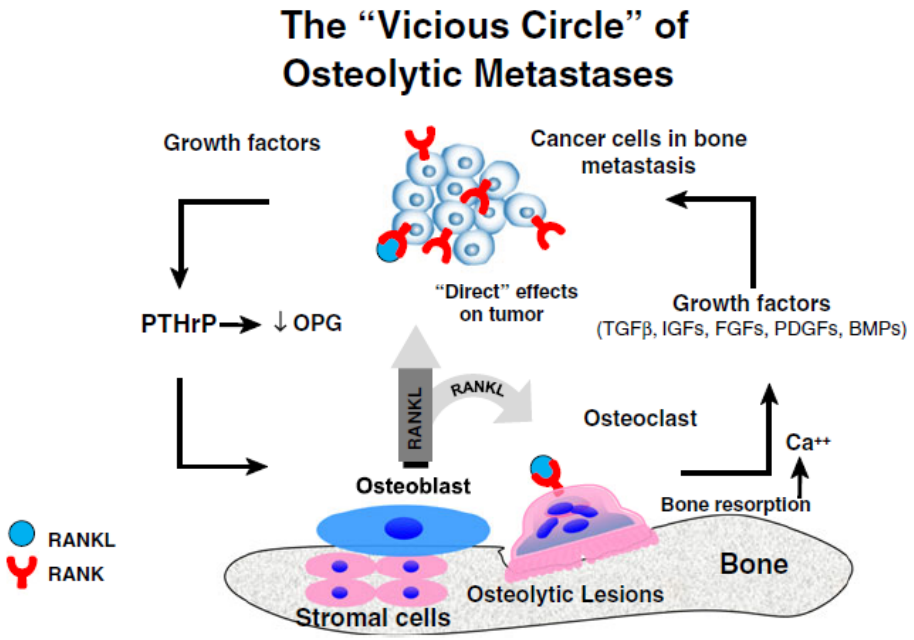

FIGURE 6 THE VICIOUS CYCLE IN OSTEOLYTIC METASTASIS. Tumour cells stimulate bone destruction by production of PTHrP and induction of osteoclastogenesis. The osteoclasts in turn release growth factors from the bone matrix further supporting osteoclastogenesis and stimulating tumour cells to expand and produce more PTHrP. Adapted from Roodman *et al* [205].

1.3.2.4 Model of osteoblastic bone metastases in prostate cancer

The model of PCa bone metastasis is not well understood. PCa cells can influence bone homeostasis by secreting paracrine factors that regulate osteoblast proliferation or differentiation, including BMPs, TGF-β, IGF, PDGF, VEGF, endothelin-1 (ET-1), urokinase-type plasminogen activator (uPA) and PSA. These factors can support osteoblast proliferation directly (BMP, TGF, IGF, PDGF, VEGF and ET-1) or influence osteoblast proliferation by modifying growth factors present in the bone microenvironment (uPA and PSA) [207, 208]. ET-1 is expressed by osteocytes, osteoblasts, osteoclasts and vascular endothelial cells. It stimulates mitogenesis in osteoblasts and enhances the effect of other osteoblast-stimulatory factors to induce bone formation [209]. Prostate epithelium produces ET-1 and expresses its both A and B receptors (ETA and ETB). Prostate cancers express ET-1 and mostly ETA receptors [210]. Exogenous ET-1 via ETA receptors increases the proliferation of PCa cells through enhancement of mitogenic effects of IGF-1, IGF-2, PDGF, epidermal growth factor (EGF), and FGF-2 [209]. The paracrine effects of tumour-produced ET-1 on osteoblasts leads to their activation. The activated osteoblasts deposit new unmineralised matrix for bone formation, which provides a more fertile 'soil' for tumour cells, enriched with growth factors and BMPs. These factors help PCa cells survive and proliferate in the bone

microenvironment [170, 171, 211]. Breast cancers are also known to produce ET-1 and they express both, ETA and ETB receptors [212]. Culture media from osteoblastic MCF-7 and T47D cell lines known to produce ET-1, can stimulate new bone formation and osteoblast proliferation, which is blocked by administration of ETA antagonist [209].

Similar to other malignant cells, PCa cells can release cytokines that induce osteoclastogenesis, including PTHrP, IL-1, IL-6 and M-CSF. PTHrP is produced by normal prostate epithelial cells, and its immunoexpression increases with cancer progression. Upregulation of PTHrP in PCa cells can regulate malignant tumour growth in an autocrine manner and PTHrP expression can protect prostate and other cells from apoptosis [194]. As PTHrP expression in breast cancer bone metastases is a driving force of osteolytic lesions, it is unclear why PTHrP is overexpressed in osteoblastic PCa bone metastases. The possible explanation lies in proteolytic activity of PSA. Contrary to breast cancer, PSA producing PCa cells have ability to cleave PTHrP, an event that switches the downstream pathway from osteolytic to osteoblastic. Cleavage of PTHrP leads to its inactivation. On the other hand, the cleaved NH2-terminal region has a homology with endothelin-1, therefore can act through ETA receptor pathway as a mitogenic factor for osteoblasts [200, 201]. Tumour-secreted proteases such as PSA and uPA can also locally increase the amount of growth factors. uPA can cleave and activate latent form of TFG-β produced by osteoblasts. Both, uPA and PSA can also separate IGF-I from its binding protein IGF-BP3, therefore increasing the local amounts of free IGF in the bone microenvironment [194, 200].

PCa cells can also secrete bone morphogenic proteins (BMPs), the most potent stimulators of osteoblastogenesis. Primary and metastatic PCas have a different pattern of BMP expression and adopt different signalling pathways downstream of the BMP receptor. Most BMPs and their receptors are expressed in normal prostate tissue. With cancer progression, pattern of BMPs expression changes. BMPs production by PCa cells induces the osteoblastic activities leading to a predominantly osteoblastic lesion. In return, BMPs synthesised by osteoblasts or released from bone matrix enhance the growth and aggressiveness of PCa cells, allowing more BMPs to be produced from the tumour cells and sustaining the ‘vicious cycle’ [193, 213].

In addition to this ‘vicious cycle’, at a certain stage, both tumour-derived factors and osteoblasts expressing RANKL can activate osteoclasts, leading to some level of bone resorption, and subsequently generating bigger spaces for dominant osteoblastic lesions. The cytokines released from bone matrix during bone resorption can also

enhance this ‘vicious cycle’ through facilitating the proliferation of both PCa cells and osteoblasts [193, 194].

Current chemotherapy regimens mainly debulk the tumour and palliate symptoms, but cannot eradicate late stage disease. They usually slow progression of lesions and reduce bone-related skeletal events (SRE; e.g. bone pain and pathological fractures). The standard bone-targeting treatment for PCa includes bone-seeking radiopharmaceuticals like strontium-89 (89Sr; calcium analog preferentially taken up at areas of increased bone turnover such as osteoblastic metastases) [195, 211, 214] and bisphosphonates (e.g. zoledronic acid), analogs of pyrophosphates that inhibit osteoclasts function [170, 191, 195, 214]. Recently, new bone-targeted radiopharmaceutical, the alpha-emitting agent Ra223 was introduced into clinical practice, showing increased overall survival in patients with mCRPC [215].

Better understanding of the molecular mechanisms of PCa bone metastases is needed in order to identify new therapeutic targets and develop better treatment options. Many clinical trials already explore blockage of the RANK/RANKL/OPG axis as a potential therapeutic target for bone metastases. The anti-RANKL monoclonal antibody, Denosumab, proved to be a potent inhibitor of osteoclastogenesis and bone resorption and has been shown to reduce SRE [170, 191]. Atrasentan, an ETA receptor antagonist, has been shown to prevent osteoblastic bone metastases in mouse models and is tested in clinical trials for a wide range of solid tumours, including PCa [191, 195].

1.4 Aims

The aim of this project is to study genomic alterations in PCa bone metastases in order to identify potential genomic mechanisms driving PCa progression. Identification of such genetic factors could aid treatment choice for patients with advanced lethal disease or help to develop better treatment strategies to improve patient management and possibly prolong survival. Genome-wide analysis with high density Affymetrix SNP 6.0 arrays will be performed on available fresh frozen PCa bone metastases. Genomic copy number changes will be identified with 'in house' GOLF software and scrutinised further with emphasis on recurrent chromosomal rearrangements.

Some of the detected recurrent genomic changes in bone metastases will be selected for further analysis based on review of available literature on genomic alterations in PCa. Particular attention will be paid to recurrent genomic events which were previously sporadically found in primary tumours as they could be a driving force for cancer cells at primary site to acquire metastatic potential. Next, we will analyse copy number status of chosen genetic alterations (concentrating on regions with possible driver genes) by fluorescence *in situ* hybridisation (FISH) in larger cohorts of FFPE PCa bone metastases as well as in primary tumours and non-malignant BPH samples. Immunohistochemistry (IHC) staining will be also performed to see if observed gene alterations affect expression of coded by them proteins.

Following FISH and IHC analysis, *in vitro* cell lines models will be generated with stable overexpression and downregulation of relevant genes in order to investigate how they drive PCa progression. Impact of gene deregulation on several cellular processes involved in malignant phenotype will be analysed, including proliferation, migration and invasion. If unknown, potential downstream targets or pathways of these genes will be analysed to better understand gene function and explore possible avenues for therapeutic intervention.

CHAPTER 2

Material and Methods

2.1 Clinical samples

Tissue microarray (TMA) blocks containing prostate tissue cores from 152 FFPE primary PCa and 55 BPH cases were prepared from patient samples obtained from The Barts and The London Hospital NHS trust and Whipps Cross Hospital in London under ethical approval. Four fresh frozen primary PCa and four BPH samples were obtained from The Barts and The London Hospital NHS trust. Six fresh frozen and 43 FFPE (including 6 cases for which fresh tissue was available) PCa bone metastases were obtained under ethical approval from The Robert Jones and Agnes Hunt Orthopaedic Hospital in Oswestry, Shropshire. All fresh frozen samples of PCa bone metastases came from patients with advanced PCa who were treated for pathological bone fractures. All available information about these samples is listed in Table 3.

TABLE 3 AVAILABLE PATIENT AND TUMOUR INFORMATION FOR FRESH FROZEN PCA BONE METASTASES.

Sample ID	Patient age	Sample origin	Type of metastasis	Additional information
Sample 1	83	right tibia	osteoblastic	
Sample 2	76	proximal left femur	mixed osteoblastic/ osteolytic	widespread tumour
Sample 3	86	femoral head, left hip	osteoblastic	widespread tumour, bisphosphonates treatment
Sample 4	64	proximal femur including femoral head		widespread tumour
Sample 5	77	proximal left femur		widespread tumour
Sample 6	67	left proximal humerus	osteoblastic	extensive necrosis

TMA sections of FFPE cases of conservatively managed clinically localised PCas diagnosed by transurethral resection of the prostate (TURP) were obtained from Prof Colin Cooper. These samples were part of Transatlantic Prostate Group (TAPG) PCa cohort containing in total 709 cases. Detailed description of the cohort is available

elsewhere [216]. Over 10 years follow up data were available for those patients and were used to assess the prognostic value of 6q16 deletion in the early stage of PCa.

2.2 Cell lines and cell culture

Five PCa cell lines, 22RV1, PC3, DU145, LNCaP and VCaP, and two SV40-immortalised prostate epithelial cell lines, PNT1A and PNT2, were used in this project. Additionally, human embryonic kidney HEK293 cell line was also used. All cell lines were tested and authenticated in 2011, using the ABI AmpF/TSR Identifier kit.

Frozen cell stocks were stored in liquid nitrogen in Dulbecco's MEM (DMEM) (Sigma Aldrich, UK) or RPMI1640 (Sigma Aldrich, UK) media with 5-10% DMSO and 20% of Foetal Calf Serum (FCS) (Sigma Aldrich, UK). All cell lines were thawed at 37°C water bath and the cell suspension was diluted in 5 ml of pre-warmed culture media, pelleted by centrifugation at 1200 rpm for 5 minutes and resuspended in culture media. After thawing, cells were grown under standard conditions (5% CO_2 and 37°C) in RPMI1640 or DMEM with 10% FCS and 1% penicillin/streptomycin (100 units/ml). Cells were passaged after reaching 80-90% confluence.

2.3 Hematoxylin-eosin (H&E) staining

Fresh frozen sections were fixed in 100% methanol for 10 min and subsequently air-dried. FFPE sections were first dewaxed in 2 changes of xylene, 5 min each and rehydrated in series of alcohols (100%, 90% and 70% ethanol, 5 min each). Slides were then rinsed in water and placed in haematoxylin solution for 10 min, differentiated in 1% acid ethanol for few seconds, washed under running tap water for 5 min and counterstained with eosin solution for 1 min. Next, slides were dehydrated with 90% and 100% ethanol (3 min each), cleared in 2 changes of xylene (5 min each) and mounted with xylene based mounting medium (DPX, Sigma, UK).

2.4 DNA extraction

2.4.1 Fresh frozen samples and cell lines

Primary PCa and BPH frozen tissue was first cut using cryostat (ThermoFisher, UK) and one slide was H&E-stained to guide subsequent macrodissection using sterile blade and stereo microscope. Five to ten sections were used per sample. For bone metastases, a small piece of frozen tissue was used for DNA extraction. The tissue was mashed and placed in 500 µl of TEN buffer (10 mM Tris 8.0, 10 mM EDTA, 150 mM NaCl). Cell lines

were first trypsinised, centrifuged (1200 rpm, 5 min), washed with PBS and then resuspended in 500 µl of TEN buffer. Next, for all samples SDS (1% vol) and proteinase K (0.5 mg/ml) were added and samples incubated at 50°C for 3-24 h (until completely digested). After complete digestion, samples were incubated with RNAse A (100 µl/ml) for 1 h at 37°C to digest the RNA. After incubation regular phenol/chloroform extraction was performed. Samples were mixed with equal volume of phenol, shaken in order to separate DNA from proteins and cell debris, and centrifuged for 15 min at 13000 rpm. The aqueous top layer containing DNA was transferred to another tube and equal volume of 50% phenol/chloroform solution was added to the samples. After 15 s of firm shaking, samples were centrifuged (13000 rpm, 15 min) and DNA top layer separated and cleaned again with equal volume of chloroform. Eventually, DNA was precipitated with sodium acetate (1/10 of sample volume) and 2.5 volume of ethanol for 30 min at -80°C. After centrifugation (13000 rpm, 15 min), DNA pellet was washed with 70% ethanol and resuspended in DEPC (diethylpyrocarbonate, 0.1%)-treated water. DNA concentration and quality were checked by Nanodrop Spectrophotometer (Thermofisher, UK). The purity of DNA (same for RNA) was considered as sufficient when the ratio of absorbance at 260/280 nm and 260/230 nm was between 1.8 and 2.2. Samples were stored at -20˚C until further processing.

2.4.2 Simultaneous DNA and RNA extraction

DNA and RNA extraction from single cell line samples was done with TRIzol reagent (Invitrogen, Life Technologies, UK) according to manufacturer's instructions. Cells (≤ 1 x 10^6 cells) were tripsinised, centrifuged at 1200 rpm for 5 min and pellet resuspended in 1ml of TRIzol. Subsequently, chloroform (1/20 volume) was added and, after a quick shake, samples were left at room temperature for 3 min for RNA to separate from the cellular DNA and proteins. After centrifugation at 4°C at 13,000 rpm for 15 min, the upper aqueous layer containing RNA was moved to a fresh vial and RNA was then precipitated by adding 500 µl of isopropanol (bottom organic layer was saved for simultaneous DNA extraction). After centrifugation at 4°C at 13,000 rpm for 10 min, supernatant was removed and the precipitated RNA was washed with fresh 80% ethanol, air-dried and resuspended in 25 µl of DEPC-treated water. RNA quality and quantity was assessed using Nanodrop. All RNA samples were stored at -80°C for further analysis.

The bottom organic layer was used for DNA extraction. Any remaining aqueous phase containing RNA was removed. 0.3 ml of 100% ethanol was added to the samples, followed by gentle mix and incubation at room temperature for 2–3 min. Next, samples

were centrifuged at 2000 *g* for 5 min at 4°C to pellet the DNA. After centrifugation, the phenol-ethanol supernatant was removed and the DNA pellet washed with 1 ml of sodium citrate/ ethanol solution (0.1 M sodium citrate in 10% ethanol, pH 8.5) for 30 min at room temperature. Samples were then centrifuged at 2000 g for 5 min at 4°C and wash step followed centrifugation performed once more. Eventually, samples were rinsed with 1.5 ml of 75% ethanol for 20 min at room temperature and centrifuged at 2000 g for 5 min at 4°C. Supernatant was discarded and DNA pellets air-dried and resuspended in 0.3–0.6 ml of 8mM NaOH. Once DNA pellets dissolved, pH was adjusted to 7.0 with HEPES (4-(2-Hydroxyethyl)piperazine-1-ethanesulfonic acid, N-(2-Hydroxyethyl)piperazine-N′-(2-ethanesulfonic acid)) buffer. DNA concentration and quality were checked by Nanodrop. DNA samples were stored at -20^{o}C for future use.

2.4.3 FFPE samples

H&E stained slide was examined by a pathologist and area of cancer/normal tissue circled with the marker pen. Those slides were used for reference when cancer lesions from FFPE tissue sections were scraped from unstained slides using a sterile scalpel and collected into 1.5 ml tubes. FFPE sections were first dewaxed in three xylene washes, 7 minutes each and air dried before macrodissection. Ten sections were dissected for each case and directly resuspended in 500 µl of TEN buffer. Next, sodium dodecyl sulphate (SDS, 1% vol) and proteinase K (0.5 mg/ml) were added and samples incubated at 50°C for 2-3 days (until completely digested). After complete digestion, samples were incubated with RNAse A (100 µl/ml) for 1 h at 37°C to digest the RNA. Next, regular phenol/chloroform extraction was performed as described above. DNA concentration and quality were checked by Nanodrop. The integrity of DNA for clinical samples was assessed by agarose gel electrophoresis. 4 µl of DNA mixed with 1 µl of loading buffer was loaded into 1% gel (1 g agarose in 100 ml of 1X TBE (Tris-borate-EDTA) buffer supplemented with 5% ethidium bromide). DNA was run on the gel at 120V for 30-60 min in 1X TBE buffer, and the resolving band in the gel was checked under ultraviolet (UV) light. Samples were stored at -20˚^{o}C until further processing.

2.5 Sample preparation for SNP 6.0 array analysis

Six fresh-frozen PCa bone metastases were used for genome-wide analysis. Genome-Wide Human Single Nucleotide Polymorphis (SNP) 6.0 Arrays were purchased from Affymetrix (Santa Clara, CA, US). A single array contains 906,600 SNPs and 946,000 probes for the detection of copy number variation. The median inter-marker distance

over all SNP and copy number markers combined is less than 700 bases. Samples were prepared strictly according to the manufacturer protocol (Affymetrix, Santa Clara, CA, US). The SNP array assay involves many consecutive steps such as: genomic DNA digestion, ligation, dilution, PCR, fragmentation, labelling, hybridisation, washing, staining, scanning and SNP data analysis. Genome-Wide Human SNP Nsp/Sty Assay Kit 5.0/6.0 was used for SNP array DNA preparation and hybridisation.

2.5.1 Restriction enzyme digestion

Genomic DNA was diluted to required 50 ng/µl with reduced TE buffer (10 mM Tris-HCl, 0.1 mM EDTA, pH 8.0). Digestion master mix was prepared on ice in pre-PCR clean hood (**TABLE** 4). For each sample 5 µl of genomic DNA was mixed with 14.75 µl of the master mix in a PCR tube. The digestion reactions were performed in a PCR machine using the following program: 37ºC for 2 h, 65ºC for 20 min and 4ºC forever.

TABLE 4 RESTRICTION DIGESTION MIX PREPARATION.

Reagents	Volume (µl)
NE buffer 2 (10x) (for NspI)/NE buffer 3 (10x) (for StyI)	2
BSA, 10x (1 mg/ml)	2
NspI (10 U/µl) or StyI (10 U/µl)	1
H_2O	9.75
Total	14.75

2.5.2 Ligation

Ligation master mix was prepared on ice (Table 5) and mixed with digested DNA. Adaptor ligation reaction was performed in PCR machine using following program: 16ºC for 3 h, 70ºC for 20 min and 4ºC forever. After adaptor ligation DNA samples were diluted to 100 µl final volume with 75 µl water for subsequent PCR amplification.

TABLE 5 LIGATION MIX PREPARATION.

Reagents	Volume (µl)
Adaptor Nsp I or Sty I *	0.75
T4 DNA Ligase (400 U/µl)	2
T4 DNA Ligase buffer (10x)	2.5
Total	5.25

*: part of Genome-Wide Human SNP Nsp/Sty Assay Kit 5.0/6.0.

2.5.3 PCR

The PCR master mix was prepared on ice (Table 6). Three PCR reactions were prepared for each StyI digested sample and four for each NspI digested sample. For each reaction 10 µl of diluted ligated DNA sample was mixed with 90 µl PCR master mix. For negative control 10 µl of water was used instead of DNA solution. The PCR cycling conditions were as follow: initial DNA denaturation at 94ºC for 3 min, followed by 30 cycles of: 94ºC for 30 s, 60ºC for 30 s and 68ºC for 15 s. Final extension step at 68ºC for 7 min was added at the end. Expected PCR product should be a DNA smear with size ranging between 200 and 1100 bp. 3 µl of PCR product mixed with 1 µl of 10x loading buffer was run on 2% agarose gel at 120 V for 30 min to confirm the size.

TABLE 6 PCR MASTER MIX PREPARATION.

Reagents	Volume (µl)
TITANIUMTM Taq PCR buffer (10x)	10
G-C melt (5 M)	20
PCR Primer 002 (100 µM) *	4.5
dNTP (2.5 mM each)	14
TITANIUMTM Taq DNA Polymerase (50x)	2
H_2O	39.5
Total	90

*: part of Genome-Wide Human SNP Nsp/Sty Assay Kit 5.0/6.0.

2.5.4 PCR product purification

Al seven PCR reaction products for each sample were pooled together in one vial and mixed thoroughly with 1 ml of magnetic beads. Samples were incubated at room temperature for 10 min to allow DNA binding to the magnetic beads. Next, samples were

centrifuged at 16000 g for 3 min and placed on the magnetic stand where supernatant was carefully removed without disturbing the bead pellet. DNA bound to the beads was then washed with 1.5 ml of 75% ethanol and samples centrifuged for 3 min at 16000 g. After centrifugations samples were placed again on the magnetic stand, supernatant removed and leftovers of ethanol allowed to evaporate by leaving the vials uncapped at room temperature for 15 min. After drying, 55 µl of elution buffer EB was added to each tube and samples placed on a benchtop MixMate® mixer (Eppendorf, UK) at 1150 rpm for 10 min in order to resuspend the DNA into solution. Eventually, the samples were centrifuged for 5 min at 16000 g, placed on the magnetic stand for 5 min to allow all beads to attach to the vials wall, and the supernatant containing samples' DNA was retrieved into fresh vials. Final concentration of DNA into each sample should be 5.0 to 6.0 µg/µl, which was confirmed by nanodrop (before nanodrop samples were diluted 100 times in water: 2 µl of each sample plus 198 µl of water).

2.5.5 Fragmentation

45 µl of purified amplified DNA was further fragmented by adding 5 µl of 10X fragmentation buffer and 5 µl of diluted fragmentation reagent (Table 7). The fragmentation reaction was performed in PCR machine using following program: 37ºC for 35 min, 95ºC for 15 min and 4ºC forever. Expected average size of fragmented DNA should be below 180 bp which was confirmed by running 4 µl of fragmented PCR product on 2% agarose gel at 120 V for 30 min.

TABLE 7 FRAGMENTATION REAGENT PREPARATION.

Reagents	Volume (µl)
10x Fragmentation Buffer*	12
Fragmentation Reagent (3 U/µl)*	1
H_2O	106
Total	120

*: part of Genome-Wide Human SNP Nsp/Sty Assay Kit 5.0/6.0.

2.5.6 Labelling

DNA fragments end-labelling with biotin, necessary for subsequent hybridisation to array chip was performed with terminal deoxynucleotidyl transferase (TdT) (Table 8**)**. 19.5 µl of labelling mix was added to each sample of fragmented DNA and labelling was performed on PCR machine for 4 hours at 37ºC. After labelling TdT was inactivated by heating the samples at 95ºC for 15 min.

TABLE 8 LABELLING MIX PREPARATION.

Reagents	Volume (µl)
5X TdT Buffer*	14
TdT (30 U/µl)*	3.5
Genechip® DNA Labelling Reagent (30 mM)*	2
Total	19.5

*: part of Genome-Wide Human SNP Nsp/Sty Assay Kit 5.0/6.0.

2.5.7 Hybridisation

Hybridisation mixture was prepared as shown in Table 9. The samples were then submitted to the array platform controller, Ms Tracy Chaplin, for final processing. For each sample hybridisation mix was denatured at 100ºC for 10 min and immediately placed on ice for another 10 min. Next, the samples were brought to 49ºC (1 min incubation) and 200 µl of each hybridisation mix was injected onto separate SNP array chip and incubated at 49ºC for 16 to 18 h in a rotating GeneChip® hybridisation oven 640 (Affymetrix, Santa Clara, CA, US) at 60 rpm.

TABLE 9 HYBRIDISATION MIXTURE PREPARATION.

Reagents	Volume (µl)
MES (12X; 1.22 M)*	12
DMSO (100%)	13
Denhardt's Solution (50X)	13
EDTA (0.5 M)	3
Herring sperm DNA (HSDNA) (10 mg/ml)	3
Human Cot-1 DNA® (1 mg/ml)	3
Tween-20 (3%)	1
Tetramethylammonium chloride (TMACL) (5 M)	140
OCR,100**	2
Labelled DNA	70
Total	260

*: 1000 ml of 12xMES Buffer: 70.4 g of MES hydrate, 193.3 g of MES sodium salt, 800 ml of DEPEC treated water. pH 6.5 - 6.7.
**: part of Genome-Wide Human SNP Nsp/Sty Assay Kit 5.0/6.0.

2.5.8 Washing and Staining

After hybridisation, unhybridised mixtures were removed from the chips, and the chips were washed and stained with the mixture of streptavidin, a biotin-binding protein covalently attached to a fluorescent label - R-phycoerythrin, and biotinylated antibody according to the Fluidics Protocol (Table 10). All steps were performed on GeneChip® Fluidics Station 450.

TABLE 10 WASHING AND STAINING PROCESS.

Step	Procedure
Post Hyb Wash	6 cycles of 5 mixes/cycle with Wash Buffer A[a] at 25ºC
Post Hyb Wash	6 cycles of 5 mixes/cycle with Wash Buffer B[b] at 45ºC
Stain	Stain the probe array for 10 minutes in Streptavidin Phycoerythrin (SAPE) at 25ºC
Post Stain Wash	6 cycles of 5 mixes/cycle with Wash Buffer A at 25ºC
2nd Stain	Stain the probe array for 10 minutes in antibody solution [c,d] at 25ºC
3rd Stain	Stain the probe array for 10 minutes in SAPE solutione at 25ºC
Final Wash	10 cycles of 6 mixes/cycle with Wash Buffer A at 30ºC. The holding temperature is 25ºC
Filling Array	Fill the array with Array Holding Buffer

a: Wash Buffer A: 300 ml of 20x saline-sodium-phosphate-EDTA (SSPE), 1 ml of 10% Tween 20, 699 ml of water, filtered with 0.2 µM filter.
b: Wash Buffer B: 30 ml of 20x SSPE, 1 ml of 10%Tween 20, 969 ml of water, filtered with 0.2 µM filter.
c: Stain Buffer: 666.7 µl of water, 300 µl of 20x SSPE, 3.3 µl of 3% Tween 20, 20 µl of 50x Denhardt's blocking solution (1% Ficoll (type 400), 1% polyvinylpyrrolidone, and 1% bovine serum albumin).
d: Antibody stain solution: 5 ml of 0.5 mg/ml biotinylated antibody and 495 µl of Stain Buffer.
e: SAPE solution: 5 µl of 1 mg/ml SAPE and 495 µl of Stain Buffer.
f: Array Holding Buffer: 8.3 ml of 12x MES Stock Buffer, 18.5 ml of 5M NaCl, 0.1 ml of 10% Tween 20 and 73.1 ml of water.

2.5.9 Scanning

After post-hybridisation washes, the array chip was scanned by Affymetirx Scanner 7G and signal intensity data were processed (including QC) using the Affymetrix Genechip Operating Software 1.4 (Affymetrix, Santa Clara, CA, US).

2.5.10 SNP array data analysis

Signal intensity data from SNP arrays were analysed using in-house Genome-Oriented Laboratory File, GOLF (V4.1) software [24, 217]. The NCBI annotation of the human reference genome (NCBI build 36.2) was applied to define the genomic regions. Chromosomal copy number alterations were determined based on the log2 ratio of signal intensity from the PCa metastatic sample versus the average pooled signal intensity of seven unrelated control prostate samples. The control samples were available from previous analysis of primary PCa collected from prostatectomy specimens and contained DNA from normal prostate tissue adjacent to the tumour [218, 219]. Chromosomal gain and loss events were considered if the signal intensity ratio of the mean of 20 contiguous probes was significantly outside of 0±0.4 log2 ratio. Regions with copy number alterations were visually inspected and manually selected from the original SNP intensity plots generated by GOLF software.

2.6 Fluorescent *in situ* hybridisation (FISH)

2.6.1 FISH probe preparation

2.6.1.1 Bacterial artificial chromosome (BAC) DNA preparation

The BAC clones used for FISH probes preparation were obtained from the Institute of Cancer Research (Sutton, UK). Used clones and location of genes of interest are listed in Table 11. BAC clones were streaked for single colonies on standard Luria-Bertani (LB) agar (most widely used medium for the growth of bacteria) with 20 µg/ml of chloromphenicol (Sigma, UK) and grown at 37°C for 16 h. Single colony for each BAC was restreaked into 5 ml of broth liquid (LB) media supplemented with 12.5 µg/ml chloromphenicol and cultured at 37°C on the shaker at 225-300 rpm for 16 h. Alkaline lysis was performed for BAC plasmid extraction, using P1, P2, P3 solutions and modified protocol from Qiagen maxiprep kit. Briefly, 1ml of bacterial culture was pelleted at 13000 rpm for 5 min and resuspended in P1 solution (Tris/ EDTA buffer with RNase A). DNA was lysed with sodium hydroxide and cell debris precipitated using sodium dodecyl sulfate (SDS, anionic detergent) (150 µl of P2 solution). The cell lysate was neutralised with potassium acetate (150 µl of P3 solution) and the solution gently mixed. BAC DNA now in solution was separated from cell debris by centrifugation at 13000 rpm for 20 min. BAC DNA was precipitated from supernatant with 1 volume of ice cold isopropanol and subsequent incubation at -20°C for 30 min. BAC DNA was then pelleted by centrifugation at 13000 rpm for 15 min, washed with 80% ethanol and centrifuged again at 13000 rpm

for 5 min. The BAC DNA-containing pellet was left to air-dry, resuspended in 10 mM Tris-Cl, pH 7.5/1 mM EDTA (TE) buffer and stored at -20°C for further processing.

2.6.1.2 BAC DNA amplification, cleaning and labelling

Illustra GenomiPhi V2 DNA Amplification Kit (GE Healthcare, UK) containing Phi29 DNA polymerase and random primers was used for BAC DNA amplification according to manufacturer instructions. The bacteriophage Phi29 DNA polymerase exponentially amplify linear DNA templates via a strand displacement reaction and therefore thermal cycling is not required. DNA amplification starts after multiple random primers (hexamers) anneal to the template. When DNA synthesis proceeds to the next starting site, the Phi29 DNA polymerase displaces the newly produced DNA strand and continues its strand elongation. The displaced strands become then additional DNA templates for more primers to anneal.

Before amplification, BAC DNA was heated at 55ºC for 5 min to assure that it was well resuspended. 1µl of 300 ng/µl BAC DNA template was then mixed with 9 µl of sample buffer containing random hexamer primers, denatured at 95ºC for 3 min and cooled on ice for 5 min. Next, 9 µl of reaction buffer (with dNTPs) and 1 µl of polymerase were added to the sample, mixed and incubated at 30ºC for 1.5 h. After amplification, the Phi29 DNA polymerase was heat-inactivated at 65ºC for 10 min. The amplification is expected to generate DNA smear with average product size of 10 kb, which was confirmed by agarose gel electrophoresis.

Amplified BAC DNA was subsequently purified using standard phenol/chloroform method. 20 µl of each sample was diluted in 80 µl of TE buffer to final volume of 100 µl. Next, one volume of 1:1 phenol/chloroform was added per sample, solution mixed for 30 s and briefly centrifuged at 13,000 rpm for 2 min. The aqueous upper layer containing the amplified BAC DNA was collected into another tube, mixed vigorously with 100 µl of chloroform for 30 s and centrifuged again at 13,000 rpm for 2 min. Top layer with BAC DNA was moved to the fresh tube and DNA precipitated with 2.5 volumes of isopropanol at -20°C for 30 min. DNA was then pelleted by centrifugation at 13,000 rpm at 4°C for 20 min, washed with fresh 80% ethanol, centrifuged at 13,000 rpm at 4°C for 10 min and after supernatant removal left to air-dry at room temperature. Finally dried DNA was resuspended in 15 µl of TE buffer. The concentration of the amplified BAC DNA was determined by Nanodrop 1000 spectrophotometer (NanoDrop Technologies, Wilmington, US) (expected ~70-150 ng/ml).

BAC DNA labelling was done with BioPrime® DNA Labeling System (Invitrogen, Life Technologies, UK) according to the manufacturer protocol. 300 ng of amplified BAC DNA was diluted with DEPC-treated water to a final volume of 24 µl, and mixed with 20 µl of random primers (octamers). The mixture was denatured at 95°C for 5 min. For biotin-14-dCTP probe labelling (red probe), 5 µl of 10 x dNTP kit biotinylated mixture was added to the DNA/primer mixture. For digoxigenin (DIG)-11-dUTP probe labelling (green probe), 1.75 µl of DIG-11-dUTP (Roche, UK) in combination with 5 µl of special 10x dNTP mixture containing 1mM dATP, dGTP, dCTP, and 0.65 mM dTTP was used. Next, 1 µl of Klenow fragment polymerase from the kit was added and the labelling reaction was performed at 37°C for 3 h. The labelling was stopped with 5 µl of stop buffer. All labelled probes were cleaned on Microspin G50 columns (GE Healthcare, UK). Purified DNA was quantified by Nanodrop (expected ~90-150 ng/µL). 30 µl of COT-1 human DNA (Roche, UK) and 1 µl of herring sperm DNA (Sigma, UK) were added to prevent unspecific probe hybridisation. Total DNA was then precipitated with 4M NaCl (1/10 of sample volume) and 2.5 volumes of 100% ethanol. Probe DNA was pelleted by centrifugation at 13,000 rpm at 4°C for 20 min, washed with 80% ethanol, centrifuged again at 13,000 rpm at 4°C for 10 min, and after supernatant removal and air-drying, resuspended in 20 µl of DEPC-treated water and stored at -20°C freezer until further use.

2.6.2 Cell and tissue pre-treatment

Cells from culture were trypsinised, centrifuged (1200 rpm, 5 min), washed with PBS and resuspended in 15 ml of fixative (3:1 methanol: acetic acid). After 15 min fixation at room temperature, cells were pelleted at 1200 rpm for 5 min and resuspended in 15 ml of fresh fixative. This procedure was repeated twice and the last time cells were resuspended in small volume (200 - 500 µl) of fixative, dropped on slides using plastic pipette and allowed to air-dry. The slides were then stored at -20°C until further use. Immediately before FISH, slides were pre-treated for 10 min with 70% acetic acid to remove remains of cytoplasm, washed in PBS (2 x 5 min), dehydrated with 70%, 90% and 100% ethanol (3 minutes each) and air-dried.

FFPE tissue from clinical samples was dewaxed with xylene (2 x 5 min), washed with ethanol (2 x 5 min) and rehydrated in water (2 x 3 min). Slides were then boiled in tissue pre-treatment solution for 15 min, followed by 5 min enzyme digestion to break cell membranes and expose nuclei for better FISH probe access (SPOT-Light Tissue Pre-

treatment kit, Invitrogen, Life Technologies, UK). Eventually, slides were washed in water (2 x 3 min) and air-dried.

2.6.3 Hybridisation and post-hybridisation washes

1 µl of the DIG labelled probe (chromosome 1 centromere) and 1 µl of combined 4 biotin labelled probes (0.25 µl each; either for *CCND1* or *FBXL4* locus) were mixed with 10 µl of hybridisation buffer (60%formamide, 12% dextran sulphate, 2.4x SSC (sodium chloride, sodium citrate) buffer, 14 mM EDTA pH 8.0 and salmon sperm, 400 µg/ml). The mixture was then applied on pre-treated slides, which were subsequently coverslipped. Coverslips were sealed with rubber cement. Slides were denatured at 95°C for 10 min, placed in the humid chamber and probe hybridisation allowed overnight at 37°C. Next day (after ~16h) coverslips were removed and slides underwent standard post-hybridisation washes at 42°C: twice in 50% formamide/2x SSC and twice in 2x SSC, 5 min each. After 3 min wash with 4x SSC/0.5% Tween-20 (SSCT) buffer, slides were blocked with 200 µl of 5% milk/SSCT solution (SSCTM) for 15 min at 37°C. Next, blocking solution was removed and slides were incubated with 200 µl of SSCTM with 1 µl of the streptavidin-Cy3 conjugate (Sigma, UK) at 37°C for 10 min. After incubation slides were washed 3 x 2 min with SSCT. Next, 200 µl of SSCTM with 1 µl of anti-DIG-FITC antibody (Roche, UK) was added to each slide and slides incubated again at 37°C for 10 min. Eventually, slides were washed with SSCT (2 min), PBS (2 x 5 min), dehydrated in 70% ethanol (20 s) and air-dried. Slides were then coverslipped with Vectashield antifade containing DAPI (4',6-Diamidino-2-Phenylindole, Dihydrochloride, nuclear stain), and stored at 4°C before evaluation under the microscope.

TABLE 11 BAC CLONES USED FOR FISH PROBES PREPARATION

Gene or region of interest	BAC clone	Labelled FISH probe colour
Chr6q16 deletion:	RP11-639P13	Red
	CTD-2073H5	Red
	RP11-258I9	Red
	CTD-2281M23	Red
Chr11q13 gain:	CTD-2009H2	Red
	RP11-681H17	Red
	RP11-278A17	Red
	RP11-599F23	Red
Chr1 centromere:		Green control probe for 6q16 and 11q13 regions
Chr6p12.3 control:	RP11-727H16	Green control probe for TAPG cohort

FISH slides were scanned and analysed using the Applied Imaging Ariol® System (Applied Imaging, San Jose, CA, USA). A minimum of 100 cells with clear hybridisation signals were counted per sample. FISH score for each locus in PCa samples was normalised to results from BPH cases serving as nonmalignant controls. Standard mean value of positive findings in ten control specimens (BPH) +3SD was used as a positive cut-off point [220, 221], which for both, *CCND1* and *FBXL4* loci was ≥30% of nuclei with copy number change.

2.7 RNA expression analysis

2.7.1 RNA extraction

RNA was extracted with TRIzol reagent (Invitrogen, Life Technologies, UK) according to manufacturer's instructions. Treated and untreated cells (≤ 1 x 10^6 cells) were washed with PBS before adding 1ml of TRIzol. For bone metastases less than 1 mg of tissue scrapes was mashed on ice and immediately mixed with 1 ml of TRIzol. Subsequently, chloroform (1/20 volume) was added and, after a quick shake, samples were left at room temperature for 3 min for RNA to separate from the cellular DNA and proteins. After centrifugation at 4°C at 13,000 rpm for 15 min, the upper aqueous layer containing RNA was moved to a fresh vial and RNA was then precipitated by adding 500 µl of isopropanol. After centrifugation at 4°C at 13,000 rpm for 10 min, supernatant was removed and the precipitated RNA was washed with fresh 80% ethanol, air-dried and

resuspended in 25 µl of DEPC-treated water. RNA quality and quantity was assessed using Nanodrop. All RNA samples were stored at -80°C for further analysis.

2.7.2 Complementary DNA (cDNA) synthesis

cDNA synthesis was performed using Moloney Murine Leukemia Virus Reverse Transcriptase, RNase H Minus, Point Mutant (M-MLV RT (H–)) supplied with reaction buffer (Promega, UK). Total of 1 µg of RNA (per sample) diluted in DEPC-treated water to a final volume of 11 µl was mixed with 1 µl of random hexamers (Applied Biosystem, Life Technologies, UK) and denatured at 72°C for 5 min. After 5 min incubation on ice, 6 µl of 5x M-MLV RT buffer and 10 µl of 2.5 mM dNTP (Roche, UK) were added and cDNA synthesis was performed at 42°C for 1 h, followed by enzyme inactivation by heating at 95°C for 5 min. Eventually, RNA was digested by adding 1 µl of RNase H (Invitrogen, Life Technologies, UK) and heating the mixture at 42°C for 20 min. Samples were stored at -20°C for future use.

2.7.3 Quantitative Polymerase Chain Reaction (qPCR)

qPCR reactions were prepared with Taqman Universal PCR Master Mix (Applied Biosystem, Life Technologies, UK), using TaqMan Gene Expression Assays (Applied Biosystem, Life Technologies, UK) or Copy Number Assays (CNAssays) listed in Table 12. TaqMan *GAPDH* Expression Assays (Applied Biosystem, Life Technologies, UK) was used as an endogenous control for expression assays and *RPPH1* (14q11.2, coding RNase P) Copy Number Reference Assay for CNAssays.

For cyclin D1b splice variant detection, POWER SYBR Green assay was chosen (Applied Biosystems, Life Technologies, UK) as there is no commercially available TaqMan expression assay. Primers used were described elsewhere [222]. Forward primer (GTGCCACAGATGTGAAGTTC) spans the junction of exon 3 and 4, and reverse primer (GGACATCACCCTCACTTAC) lays within beginning of intron 4. This primer combination avoids possibility of amplification of genomic DNA or full length cyclin D1a variant. Amplicon length is 175 bp. β-actin primers were used as endogenous control (forward: TCTTCCAGCCTTCCTTCCT, reverse: GCAGTGATCTCCTTCTGCAT, amplicon size: 175 bp).

To assure reaction specificity, melting curves were performed along the SYBR Green based qPCR to detect potential primer – dimers or unspecific amplification products, and 2% agarose gel was run for each plate after completion of qPCR. All samples were

prepared according to manufacturer recommendations. PCR mixture content is listed in Table 13.

TABLE 12 LIST OF USED TAQMAN ASSAYS.

Gene	TaqMan assay type	Assay ID/part number	Exon boundary
GAPDH	Gene Expression Assay	Hs02758991_g1/4331182	6-7
CCND1	Gene Expression Assay	Rn00432360_m1/4331182	4-5
FBXL4	Gene Expression Assay	Hs00273315_m1/4351370	5-6
CCND1	Copy Number Assay	Hs01425024_cn	1
FBXL4	Copy Number Assay	Hs02961727_cn	9
RPPH1	Copy Number Reference Assay	4403328	16

TABLE 13 QRT-PCR MASTER MIX.

Reagents	Volume (µl)
TaqMan Universal PCR Master Mix/ POWER SYBR Green Master Mix	10
DEPC-treated water	8
TaqMan Gene Expression Assays/ CNAssay/ cDNA specific primers	1
cDNA (or 15-25 ng of DNA for CNAssay)	1
Total volume	20

Samples in MicroAmp® fast optical 96-well reaction plates (Applied Biosystems) were loaded on an ABI 7500 Real-Time PCR System (Applied Biosystems, UK) with default settings. Cycling conditions are listed in Table 14. Samples were run in triplicates. RNA levels were calculated using relative quantification method. DNA copy number was calculated according to manufacturer instructions: samples were run with absolute quantification program and data were loaded into CopyCaller software (version 2.0) for copy number quantification (Applied Biosystems, UK).

TABLE 14 STANDARD QPCR PROGRAM.

Step	Temperature (˚C)	Time
Denaturation	95	10 min
40 cycles of subsequent:		
Denaturation	95	15 sec
annealing and extension	60	1 min

2.8 Protein analysis

2.8.1 Western blot (WB)

2.8.1.1 Protein extraction

Protein extraction was done on ice with freshly prepared lysis buffer (Table 15). 100-200 µl of lysis buffer was added to each well of 6-well plate and cells were mechanically homogenised with a cell scraper. Cell lysates were incubated on ice for 30 min with vortexing every 5-10 min. Eventually, cell lysates were spin at 1000 g for 2 min to remove cell debris. The supernatant was collected and stored at -80°C until further use.

TABLE 15 LYSIS BUFFER PREPARATION.

Reagent	Volume (µl)
50mM TRIS/150 mM NaCl pH 8.0	752
10% Triton X-100	100
protease inhibitor cocktail 7x	143
phosphatase inhibitor	5
Total volume	1000

2.8.1.2 Bradford assay

The Bradford assay relies on the binding of the dye Coomassie Blue G-250 to protein. Protein binding stabilises the anionic form of the dye, causing a visible colour change (reaction turns blue). The quantity of protein can be estimated by determining the amount of dye in the blue ionic form by measuring the absorbance of the solution at 565 nm. Measurements were done in 96-well plates and in duplicates for each sample. 10 µl of each protein solution was added to 190 µl of diluted to 1x Protein Assay Dye Reagent Concentrate (BioRad, UK). Protein concentration was quantified relative to the standard curve constructed from bovine serum albumin (BSA) standard solutions (125, 250, 500,

750, 1,000, 1,500 and 2,000 µg/ml, Fisher Scientific, UK). Briefly, 10 µl of BSA standard solutions or relevant protein lysates were added to 190 µl of diluted to 1x Protein Assay Dye Reagent Concentrate. Samples and standards were loaded on plate reader (Opsys MR Microplate Reader, DYNEX, VA, US) for standard curve preparation and sample quantification. Absorbance of sample was then compared to standard curve prepared with BSA protein standards and concentrations calculated with Revelation Quicklink software version 4.25.

2.8.1.3 Sodium Dodecyl Sulphate-PolyacrylAmide Gel Electrophoresis (SDS-PAGE) and PVDF membrane transfer

Protein samples (15-50 µg) were diluted in 1x NuPAGE® LDS Sample Buffer (BioRad, UK) containing Coomassie G250 and Phenol Red. Tertiary protein structure was disrupted by adding 1x reducing buffer (BioRad, UK). Samples were denatured at 97°C for 10 min.

Classic SDS-PAGE Laemmli system was used. The gel was divided into an upper 'stacking' gel of low percentage (large pore size) and low pH (6.8) used to pack proteins together after loading, and a resolving gel with a pH of 8.8 and much smaller pores. Gel recipes are listed in Table 16 and

Table 17. Addition of SDS allowed separation of the proteins by size only. Polymerisation of gels was increased by the catalysts: amonium persulphate and tetramethylethylenediamine (TEMED). After casting, gels were assembled into running module (BioRad, UK), which was filled with 1x Tris-Glycine-SDS PAGE Running Buffer (0.25 M Tris base, 1.92 M glylcine, 1% SDS, National Diagnostics, UK). Denatured protein samples (95°C for 5 min) and Spectra™ Multicolor Broad Range Protein Ladder (Fisher Scientific, UK) were then loaded on the gel. Gel electrophoresis was done at 100-120 V for 1.5 h.

After electrophoresis proteins were transferred on Polyvinylidene difluoride (PVDF) membrane (Immobilon-P Membrane, 0.45 µm, Millipore, UK). PVDF membrane was pre-treated by sequential 1 min washes in 100% methanol, water and the transfer buffer (10% Tris-Glycine Buffer (0.25 M Tris base and 1.92 M glycine, National Diagnostics, UK), 20% methanol, 70% distilled water). Protein transfer to the PVDF membrane was done by wet transfer method. Transfer cassette with the gel and the PVDF membrane covered by blotting paper and sponges was submerged in the tank with transfer buffer and ice container (for cooling), and an electrical field was applied. Protein transfer was done at 200 mA for 120 min. After transfer membrane was washed briefly in water.

TABLE 16 10% RESOLVING GEL PREPARATION.

Reagent	Volume
ProtoFLOWGel 37:5:1 (Flowgen Bioscience, UK)	6.6 ml
4x ProtoFLOWGel Resolving Buffer (Flowgen Bioscience, UK)	5 ml
H_2O	8.2 ml
TEMED (Sigma, UK)	20 µl
Amonium persulphate 10% (Sigma, UK)	200 µl

TABLE 17 STACKING GEL PREPARATION.

Reagent	Volume
ProtoFLOWGel 37:5:1 (Flowgen Bioscience, UK)	1.3 ml
ProtoFLOWGel Stacking Buffer (Flowgen Bioscience, UK)	2 ml
H_2O	6.1 ml
TEMED (Sigma, UK)	10 µl
Amonium persulphate 10% (Sigma, UK)	50 µl

2.8.1.4 Antibody incubation and protein detection

To prevent non-specific background binding of the primary and/or secondary antibodies, membrane was blocked with 5% BSA (powder milk for FBXL4) solution in Tris Buffer Saline/0.1% Tween-20 (TBST) for 30 min. After blocking, membrane was incubated with primary antibody diluted in 5% BSA (powder milk for FBXL4) /TBS buffer overnight at 4°C under agitation. All antibodies used are listed in Table 18. Next day, membrane was washed 3 x 7 min in TBST and incubated in secondary peroxidase conjugated antibody diluted in 5% milk/TBST buffer for 1 h at room temperature on rocking platform. After incubation membrane was washed 3 x 7 min again with TBST buffer.

Protein detection was done with Immobilon Western Chemiluminescent HRP Substrate (Millipore, UK) or with SuperSignal™ West Femto Maximum Sensitivity Substrate (Thermo Fisher, UK), which is an ultra-sensitive enhanced chemiluminescent substrate for low-level protein detection, containing luminol and horseradish peroxidise (HRP) solutions. After TBST wash, 1 ml of chemiluminescent HRP substrate was added on the membrane, which was then incubated for 1 min at room temperature. Stained protein

bands were subsequently captured on X-ray film (Fuji Photo Film, Fisher Scientific, UK). Exposure time was different for each antibody and varied from 1 s to 30 min. β-actin protein bands were used as protein load control. Membrane was eventually washed thoroughly in several changes of TBST, dried and stored at 4°C for future use.

TABLE 18 PRIMARY AND SECONDARY ANTIBODIES USED FOR WESTERN BLOT.

Antibody	Cat. No./ Manufacturer	Dilution
FBXL4, mouse polyclonal Ab	ab172441, Abcam, UK	1:1000
FBXL4, rabbit polyclonal Ab	ab153812, Abcam, UK	1:1000
FBXL4, rabbit polyclonal Ab	ab181704, Abcam, UK	1:1000
FBXL4, mouse monoclonal Ab	sc-376102, Santa Cruz, US	1:1000
FBXL4, mouse monoclonal Ab	sc-81270, Santa Cruz, US	1:500
Flag, rabbit polyclonal Ab	F7425, Sigma-Aldrich, UK	1:500
Flag, mouse monoclonal Ab, Clone M2	F1804, Sigma-Aldrich, UK	1:200
N-cadherin, mouse monoclonal Ab	ab98952, Abcam, UK	1:1000
E-cadherin, mouse monoclonal Ab	M106, Takara, France	1:1000
Vimentin, rabbit monoclonal Ab	AC-0024, Epitomics, UK	1:1000
FAK, mouse monoclonal Ab	05-537, Millipore, UK	1:1000
Phospho-FAK (Y397), rabbit monoclonal Ab	ab81298, Abcam, UK	1:250
Anti-β-Actin, mouse monoclonal Ab, clone AC-15	A5441 Sigma Aldrich, UK	1:2000
Goat Anti-Mouse IgG (H+L), Peroxidase Conjugated	32430 Fisher Scientific, UK	1:2000
Goat Anti-Rabbit IgG (H+L), Peroxidase Conjugated	32460 Fisher Scientific, UK	1:2000

2.8.2 Immunochistochemistry (IHC)

2.8.2.1 Cell lines

Stable HEK293 cells overexpressing FBXL4 with related controls (wild type (wt) HEK293 and HEK293 transfected with empty vector (EV)) and 22RV1 single clones with FBXL4 knockdown by shRNA (shFBXL4) with adequate controls (wt 22RV1 and 22RV1 transfected with non-targeting shRNA (NT)) were stained for FBXL4 and ERLEC1. All antibodies used for IHC including dilutions are listed in Table 19.

TABLE 19 PRIMARY ANTIBODIES USED FOR IHC/IF.

Antibody	Cat. No./ Manufacturer	Dilution
FBXL4, mouse polyclonal Ab	ab172441, Abcam, UK	1:100
FBXL4, rabbit polyclonal Ab	ab153812, Abcam, UK	1:500
FBXL4, rabbit polyclonal Ab	ab181704, Abcam, UK	1:1000
FBXL4, mouse monoclonal Ab	sc-376102, Santa Cruz, US	1:1000
FBXL4, mouse monoclonal Ab	sc-81270, Santa Cruz, US	1:50
Flag, mouse monoclonal Ab, Clone M2	F1804, Sigma-Aldrich, UK	1:100
Cyclin D1 (SP4), rabbit monoclonal Ab	VPRM03, Vector Laboratories, UK	1:50
ERLEC1, rabbit polyclonal Ab	ab102046, Abcam, UK	1:200

Four different FBXL4 antibodies were tested for immunohistochemistry using stable HEK293 cells overexpressing FBXL4 as a positive control. ERLEC1 antibody was previously confirmed to be specific using WB. Cells were seeded in full DMEM medium onto glass slides and allowed to attach and grow for 2 days. During that time, HEK293 cells were treated with tetracycline to induce FBXL4 expression. Next, medium was removed, cells rinsed with PBS and fixed with 10% formalin in PBS for 20 min. After fixation slides were rinsed in PBS 2x5 min and permeabilised with 0.2% Tween 20 in PBS for 10 min. Next, slides were washed in PBS 2x5 min and incubated with primary

antibody for 1 h at the dilutions specified in Table 19. Primary antibodies were diluted in PBS with 1% BSA. After incubation primary antibody solution was washed off with PBST buffer (2x3 min) and secondary biotinylated universal antibody (Vectastain Universal Elite ABC Kit, Vector Lab, UK) diluted in PBS was applied for 30 min. After rinse with PBST (2x3 min), slides were incubated with avidin-peroxidise complex (Vectastain Universal Elite ABC Kit, Vector Lab, UK) for 20 min. Slides were rinsed again with PBST (2x3 min). Colour development was done by applying 3,3′-Diaminobenzidine (DAB) solution (BioGenex, UK) for 10 min. Slides were then conterstained with haematoxylin for 3 min, differentiated in 70% acid ethanol for few seconds and washed under running tap water for 5 min. Eventually, slides were dehydrated through series of 70%, 90% and 2x100% ethanols (3 min each), cleared with two changes of xylene (5 min each) and mounted with xylene based mounting medium (DPX, Sigma, UK).

2.8.2.2 FFPE tissue sections

FFPE clinical samples were cut at 4 µm with microtome (Leica, UK). Tissue sections were then dewaxed in 2 changes of xylene (5 min each) and rehydrated through series of alcohols (100%, 90% and 70% ethanol, 5 min each). Endogenous peroxidise was blocked by incubation in 3% H_2O_2 solution in methanol for 10 min. For FBXL4 and ERLEC1 antibodies antigen retrieval was performed by pressure-cooking the slides in citric acid solution, pH 6.0 (Vectastain, UK) for 10 min and immediately cooled under running tap water. For cyclin D1 antibody only, antigen retrieval was performed by microwaving the slides in TRIS-based, high pH solution (Vectastain, UK) for 15 min, followed by 30 min cooling on bench. After antigen retrieval slides were rinsed in water and placed in TBST, pH 7.6 for 2 min. Next, slides were incubated at room temperature for 1 h with primary antibody diluted in PBS with 1% BSA. Normal tonsil tissue was used as a positive control for cyclin D1 (basal layer of squamous epithelium is cyclin D1 positive) and BPH section served as a positive control for FBXL4. Primary antibody solution was washed off with TBST buffer (2x3 min) and secondary biotinylated universal antibody (Vectastain Universal Elite ABC Kit, Vector Lab, UK) diluted in PBS was applied for 30 min. After rinse with TBST (2x3 min), slides were incubated with avidin-peroxidise complex (Vectastain Universal Elite ABC Kit, Vector Lab, UK) for 20 min. Slides were rinsed again with PBST (2x3 min). Colour development was done by applying 3,3′-Diaminobenzidine (DAB) solution (BioGenex, UK) for 10 min. Slides were then conterstained with haematoxylin for 3 min, differentiated in 70% acid ethanol for few seconds and washed under running tap water for 5 min. Eventually, slides were dehydrated through series of 70%, 90% and 2x100% ethanols (3 min each), cleared with

two changes of xylene (5 min each) and mounted with xylene based mounting medium (DPX, Sigma, UK). After drying, slides were examined under light microscope and scored for protein expression by pathologist, Dan Berney. Cyclin D1 nuclear expression was scored for staining intensity (score 1-weak, 2-medium, 3-strong) and percentage of stained nuclei (0-100%). FBXL4 cytoplasmic expression was scored for intensity only.

2.8.3 Immunofluorescence (IF)

For IF cells were grown on coverslips in 2 ml of medium/well in 6 well plate. Stable 22RV1 cells transfected with shRNA were grown on coverslips for 2 days; stable T-Rex-293 cells were treated for 48h with tetracycline and HEK293 cells transfected with ERLEC1 siRNA were allow to grow till 48 h post-transfection. If mitochondria staining was required, cells were incubated with 100 nM of MitoTracker Red CMXRos (M7515, Life Technologies, UK) for 30 min before proceeding to PBS rinse and cell fixation. Cells were washed with 2 ml PBS and fixed in 10% formalin for 20 min. After washing coverslips with PBST 2x5 min, cells were permeabilised with 0.2% Tween in PBS for 10 min, washed again in two changes of PBS, 5 min each and unspecific antibody binding blocked with 1% BSA in PBS. Blocking solution was then removed and coverslips were incubated at room temp for 1 h with 100 µl of primary antibody diluted in blocking solution: mouse anti-Flag (1:100), mouse anti-FBXL4 (1:50), mouse anti-FAK (1:100), or rabbit anti-ERLEC1 (1:20). For antibodies details please see Table 18 and Table 19. Negative control slide was incubated with primary antibodies diluent only. Primary antibodies were washed with PBS, 2x5 min and Donkey anti-Rabbit IgG Secondary Antibody, Alexa Fluor® 488 conjugate (Life Technologies, UK) or Goat anti-Mouse IgG Secondary Antibody, Alexa Fluor® 488 conjugate (Life Technologies, UK) were applied at dilution 1:100 in PBS for 30 min. For single IF staining, cells were then washed in PBS for 2x5 min, air-dried and covered with antifade containing DAPI (Invitrogen, UK). For double IF staining, cells were next incubated for 40 min with Alexa Fluor 595 Phalloidin (Life Technologies, UK) diluted 1:40 (methanol stock 200U/ml) for F-actin staining. Next cells were washed in PBS for 2x5 min, air-dried and covered with antifade containing DAPI (Invitrogen, UK).

Fluorescence signal (green for ERLEC1/ FBXL4, red for mitochondria/ F-actin and blue for nuclei) was checked using Axioplan microscope or confocal microscope LSM710. Signal intensity was compared to control cells. Slides were stored at 4^{o}C and protected from light.

2.9 *FBXL4* gene knockdown

2.9.1 Gene knockdown with small interfering RNA (siRNA)

Cells were seeded 24 h before transfection in 6 well plates at 40-50% confluence (Table 20). No antibiotic was added to the growth medium. All siRNAs used were resuspended to 20 µM stock solution according to manufacturer instructions and are listed in Table 21.

TABLE 20 CELL SEEDING DENSITIES FOR SIRNA KNOCKDOWN.

Cell line	Medium	6 well plate
HEK293	DMEM	$7x10^4$ /well
22RV1	DMEM	$12x10^4$ /well
DU145	DMEM	$10x10^4$ /well
PC3	DMEM	$7x10^4$ /well

TABLE 21 LIST OF SIRNAS USED FOR KNOCKDOWN EXPERIMENTS.

siRNA	Manufacturer/cat.no.	Targeted gene
ON-TARGET*plus* SMARTpool	Dharmacon/ L-003210-00	*CCND1*
ON-TARGET*plus* SMARTpool	Dharmacon/L-013564-00	*FBXL4*
ON-TARGET*plus* SMARTpool	Dharmacon/ L-010658-00	*ERLEC1*
ON-TARGET*plus* Non-targeting Control Pool	Dharmacon/ D-001810-10	none

Cells were transfected with 100 nM of siRNA/well. For each well of the 6 well-plate, 5 µl of the siRNA (20 µM stock) was mixed with 180 µl of plain culture medium in 1 vial. In another separate vial 5 µl of oligofectamine (Invitrogen, Life Technologies, UK) was mixed with 20 µl of plain culture medium. Both tubes were incubated at room temperature for 5 min. The content of both tubes was then mixed together and incubated for another 20 min at room temperature. Next, 790 µl of plain medium was added to the mixture. Meantime, cells in the 6-well plate were washed with PBS and 1 ml of siRNA mixture was added to each well. Plates were then placed in the incubator for 4 h to allow siRNA enter the cells. After 4 h, 500 µl of culture medium with 30% of FCS was added to each well and plates were incubated under standard conditions for 24, 48 or 72 h. For each experiment time point, equal numbers of wells were prepared with siRNA targeting gene of interest, non-targeting siRNA and control cells not treated with siRNA.

For 96 well plate reagents volumes were adjusted accordingly. Cells were transfected with 10 nM of siRNA/well. For each well of the 96 well-plate, 0.5 µl of the suitable siRNA (20 µM) was mixed with 16 µl of plain culture medium in 1 vial. In another separate vial 0.5 µl of oligofectamine (Invitrogen, Life Technologies, UK) was mixed with 3 µl of plain culture medium. Both tubes were incubated at room temperature for 5 min. The content of both tubes was then mixed together and incubated for another 20 min at room temperature. Meantime, old medium was removed from the plates and 80 µl of fresh plain DMEM was added to each well. After incubation, 20 µl of siRNA mixture was added to each well and placed in the incubator for 4 h to allow siRNA enter the cells. After 4 h, 50 µl of culture medium with 30% of FCS was added to each well and plates were incubated under standard conditions for 24, 48 or 72 h. For each experiment time point, equal numbers of wells were prepared with siRNA targeting gene of interest, non-targeting siRNA and control cells not treated with siRNA.

2.9.2 Gene knockdown with short hairpin RNA (shRNA) constructs

Transduction-ready high-titer GIPZ lentiviral particles with TurboGFP (allowing the visual marking) were purchased from Thermo Fisher Scientific, UK (Figure 7). Three different GIPZ shRNA against FBXL4 were obtained at titres (number of viral particles or transducing units present per ml of solution): shFBXL4_1, 2.75 x 10^8 TU/ml; shFBXL4_2, 4.12 x 10^8 TU/ml and shFBXL4_3, 8.24 x 10^8 TU/ml. The GIPZ Non-silencing lentiviral shRNA vector (8.24 x 10^8 TU/ml) and GAPDH GIPZ lentiviral shRNA vector (1.67 x 10^9 TU/ml) were purchased to serve respectively as negative and positive controls. The pGIPZ lentiviral vector can be transfected using the replication incompetent lentivirus; it contains TurboGFP which together with shRNA is part of a bicistronic transcript allowing visual marking of shRNA expressing cells as well as contain puromycin resistance gene allowing stable cell line selection (Figure 7).

Generation of stable 22RV1 cells expressing the pGIPZ lentiviral vector was based on resistance to puromycin. Determination of the minimum amount of antibiotic required to kill non-transfected cells was based on antibiotic dose response (kill curve). 22RV1 cells were seeded in 1ml of full DMEM in 24 well plates at 7.5x10^4 cells/well (60% confluence). After 24 h, full DMEM medium was replaced with fresh medium containing different concentrations of puromycin. 10 mg/ml stock solution of puromycin (Sigma, UK) in water was used to prepare a range of 11 puromycin concentrations (0 (untreated control)-15 µg/ml) to treat 22RV1 cells. After 4 days of antibiotic treatment cell viability was assessed with The CellTiter 96 Aqueous Non-Radioactive Cell Proliferation Assay (Promega, UK)

according to manufacturer instructions. 1 µg/ml of puromycin was identified as the minimal concentration of antibiotic to kill all non-transfected 22RV1 cells.

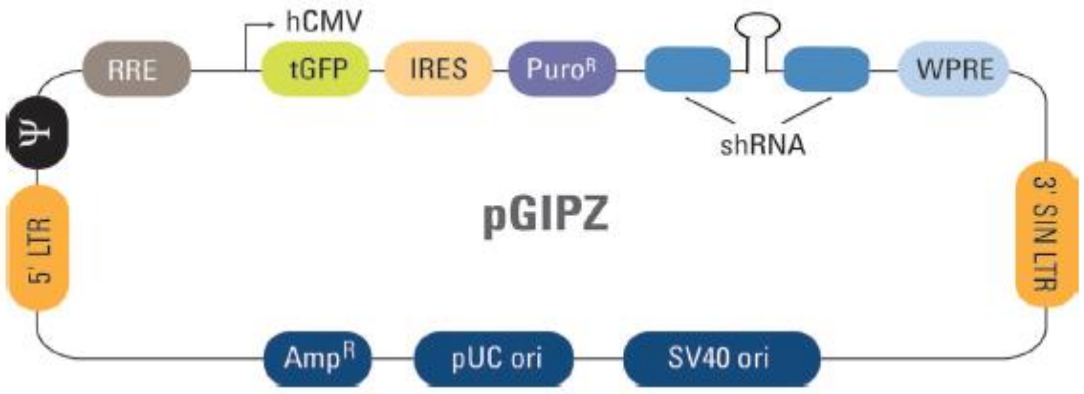

FIGURE 7. GIPZ LENTIVIRAL PARTICLES. hCMV, Human cytomegalovirus promoter drives strong transgene expression; tGFP, TurboGFP reporter for visual tracking of transduction and expression; PuroR, Puromycin resistance permits antibiotic-selective pressure and propagation of stable integrants; IRES, Internal ribosomal entry site allows expression of TurboGFP and puromycin resistance genes in a single transcript; shRNA, microRNA-adapted shRNA (based on miR-30) for gene knockdown; 5' LTR, 5' long terminal repeat; 3' SIN LTR, 3' self-inactivating long terminal repeat for increased lentivirus safety; Psi, packaging sequence allows viral genome packaging using lentiviral packaging systems; RRE, Rev response element enhances titer by increasing packaging efficiency of full-length viral genomes; WPRE, Woodchuck hepatitis posttranscriptional regulatory element enhances transgene expression in the target cells.

For viral transduction 22RV1 cells were plated at a density of $5x10^4$ cells/well (~40% confluence) in 1.5 ml of full DMEM in 24-well plates. Using these specific conditions titration of stock GAPDH GIPZ lentiviral shRNA vector (1.67×10^9 TU/ml) was performed to determine the optimum number of transducing units (TU)/ viral particles per every cell in the well (so called multiplicity of infection, MOI). To do that serial dilutions of the shRNA viral stock were made in a 96-well plate using serum free DMEM with 8 µg/ml of polybrene. Polybrene (hexadimethrine bromide, a cationic polymer) increases the efficiency of infection by neutralizing the charge repulsion between virions and cell surface. 10 µl of stock viral titer was added to 50 µl of DMEM with polybrene and mixed. 30 µl of this solution was transferred to first well of 96 well plate and mixed again with 30 µl of DMEM, making 1:2 dilution of previous concentration. Altogether, 14 serial dilutions 1:2 were prepared as listed in (Table 22); starting from 167 virus particles to 0.016/cell/30 µl volume in the final dilution.

TABLE 22. OPTIMISATION OF THE NUMBER OF TRANSDUCING UNITS (TU)/ VIRAL PARTICLES PER EVERY CELL IN THE WELL (MOI).

Well	Viral particles (µl)	Medium (µl)	MOI (viral particles/cell) in 30 µl
1	30 from stock titer	30	167
2	30 from well 1	30	83
3	30 from well 2	30	41
4	30 from well 3	30	20
5	30 from well 4	30	10
6	30 from well 5	30	5
7	30 from well 6	30	2.5
8	30 from well 7	30	1.25
9	30 from well 8	30	0.62
10	30 from well 9	30	0.31
11	30 from well 10	30	0.15
12	30 from well 11	30	0.075
13	30 from well 12	30	0.032
14	30 from well 13	30	0.0016

Once the virus dilutions were made, 22RV1 cells were washed with PBS and 220 µl of serum free DMEM with 8 µg/ml of polybrene was added to each well. Next, 30 µl of diluted virus was added (14 different dilutions, 1 dilution per well) and cell transduction performed for 6 h at 37^{o}C. After 6 h, 1 ml of full DMEM was added to each well and cells were incubated for another 72 h. Transduction efficiency was analysed by counting GFP positive colonies using immunofluorescent microscopy. After the optimal MOI was determined, 22RV1 cell transduction with 3 different stocks of pGIPZ lentiviral vector containing shRNA targeting FBXL4 was performed using exactly same conditions. The GIPZ Non-silencing lentiviral shRNA vector and GAPDH GIPZ lentiviral shRNA vector were used respectively as negative and positive controls. 72 h post transduction, old medium was replaced with 1.5 ml of full DMEM with 1 µg/ml of puromycin for positive selection of successfully transduced 22RV1 cells. Puromycin selection was continued for 2 weeks with culture medium changed every 3 days. After 2 weeks all cells were positive for GFP confirming presence of GIPZ lentiviral shRNA vector and FBXL4 knockdown was assessed at RNA level by qPCR. Cell population with best FBXL4 knockdown was chosen for subsequent single clone selection. Single clone selection was achieved by serial dilution of mixed cell population to 0-1 cell/well concentration in

96 well plates. All clones were maintained in selective medium. Wells were visually examined to assure presence of only a single colony/well before growth expansion.

2.10 *FBXL4* cloning

2.10.1 C-terminus Flag tag *FBXL4* construct preparation

Whole coding region of *FBXL4* was amplified from VCaP cDNA using PCRBIO HiFi polymerase (2 U/µl, PCR Biosystems, UK) (an error rate of approximately 1 error per 4.5 x 10^7 nucleotides incorporated) and PCRBIO 5x Reaction buffer containing 15mM MgCl2, 5mM dNTPs, enhancers and stabilizers. FBXL4 primers containing restriction sites for subsequent cloning and Flag tag sequence were ordered from Sigma (Sigma Aldrich, UK). Forward primer contained restriction site for AfI II enzyme upstream of ATG start codon (5'-AGTCTTAAGATCTAGATGGAGACTGGGGGC) and reverse primer had flag tag sequence included before stop codon and restriction site for Xho I enzyme past stop codon (5'-ACTCTCGAGTCACTTATCGTCGTCATCCTTGTAATCCTGAGTAAAGCTCTTTTTTATGAACA). The amplicon size was 1914 bp. PCR reaction mixtures and cycling conditions were prepared according to PCRBIO HiFi polymerase manufacturer instructions and listed in Table 23 and Table 24. PCR was performed using PTC-225 Thermal Cycler, MJ Research (Waltham, MA, US). Product size and PCR reaction specificity was confirmed by 1% agarose gel electrophoresis. 1 kb+ ladder (Invitrogen, Life Technologies, UK) was used as a size marker. The bulk of the sample was run on 1% low-melt agarose gel for subsequent purification with Minelute Gel extraction Kit (Qiagen, UK). Sequence of amplified FBXL4 was confirmed by Sanger sequencing. Primers for sequencing are listed in Table 25. PCR master mix and cycling conditions are listed in Table 26 and Table 27.

TABLE 23. PCR MASTER MIX.

Reagent	Volume (µl)
5x PCRBIO Reaction buffer	10
PCRBIO HiFi polymerase (2 U/ul)	0.5
Forward primer (10 µM)	3
Reverse primer (10 µM)	3
VCaP cDNA	1
water	33

TABLE 24. PCR CYCLING CONDITIONS.

Temp (^{0}C)	Time	Step	Cycling
95C	5’	initial denaturation	
95C	30’’	denaturation	Step 2-4: 35 cycles
63C	45’’	annealing	
72C	45’’	extension	
72C	10’	final extension	
4C	hold	end	

TABLE 25. PRIMERS FOR SANGER SEQUENCING OF FULL LENGTH C-FLAG *FBXL4.*

Primer pairs	Amplicon size (bp)	Annealing temp (^{o}C)
Fbxl4_1F: ATCTAGATGTCACCGGTCTTTC Fbxl4_1R: CTGAGTAAAGCTCTTTTTTATGAACA	1869	56
Fbxl4_1Fa: AGTCTTAAGATCTAGATGTCACCGGTCTTTC Fbxl4_1Ra: ACTCTCGAGTCACTTATCGTCGTCATCCTTG TAATCCTGAGTAAAGCTCTTTTTTATGAACA	1914	62
Fbxl4_1F: ATCTAGATGTCACCGGTCTTTC Fbxl4_2R: TGACCAAAGAATCTCCCATC	389	56
Fbxl4_3F: CAGAGCCAGGACTATGTGGA Fbxl4_3R: AATGCTGGCTCAGTAGTTTGC	577	58
Fbxl4_5F: TGGACAGTCTTAACAAAAAGTTTAGC Fbxl4_5R: TGCCTAAACTGAGGTGCTGA	603	58
Fbxl4_6F: CAGGCCTTAAATCTCTCCTCCT Fbxl4_1R: CTGAGTAAAGCTCTTTTTTATGAACA	654	56
FBXL4_Flag_F: AGCTCCCAAACTTGCAAAAA pcDNA4TO_Flag_R: GCGATGCAATTTCCTCATTT	458	58

TABLE 26. PCR MASTER MIX.

Reagent	Volume (µl)
10 x PCR buffer	2.5
dNTP (10mM)	0.5
Forward primer	0.5
Reverse primer	0.5
Taq polymerase	0.2
Water + cDNA	20.8
Total volume	25

TABLE 27. PCR CYCLING CONDITONS.

Step	Temperature (^{0}C)	Time	Cycling
1	95	5’	
2	95	45’’	
3	Primer set specific (56 to 62)	45’’	Step 2 – 4: 34 cycles
4	72	45’’	
5	72	10’	
6	4	hold	

2.10.2 DNA purification using Minelute Gel extraction Kit

FBXL4 band was identified under UV light in presence of gel red and excised with a scalpel. DNA was extracted from the gel with Minelute Gel extraction Kit (Qiagen, UK) according to manufacturer instructions. Three volumes of Buffer QG (solubilizes the agarose gel slice and provides the appropriate conditions for subsequent binding of DNA to the silica membrane of the MinElute column) was added to 1 volume of gel (300 µl of Buffer QG to 100 mg of gel) followed by incubation at 50°C for 10 min with periodical vortexing (until the gel slice has completely dissolved). Next, 100 µl of isopropanol (1 gel volume) was added to the sample and mixed by inverting the tube several times. DNA sample was then placed on a MinElute column and centrifuge for 1 min at 13000 rpm. The flow-through was discarded and bound DNA washed with 500 µl of Buffer QG by centrifugation for 1 min at 13000 rpm. The flow-through was discarded again and DNA washed with 750 µl of ethanol-containing Buffer PE by centrifugation for 1 min at 13000 rpm. The flow-through was discarded and the MinElute column was centrifuged again

for an additional 1 min at 13000 rpm to remove any traces of ethanol. DNA was eluted by adding 10 µl of Buffer EB (10 mM Tris·Cl, pH 8.5) on top of the column followed by centrifugation for 1 min at 13000 rpm. DNA concentration was measured with a nanodrop and stored at –20°C.

2.10.3 Cloning of *FBXL4* construct into TOPO® TA vector

Gel-purified C-Flag *FBXL4* DNA was subcloned into pCR™4-TOPO® TA Vector using TOPO® TA Cloning® Kit (Invitrogen, Life Technologies, UK). The pCR™4-TOPO® TA vector (Figure 8) is supplied linearized with 3´ thymidine (T) overhangs and covalently bound to topoisomerase I for efficient ligation of *Taq* polymerase amplified PCR products with 3´A overhangs. *Taq* polymerase has a nontemplate-dependent terminal transferase activity that adds a single deoxyadenosine (A) to the 3´ ends of PCR products. PCRBIO HiFi polymerase used to generate C-flag *FBXL4* sequence has the ability to proofread, using 3' → 5' exonuclease activity. Proofreading polymerases remove the 3´ A-overhangs necessary for TA Cloning, therefore 3´ adenines were added to the blunt-ended C-Flag *FBXL4* DNA through incubation with Taq polymerase in presence of PCR buffer and dATP (Table 28).

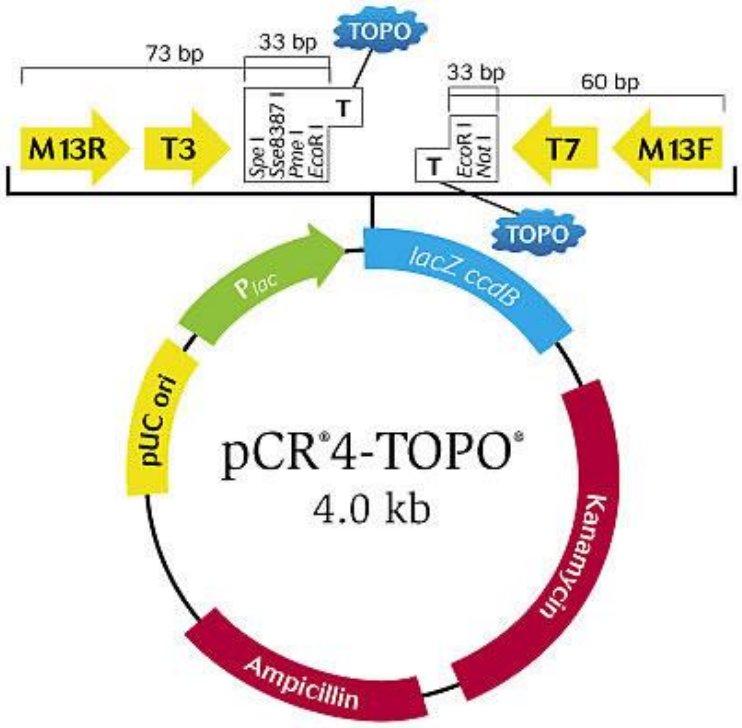

FIGURE 8. PCR™4-TOPO® TA VECTOR MAP.

TABLE 28. ADDING POLYA TAIL TO C-FLAG FBXL4 PCR PRODUCT.

Reagent	Volume (µl)	Incubation
C-Flag FBXL4 DNA (8 ng/µl)	8.7	
Taq polymerase	0.1	at 70ºC for 30 min
10mM dATP	0.2	
10X PCR buffer	1	

PCR product was directly used for TOPO cloning. Ligation was performed at room temp for 30 min according to manufacturer instructions. Reaction mixture is listed in Table 29. Ligation product was directly used for transformation of One Shot® TOP10 Chemically Competent *E. coli* cells.

TABLE 29. LIGATION MIXTURE USING TOPO® TA CLONING® KIT.

Reagent	Volume (µl)
Fresh ampli Taq PCR product (30 ng/µl)	4
Salt Solution	1
pCR4 TOPO TA vector (10 ng/µl)	1
Final volume	6

2.10.4 Transformation of Chemically Competent Cells

One Shot® TOP10 Chemically Competent *E. coli* cells supplied with S.O.C Medium (2% tryptone, 0.5% yeast extract, 10 mM NaCl, 2.5 mM KCl, 10 mM $MgCl_2$, 10 mM $MgSO_4$, and 20 mM glucose) were purchased from Invitrogen, UK. Agar plates with 100 µg/ml ampicillin (selective antibiotic for cells transformed with pCR™4-TOPO® TA Vector) were freshly prepared before transformation. One Shot® Chemically Competent Cells and ligation product were thawed on ice. 2 µl of ligation product was directly pipetted into 25 µl of competent cells, gently mix by tapping and incubated on ice for 30 min. Next, competent cells were heat-shocked at 42°C for exactly 30 seconds on the hot block and 125 µl of pre-warmed S.O.C medium was added, following 1 h incubation on shaker at 37°C and at 225 rpm. After incubation, 100 µl of cell mixture was spread on selective agar plate and incubated overnight at 37°C (16 h). Next day, several single colonies were transferred into separate tubes with 10 ml selective LB BROTH medium and incubated on a shaker at 37°C and at 225 rpm for 16 h. C-Flag *FBXL4* pCR™4-TOPO® TA vector

was purified with Wizard® *Plus* Minipreps DNA Purification System (Promega, UK). Insert size was confirmed by restriction digestion.

2.10.5 Plasmid purification with The Wizard® Plus Minipreps DNA Purification System

The Wizard® *Plus* Minipreps DNA Purification System was used for small scale plasmid purification for confirmation of correct cloning results. This system can be used to isolate any plasmid from *E.coli* hosts below 20 kb in size. Purification procedure was done following protocol supplied with the kit. About 2 ml of C-Flag *FBXL4* pCR™4-TOPO® TA vector containing bacterial growth was pelleted by centrifugation for 10 min at 10000 g. Cell pellet was resuspend in 250 µl of Cell Resuspension Solution (Tris-EDTA buffer with RNase A) and lysed for 5 min at room temp with 250 µl of Cell Lysis Solution (SDS + NaOH). Lysis was stopped by adding 350 µl of Neutralization Solution (containing potassium acetate). Cell debris were removed by pelleting at 14000 g in a microcentrifuge for 10 minutes. The cleared plasmid containing lysate was transferred to spin column and centrifuged at maximum speed for 1 min at room temperature. Column was then washed twice with Column Wash Solution following plasmid elution with 100 µl of Nuclease-Free Water. Plasmid quality and quantity was assessed using a nanodrop. C-Flag *FBXL4* insert size was confirmed by restriction digestion.

2.10.6 Restriction digestion of C-Flag *FBXL4* pCR™4-TOPO® TA vector and subcloning into pcDNA4/TO expression vector

All restriction enzymes and additional reagents were purchased from New England Biolabs, UK. Reaction mixture is listed in Table 30. Digestion was performed at 37^{o}C for 2 h. Enzymes were inactivated by heat (65^{o}C) for 20 min. C-Flag *FBXL4* DNA fragment size was confirmed by 1% agarose gel electrophoresis. DNA samples from clones with correct C-Flag *FBXL4* DNA fragment size were subjected to Sanger sequencing using primers described in Table 25. Clone for which intact sequence of C-Flag *FBXL4* DNA insert was confirmed by Sanger sequencing was used for subsequent cloning into pcDNA4/TO vector.

TABLE 30. RESTRICTION DIGESTION REACTION MIX.

Reagent	Volume (µl)
Afl ll	1
Xhol	1
10 x BSA	3
10 x buffer 4	3
C-Flag *FBXL4* pCR™4-TOPO® TA vector (100 ng/µl)	4
WATER	18
Total volume	30

2.10.7 Subcloning C-Flag *FBXL4* fragment into pcDNA4/TO expression vector

pcDNA4/TO expression vector was purchased from Invitrogen, UK as a part of a Tetracycline-Regulated Expression System for Mammalian Cells (T-REx™ System) containing pcDNA4/TO expression vector (Figure 9) and pcDNA6/TR regulatory vector (Figure 10). pcDNA4/TO inducible expression plasmid is designed for expression of gene of interest under the control of the strong human cytomegalovirus immediate-early (CMV) promoter and two tetracycline operator 2 (TetO2) sites. pcDNA6/TR regulatory plasmid encodes the Tet repressor (*Tet*R) under the control of the human CMV promoter. In the absence of tetracycline, the Tet repressor forms a homodimer which binds to each TetO2 sequence in the promoter of the inducible expression vector and represses transcription of gene of interest. Addition of tetracycline leads to its binding to Tet repressor homodimer, preventing it from binding to the Tet operator. The Tet repressor: tetracycline complex then dissociates from the Tet operator and allows induction of transcription from the gene of interest. Transfection of pcDNA4/TO vector without regulatory vector will lead to constitutive gene expression.

1 µg of C-Flag *FBXL4* pCR™4-TOPO® TA vector and pcDNA4/TO expression vector were digested with Afl II and Xho I restriction enzymes as described in Table 30 and the whole reactions run on a low-melt agarose gel. C-Flag *FBXL4* fragment and linear pcDNA4/TO vector were then extracted from the gel and purified as described in chapter 2.10.2.

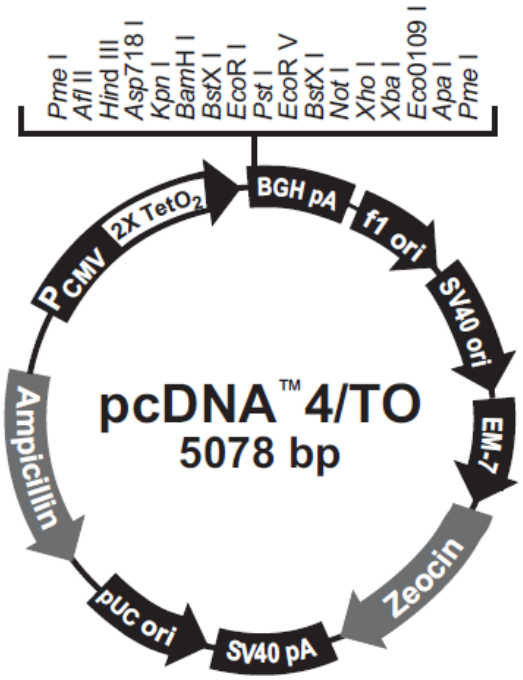

FIGURE 9. PCDNA4/TO VECTOR MAP. Part of Invitrogen T-REx™ System (A Tetracycline-Regulated Expression System for Mammalian Cells).

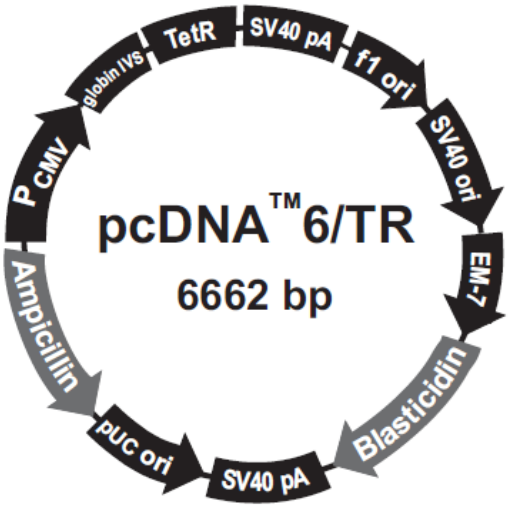

FIGURE 10. PCDNA6/TR VECTOR MAP. Part of Invitrogen T-REx™ System (A Tetracycline-Regulated Expression System for Mammalian Cells).

Next, the fragments were ligated using Rapid DNA Ligation Kit (Invitrogen, UK), according to manufacturer instructions. Ligation mix was prepared as described in Table 31.

TABLE 31. DNA LIGATION MIX.

Reagent	Volume (µl)
pcDNA4/TO linear vector (36 ng/µl)	1
C-Flag *FBXL4* DNA fragment (10 ng/µl)	9
T4 DNA Ligation Buffer (vial 1)	10
T4 DNA Ligase (vial 3)	1

Ligation reaction was allowed to proceed for 1 h at room temp. 1 µl of ligation mix was then used to transform TOP10 cells as described in chapter 2.11.5, using zeocin (50µg/ml) as a selective antibiotic. 12 bacterial single colonies were picked next day and expanded into 10 ml liquid BROTH. After 16 h incubation on shaker at 37ºC, C-Flag *FBXL4* pcDNA4/TO vector DNA was extracted from bacteria as described in chapter 2.11.6. Restriction digestion reaction with Afl ll and Xho l was performed for 2 h (Table 32) and digestion products were run on 1% agarose gel to confirm insert size. DNA samples from single clones with correct C-Flag *FBXL4* fragment size were send for sequencing using sequencing primers described in chapter 2.10.1.

TABLE 32. C-FLAG *FBXL4* PCDNA4/TO VECTOR RESTRICTION DIGESTION.

Reagent	Volume (µl)
Afl ll	1
Xhol	1
10 x BSA	3
10 x buffer 4	3
C-Flag *FBXL4* pcDNA4/TO vector DNA (100 ng/µ)	4ul (400 ng)
WATER	18
Total volume	30

2.10.8 Large scale pcDNA4/TO expression vector with C-terminus Flag tag *FBXL4* construct amplification

After restriction digestion and sequencing validation of correct C-Flag FBXL4 insert, 1 ml of the same bacterial culture in selective LB BROTH medium (chapter 2.10.4) was added to 100ml of selective LB BROTH medium and incubated on shaker at 37°C and at 225 rpm for 16 h for maxi scale plasmid purification. Next day cells were pelleted by centrifugation for 15 min at 6000 g at 4°C. Plasmid extraction and purification was done

using the EndoFree Plasmid Maxi Kit and supplied protocol (Qiagen, UK). Briefly, bacterial pellet was resuspended in 10 ml of Buffer P1 (50 mM Tris-Cl, pH 8.0, 10 mM EDTA, 100 µg/mL RNase A) and lysed with 10 ml of Buffer P2 (200 mM NaOH, 1% SDS) for 5 min at room temperature. Cell debris were precipitated with 10 ml of chilled Buffer P3 (3.0M potassium acetate, pH 5.5) and whole lysate was immediately poured into the QIAfilter Cartridge. After 10 min incubation at room temp cell lysate was filtered into a 50 ml tube. Next, 2.5 ml of Buffer ER was added to the filtered lysate, mixed and incubate on ice for 30 min. After incubation filtered lysate was loaded onto a QIAGEN-tip 500 and allowed to go through the resin by gravity flow. Resin – bound plasmid was washed twice with 30 ml Buffer QC and eluted with 15 ml Buffer QN. Plasmid DNA was then precipitated by adding 10.5 ml isopropanol and pelleted by centrifugation at 15000 g for 30 min at 4°C. Plasmid pellet was washed with 5 ml of endotoxin-free 70% ethanol, air – dried and resuspended in endotoxin-free Buffer TE to the concentration of 2 µg/µl. 300 ng of purified plasmid was again digested with Afl ll and Xho l restriction enzymes for insert size confirmation.

2.11 Transient FBXL4 overexpression

Cells were seeded 24 h before transfection in 6 or 96 well plates at densities listed in Table 33 in order to achieve 70-90% confluence. No antibiotic was added to the growth medium.

TABLE 33. CELL SEEDING DENSITIES FOR GENE OVEREXPRESSION.

Cell line	Medium	6 well plate	96 well plate
22RV1	RPMI	$40x10^4$ /well	$1x10^4$ /well
PC3	RPMI	$30x10^4$ /well	$0.5x10^4$ /well
DU145	DMEM	$40x10^4$ /well	$1x10^4$ /well
HEK293	DMEM	$40x10^4$ /well	$1x10^4$ /well

Cells were transfected with 2 µg/well of C-Flag *FBXL4* plasmid DNA. For each well of 6 well plate, 1 µl of 2 µ/µl plasmid DNA was mixed with 249 µl of plain culture medium in 1 vial. In another separate vial, 5 µl of lipofectamine (Invitrogen, Life Technologies, UK) was mixed with 245 µl of plain culture medium. Both tubes were incubated at room temp for 5 min. After 5 min content of both tubes was mixed together and incubated for another 20 min. Meantime, cells were washed with PBS and 1.5 ml of plain medium was added to each well. After 20 min incubation, 500 µl of transfection mixture was added to each

well of 6 well plate. Plates were placed in the incubator for 6 h to allow plasmid DNA to enter the cells. After 6 h, transfection medium was aspirated and replaced with culture medium with 10% FBS. For 96 well plates volumes were reduced to fit 200 µl/well volume, with 0.5 µg of plasmid DNA/well. For each experiment/time point, equal number of wells was prepared with plasmid DNA targeting gene of interest, empty plasmid and control, untreated cells. As a transfection rate control pmaxGFP Vector (Lonza, US) was used.

2.12 Production of stably transfected cells with C-Flag *FBXL4* plasmid DNA

2.12.1 Production of cells constitutively overexpressing *FBXL4*

PC3 and DU145 cells were transfected with C-Flag FBXL4 plasmid DNA as described in chapter 2.11. After 48 h cells were treated with selective antibiotic, zeocin at 300 µg/ml of full DMEM medium for 4 weeks. Zeocin is a copper-chelated glycopeptide antibiotic, which causes cell death by intercalating into DNA and cleaving it. pcDNA4/TO vector contains the *Sh ble* gene, which product inactivates zeocin by binding to the antibiotic. Therefore, cells retaining pcDNA4/TO vector are resistant to zeocin treatment. During that time medium was replaced every 3 days (to sustain steady levels of fresh antibiotic) and death of non-transfected cells and outgrow of transfected cells was observed. After two weeks of selection, *FBXL4* expression levels were checked by qPCR in 3 consecutive weeks to assess gene overexpression. Additionally, PCR of flag tag region was performed to confirm presence of C-Flag *FBXL4* plasmid DNA in those cells. Regular PCR master mix and cycling conditions were applied as described in Table 26 and Table 27, using forward primer within last exon of *FBXL4* and revere primer located within pcDNA4/TO vector (Table 34).

TABLE 34. PRIMERS FLANKING FLAG REGION OF C-FLAG *FBXL4* PCDNA4/TO VECTOR.

Primer pairs	Amplicon size (bp)	Annealing temp (°C)
FBXL4_Flag_F: AGCTCCCAAACTTGCAAAAA pcDNA4TO_Flag_R: GCGATGCAATTTCCTCATTT	458	58

2.12.2 Tetracycline - inducible system for FBXL4 overexpression

22RV1 cells (single clone) containing pcDNA6/TR regulatory vector were generated previously in our laboratory by Dr Marc Yeste-Velasco and maintained in full DMEM

medium with 5 µg/ml of blasticidin (selective antibiotic). Blasticidin is a peptidyl nucleoside antibiotic that inhibits protein synthesis by interfering with the peptide-bond formation in the ribosomal machinery. Resistance to blasticidin is conferred by the blasticidin resistance gene (bsr) present in the pcDNA6/TR regulatory vector, which codes for blasticidin-S deaminase.

Commercial T-REx™-293 cells were purchased as a part of T-REx™ System and maintained in full DMEM medium with 5 µg/ml of blasticidin. Both cell lines were transfected with C-Flag *FBXL4* expression vector and maintained in full DMEM medium with 5 µg/ml of blasticidin and 400 µg/ml of zeocin as described in chapter 2.12.1. After 2 weeks of selection, cells were seeded in 6 well plates at 60% confluence and 1 µg/ml of tetracycline was added to some wells to induce expression of *FBXL4* from expression vector. After 24 h of tetracycline treatment, RNA was extracted and *FBXL4* overexpression checked by qPCR. *FBXL4* expression levels were checked by qPCR in 3 consecutive weeks. Additionally, PCR of flag tag region was performed to confirm presence of C-Flag FBXL4 plasmid DNA in those cells. Regular PCR master mix and cycling conditions were applied as described in chapter 2.12.1.

For C-Flag FBXL4 T-REx™-293 cells single clones were generated through serial dilutions, including control clones with empty pcDNA4/TO vector. After additional 2 weeks of selection, *FBXL4* expression levels were checked by qPCR in all clones and clone with highest *FBXL4* expression was chosen for further experiments. To assess if continuous treatment with tetracycline leads to constant and stable *FBXL4* overexpression, C-Flag *FBXL4* T-REx™-293 cells were kept at 60% confluence and subjected to continuous tetracycline treatment for 60 days with periodical assessment of FBXL4 expression by qPCR and presence of C-Flag FBXL4 pcDNA4/TO expression vector by PCR of the flag tag region.

2.13 Cell viability assay

Cells were seeded into 96-well plates at 40-50% confluence (0.3-0.5 x 10^4 cells/well) and siRNA knockdown was performed as described in section 2.9.1. Viability was assessed 48 and 72 h post siRNA transfection with The CellTiter 96 Aqueous Non-Radioactive Cell Proliferation Assay (Promega, UK) according to manufacturer instructions. This colorimetric assay is composed of solutions of a tetrazolium compound [3-(4,5-dimethylthiazol-2-yl)-5-(3-carboxymethoxyphenyl)-2-(4-sulfophenyl)-2H-tetrazolium, inner salt (MTS) and an electron coupling reagent (phenazine methosulfate; PMS). MTS

is bioreduced by cells into a formazan product that is soluble in tissue culture medium. The absorbance of the formazan at 495 nm is then measured directly from the plate. The quantity of formazan product is directly proportional to the number of living cells in culture. Briefly, at each time point 200 µl of old culture media was replaced with 100 µl of fresh medium. MTS and PMS reagents were mixed together at ratio1:20 and 20 µl of this solution directly added to each well of cultured cells. Cells were the incubated at 37ºC for 2-6 h. Absorbance was measured using plate reader (Opsys MR Microplate Reader, DYNEX, VA, US). Wells containing only culture medium were used as a background control. Three biological repeats of experiment were performed. Statistical difference in cell viability between *FBXL4* knockdown cells and control cells transfected with non-targeting siRNA was assessed using paired t-test.

2.14 Cell migration assay

Cell migration was assessed by transwell migration assay. DU145, PC3 and 22RV1 cells were seeded in 6-well plates and transfected with anti *FBXL4* siRNA as described in chapter 2.9.1. Stable HEK293 were treated with tetracycline for 48-72 h before transwell assay. For transwell assay cells were trypsinised 48 h post transfection/tetracycline treatment and seeded into transwell inserts with 8 µm pore size (BD Biosciences, US) at $3x10^4$ cells/well for PC3 and DU145, $5x10^4$ for 22RV1 and $7x10^4$ for HEK293. Before cell seeding, 650 µl of DMEM medium with 10% FCS (acting as chemoatractant) was pipetted into wells and inserts placed on top of the wells. Meantime, cells were trypsinised from 6-well plate, centrifuged at 1200 rpm for 5 min and resuspended in 300 – 500 µl of medium with 1% serum. Next cells were counted and seeded into inserts at density mentioned above in 200 µl of medium with 1% serum to form confluent layer. Cells were allowed to migrate across the membrane for 24 h. After 24 h (72 h post transfection), inserts were washed with PBS and fixed in 10% formalin in PBS, rinsed in PBS 2 x 5 min and not migrated cells from the top of the insert membrane gently removed with cotton buds. Next, migrated cells attached to the bottom of the membrane were stained with hematoxylin for 20 min. After staining inserts were washed in tap water for 5 min and dehydrated in 70%, 90% and 100% ethanol for 5 min. Next, membranes with migrated cells were cut from the inserts with scalpel blade, rinsed in xylene and mounted on the glass slides in DPX mounting medium. After drying, slides were scanned using the Applied Imaging Ariol® System (Applied Imaging, San Jose, CA, USA). Equal size area on each membrane was marked for cell counting.

2.15 Cell invasion

2.15.1 Matrigel invasion

BD BioCoat™ BD Matrigel TM Invasion Chamber, 8.0 µm PET Membrane 24-well Cell Culture Inserts were purchased from (Corning, BD Biosciences, US). Invasion chambers were stored at -20^{o}C and brought to room temp before placing them in incubator at 37^{o}C for 30 min. Invasion assay was performed in the same manner like the transwell migration assay (see chapter 2.14).

2.15.2 Collagen invasion

2.15.2.1 Single cell collagen invasion assay through native collagen type-I matrice

Single-cell collagen invasion model was performed according to de Weaver *at al* (Figure 11) [223]. 3 mg/ml collagen I solution extracted from rat tail (the most common fibrillar collagen found in skin, bone, tendons, and other connective tissues) was purchased from Applied Biosystems, UK. All ingredients for 1 mg/ml collagen mixture preparation were kept on ice at all time. 1.2 ml of 1 mg/ml collagen solution prepared as described in Table 35 was added per well of 6 well plate and immediately plates were placed in tissue culture incubator at 37^{o}C where the collagen was allowed to solidify for 1 h. Meanwhile, PCa cells at 48 h post *FBXL4* knockdown along with controls were tripsinised, spun down at 1200 rpm for 5 min, resuspended in full DMEM and counted. 100,000 cells were resuspended in 1.5 ml of full DMEM and added per well in triplicates. Plates then were placed in the incubator and cells allowed to invade collagen for 24 h. After 24 h cells with cellular extensions (pseudopodia) invading the collagen matrix were counted in 10-15 microscope fields (at 200x magnification).

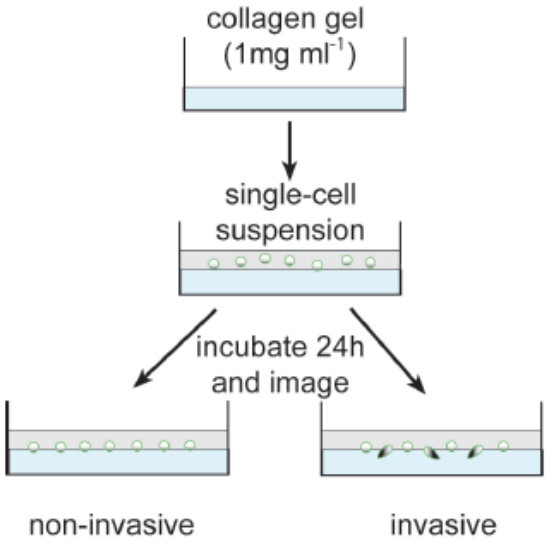

FIGURE 11. PROTOCOL FOR SINGLE CELL INVASION THROUGH COLLAGEN. Adapted from de Weaver *at al* [223].

TABLE 35. 1 MG/ML COLLAGEN PREPARATION.

Solutions	Volume (ml)
Collagen 3mg/ml	6
CMF-HBSS	5.8
10xDMEM	1.3
NaHCO3	1.3
DMEM full medium	3.4
NaOH 1M	0.2
Final volume	18

2.15.2.2 Single cell invasion assay through collagen type-I/Matrigel matrix

Single cell invasion assay through collagen type-I/Matrigel (1.6 mg/ml/~50%) matrix was adopted from Godinho et al [224]. BD Matrigel Matrix Growth Factor Reduced was purchased from Applied Biosystems, UK. 1.6 mg/ml collagen/~50% matrigel was prepared on ice according to Table 36.

TABLE 36. COLLAGEN-MATRIGEL MATRIX COMPOSITION.

Ingredient	Volume (µl)
collagen(3 mg/ml)	1599
10xDMEM	187.5
NaOH 1M	30
Matrigel GFR	1401
volume	3000.0

200 µl of collagen solution was added per well of 24 well plate and allowed to solidify in incubator for 1 h. Meanwhile, stable 22RV1 shFBXL4 PCa cells along with controls were tripsinised, spun down at 1200 rpm for 5 min, resuspended in 2% FCS DMEM and counted. 4000 cells were resuspended in 0.5 ml of 2% FCS DMEM with 2% Matrigel and added per well in triplicates. Plates then were placed in the incubator and cells allowed to invade collagen for 72 h. After 72 h cells with cellular extensions (pseudopodia) invading the collagen matrix were counted in 10-15 microscope fields (at 200x magnification).

CHAPTER 3

Genome-wide alterations in PCa bone metastases

3.1 Introduction

The most common metastatic site of PCa is bone: around 90% of patients dying from this disease have skeletal metastases [193, 194]. Once tumours metastasize to bone, they are incurable and result in significant disease morbidity. Better understanding of bone metastases is needed in order to develop more efficient approaches and novel therapies to manage aggressive metastatic disease. It is well established that PCa has a genetic background and with abundance of prostatectomy specimens, there have been many genomic studies concentrating on genetic changes in primary PCa [165, 225-227], while difficulty in obtaining specimen from metastatic sites hindered genetic analysis of PCa metastases [139].

Presence and extent of genomic changes in PCa bone metastases, the most common site of PCa spread is particularly understudied due to difficulty in obtaining good quality, high in tumour content samples. As PCa bone metastases are assessed by imaging methods, research samples usually come from autopsies [153, 167, 228, 229], unless as in recent studies, patients are specifically consented for bone biopsy [138, 230, 231]. As bone metastases result in significant disease morbidity with limited success of palliative treatment [232], better understanding of genomic changes in PCa bone metastases could lead to new bone-oriented treatment options, or identification of possible new predictive markers for metastatic cancer spread. Thanks to collaboration with The Robert Jones and Agnes Hunt Orthopaedic Hospital in Oswestry, Shropshire, we had a unique opportunity to look at genomic changes in PCa bone metastases from patients with advanced PCa who were treated there for pathological bone fractures caused by PCa.

3.2 Results

3.2.1 Sample and SNP 6.0 array data quality control

Direct assessment of tumour purity in six fresh frozen samples of bone metastases prior to SNP analysis was impossible due to difficulty in sectioning of hard bone tissue. Therefore, FFPE samples (all decalcified with formic acid) from the same patients were H&E stained to indirectly estimate tumour cell content in fresh frozen specimens. Samples 2, 4, 5 and 6 showed very high tumour content of >80%. Samples 1 and 3 had less abundant tumour content of about 50% (Figure 12).

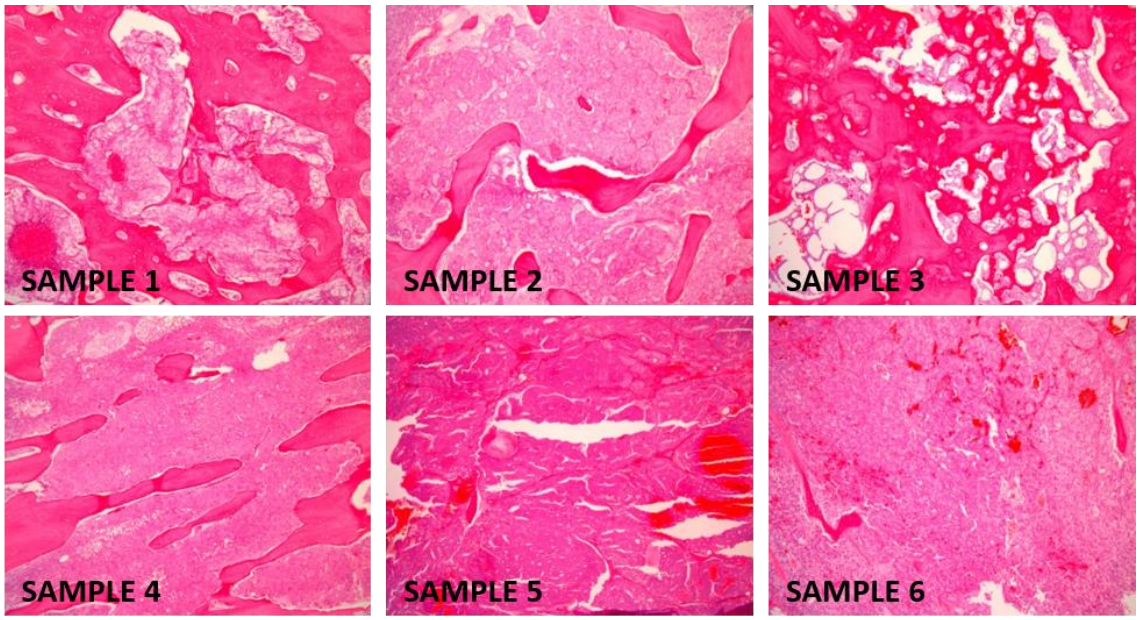

FIGURE 12. CANCER PURITY IN FFPE DECALCIFIED PCA BONE METASTASES SAMPLES DERIVED FROM THE SAME PATIENTS AS FRESH FROZEN SPECIMENS. Samples 2, 4, 5 and 6 show widespread tumour, while metastatic samples 1 and 3 are less tumour rich with more bone tissue present. Tumour content for each sample was assessed by a pathologist, Prof. Dan Berney.

PCa bone metastases DNA quality was assessed by running 0.5-1 µg of DNA (dependent on sample availability) on 1% agarose gel (Figure 13A). Good quality DNA shows single high molecular size band on the gel with minimal smear of fragmented DNA. DNA integrity was reasonably good for samples 4, 5 and 6. The other three samples showed more degradation represented as a smear on the gel, while still displaying strong high molecular size band of intact DNA.

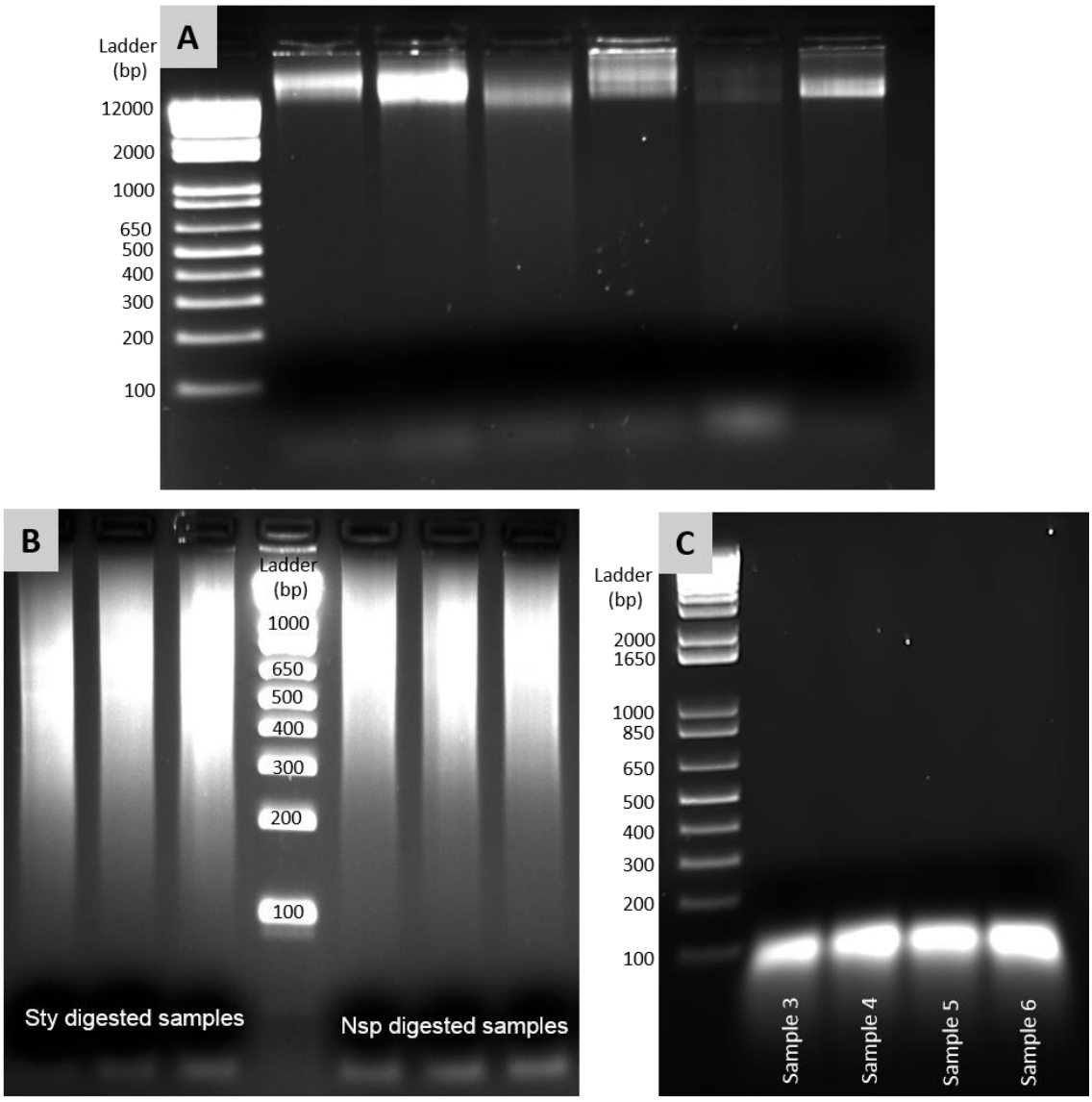

FIGURE 13. AGAROSE GEL ELECTROPHORESIS BASED QUALITY CONTROL STEPS DURING SAMPLES PREPARATION FOR SNP 6 ARRAYS. (A), Good initial genomic DNA quality of six PCa bone metastases was confimed by the presence of a high molecular weight band of DNA with minimal low quality smear of DNA fragments. (B), Samples quality control (examples) after initial DNA fragmentation and fragments amplification by PCR. Fragmentation with both, Sty and Nsp enzymes resulted in DNA smears of expected 250-1100 bp size. (C), Last quality check (examples) after final DNA fragmentation. All samples show correct DNA fragment size below < 180 bp.

All samples were processed for Affymetrix SNP 6.0 arrays according to manufacturer instructions (Affymetrix, Santa Clara, CA, US). Three quality checks were performed during samples preparation prior to hybridization on GeneChip arrays in order to exclude experimental errors. First check was to verify PCR product size by 2% agarose gel electrophoresis after initial genomic DNA restriction enzyme digestion, adaptor ligation and DNA fragments amplification by PCR. All samples were successfully amplified and

had correct DNA fragment size distribution within 250-1100 bp (example in Figure 13B). Next was the quantity check of the pooled and purified PCR products. PCR product concentration for all samples was verified by nanodrop and fell well within recommended range of 5.0 to 6.0 µg/µl. Third quality check was to confirm DNA fragments size by 2% agarose gel electrophoresis after final DNA fragmentation with DNase I. All samples were successfully fragmented with correct fragment size <180 bp (examples in Figure 13C). Once the adequate quality of all samples was confirmed, they were hybridised onto GeneChips and data collected from processed SNP arrays was assessed for quality with Affymetrix Genotyping Console software (Affymetrix, Santa Clara, CA, US). An estimate of the overall quality for each individual sample was performed by calculation of QC Call Rate (QCR) for a default set of 3022 SNPs. This quality control step is used to identify poor quality samples. Two samples exhibited QC Call Rate slightly below recommended 86% cut off (sample 5 - 85.1% and sample 6 - 85.8%) while another four had good initial QC Call Rate between 90% and 95% (Table 37), confirming adequate quality for subsequent genotyping analysis with the genotype calling algorithm Birdseed v2 software (Affymetrix, Santa Clara, CA, US). The Birdseed algorithm performs a multiple-chip analysis to estimate signal intensity for each allele of each SNP and makes genotype calls (A-signal vs. B-signal). The Birdseed algorithm accurately determined the genotype calls of each PCa bone metastasis sample with overall call rate of over 95% (Table 37).

TABLE 37 QUALITY CONTROL OF SNP ARRAY DATA GENERATED FOR THE PCA BONE METASTASES.

Sample	QC call rate (%)	Birdseed v2 Call Rate (%)
1	93.5	97.1
2	90.5	96.4
3	91.3	95.5
4	90.3	95.1
5	85.1	95.0
6	85.8	95.5

3.2.2 Genomic copy number changes detected in PCa bone metastases

Generated SNP array data were analysed for copy number changes with GOLF v4.1 software using combined set of 7 normal prostate samples as normal control, as

described in materials and methods. Genomic copy number changes detected in the six fresh frozen tissues of PCa bone metastases are visualised in Figure 14.

Surprisingly, many of detected genomic changes displayed very similar if not identical chromosomal breakpoints present in over half of the samples (Table 38) and included gains at 1p36.3, 1q32.1-32.2, 2q14.3, 3p26.1-24.3, 3p22.3, 3q29, 4p16, 5p15.33, 5q35.2-35.3, 6p21.1, 6q27, 7p22.3-22.1, 7q11.23, 7q21.3-22.1, 7q32.1-32.2, 7q36.3, 8q24.3, 9p13.3-13.1, 9q34.11-34.3, 11p15.5-15.4, 11p12-11.2, 11q12.3-14.1, 12p13.33-q13.32, 12q13.11-14.1, 12q23.3-24.21, 12q24.23-24.31, 12q24.33, 13q32.2-32.3, 13q34, 14q32.2-32.33, 15q14-21.1, 16p13.3, 16p12.1-11.2, 16q24.2-q24.3, 17q24.3-25.3, 21q22.2-22.3, 22q11.21-11.22, 22q12.1-12.3,and 22q12.3-13.33, and losses at 9q32-33.2, 10q25.1, 16q21, 17q21.33-q22, and 17q24.3.

Another group of copy number changes detected in PCa bone metastases were more heterogeneous in location and chromosomal breakpoints. However, there were overlapping common regions shared by two or more samples (Table 39). The most common regions of copy number change in this group were losses at 6q14.1-23.1 (six cases), 8p23.3-q11.21 (four cases) and 17p13.3-12 (three cases), and gains at 20q11.21-13.33 (three cases) and Xq11.1-28 (three cases), with minimal overlapping regions (MOR) at 6q16.1-16.2, 8p23.2-21.1, 17p13.1-12, 20q13.12-13.32 and Xq12-13.1, respectively. Most regions of shared copy number changes were present in two cases with MOR at 3q21.2-q29, 4p14-13, 8q11.21-23.1, 8q23.3-24.3, 14q24.2-24.3 and 20q13.12-13.32 for gains, and 2p13.1-11.1, 2q22.1-q23.3, 4q28.1, 5q14.3-22.1, 10q23.31, 11q22.2-24.2, 13q13.2-31.1, 18q21.2-21.31, 18q21.33-22.3 and 20p12.3-12.2 for losses. One sample had deletion at 21q22 between *TMPRSS2 and ERG* region.

Examples of copy number changes are shown in Figure 15 - 19. Different size losses at 6q14.1-23.1 found in all 6 cases with MOR at 6q16.1-16.2 are shown in Figure 15. Various size losses of most of the p arm of chromosome 8 with gains of 8q are displayed in Figure 16. Copy number gain at AR locus, Xq12 is depicted in Figure 17. Examples of recurrent copy number gains with very similar/identical breakpoints are depicted in Figure 18. Figure 19 shows identical chromosomal breakpoints at chromosome 16 in most of the samples.

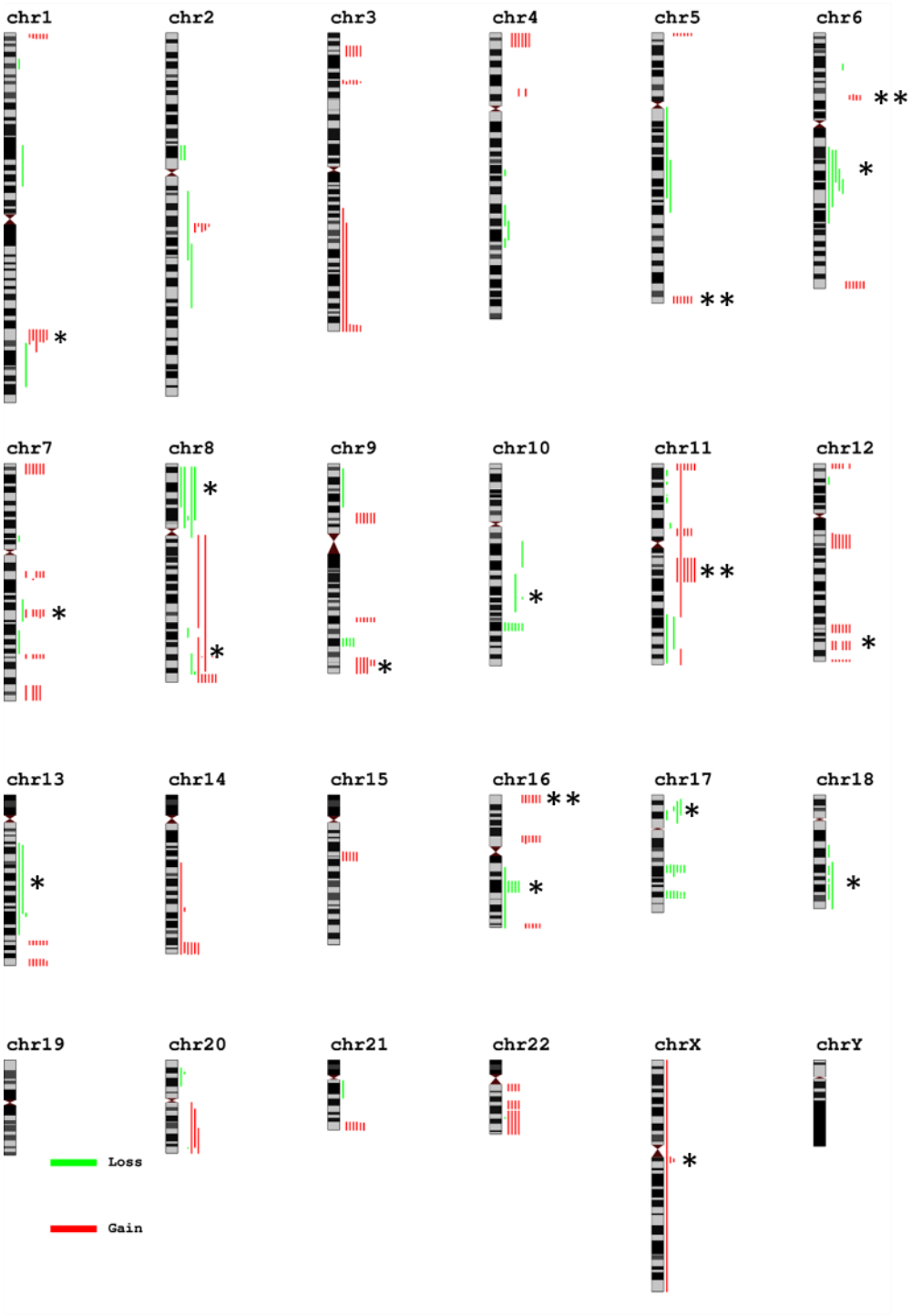

FIGURE 14. SUMMARY OF ALL REGIONS WITH COPY NUMBER CHANGES IN 6 PCA BONE METASTASES DETECTED BY SNP 6.0 ARRAY ANALYSIS. Each line on the right corresponds to an aberration in the associated chromosome regions. Red lines denote gains and green lines denote losses. Data is displayed with Genomic Recurrent Event ViEwer software (http://www.well.ox.ac.uk/GREVE/). * previously reported high frequent genomic alteration regions in mCRPC, including distant metastases [119, 121, 138, 150-153, 167, 228]. Double ** regions previously linked to liver and lymph node metastases [151].

TABLE 38 COMMON COPY NUMBER CHANGES WITH THE SAME GENOMIC BREAKPOINTS PRESENT IN MORE THAN HALF OF THE PCA BONE METASTASES.

Chromosome	Genomic region with copy number change (genes linked to PCa)	No of cases
Gains:		
1	1p36.3	6
	1q32.1-32.2	6
2	2q14.3	5
3	3p26.1-24.3	5
	3p22.3	6
	3q29	6
4	4p16	6
5	5p15.33	6
	5q35.2-35.3	6
6	6p21.1	4
	6q27	6
7	7p22.3-22.1	6
	7q11.23	6
	7q21.3-22.1 (*CDK6*)	5
	7q32.1-32.2	5
	7q36.3	4
8	8q24.3	4
9	9p13.3-13.1	6
	9q34.11-34.3	4
11	11p15.5-15.4	5
	11p12-11.2	5
	11q12.3-14.1 (*CCND1*)	5
12	12p13.33-13.32	5
	12q13.11-14.1 (*CDK2, CDK4*)	6
	12q23.3-24.21	6
	12q24.23-24.31	5
	12q24.33	6
13	13q32.2-32.3	6
	13q34	6
14	14q32.2-32.33	5

15	15q14-21.1	5
16	16p13.3	6
	16p12.1-11.2	6
	16q24.2-24.3	5
17	17q24.3-25.3	6
21	21q22.2-22.3	6
22	22q11.21-11.22	4
	22q12.1-12.3	4
	22q12.3-13.33	4
Losses:		
9	9q32-33.2	4
10	10q25.1	6
17	17q21.33-22	6
	17q24.3	6

TABLE 39. COPY NUMBER CHANGES WITH DIFFERENT GENOMIC BREAKPOINTS IN PCA BONE METASTASES.

Chromosome	Minimum overlapping Region (genes linked to PCa)	Altered genomic region
Gains:		
3	3q21.2-29 (*PIK3CA*)	3q13.31-29 (sample 5)
		3q21.2-29 (sample 2)
8	8q11.21-23.1 (*NCOA2*)	8q11.21-23.1 (sample 6)
		8q11.21-24.3 (sample 3)
	8q23.3-24.3 (*MYC, PSCA*)	8q11.21-24.3 (sample 3)
		8q23.3-24.3 (sample 6)
14	14q24.2-24.3	14q21.3-32.33 (sample 6)
		14q24.2-24.3 (sample 4)
20	20q13.12-13.32	20q11.22-13.32 (sample 6)
		20q13.12-13.33 (sample 4)
		20q11.21-13.33 (sample 5)
X	Xq12-13.1 (*AR*)	Xq11.1-13.1 (sample 6)
		Xq12-13.1 (sample 4)

		Xq11.1-28 (sample 5)
Losses:		
2	2q22.1-23.3	2q22.1-32.1 (sample 2)
		2q12.2-23.3 (sample 5)
4	4q28.1	4q26-28.1 (sample 6)
		4q28.1 (sample 5)
5	5q14.3-22.1 (*CHD1*)	5q11.2-22.1 (sample 5)
		5q14.3-23.1 (sample 3)
6	6q16.1-16.2 (*FBXL4*)	6q14.1-22.32 (sample 6)
		6q14.1-22.1 (sample 5)
		6q14.1-16.2 (sample 3)
		6q16.1-21 (sample 2)
		6q15-21 (sample 1 and 4)
8	8p23.2-21.1 (*NKX3.1*)	8p23.3-11.1 (sample 4)
		8p23.3-q11.21 (sample 2, 3, 5)
10	10q23.33 (*PTEN*)	10q23.33 (sample 4)
		10q22.1-24.1 (sample 2)
11	11q22.2-24.2	11q22.1-25 (sample 5)
		11q22.2-24.2 (sample 6)
13	13q13.2-31.1 (*RB*)	13q13.1-31.3 (sample 6)
		13q13.2-31.1 (sample 2)
17	17p13.1-12 (*TP53*)	17p13.3-p12 (sample 6)
		17p13.2-11.2 (sample 2)
		17p13.1-11.2 (sample 4)
18	18q21.2-21.31	18q21.1-23 (sample 6)
		18q21.2-21.31 (sample 4)
	18q21.33-22.3	18q21.1-23 (sample 6)
		18q21.33-22.3 (sample 4)
20	20p12.3-12.2	20p12.3-12.2 (sample 2)
		20p12.3-12.1 (sample 4)

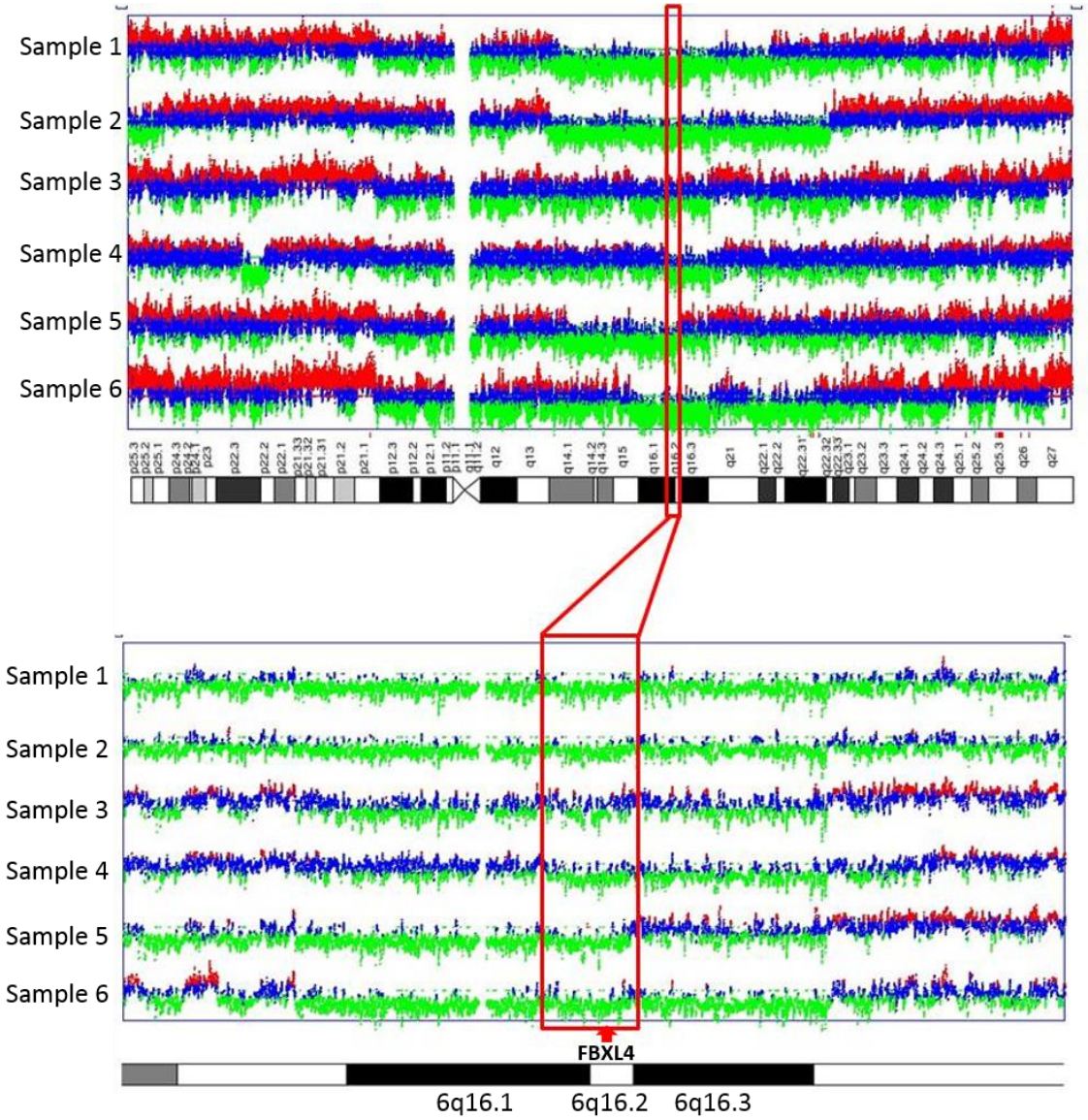

FIGURE 15. COPY NUMBER LOSS AT 6Q PRESENT IN SIX PCA BONE METASTASES. Loss at 6q spans region between 6q14.1 and 6q22.32, depending on the sample (top). Minimum overlapping region for all six samples can be distinguished at 6q16.2 (98 – 99 kb, red box) and is magnified in the bottom panel with marked *FBXL4* locus, a possible dirver for this alteration. Normal copy number is depicted in blue, loss in green and gain in red.

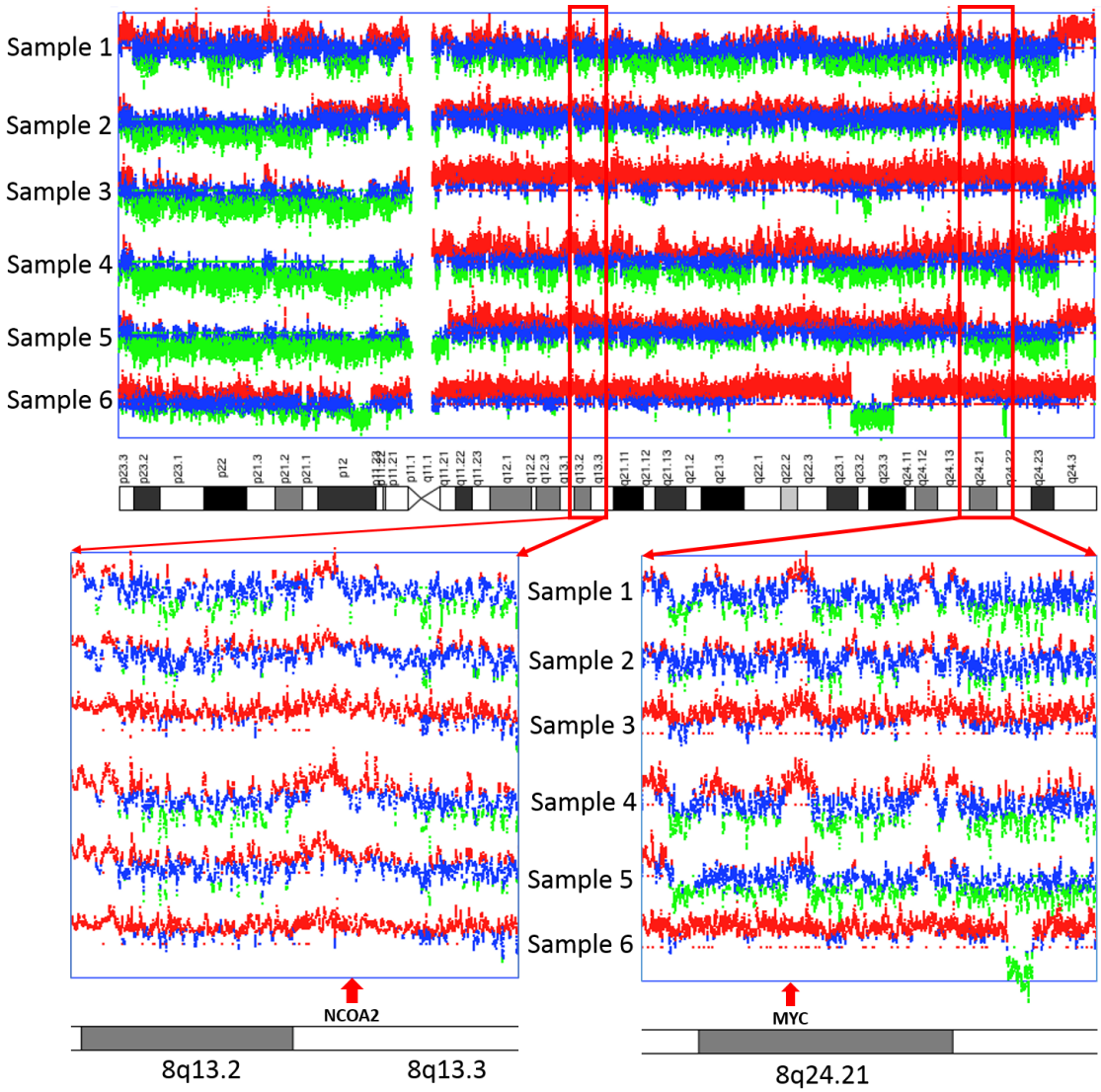

FIGURE 16. COPY NUMBER CHANGES DETECTED ON CHROMOSOME 8 IN PCA BONE METASTASES. Most of p arm was lost in four samples (samples 2-5) while one tumour displayed only small loss at p12 (sample 6) and another did not show loss of 8p (sample 1). Two tumours had 8q arm gain except for losses at q23 (sample 6) and q24.23 (sample 3). All samples displayed gain at q24.3. Lower panel shows magnified regions with NCOA2 and MYC loci, the two most commonly cited drivers for 8q gain in PCa. Normal copy number is depicted in blue, loss in green and gain in red.

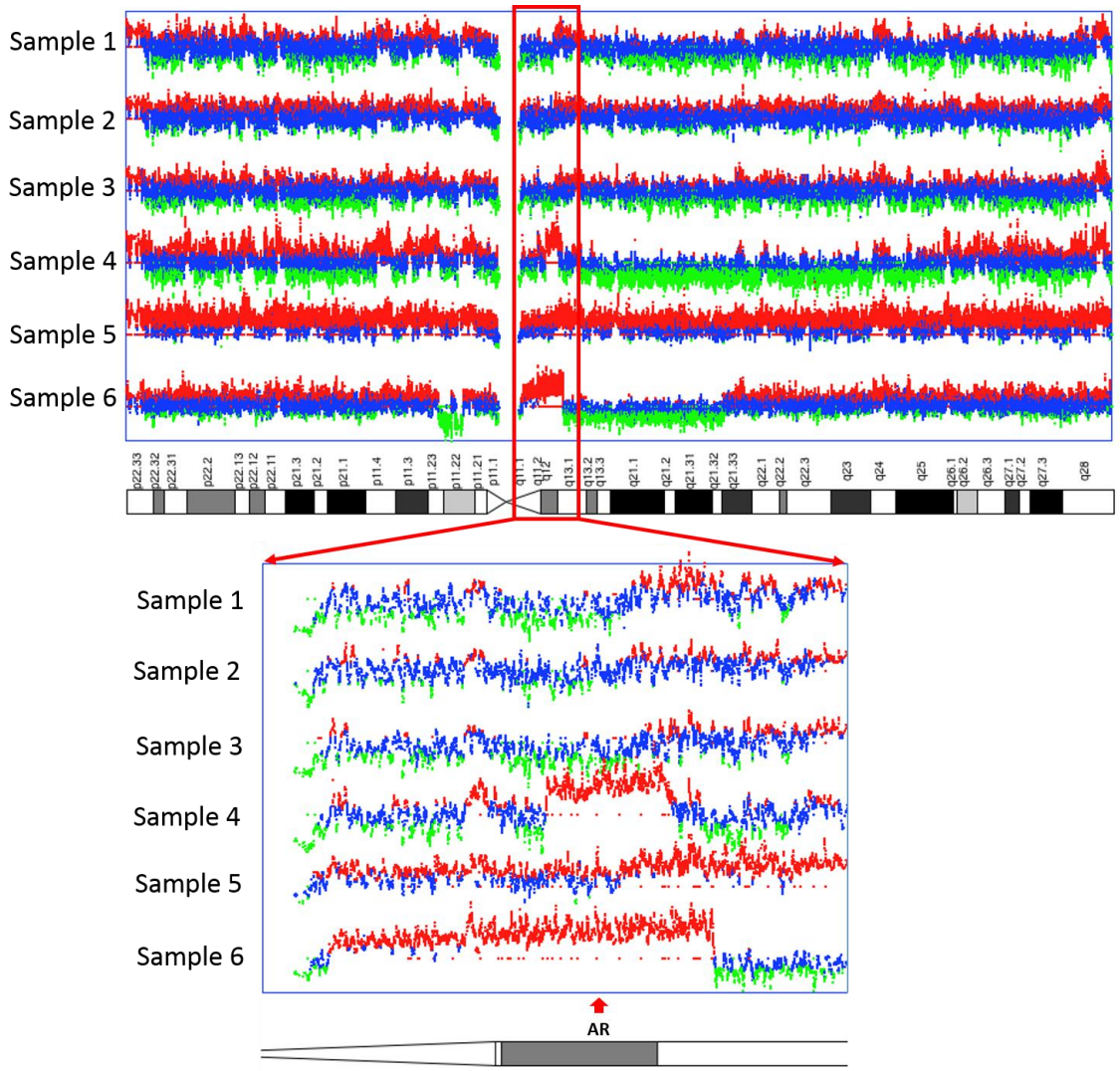

FIGURE 17. COPY NUMBER GAIN ON CHROMOSOME X AT AR LOCUS. Two samples display gains within AR locus located at Xq12, while one sample shows whole chromosome X gain. The magnified Xq12 gain region with marked AR locus is shown in lower panel. Normal copy number is depicted in blue, loss in green and gain in red.

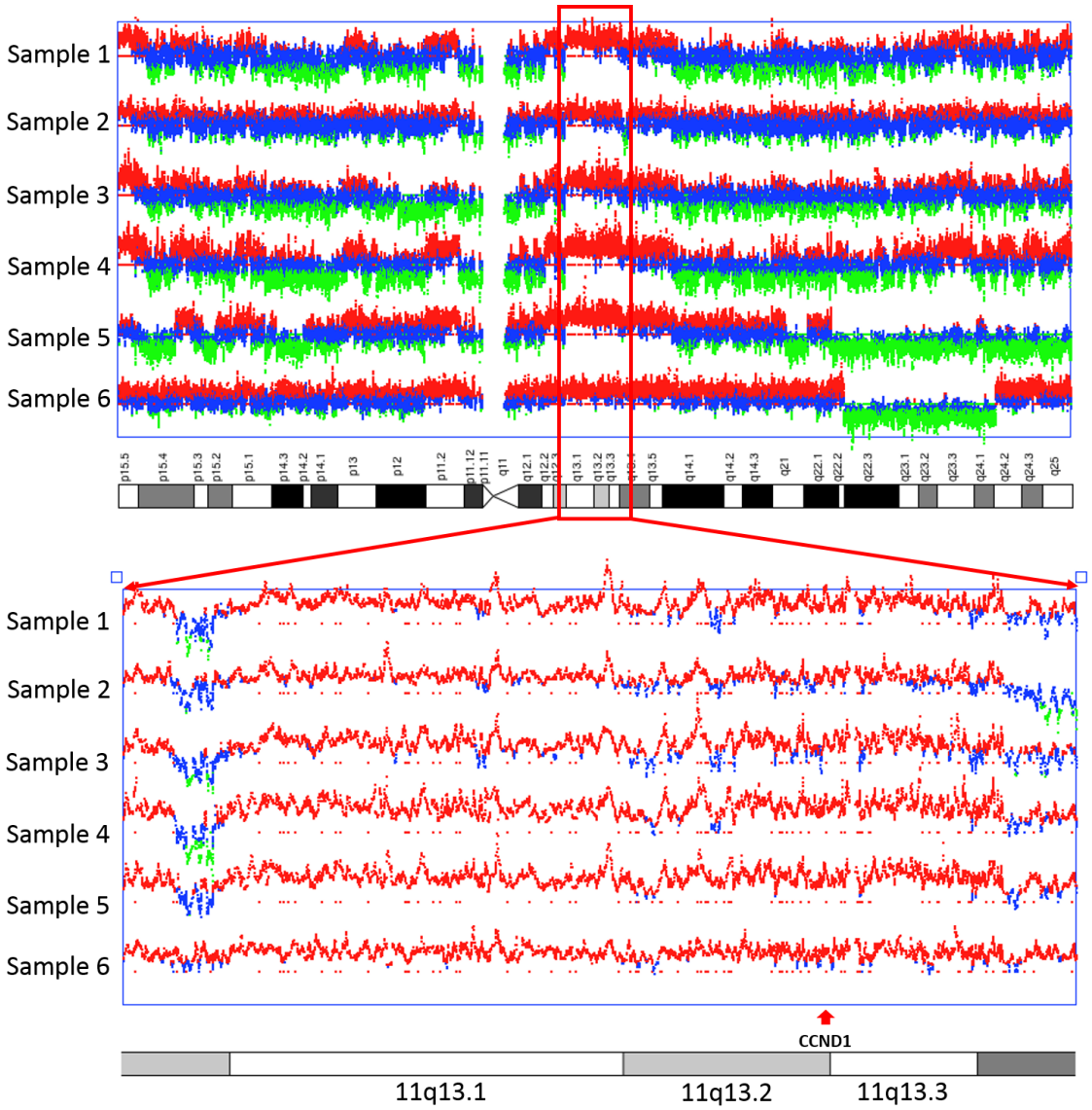

FIGURE 18. COPY NUMBER CHANGES PRESENT ON CHROMOSOME 11 IN PCA BONE METASTASES. All samples display gain at p15.5 and q13.1-14.1 while five samples also show gain at p11.2. Magnified region of q13.1-14.1 gain is displayed in lower panel and contains *CCND1* oncogene, which we propose to be a potential driver for this genomic alteration. Normal copy number is depicted in blue, loss in green and gain in red.

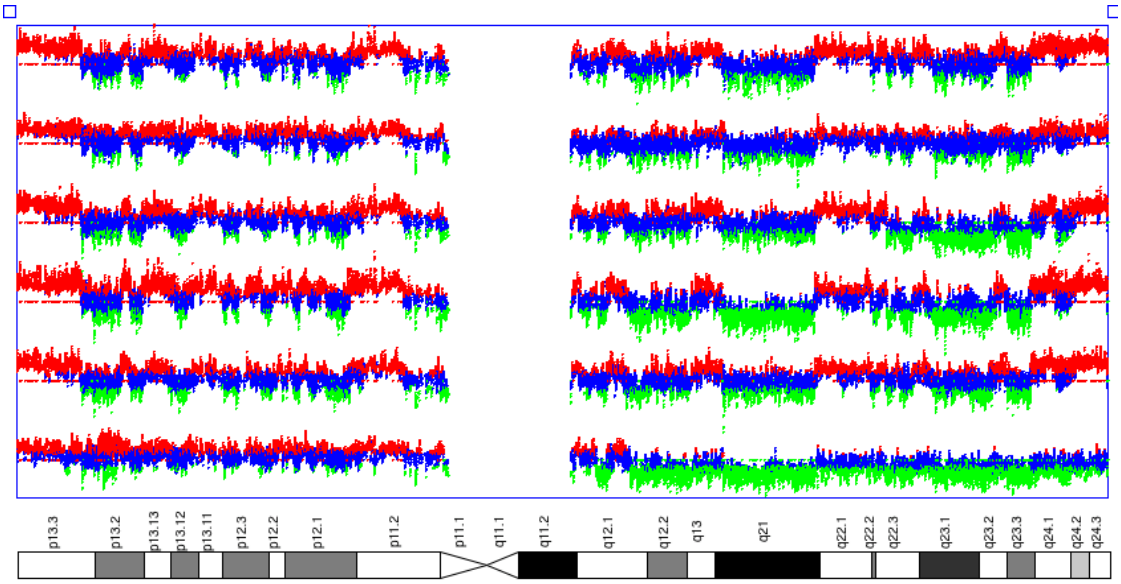

FIGURE 19 COPY NUMBER CHANGES AT CHROMOSOME 16. All samples display almost identical pattern of copy number change (apart from sample 6 with most of q arm loss) with gains at 16p13.3, 16p12.1-11.2 and losses at 16q21-22.2 and 16q24.2-24.3. Gains at 16p13.3-p11.2 and losses at 16q11.2-q21 are the 3rd most common gains and losses in metastatic PCa and 2-3 times more frequent in metastatic than in primary PCa [121]. No driver genes for this regions were found. Normal copy number is depicted in blue, loss in green and gain in red.

3.2.3 Confirmation of copy number changes in six fresh frozen bone metastases

Two regions with copy number alterations shared by all PCa bone metastases were selected for copy number change confirmation using qPCR method. TaqMan genomic Copy Number Assays directed at *CCND1* and *FBXL4* genes were chosen to confirm copy number gain at 11q13 and loss at 6q16.3, respectively. Relative DNA copy number was analysed with CopyCaller Software v2.0 (Applied Biosystems, UK) using normal male DNA as 2n copy number control and RNase P TaqMan Copy Number Reference Assay located at 14q11.2 as endogenous control (Figure 20). Copy number analysis by qPCR at 6q16 correlated with SNP 6.0 results in all six PCa bone metastases. Copy number at *FBXL4* locus varied from 1.0 – 1.2 (samples 4, 5 and 6) through 1.4 (samples 2 and 3) to 1.9 (sample 1). Copy number analysis by qPCR at *CCND1* locus correlated with SNP 6.0 results in 3/6 samples. Samples 5 and 6 showed *CCND1* copy number around 3, while sample 2 had only slightly elevated copy number of 2.4. Samples 1, 3 and 5 showed neutral copy number at *CCND1* locus.

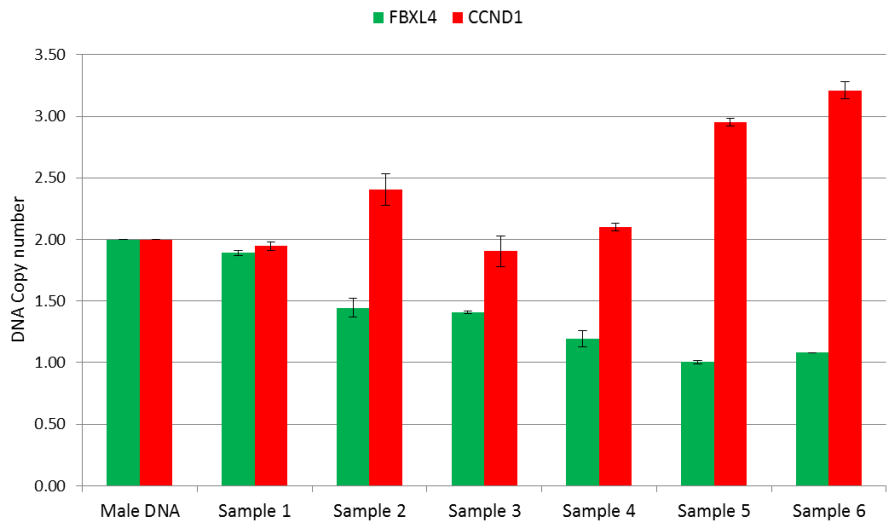

FIGURE 20. RELATIVE COPY NUMBER CONFIRMATION AT 11Q13 AND 6Q16 USING QPCR. Copy number was analysed with CopyCaller Software v2.0 (Applied Biosystems, UK) and normalised to commercial healthy male DNA. *RPPH1* (Rnase P) Copy Number Reference Assay located at 14q11.2 was used as endogenous control.

3.3 Discussion

Genomic alterations in metastatic PCa might reveal important biological insights into this lethal stage of PCa. Metastatic tumours often share common genomic alterations with primary tumours but display them at higher frequency [115, 150, 151]. These common genetic changes together with subsequently acquired novel genetic alterations may confer a selective advantageous phenotype, which allows the subset of cancer cells to disseminate from primary site and/or successfully establish distant metastases [169, 172]. Identification of genetic changes that facilitate tumour progression to metastatic stage, as well as metastatic site-specific alterations could help with patient stratification into treatment groups or help to predict patient outcome.

3.3.1 The common regions with copy number changes with same chromosomal breakpoints

In the current study we performed genome-wide analysis of six PCa bone metastases obtained from sites of pathological bone fractures occurred due to prostate tumour spread. Subsequent data analysis with 'in house' developed GOLF software uncovered widely spread genetic changes in all metastatic samples. Many of detected genomic changes displayed very similar if not identical chromosomal breakpoints present in over half of the samples (Table 38) and included gains at 1p36.3, 1q32.1-32.2, 2q14.3, 3p26.1-24.3, 3p22.3, 3q29, 4p16, 5p15.33, 5q35.2-35.3, 6p21.1, 6q27, 7p22.3-22.1,

7q11.23, 7q21.3-22.1, 7q32.1-32.2, 7q36.3, 8q24.3, 9p13.3-13.1, 9q34.11-34.3, 11p15.5-15.4, 11p12-11.2, 11q12.3-14.1, 12p13.33-q13.32, 12q13.11-14.1, 12q23.3-24.21, 12q24.23-24.31, 12q24.33, 13q32.2-32.3, 13q34, 14q32.2-32.33, 15q14-21.1, 16p13.3, 16p12.1-11.2, 16q24.2-q24.3, 17q24.3-25.3, 21q22.2-22.3, 22q11.21-11.22, 22q12.1-12.3,and 22q12.3-13.33, and losses at 9q32-33.2, 10q25.1, 16q21, 17q21.33-q22, and 17q24.3. Presence of so many genomic changes with the same breakpoints in most cases suggests that they may be artefacts caused by technical error, as it is unlikely that all metastatic cases studied show such high similarity of genomic alterations. These artefact changes described above may cover true genomic regions of reccurent copy number gains or losses existing in these six samples. The source of the error is not clear but it could originate from the arrays processing or DNA quality. Error from arrays processing was tested by processing one primary PCa sample, which was previously analysed in our laboratory by SNP array, and comparing generated genomic profile to the profile acquired previously. New genomic profile of primary PCa sample was very similar to the one generated previously and different from profiles generated for metastatic samples. This result suggests that array processing might not be the main source of observed artificial genomic changes. Starting DNA quality will also have an impact on downstream sample processing. Additionally, as all samples were collected from sites of bone fracture, they may be contaminated with necrotic and apoptotic cells containing fragmented DNA [233, 234]. The fragmented and partially digested DNA from necrotic tissue may have over-representation of more digestion resistant DNA fragments whose presence could artificially enrich copy number of certain parts of genomic sequence.

These described above potential artefacts make the evaluation of detected genomic changes with the same breakpoints less reliable. However, previous reports on genomic rearrangements associated with advanced PCa included several copy number changes falling in these regions (Table 38). For example, gains at 5q35.2-35.3, 11q13.2, 16p13.3 and 6p21.1 were reported in liver and lymph node PCa metastases [151]. Interestingly, located within 6p21.1 gain *VEGF* oncogene has been reported to promote osteoblastic lesion formation at PCa bone metastatic sites [235]. Gain at 11q13.2 contained *CCND1* oncogene, which is commonly gained/amplified in mCRPC [138, 167]. Gains at 1q32 and 7q22.1 were also frequently found in mCRPC [150, 152, 153]. Gain of 1q32 was one of the most common alterations found in disseminated tumour cells from patients with metastatic PCa (45%), and was detected in 50% of the deadly metastatic PCa [150]. Frequent gains at chromosome 7 and gains at 9q34.11, 12q24.31, 16p13.3 or 16p12.2-

11.1 observed in our bone metastases were also previously reported to be significantly more common in soft tissue metastases (40-55% and >30%, respectively) from deadly mCRPCs than in localised PCa [151]. Validation of these highly similar genomic changes with different method is required to definitively assess their prevalence in PCa bone metastases.

3.3.2 The common regions with copy number changes with different chromosomal breakpoints

Another group of genomic changes detected in PCa bone metastases consists of variable size copy number alterations sharing overlapping region between two or more samples. Particularly interesting within this group were minimal overlapping regions shared by at least half of the samples and included losses at 6q16.1-16.2 (6 cases), 8p23.2-21.1 (4 cases) and 17p13.1-12 (3 cases), and gain at 20q13.12-13.32 (3 cases) and Xq12-13.1 (3 cases). Detection of various size copy number loss at 6q14-22, present in all 6 metastatic samples is in agreement with several reports of frequent deletion within 6q13-q22 in advanced mCRPC [119, 150, 151, 236]. Minimal overlapping region at 6q16 could play an important role in metastatic cancer progression, as LOH at 6q16 was previously mentioned as the only LOH region showing a tendency towards higher degree of copy loss in metastatic and low differentiated tumours [226]. Therefore 6q16 loss was chosen for further analysis.

Frequent loss of 8p (4/6) and recurrent gain of 8q (2/6) found in our metastatic samples correspond closely to other reports on PCa, as these alterations are most commonly detected in PCa, especially in metastatic disease [138, 167, 237-239]. Simultaneous 8p loss and 8q gain was also found more frequently in circulating tumour cells (CTC) from patients with metastatic than localised disease [150]. The 8p21 region was previously reported as the most frequent site of LOH in PCa and PIN [115]. Loss of 8p21 together with loss of *PTEN* at 10q23.33 (found in 2/6 of our bone metastases) are most commonly reported events involved in progression from PIN to PCa [141]. *PTEN* loss is very common in primary and metastatic PCa (40% of cases) [115, 138, 153, 228, 230]. As an early event in PCa progression, loss of *PTEN* is considered as one of the drivers of tumorigenesis [167, 230]. However, based on mouse models *PTEN* loss alone does not induce development of invasive tumours [240]. Interesting study on mice single and double knockout for *PTEN* and *SMAD4* genes revealed that mice with both genes knockout develop highly aggressive invasive PCa and die within 32 weeks [241]. Therefore, it is possible that *PTEN* loss can lead to advanced metastatic disease when combined with concomitant deregulation of other genes such as *SMAD4*. *SMAD4* is

consistently downregulated in PCa [241] and the region of 18q21.2, which harbours *SMAD4*, was found deleted in 30% of 17 soft tissue metastases [242]. We did not detect *SMAD4* copy number loss in our 6 bone samples; however, we cannot exclude gene downregulation by post-transcriptional mechanisms.

Copy number loss at 17p13.3-11.2 found in half of bone metastases (minimal overlapping region 17p13.1-12) was also commonly detected in 14 deadly metastatic PCa [151]. Letouze *et al* [152] used SNP 6.0 data from 14 PCa patients with multiple metastatic sites to reconstruct the tumour progression tree in each patient and to find a signature copy number pattern of the common precursor clone for each sample. Interestingly, most frequently detected changes in the precursor clones were also frequent in our samples, including loss of 8p21, 17p13-11 and 6q14-21, and gain of 8q24. As precursor clones would onset the metastasis, these recurrent abbreviations may play a role in metastatic progression.

Taylor *et al* [115] based on copy number alterations analysis of 181 primary tumours and 37 metastases distinguished two separate subgroups of tumours: those with minimal copy number alterations (clusters 1-4), mainly containing primary tumours, and those with substantial copy number alterations (clusters 5 and 6), that included most of the metastatic samples analysed. Cluster 5 contained 6/8 bone metastases studied and was characterised by presence of common genomic alterations, such as loss of 6q, 13q, 16q and 18q. Our bone metastases also displayed variable size losses within 6q14.1–q22.32 (all cases), 13q13.1-q31.1 (2/6), 16q12.1-q24.3 (2/6) and 18q21.1-q23 (2/6). In Taylor *et al* study cluster 5 tumours had an extremely unfavourable prognosis. Together with 8p losses and 8q gains, losses at 13q, 16q and 18q are most commonly found in mCRPCs, as reported in a study of 150 samples of mCRPC collected from different metastatic sites (lymph nodes, bones, liver, soft tissue) [138] and another cohort of 54 metastatic samples (including bone metastases) from 10 mCRPC patients [167].

Gain of *AR* at Xq12 is usually linked to progression from localised to metastatic disease [141], with focal amplifications of *AR* restricted to mCRPC [115, 138, 167, 230]. Unsurprisingly, two of our bone metastases had gain within Xq12-13.1 and one sample had a whole chromosome X gain.

Copy number loss at common TSG loci was also present in our PCa bone metastases. Loss of 17p13.1-12 (*TP53* at 17p13.1) was found in 3/6 (sample 2, 4, and 6), 13q13-31 (*RB1* at 13q14.1) in 2/6 (sample 2 and 6), and 12p13.31-13.1 (*CDKN1B* at 12p13.1,

coding p27) and 9p24.2-21.1 (*CDKN2* at 9p21.3, coding p16) were present in a single tumour (sample 5). Taylor *et al* [115] in his subset of primary and metastatic tumours found peaks of deletion in regions targeting *RB1* (13q14.2), *TP53* (17p13.1), and broader deletions at 12p13.31-p12.3, containing *CDKN1B* (12p13.1). They found *RB1* loss in 37% of metastatic PCa versus 5% of primary PCa and loss of *CDKN1B* in 47% of metastatic PCa versus 24% of primary tumours. Holcomb *et al* [151] reported loss of *RB1* locus in 79% of soft metastases from mCRPC patients and Liu *et al* [228] found homozygous deletions at *CDKN2A* locus in single PCa metastatic sample. However, in recent NGS-based study, Robinson *et al* [138] found *RB*, *CDKN1B* and *CDKN2A* loss/mutations at lower frequencies of 21%, 4% and 2.7% in 150 PCa metastatic samples. As those genes are involved in one pathway, inactivation of any of them will lead to pathway disruption. Functional inactivation of p16 and Rb tumour suppressor proteins is generally mutually exclusive in human cancers [243, 244], which is also the case in our samples. Moreover, overexpression of cyclin D1, e.g. as a result of *CCND1* copy number gain, would have the same effect on cell proliferation (unrestrained) as loss of p16 and Rb [244, 245]. Interestingly, we confirmed copy number gain at *CCND1* locus in exactly same three PCa bone metastases that had loss of *CDKN2* or *RB1*. It is possible that in those samples additional gain of *CCND1* was necessary to efficiently stimulate cell cycle progression. In lung cancer cyclin D1 overexpression coexist with loss of Rb or p16 and it has been suggested that overexpression of cyclin D1 may be an early event in this cancer, followed either by Rb loss, as occurs in SCLC, or by loss of p16 expression, a common event in NSCLC [246]. Cyclin D1 overexpression followed by Rb loss has also been proposed for parathyroid cancer progression [247].

One bone metastasis displayed deletion at 21q22.2-22.3 locus between *ERG* and *TMPRSS2* genes, an event commonly found in PCa [122, 151, 228]. *TMPRSS2-ERG* rearrangement is considered as an early event in PCa carcinogenesis and its status in primary tumours is carried over to the metastatic sites, but is not acquired *de novo* at metastatic site, suggesting that is not necessary for PCa progression [228]. Currently, the significance of the *TMPRSS2-ERG* rearrangement in PCa is not clear, as associations with both poor [128] and good prognosis [131] have been reported.

3.3.3 Copy number confirmation at *CCND1* and *FBXL4* locus

Copy number analysis of *FBXL4* locus by qPCR confirmed loss of the region in all 6 samples analysed by SNP array but only 3/6 of PCa bone metastases with copy number gain at 11q13 detected by SNP array showed gain at *CCND1* locus with TaqMan

CNAssay. Lack of copy number gain detection in the other 3 cases could be due to specificity of a relative quantification method used for copy number analysis. The qPCR method is widely used for copy number confirmation. However, as qPCR compares threshold cycles (Ct) between the target gene (target CNAssay) and a reference sequence (reference CNAssay) to generate ΔCt values, which are used for copy number variation (CNV) calculation, it highly relies on the assumption that amplification efficiency of both assays that are competing in a single reaction is equal. Differences in amplification efficiencies between target and reference amplicons would cause variations in ΔCt that can result in artifactual copy number assignments. It has been shown that as little as a 4% change in amplification efficiency could result in an error of up to 400% in ΔCt calculation [248, 249]. Unfortunately, at present, there is no accepted procedure to evaluate PCR efficiency from a single run, hence some methods can overestimate and others underestimate the true PCR efficiency [249]. qPCR methods are also prone to false copy number assignments if DNA concentration and quality are not optimal and inhibitory components from insufficiently purified DNA may also cause significant reduction in the sensitivity of qPCR assays [248, 249]. Most importantly, the analysis assumes that substitutional mismatches at either the test or reference locus primer binding sites do not lead to 'drop-out' of one or more copies. Any genetic changes within regions where primers and probe attach (e.g. polymorphism or point mutations) could affect qPCR efficiency and lead to failure of polymorphic copy to amplify, therefore reducing amount of PCR product [250, 251]. *CCND1* sequence is particularly rich in polymorphic sites (over 100 SNPs identified) [252], and unfortunately, they could not be avoided in TaqMan assay used in this study.

There is also the possibility of some sample or SNP array processing error which could potentially cover the true genetic alteration as this particular copy number gain is one of previously discussed genetic regions with exactly the same breakpoints in all samples.

CHAPTER 4

Analysis of 11q13 gain/*CCND1* gene in PCa

4.1 Introduction

4.1.1 The 11q13-14 gain and potential driver genes

One of the common genetic changes detected in all PCa bone metastases analysed was gain of 11q13-14. Gains within 11q12-24 region were previously found at higher frequency in more advanced/metastatic PCa than in localised tumours [150, 151, 226]. The smaller 11q13 region is especially frequently gained in a variety of tumours, including breast [253], ovarian [254], HNSCC [255, 256], bladder [257] and oral [258]. The common 11q13-14 gain detected in our 6 bone metastases spans over 15 Mbs and contains more than 300 genes. For such kind of gene rich region, it is always difficult to assess which of these genes is a potential driver for observed genomic alteration [259]. However, based on previous reports, the most frequently named potential candidate drivers within 11q13 gain are: *CCND1*, *EMSY*, *FGF3* and *FGF4* [255, 258].

EMSY gene is located at 11q13.5 and has been found amplified in sporadic breast cancer (13%) and higher-grade ovarian cancer (17%), where it was associated with worse survival, particularly in node-negative breast cancer [254]. *EMSY* encodes a protein that binds to and inhibits the activity of *BRCA2*, suggesting its involvement in DNA repair in non-hereditary breast and ovarian cancers [254]. However in vitro study showed lack of benefit from *EMSY* amplification when considering cells sensitivity to agents targeting cells with defective homologous recombination [260]. Interestingly, *EMSY* genetic variants were reported to contribute to PCa predisposition [261, 262].

Other potential candidate drivers, FGF3 and FGF4, are frequently amplified together with *CCND1* in many cancers, including bladder, breast and squamous cell carcinoma of the lung and head and neck [257, 263]. In recent NGS study they were found amplified in in 22 of 391 cancer patients (5.6%) [264]. In breast cancer, *FGF3* amplification was found to be a good indicator of prognosis in the subgroup of progesterone-receptor-negative patients [253]. However in PCa *FGF3* amplification is rare or absent [265, 266], therefore it is unlikely to be involved in PCa carcinogenesis. Based on mouse model FGF3 overexpression may lead to benign epithelial hyperplasia. Transgenic mice, which carry the *FGF3* gene driven by the MMTV promoter/enhancer develop pronounced mammary gland hyperplasia (female) or benign epithelial hyperplasia similar to BPH [267].

Based on widespread evidence of *CCND1* oncogene involvement in human cancer, it seems to be most likely target gene of 11q13 gain/amplification [268]. Copy number gain/amplification specifically at *CCND1* locus was recently commonly found at different

metastatic sites (including bone) in mCRPC [138, 167] and several metastatic PCa cell lines including PC3, DU145 and VCaP are known to have 11q copy number gain [218]. Chromosomal rearrangement, amplification and mutation of the *CCND1* gene have been reported in many types of human cancers, including mantle cell lymphomas, parathyroid adenomas, breast, prostate, colon, lung, bladder and liver adenocarcinomas, squamous carcinomas of the esophagus and head and neck [252, 269]. Tissue culture-based experiments showed that cyclin D1, a *CCND1* gene product, acts as a collaborative oncogene that enhances oncogenic transformation of other oncogenes (i.e. *Ras, Src, E1A*) in cultured cells [270]. Cyclin D1 was indicated in acquisition of invasive phenotype by breast cancer cells and their local invasion to surrounding tissue [271]. Cyclin D1 deficient mice were resistant to breast cancer induced by the *HER2* or *Ras* oncogenes [269]. Cyclin D1 overexpression also contributes to the resistance of tumour cells to chemotherapeutic agents such as cisplatin [272]. In PCa cell lines cyclin D1 inhibits *FOXO*-mediated anoikis (programmed cell death induced by detachment of anchorage-dependent cells from the surrounding extracellular matrix) and therefore may contribute to tumourigenesis by promoting anchorage-independent cell survival [273].

4.1.2 Cellular function of *CCND1* product, cyclin D1

CCND1 gene is located at chromosome 11q13.3 (Figure 21).

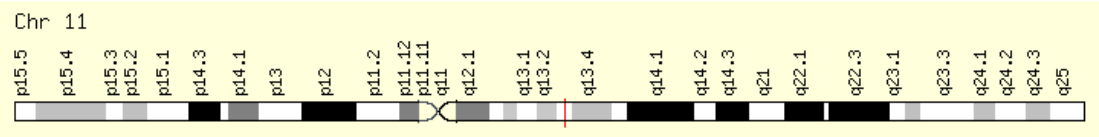

FIGURE 21. *CCND1* LOCATION ON CHROMOSOME 11Q13. Red line marks *CCND1* position. Adopted from www.genecards.org.

Cyclin D1 belongs to conserved cyclin family, which function as regulatory subunits for the cyclin-dependent kinases (CDKs). 29 cyclins and more than 20 CDKs have been identified in mammalian cells [274]. All cyclins share a conserved domain of 150 amino acid residues called the “cyclin box”, which mediates binding to CDKs. D, E, A, and B-type cyclins in complexes with relevant CDKs are known to directly regulate the cell cycle: through phosphorylation of different substrates they trigger transition to distinct cell cycle phases [275]. D-type cyclins (D1, D2, and D3) are G1-specific cyclins that associate with CDK4 or CDK6, and promote cell cycle progression during G1 phase. Unlike other cyclins, expression and accumulation of D-cyclins are strongly dependent

on extracellular mitogenic signals, therefore they are regarded as mitogenic sensors that transmit signals from the extracellular environment to the cell cycle machinery [276, 277]. The ability of Cyclin D1 to activate CDK4/6 is the most extensively documented mechanism for its oncogenic action. Activation of CDK4/6 leads to phosphorylation and inactivation of the tumour suppressor protein Rb. Rb serves as a gatekeeper of the G1 phase and its inactivation by cyclin D1/CDK4/6 results in release of E2F transcription factors and activation of genes that are essential for advances into the late G1 and S phases [278] (Figure 22). Upregulation of cyclin D1 expression and CDK4/6 activation would therefore lead to mitogen independent cell proliferation and overriding checkpoints controlling genomic integrity and stability [268]. In normal cells, cyclin D1 levels are tightly controlled at transcriptional, posttranscriptional and protein levels [279]. Cyclin D1 degradation is triggered by phosphorylation of its Thre286 residue through glycogen synthase kinase 3β (GSK3β). Under normal conditions, phosphorylation of cyclin D1 leads to nuclear export and subsequent rapid ubiquitin-dependent proteolysis [279].

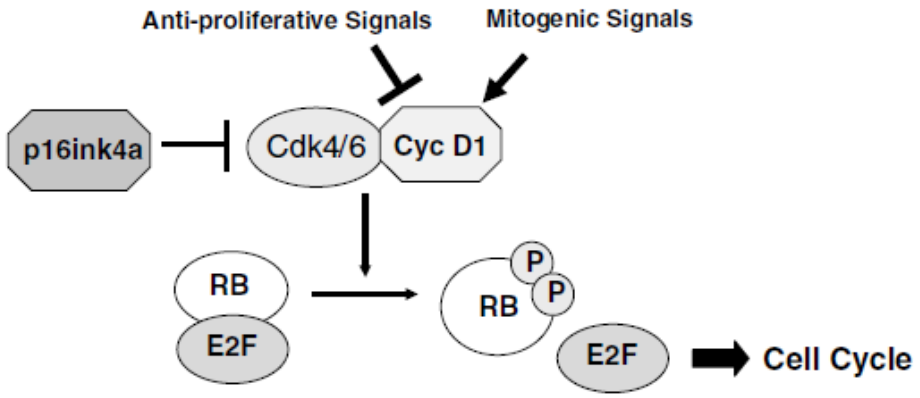

FIGURE 22. CYCLIN D1 FUNCTION. pRb is phosphorylated by G1 phase cyclins, cyclin D1 and cyclin E, which leads to its inactivation and release of E2F transcription factors. Adapted from Knudsen *et al* [252].

Cyclin D1 localisation and stability can also be altered by mRNA splicing due to polymorphism (G/A870) of the *CCND1* locus, which has been reported to associate with increased cancer risk or poor prognosis for a number of cancers, including prostate [280]. The G/A870 polymorphism alters a splice donor site at the exon 4-intron 4 boundary (introduces a premature stop codon within intron 4) and the A allele predispose for the production of an alternative transcript b, which lacks exon 5. The C-terminus of cyclin D1b lacks located within exon 5 PEST domain, involved in protein destabilisation, and a phosphorylation site Thre286, regulating nuclear export and cyclin D1 turnover possibly leading to increased cyclin D1b stability and inability to be exported from the nucleus

(Figure 23) [252]. Cyclin D1b expression was confirmed to be largely nuclear, but didn't show increased stability and as oppose to full variant (cyclin D1a), was found to be a poor activator of CDK4-dependent Rb phosphorylation [281]. Nonetheless, cyclin D1b seems to have enhanced oncogenic capacity compared to full-size cyclin D1a, possibly due to other functions than Rb inactivation. The cyclin D1b transcript is present in multiple cancers, including Ewing's sarcoma, mantle cell lymphoma, oesophageal, colon and breast cancers [282]. Based on mouse fibroblast models, cyclin D1b (but not cyclin D1a) induced tumour formation and anchorage independence, and in breast cancer cells induced resistance to therapeutic intervention [282].

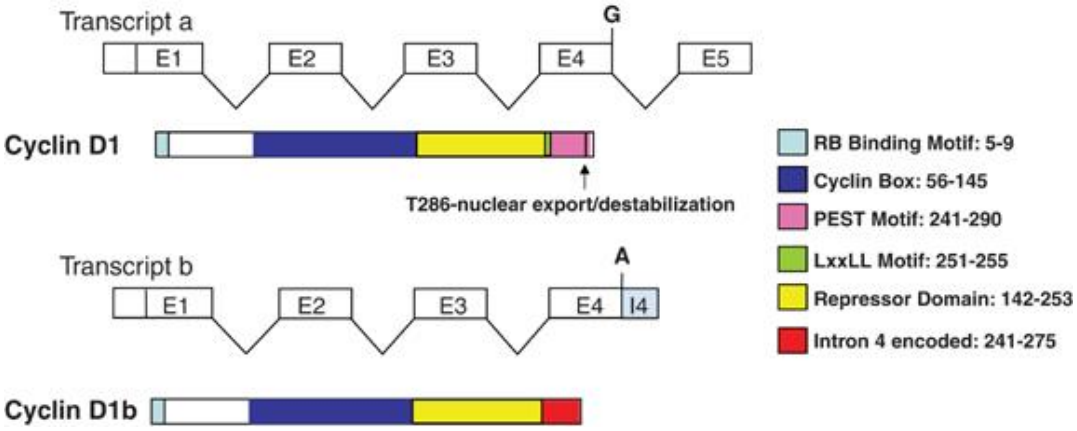

FIGURE 23. DIFFERENCE IN DOMAIN STRUCTURE OF CYCLIN D1 AND D1B. Adopted from Knudsen *et al* [252].

In prostate, expression of full length cyclin D1a transcript increases in response to androgen stimulation of AR, which leads to subsequent CDK4 protein activation necessary for cell-cycle progression [283]. Prostate cancers require AR for survival and progression and androgen withdrawal therapy is the common treatment for PCa. Interestingly, accumulated cyclin D1a induces a negative feedback loop by directly binding to and inhibiting AR transcriptional activity, thus regulating the strength and duration of AR signalling and limiting further cellular proliferation [284]. Cyclin D1b fails to control AR activity: is deficient in its ability to regulate AR-dependent transcription and lost the ability to attenuate androgen-dependent proliferation. At the same time it can promote cell cycle progression in AR-dependent PCa [252, 285].

4.2 Results

4.2.1 FISH analysis of 11q13/*CCND1* gain in larger cohort of metastatic and primary PCa samples

I performed FISH analysis of *CCND1* locus in 43 bone metastases and 152 primary cancers to determine its copy number status. BPH TMAs (55 cases) were used as a non-neoplastic control for FISH signal evaluation and counting. FISH analysis of 11q13/*CCND1* region was successfully performed in all BPH cases, 22/43 of PCa bone metastases. 142/152 cases showed good quality FISH signal at 11q13/*CCND1* and 10 (7%) of them had copy number gain at this locus. Overall, there was a significant difference in frequency of copy number change at 11q13/*CCND1* locus between primary tumours and bone metastases ($p<0.0001$, Chi-square test) with more frequent copy number change in bone metastases (Table 40). Examples of copy number gain are shown in Figure 24.

TABLE 40 FREQUENCY OF CCND1 GAIN DETECTED BY FISH IN PRIMARY AND METASTATIC PCA

PCa type	11q13 copy number gain		p value
	positive	negative	
Primary PCa	10/142 (7%)	132/142 (93%)	<0.0001
Bone metastases	12/22 (54.5%)	10/22 (45.5%)	

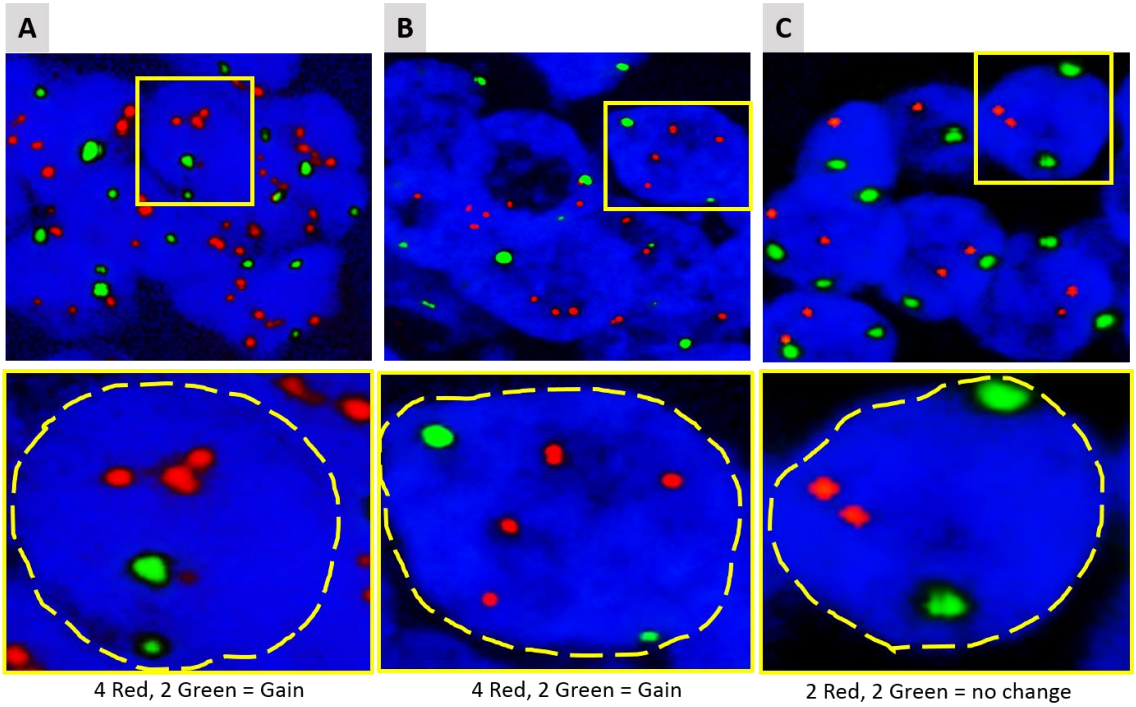

FIGURE 24. REPRESENTATIVE FISH IMAGES OF COPY NUMBER CHANGES AT 11Q13 IN PROSTATE SAMPLES. (A) *CCND1* copy number gain in bone metastasis; (B), *CCND1* gain in primary PCa; (C), BPH with neutral copy number at *CCND1* locus. Red, *CCND1* locus; green, control locus; blue, nuclei (DAPI). A minimum of 100 nuclei (cells) with clear hybridization signals were counted per tissue sample. Nuclei with same number of red and green signals were considered as no copy number change. Nuclei with more red than green signal were considered as positive for CCND1 copy number gain. Lower panel shows enlarged single nuclei (depicted in yellow dotted line) from the top pictures (yellow boxes) to illustrate copy number assessement for each exemplar nucleus. The percentage of nuclei with more red signals than green signals were determined per sample and the widely accepted cutoff calculated as the mean of false-positive findings in ten non-malignant controls (BPH samples) plus three times the standard deviation (mean % ± 3SD) was used for CCND1 copy number status evaluation in each sample.

4.2.2 Cyclin D1 protein immunoexpression in FFPE PCa samples

IHC for cyclin D1 was successfully performed in all 43 bone metastases and 152 primary PCa (staining examples shown in Figure 25 and Figure 26). Cyclin D1 staining was observed mainly in nuclei, however some degree of cytoplasmic expression was also noted. Only nuclear expression was used for analysis [286] and both: staining intensity as well as percentage of stained nuclei were assessed in each sample.

Forty of 43 (90%) bone metastases showed various levels of cyclin D1 immunoexpression with remaining three cases negative for cyclin D1 staining. Most of the cases positive for cyclin D1 were strongly stained (23/40, 57.5%; intensity score 3, e.g. sample 4, Figure 25) with only 6 tumours showing low staining intensity (6/40, 15%;

intensity score 1, e.g. sample 3, Figure 25). Mean percentage of stained nuclei was 21.2% with most of the tumours expressing cyclin D1 in 10-30% of cells (29/40, 72.5%).

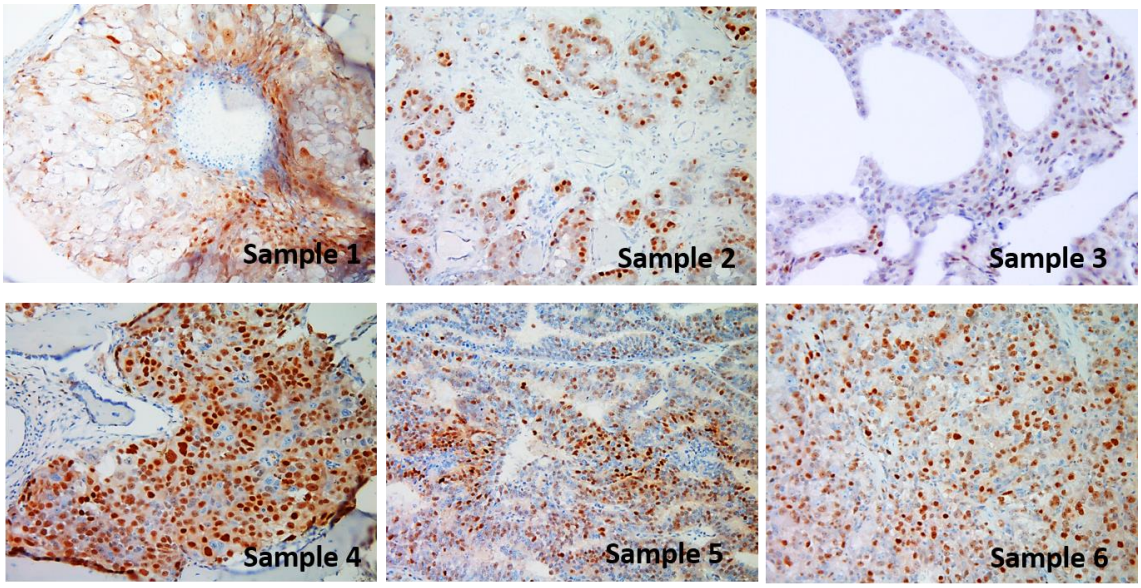

FIGURE 25. EXAMPLES OF CYCLIN D1 IHC IN BONE METASTASES. Matched FFPE samples to six fresh frozen bone metastases showed wide range of cyclin D1 staining, with staining intensity from weak (sample 3) to strong (samples 4) in 10% (sample 1, 2, 3) to 70% of nuclei (sample 4).

For the six bone metastases with available SNP array data, cyclin D1 expression was analysed in context of genetic alterations in *CCND1/RB/CDKN2A* and *TP53/CDKN1A* pathways (Table 41). All three cases with confirmed *CCND1* copy number gain by qPCR had loss of *TP53*. Two of these cases had also loss of RB, while Sample 5 which was negative for *RB* loss had instead *CDKN2A* loss. All three cases showed medium cyclin D1 staining intensity with 10-40% positively stained nuclei. Two of the three samples negative for *CCND1* gain had weak cyclin D1 expression in 10-20% of nuclei suggesting low activation of this pathway while the third sample (Sample 4) had strong cyclin D1 expression in 70% of nuclei indicating strong pathway activation. All these three cases did not display additional genetic changes in *CCND1/RB/CDKN2A* and *TP53/CDKN1A* pathways.

TABLE 41. CYCLIN D1 EXPRESSION ON THE BACKGROUND OF GENETIC CHANGES IN *CCND1/RB/CDKN2A* AND *TP53/CDKN1A* PATHWAYS

PCa bone metastases	*CCND1* gain (qPCR)	Cyclin D1 Int	Cyclin D1 %	*RB* loss	*CDKN2A* (p16) loss	*TP53* loss	*CDKN1A* (p21) loss
Sample 1	-	1	20	-	-	-	-
Sample 2	+	2	10	+	-	+	-
Sample 3	-	1	10	-	-	-	-
Sample 4	-	3	70	-	-	-	-
Sample 5	+	2	20	-	+	+	-
Sample 6	+	2	40	+	-	+	-

Of 152 primary PCa, 130 were positive for cyclin D1 expression (85.5%). Most of the cyclin D1 positive primary tumours showed moderate (53/130, 40.8%; intensity score 2) to strong staining intensity (49/130, 37.7%; intensity score 3) with only 28/130 (21.5%) cases displaying weak staining (intensity score 1). Majority of the tumours had cyclin D1 expression in 10-30% of nuclei (112/130, 86.1%) with only 12 cases having cyclin D1 expression in more than 30% of nuclei (9.2%), including two tumours with all cells stained for cyclin D1 (Figure 26, last in top panel). There was no correlation between cyclin D1 staining intensity (cut off ≥2) and Gleason score (41 tumours with GS<7, 46 with GS=3+4, 31 with GS=4+3 and 24 with GS>7; p=0.2276, X^2 test) or with tumour stage (T1+T2 (2+51 tumours) vs T3 (19 tumours); p=0.7626, Fisher exact test).

BPH samples used as non-malignant control also commonly stained for cyclin D1 (33/44, 78.6%) but to lesser extent than tumour tissue (median staining intensity = 1 and median % of stained nuclei = 10%, Figure 26, bottom panel). Staining was often focal with only some of the glands stained.

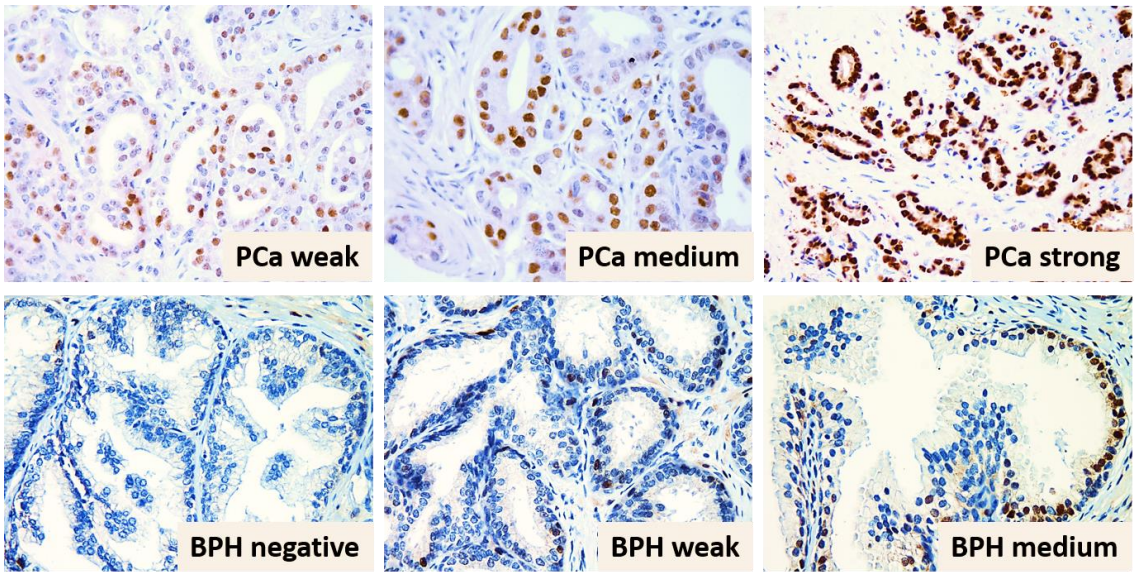

FIGURE 26. EXAMPLES OF CYCLIN D1 IHC IN PRIMARY PCA AND BPH. Top panel: representative range of cyclin D1 staining intensity in PCa with mostly low percentage of stained nuclei. One of two cases with all nuclei strongly stained is also shown (PCa strong). Bottom panel: BPH samples were also mostly positive for cyclin D1 but stained weak to moderate with most cases showing focal stain in ≤20% of nuclei.

Cyclin D1 staining intensity had a tendency to be stronger in bone metastases than in primary tumours. Median staining intensity of bone metastases was higher than primary tumours (3 versus 2, p= 0.0152, two sided Mann-Whitney U test). 34/43 (79.1%) of bone metastases and 102/152 (67.1%) of primary tumours had intensity score ≥ 2 (Chi-square test, p=0.1869) but only 32.2% (49/152) of primary tumours expressed very strong staining intensity (score 3) compared to 53.5% (23/43) of bone metastases (Chi-square test, p=0.015, Figure 27A and B). The percentage of stained nuclei was similar in both groups with median and average values around 20% (p=0.270, two sided Mann-Whitney U test, Figure 27C and D, Table 42). For both, bone metastases and primary tumours, most of the cases had cyclin D1 expression present in 10-30% of nuclei with minority of cases expressing cyclin D1 in more than 30% of nuclei and two tumours (both primary PCa) showing 100% cyclin D1 positivity (Figure 27C).

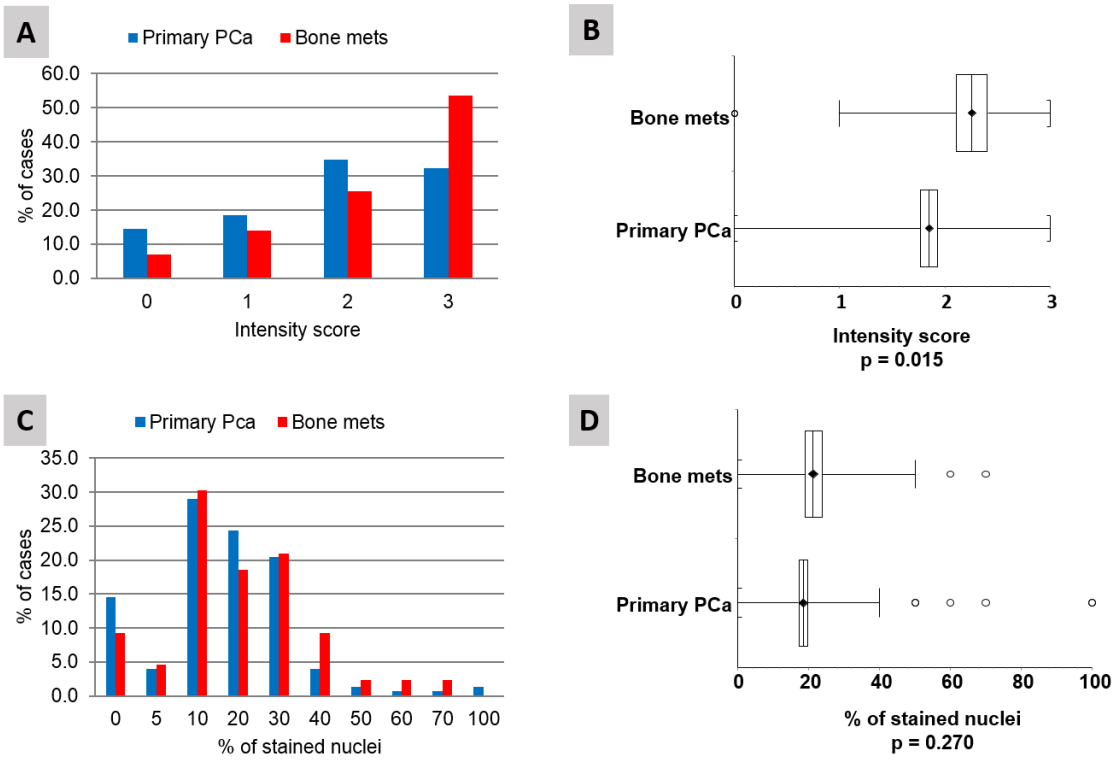

FIGURE 27. COMPARISON OF CYCLIN D1 IMMUNOEXPRESSION IN PRIMARY AND METASTATIC PCA SAMPLES. Bone metastases show higher intensity of cyclin D1 expression than primary tumours (A) with significantly higher mean cyclin D1 staining intensity than primary PCa (B). However, bone metastases show similar percentage of stained nuclei to primary tumours (C) with no difference in mean percentage of stained nuclei between those two groups (D).

TABLE 42 MEDIAN AND AVERAGE CYCLIN D1 IMMUNOEXPRESSION IN PRIMARY PCA AND BONE METASTASES.

Samples	Score type	Median	Mean (SD)
Primary PCa	intensity	2	1.85 (1.0)
Bone metastases		3	2.26 (1.0)
Primary PCa	% of stained nuclei	20	18.49 (15.9)
Bone metastases		20	21.16 (15.9)

4.2.3 Correlation between cyclin D1 expression and 11q13/*CCND1* copy number gain

Cyclin D1 expression measured by IHC and 11q13/*CCND1* copy number gain assessed by FISH were both available for 164 cases, including 22 bone metastases and 142 primary PCa. Twelve PCa bone metastases and 10 primary tumours were positive for

11q13/*CCND1* copy number gain with average number of affected nuclei 53% and 43%, respectively. All samples with gain were positive for cyclin D1 staining. Correlations between cyclin D1 expression and 11q13/*CCND1* copy number gain were calculated with two sided Mann-Whitney U test. Bone metastases positive for 11q13/*CCND1* gain showed either moderate or strong cyclin D1 staining intensity. Tumours with 11q13/*CCND1* neutral copy number displayed similar staining intensity to samples with 11q13/*CCND1* gain, apart from two cases with weak staining. Most of the cases with 11q13/*CCND1* gain had cyclin D1 expression present in 30% of nuclei (7/12), while tumours without gain showed cyclin D1 IHC mostly in 10% or 20% of nuclei (5/10 and 3/10, respectively). However, there was no significant difference in cyclin D1 IHC between those two groups (p=0.599 for staining intensity and 0.334 for percentage of stained nuclei).

All primary tumours with 11q13/*CCND1* gain, similar to bone metastases, showed either medium or strong cyclin D1 staining intensity, while 34.8% (46/132) of tumours with neutral copy number had weak or no cyclin D1 expression (p=0.002). Half of the tumours with 11q13/*CCND1* gain showed cyclin D1 expression in 30% of cell nuclei, while cases with neutral copy number at 11q13/*CCND1* had mostly cyclin D1 expression present in 10% of cells (p=0.01).

When primary and metastatic tumours were grouped together based on 11q13/*CCND1* copy number status, cases with 11q13/*CCND1* gain had stronger cyclin D1 median staining intensity than cases with 11q13/*CCND1* neutral copy number (p<0.0001, Figure 28A and B). Tumours with 11q13/*CCND1* gain also showed staining in more cell nuclei than cases without gain (p=0.003, Figure 28C and D).

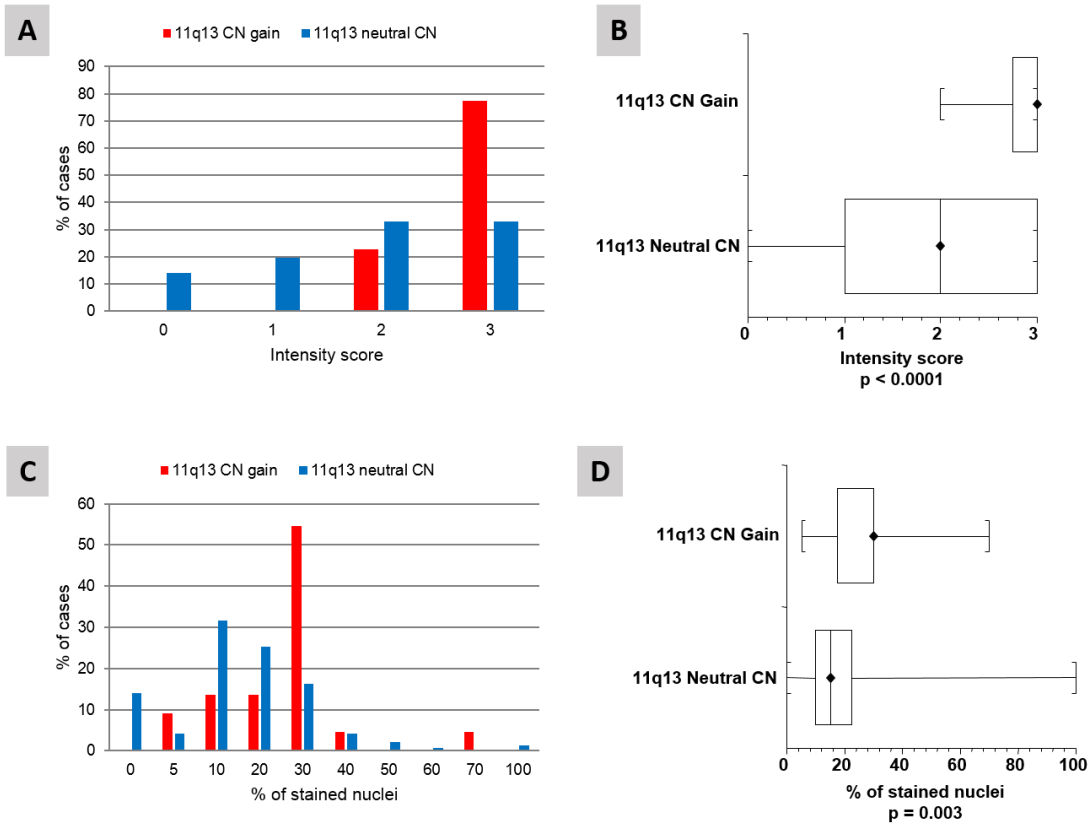

FIGURE 28. PCA WITH 11Q13 GAIN SHOW SIGNIFICANTLY STRONGER CYCLIN D1 IMMUNOEXPRESSION AND IN MORE CELL NUCLEI THAN CASES WITH NEUTRAL COPY NUMBER AT *CCDN1* LOCUS. (A), staining intensity distribution; (B), significant difference in median staining intensity; (C), percentage of stained nuclei score and (D), significant difference in median percentage of stained nuclei between the two groups.

4.2.4 Cyclin D1 transcripts expression in prostate samples

qPCR for full length cyclin D1a transcript was performed with TaqMan expression assay located at exon 4-5 junction, present only in transcript a. Cyclin D1b transcript was quantified with specifically designed primers targeting junction of exon 3 and 4 (forward) and beginning of intron 4 (reverse) and SYBR Green assay.

Both cyclin D1 transcripts expression was tested in prostate cell lines. All prostate cell lines analysed expressed both transcripts, except for VCaP, which had highest levels of cyclin D1b but had undetectable levels of cyclin D1a. 22RV1 highly expressed both transcripts, followed by PC3, DU145 and LNCaP cells. PNT1A and PNT2 cell lines derived from normal PCa epithelium had lowest cyclin D1a and b RNA expression (Figure 29). As the *CCND1* A/G status at 870 polymorphic site is already known for prostate cell lines, the relation between polymorphism and cyclin D1 transcripts

expression was analysed. Cyclin D1a and b transcripts expression levels did not correlate with A/G870 polymorphism and they also did not correlate with *CCND1* copy number status. 22RV1 (A/A870, no *CCND1* gain) and VCaP (*CCND1* gain) showed higher cyclin D1 expression than PC3 (A/G870, *CCND1* gain), DU145 (A/A870, no *CCND1* gain) or LnCaP (A/G870, no *CCND1* gain), which had similar but much lower levels of cyclin D1 transcripts.

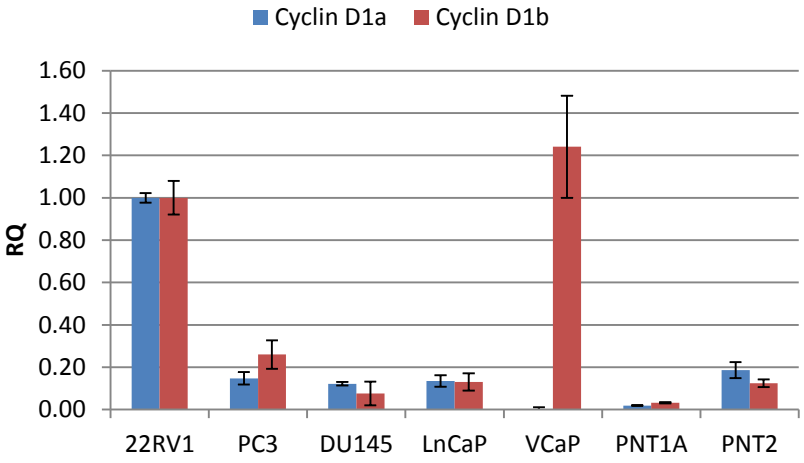

FIGURE 29. RNA EXPRESSION OF FULL LENGTH CYCLIN D1A AND ITS ALTERNATIVE SPLICE VARIANT, CYCLIN D1B IN PROSTATE CELL LINES.

For clinical samples qPCR quantification was possible in 5/6 bone metastases (samples 2 to 6), 4 primary tumours (WX samples) and 5 BPH samples. One metastatic sample (sample 1) was excluded from analysis due to poor RNA quality (no product was detected with cyclin D1 or β-actin primers after 40 cycles of qPCR).

Both cyclin D1 transcripts were detected in most of bone metastases, primary tumours, and all BPH samples (Figure 30). 5/9 cancer samples and 2/5 BPH samples expressed more cyclin D1b than cyclin D1a transcript (Figure 30, red boxes). Cyclin D1a transcript levels varied widely across the samples while Cyclin D1b levels were more consistent (Figure 31A). There was no correlation between cyclin D1a and cyclin D1b levels across the samples (p=0.1301, Spearman's rank test, Figure 31B).

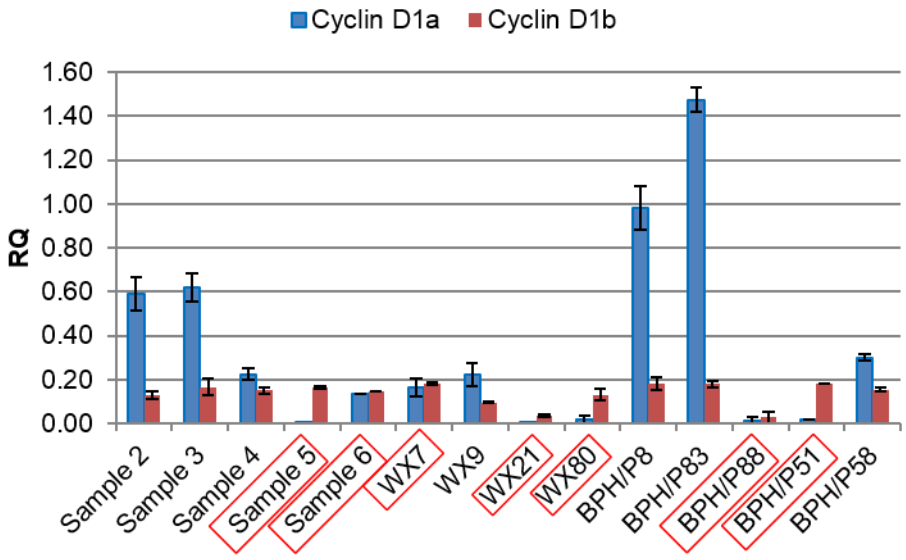

FIGURE 30. CYCLIN D1 TRANSCRIPTS EXPRESSION IN PROSTATE CLINICAL SAMPLES BY QPCR. Samples in red boxes express more cyclin D1b transcript. PCa bone metastases are positioned left (sample 2-6), primary tumours in the middle (WX cases), and BPH samples on the right. Presented RQ values were calibrated to expression levels in 22RV1 cell line.

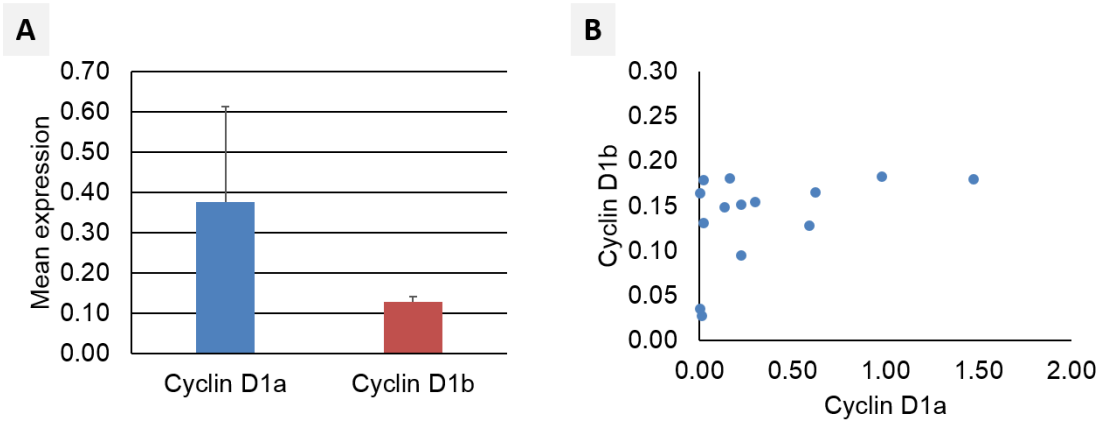

FIGURE 31. CYCLIN D1 TRANSCRIPTS EXPRESSION ACROSS PROSTATE CLINICAL SAMPLES BY QPCR. (A), mean transcript expression in all clinical prostate samples tested. (B), no correlation between cyclin D1a and b transcripts in the same patient set.

4.3 Discussion

4.3.1 11q13/*CCND1* gain is more prevalent in metastatic than primary PCa

MOR of copy number gain at 11q13-14 found in all analysed bone metastases falls within 11q12-24 region, which was previously found at higher frequency in more advanced/ metastatic PCa than localised tumours [150, 151, 226]. *CCND1* oncogene coding for cyclin D1 protein is the best candidate driver gene for this gained chromosomal region, as cyclin D1 overexpression is commonly involved in human cancer. Recent study found frequent *CCND1* gain/amplification at various metastatic sites (including bone) of mCRPC, implicating cyclin D1 involvement in advanced metastatic disease [138].

Further investigation of FFPE samples by FISH showed significantly higher prevalence of *CCND1* gain in bone metastasis (54.5%, 12/22) than in primary tumours (7%, 10/142; $p<0.0001$). Enrichment of metastatic samples in *CCND1* gain suggests its involvement in PCa tumour progression and metastasis. Similar to our study, Das *et al* [287] reported gain of 11q13 at *CCND1* locus to be more common in patients with bone metastasis (67%, 4/6) than in those without distant metastasis (23%, 9/40); unfortunately they had very limited number of bone samples. Additionally, they found significant association of 11q13 gain with higher Gleason score (Gleason 8-10, 50% versus 5-7, 12%). Another study looked at high level of *CCND1* amplification (≥ 3 fold) and considered it as a rare event in PCa, present in 2/172 (1.2%) of the primary tumours, 3/38 (7.9%) of local recurrences, and in 2/43 (4.7%) of the metastases (other than bone) [288]. We too, rarely saw high amplification of *CCND1* - only in 2 bone metastases and in none of the primary PCa. Presence of low copy number gain was unfortunately not included in their report. Recent study of 150 mCRPC biopsies from different metastatic sites, including 43 bone samples, found 11q13-14 region commonly gained in those samples, with *CCND1* amplification present in 9% of metastatic cases [138].

4.3.2 Cyclin D1 IHC staining intensity is stronger in bone metastases than in primary tumours

Following FISH analysis of 11q13/*CCND1* locus, cyclin D1 expression with IHC was examined in the same set of prostate samples. BPH samples commonly expressed cyclin D1 (33/43; 78.6%) but at low intensity and in a small proportion of nuclei (mean staining intensity = 1 and % of stained nuclei = 10%). Common but often focal cyclin D1 expression in our non-malignant samples is in agreement with other reports [289, 290], with recent study finding 72.2% (13/18) of BPH cases positive for cyclin D1 [290]. The

staining probably reflects the benign growth and enlargement of prostate glands seen in BPH condition. Cyclin D1 expression was more pronounced in cancer samples. Staining intensity had a tendency to be stronger in bone metastases than in primary tumours (median staining intensity 3 versus 2, p=0.015), with 53.5% (23/43) of bone metastases and only 32.2% (49/152) of primary tumours (p=0.018) expressing very strong staining intensity (score 3). In contrast, the percentage of stained nuclei was similar in both groups with cyclin D1 expression in 30% or less nuclei in majority of cases. Taken together, the results suggest, that similar proportion of cells express cyclin D1 in primary and metastatic tumours but with higher protein levels in bone metastases. It is possible that cyclin D1 staining positivity/intensity was affected in our FFPE bone metastatic samples by formic acid–based bone decalcification. Immunohistochemistry tests are commonly and successfully performed on decalcified bone marrow trephine biopsies obtained for bone marrow diseases. Still, suboptimal IHC results are not uncommon with weaker staining or high background leading to misinterpretation of the staining pattern [291]. Bigger excision samples are more problematic as they need to be decalcified for days and prolonged formic acid treatment was reported to reduce staining intensity [292]. As about half of our bone metastases were excision specimens, it is possible that cyclin D1 expression in those samples is underestimated due to extension of formic acid treatment.

Comparison of cyclin D1 IHC between studies is challenging due to use of different antibodies and variety of scoring systems [289, 293, 294]. Many of those antibodies exhibit limited sensitivity and specificity, and cyclin D1 IHC in pathology practice was reported as difficult, erratic, technically challenging and therefore not routinely used [286]. Reports on cyclin D1 expression in primary prostate tumours differ widely, ranging from as high as 63% (n=238) [289] - 71% (n=187) [293] to substantially lower; 11.6% (n=86) [295] - 22% (n=140) [294]. In our cohort, 85.5% (130/150) of primary PCa expressed cyclin D1, which is similar to recent study (same antibody) reporting 75.4% (64/85, cutoff >5%) primary tumours positive for cyclin D1 [296]. High grade PCa were reported to be more cyclin D1 positive than low grade tumours (18/64, 28% versus 13/76, 17%) [294] and one study found frequency of positive cyclin D1 immunoexpression (cut off ≥ 20%) significantly higher in PCa bone metastases (15/22, 68.2%) than localised tumours (10/86, 11.6%) [295]. There is an evidence, that increased cyclin D1 expression in advanced tumours can promote cancer cell migration and invasion. Fibroblasts, epithelial cells and macrophages have increased adhesion and reduced migration in the absence of cyclin D1 and cyclin D1 was reported to regulate transcription of genes that

promote migration and invasion (e.g. the Rho effector ROCK2) [268]. Furthermore, cyclin D1 may play a role in the maintenance of VEGF expression as administration of antisense to cyclin D1 in mouse models inhibited the growth of HCT116 and DLD1 xenografts. This direct anti-tumour effect of antisense to cyclin D1 was due to significant inhibition of tumour vessel formation accompanied by a significant reduction in VEGF expression [297]. Regardless of multiple studies confirming cyclin D1 role in tumorigenesis, its prognostic value in PCa is not currently clear. Early studies reported lack of independent prognostic value of cyclin D1 expression in PCa [294, 298]. In our study we looked at cyclin D1 staining intensity in relation to Gleason score and did not find correlation between these two (p=0.2276) despite using the most validated antibody (rabbit monoclonal, clone SP4), which was proven to provide results that are more consistent than those obtained with other antibodies [286]. Other studies using the same antibody also found no correlation between cyclin D1 expression and Gleason score or time to recurrence [299-301]. Lack of direct correlation of cyclin D1 with clinical features can be due to its often cooperative role in carcinogenesis with other oncogenes. Cyclin D1 is known to collaborate with HER2 or Ras oncogene to transform mammary gland epithelial cells or with c-MYC to induce B cell lymphomas in transgenic mice [278]. Indeed, in PCa cyclin D1 also seem to collaborate with other oncogenes to drive cancer progression and cyclin D1 expression was included in four gene signature (which involves inactivation of *PTEN* and *SMAD4* and activation of *CCND1* and *SPP1*), which was shown to be prognostic of PSA biochemical recurrence and to enhance the prognostic accuracy of the Gleason score in predicting metastatic lethal outcome [241]. Similarly, cyclin D1–regulated gene expression was recently associated with biochemical recurrence and poor prognosis in human PCa [302].

4.3.3 PCa samples with 11q13/*CCND1* gain show stronger cyclin D1 median staining intensity than cases with 11q13/*CCND1* neutral copy number

All samples with 11q13/*CCND1* copy number gain expressed cyclin D1. When we correlated 11q13/*CCND1* copy number status with cyclin D1 IHC, we found that bone metastases, as oppose to primary tumours, did not show correlation between cyclin D1 immunoexpression and 11q13/*CCND1* copy number status. However, when we grouped tumours based on 11q13/*CCND1* copy number status, cases with 11q13/*CCND1* gain had stronger cyclin D1 median staining intensity and showed staining in more cell nuclei than cases with 11q13/*CCND1* neutral copy number ($p<0.0001$ and 0.003, respectively), confirming correlation between 11q13/*CCND1* copy number gain and increased cyclin D1 immunoexpression. The small sample size of metastatic tumours could be the reason

for these discrepancies. It is well known that overexpression of cyclin D1 is generally much more common in cancer than can be explained by copy number gain or mutations [268]. As cyclin D1 is a key regulator of cell proliferation its expression is regulated by a variety of signalling pathways at the transcriptional level as well as post-transcriptionally, through mentioned above modulation of RNA splicing, nucleocytoplasmic transport, protein stability and degradation [279, 303]. Many factors, including mitogens such as growth factors, can induce cyclin D1 expression in cells without genetic alterations of *CCND1* locus, which would make a correlation between protein expression and gene copy number more difficult to detect. It is important to note, that although we chose the best validated antibody for cyclin D1 commercially available [286], this antibody was raised against part of C-terminus of cyclin D1 protein positioned within exon 5 of *CCND1* gene and therefore can only detect full length cyclin D1 (cyclin D1a) and not a truncated cyclin D1b protein, devoided of exon 5 [304].

Cyclin D1 overexpression in cancer is linked to cell cycle progression and increased cell proliferation [268]. Cyclin D1 induces cell cycle progression through inactivation of RB protein. Rb inactivation leads to accumulation of p16 which in turn blocks cyclin D1/CDK4 activity eventually causing cell cycle arrest [244]. Increased cell proliferation is additionally blocked by activation of p53 which leads to elevated levels of p21 and cell cycle arrest [245]. Therefore alterations within any of the genes in *CCND1/RB/CDKN2A* and *TP53/CDKN1A* pathways would impact cell proliferation. Three of the six bone metastases analysed by SNP arrays had confirmed copy number gain of *CCND1* and they all had medium cyclin D1 expression present in 10-20% of nuclei. Two of these cases had also loss of *RB*, while the other sample negative for *RB* loss displayed *CDKN2A* loss which is in agreement with general observation that inactivation of p16 and Rb TSGs is mutually exclusive in human cancers [244, 245]. These results imply that cancer cells rely on more than one mechanism to inactivate common pathway. Cyclin D1 overexpression coexist with loss of Rb or p16 in other cancers and is proposed as an early event, followed either by Rb loss, e.g. in SCLC [246] and parathyroid cancer [247] or p16 loss, e.g. in NSCLC [246]. Furthermore, all three cases with *CCND1* gain had also TP53 deletion which would protect the proliferating cells from cell cycle arrest caused by p53 dependent p21 overexpression.

4.3.4 Cyclin D1a and cyclin D1b transcript levels do not correlate with PCa progression.

Prostate cell lines including DU145, 22RV1, LAPC4, LnCaP and PC3 are known to express both cyclin D1a and D1b transcripts [285]. We also found both transcripts in most of the tested PCa cell lines, including DU145, 22RV1, LnCaP and PC3, and 2 immortalised epithelial cell lines PNT1A and PNT2. Only VCaP cells expressed high levels of cyclin D1b but had no cyclin D1a transcript. Similar to previous report [285] cyclin D1 transcripts expression levels did not correlate with A/G870 polymorphism and they also did not correlate with *CCND1* copy number status. It is plausible that in addition to genetic changes at *CCND1* locus different regulatory mechanisms as well as phase of cell cycle the cells are in are affecting cyclin D1 expression levels in PCa cells. Same can be true for our limited set of fresh-frozen clinical samples, where we also saw no relation with cyclin D1 transcripts levels and *CCND1* copy number status (known in PCa bone metastases) or cancer progression. All samples: BPH, primary PCa and bone metastases displayed cyclin D1b at similar levels and most also expressed cyclin D1a transcript but the levels varied widely across the samples. Burd *et al* [285] detected cyclin D1b in all 5 samples tested with lower levels in two matched normal tissues but higher expression in other two PIN samples compared to matched tumours. The single lymph node metastasis tested also expressed cyclin D1b. They further showed that in contrary to cyclin D1a, cyclin D1b was compromised for regulation of multiple AR target genes (including PSA), and whereas cyclin D1a significantly attenuated androgen-dependent proliferation in AR positive LnCaP cells, cyclin D1b promoted cell-cycle progression. In AR negative PC3 cells ectopic expression of either transcript did not affect cell proliferation. Therefore, they concluded that cyclin D1b expression may yield a significant growth advantage in AR-positive PCa cells. Three of our bone metastases (sample 4, 5, and 6) had copy number gain at AR locus, implying increase in AR pathway and they did not show higher cyclin D1b levels. They also seem to have less cyclin D1a transcript than cases without AR gain. However, we cannot exclude that tumours without AR gain have AR pathway activated by other means e.g. activating mutations in AR locus as they are very common in advanced PCa.

Assessment of cyclin D1b protein levels is currently hampered by lack of commercially available antibody. Comstock *et al* [282] used non-commercial cyclin D1b antibody to assess by IHC cyclin D1b expression in a cohort of microarrayed human prostate specimens (1,626 cores), containing non-neoplastic tissue, PIN lesions, and adenocarcinomas. They found that cyclin D1a and D1b showed distinct profiles in PCa,

with significant subset of tumours expressing cyclin D1b. Mean cyclin D1a levels were similar in non-neoplastic tissue, PIN or adenocarcinomas while cyclin D1b expression was elevated in tumours compared with non-neoplastic tissue ($p<0.004$), suggesting that cyclin D1b isoform may be specifically induced in PCa [282].

Persistent expression of cyclin D1 in primary and metastatic PCa tumours suggests that cancer cells requires cyclin D1 expression for their tumourigenic potential. Significantly higher frequency of *CCND1* gain in metastatic than primary tumours indicates that acquirement of 'genetic fix' allowing continuous cyclin D1 expression is advantageous for PCa cell survival and sustained metastatic growth in bone microenvironment. Further studies are necessary to assess exact function of cyclin D1 and its splice variants in PCa bone metastases.

CHAPTER 5

Analysis of 6q16/*FBXL4* loss in PCa

5.1 Introduction

Copy number losses within the 6q14-22 region were present in all 6 bone metastases with minimal overlapping region at 6q16.2. The 6q12-22 deletion is one of the most common deletions in PCa with the frequency of 22–62% [115, 119, 305]. Loss of 6q13-q22 is widely present in advanced mCRPC [119, 150, 151, 236, 306]. Genes located at 6q16 could play an important role in metastatic cancer progression as among six major loss of heterozygosity (LOH) regions in PCa (6q14-16, 8p23-11, 10q23, 13q13-21, 16q21-24 and 21q22.2), LOH at 6q14-16 was reported as the only LOH region showing a tendency towards a higher degree of copy number loss in metastatic and low differentiated tumours [226].

Only two known genes are located within 6q16.2 minimal overlapping region: *POU3F2* and *FBXL4*. *POU3F2* codes for Brn2, a member of the mammalian class III POU transcription factor family (includes Brn1, Brn2, and Oct6), which is widely expressed in the developing mammalian central nervous system and involved in cortical neural migration and neurogenesis [307, 308]. Brn2 expression is also present in melanocytes (originating from melanoblasts, a sub-population of neural crest cells), where is involved in the determination of melanocytic phenotype [309]. In melanoma lesions, cells expressing high levels of Brn2 show enhanced proliferation [310] and invasive and metastatic capacity [311]. Therefore, *POU3F2* is regarded as a proto-oncogene involved in melanocytic growth and tumourigenesis [312]. Small cell lung cancers (SCLC) are neuroendocrine tumours and similar to melanoma cell lines also overexpress Brn2, which is involved in accelerating cell proliferation and plays important roles in maintaining characteristic biological behaviour of SCLC [313]. Considering that *POU3F2* seems to be expressed only in cells of neural origin where it behaves as an oncogene, it is unlikely that this gene is a driver for 6q16 loss.

There is little known about *FBXL4* function. *FBXL4* gene product belongs to a large F-box protein family. F-box proteins are part of E3 ubiquitin protein ligase complex called the SKP1-CUL1-F-box (SCF) complex, which orchestrates phosphorylation dependent protein ubiquitination and degradation [314]. Through substrate downregulation, F-box proteins regulate diverse biological pathways that control cell growth, division, development and differentiation, signalling responses, cell survival and death [315]. Therefore, it is not surprising, that more and more evidence emerges about deregulation

of F-box proteins in human cancer and its impact on cancer development, progression and metastasis [316-318]. Several F-box proteins are known TSGs and are downregulated in cancer e.g. due to mutations (*FBXW7* in endometrial, colorectal, stomach cancer; *FBXO4* in oesophageal cancer) or deletions (*FBXO18* in melanoma), while others act as oncogenes and are overexpressed in several cancers (*SKP2* in lymphoma, prostate, colorectal, melanoma, pancreatic, breast cancer) [318]. It is possible that *FBXL4* acts as a TSG in PCa and therefore is a target gene for 6q16 loss.

5.2 Results

5.2.1 FISH analysis of FFPE samples finds 6q16/*FBXL4* loss in half of PCa bone metastases and in a small subset of primary tumours

Due to limited numbers of fresh samples available for array analysis, we used the FISH method to study *FBXL4* copy number in a larger cohort of FFPE samples, including 43 bone metastases, 152 primary tumours and 55 non-malignant BPH samples, which were used as controls. FISH analysis of *FBXL4* locus was successfully performed in 23/43 of PCa bone metastases, 145/152 of primary tumours and all BPH samples. The *FBXL4* region was lost in 11/23 (47.8%) of bone metastases and in 20/145 (13.8%) of primary tumours. None of the BPH samples harboured *FBXL4* loss. Overall, there was a significant difference in the frequency of *FBXL4* copy number loss between primary tumours and bone metastases ($p<0.0001$, Chi-square test) with more frequent *FBXL4* loss in bone metastases (Table 43). Examples of *FBXL4* copy number loss are shown in Figure 32.

TABLE 43 FREQUENCY OF *FBXL4* LOSS DETECTED BY FISH IN PRIMARY AND METASTATIC PCA.

PCa types	*FBXL4* copy number loss		p value (X^2 test)
	positive	negative	
Primary	20/145 (13.8%)	125/145 (86.2%)	0.0003
Bone metastases	11/23 (47.8%)	12/23 (52.2%)	

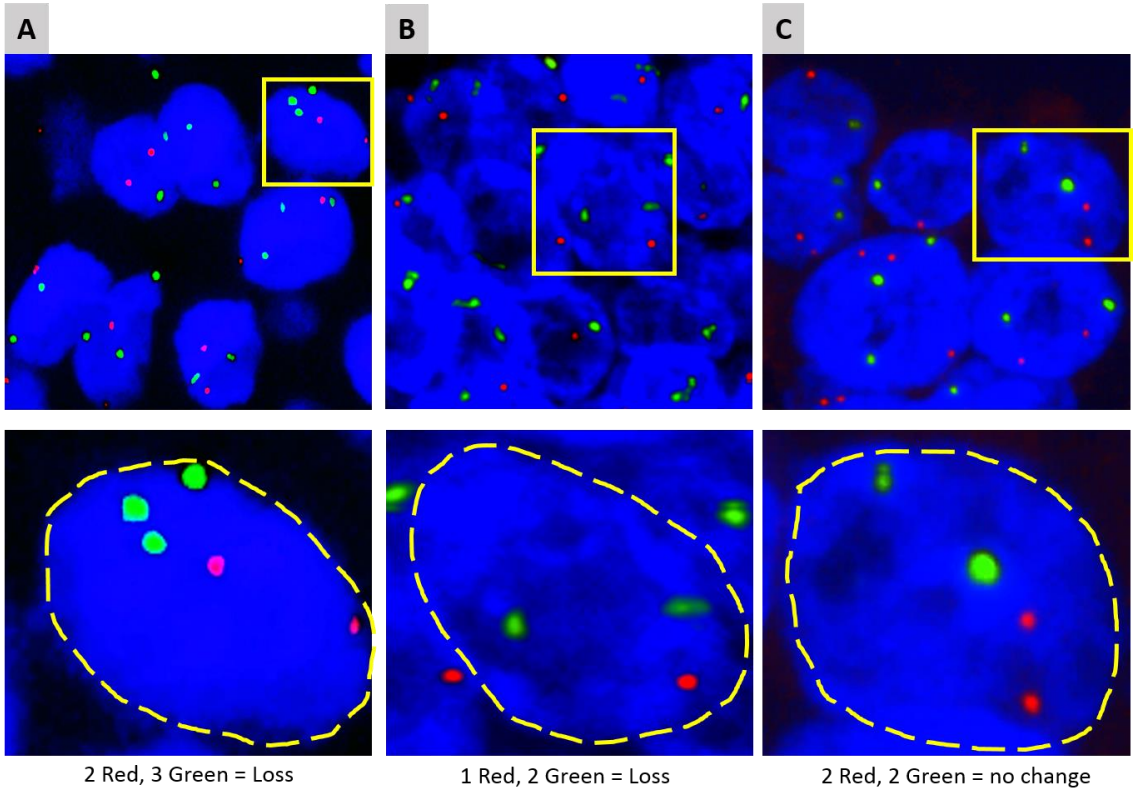

FIGURE 32. REPRESENTATIVE FISH IMAGES OF COPY NUMBER CHANGES AT FBXL4 IN PROSTATE SAMPLES. (A) and (B) respectively: *FBXL4* loss in PCa bone metastasis and primary PCa; (C), BPH with neutral copy number at *FBXL4* locus. Red, 6q16 locus; green, control locus; blue, nuclei (DAPI). A minimum of 100 nuclei (cells) with clear hybridization signals were counted per tissue sample. Nuclei with same number of red and green signals were considered as no copy number change. Nuclei with less red than green signal were considered as positive for FBXL4 copy number loss. Lower panel shows enlarged single nuclei (depicted in yellow dotted line) from the top pictures (yellow boxes) to illustrate copy number assessement for each exemplar nucleus. The percentage of nuclei with less red than green signals were determined per sample and the widely accepted cutoff calculated as the mean of false-positive findings in ten non-malignant controls (BPH samples) plus three times the standard deviation (mean % ± 3SD) was used for FBXL4 copy number status evaluation in each sample.

5.2.2 *FBXL4* copy number loss in conservatively managed localised PCa correlates with cancer progression

FBXL4 copy number status was then investigated in a large cohort of conservatively managed localised PCas diagnosed by TURP, in order to assess *FBXL4* loss as a potential cancer prognostic marker. *FBXL4* loss was present in 77/447 (17%) cases successfully analysed by FISH. *FBXL4* loss strongly correlated with high Gleason score and clinical stage (p=0.000002 and 0.0005, respectively, Table 44) as well as with PSA levels and extent of disease (p=0.00015 and 0.000049, respectively). Loss of *FBXL4* was also significantly associated with poor patient survival (HR 1.738, p=0.009; Figure 33) by univariate analysis. However, since loss of *FBXL4* was strongly correlated with

other poor prognosis factors such as PSA, the correlation with poor patient outcome lost significance in multivariate analysis when Gleason score, baseline PSA and extent of the disease were simultaneously included in the analysis model (Table 45). Therefore, although loss of *FBXL4* significantly correlates with advanced disease, it cannot be used as an independent prognostic factor for PCa survival.

TABLE 44. CORRELATION OF FBXL4 LOSS WITH GLEASON SCORES AND CLINICAL STAGES.

Parameter	No *FBXL4* loss	*FBXL4* loss	p value (X^2 test)
Gleason score <7	197	20	0.000003
Gleason score =7	97	22	
Gleason score >7	76	35	
Clinical stage T1	104	10	0.0005
Clinical stage T2	83	32	
Clinical stage T3	40	16	
Clinical stage Tx	63	11	

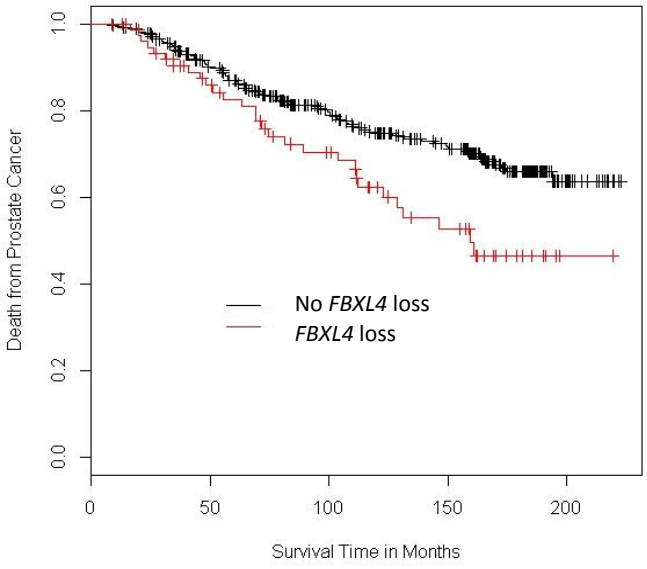

FIGURE 33. *FBXL4* LOSS IS SIGNIFICANTLY ASSOCIATED WITH DECREASED PCA SPECIFIC SURVIVAL. Kaplan–Meier survival curves represent conservatively managed localised prostate cancers with or without FBXL4 loss (HR 1.74, p=0.009).

TABLE 45. MULTIVARIATE ANALYSIS OF CLINICOPATHOLOGICAL PARAMETERS.

Parameter	HR (95% CI)	P value
FBXL4 loss	0.750	0.225
Gleason score <7 vs. =7	0.750	0.253
Gleason score >7	5.579	0.000002
PSA	1.366	0.007
Clinical stage T1	0.702	0.339
Clinical stage T2	0.964	0.901
Clinical stage T3	0.961	0.890
Extent of the disease	3.876	0.0001

5.2.3 *FBXL4* expression

5.2.3.1 *FBXL4* RNA expression is reduced in PCa

After confirmation of common *FBXL4* loss in PCa, I looked at *FBXL4* RNA expression in fresh-frozen samples from bone metastases, primary PCa and BPH. Relative *FBXL4* expression levels of all bone metastases and 3/4 primary PCa (WX samples) analysed were lower than in 6 BPH samples (Figure 34, Table 46) and the difference was statistically significant between the 3 groups (p=0.0079, Kruskal-Wallis test). Prostate cell lines also had low expression levels of *FBXL4*. 22RV1, LNCaP and VCaP cell lines with no *FBXL4* copy number loss had relatively higher *FBXL4* levels than PC3 and DU145 cell lines, which are positive for *FBXL4* loss. Surprisingly, normal epithelial cell lines immortalised with SV40, PNT1A and PNT2 displayed the lowest *FBXL4* expression (Figure 35).

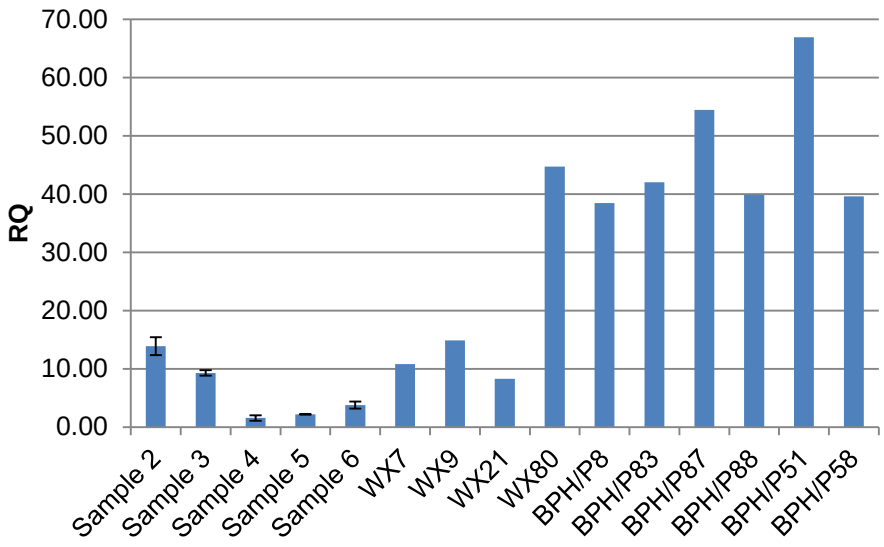

FIGURE 34 *FBXL4* EXPRESSION LEVELS IN PROSTATE CLINICAL SAMPLES MEASURED BY Q-RT-PCR. PCa bone metastases are positioned left (Sample 2-6), primary tumours in the middle (WX cases), and BPH samples on the right. RQ values presented here were calibrated to expression levels in 22RV1 cell line.

TABLE 46 DIFFERENCE IN *FBXL4* TRANSCRIPT EXPRESSION BETWEEN PCA BONE METASTASES, PRIMARY TUMOURS AND BPH SAMPLES.

Sample	*FBXL4* Median	*FBXL4* Mean	*FBXL4* SE	p value (Kruskal-Wallis test)
PCa bone metastases	3.8	6.1	2.37	0.0079
Primary PCa	12.8	18.5	7.27	
BPH	53.3	53.3	6.10	

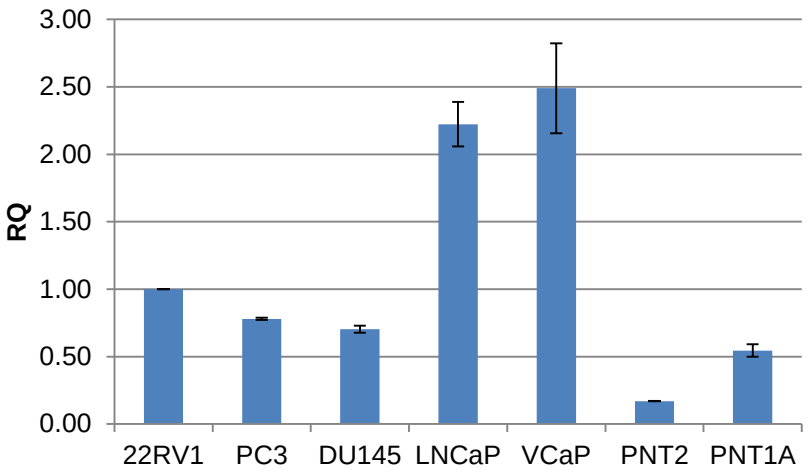

FIGURE 35 *FBXL4* EXPRESSION IN PROSTATE CELL LINES MEASURED BY QPCR. LNCaP, VCaP and 22RV1 PCa cell lines without *FBXL4* loss show higher *FBXL4* expression than PC3 and DU145 cells positive for *FBXL4* loss. Normal immortalised prostate epithelial cells PNT2 and PNT1A also have low *FBXL4* expression levels. *FBXL4* expression was measured by relative quantification method with *GAPDH* as endogenous control and 22RV1 cell line as a calibrator sample.

5.2.3.2 *FBXL4* protein expression

5.2.3.2.1 Anti-FBXL4 antibody testing using inducible protein expression in HEK293 cells

The predicted size of FBXL4 protein is 70.1 kDa. Based on RNA expression analysis, endogenous levels of FBXL4 are low in PCa cell lines, which make it difficult to test anti-FBXL4 antibodies. There are several commercially available anti-FBXL4 antibodies, however all published data is based on tagged FBXL4 protein overexpression models, implying low specificity/sensitivity of available antibodies [319-321]. Tetracycline-Regulated Expression System for Mammalian Cells (T-Rex-293 System) was used for anti-FBXL4 antibody testing. We generated stable single clones of T-Rex-293 cells containing expression vector with FBXL4 cDNA tagged at C-terminus with flag, which highly overexpressed FBXL4 from the vector upon tetracycline treatment, ensuring easier protein detection. Addition of flag tag allowed for easy monitoring of FBXL4 protein overexpression and identification of FBXL4-specific band on WB. FBXL4 overexpression upon tetracycline treatment was confirmed at RNA level by qRT-PCR (Figure 36). Of five anti-FBXL4 antibodies tested by WB and IHC, only two were specific: rabbit polyclonal from Abcam (ab153812) and mouse monoclonal antibody from Santa Cruz (sc-81270). On WB, both antibodies produced a band at 70 kDa (FBXL4 protein size) only in protein lysates from cells with FBXL4 overexpression, with rabbit antibody ab153812 performing

better and producing stronger band under less exposure time, than mouse antibody sc-81270 (Figure 37A and B). Specificity of the observed band was confirmed by two different anti-flag antibodies, which also detected the same bands in protein lysates from FBXL4 overexpressing cells, at the same time confirming FBXL4 overexpression from the vector (Figure 37C and D). Testing the antibodies for IHC showed increased staining in FBXL4 overexpressing cells for both antibodies when compared to control cells (Figure 38), proving that they are both able to detect FBXL4 protein. However, in terms of staining quality the antibodies produced opposite results to WB. Mouse antibody sc-81270 produced superior results to rabbit antibody ab153812, with sharper and much stronger staining in FBXL4 overexpressing cells (Figure 38A and B). Based on these data, all further assessment of FBXL4 protein expression by WB was done with rabbit antibody ab153812, while IHC analysis was performed with mouse antibody sc-81270.

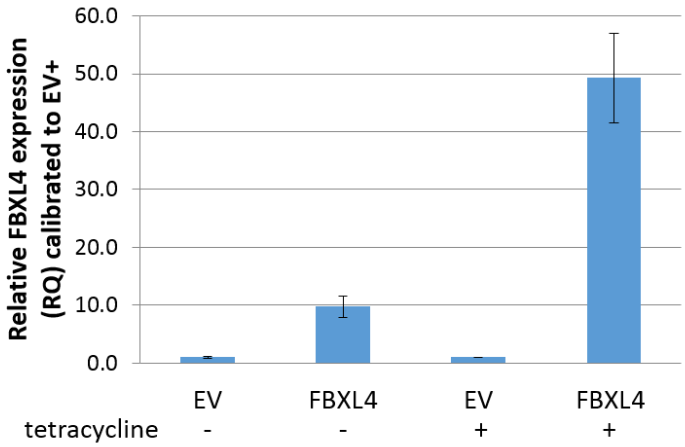

FIGURE 36. CONFIRMATION OF FBXL4 RNA OVEREXPRESSION IN HEK293 CELLS. EV, control cells with empty expression vector; FBXL4, HEK293 cells transfected with expression vector containing *FBXL4-Flag*. '-', no tetracycline treatment; '+', 1µg/ml tetracycline treatment. Error bars indicate SD; n = 3.

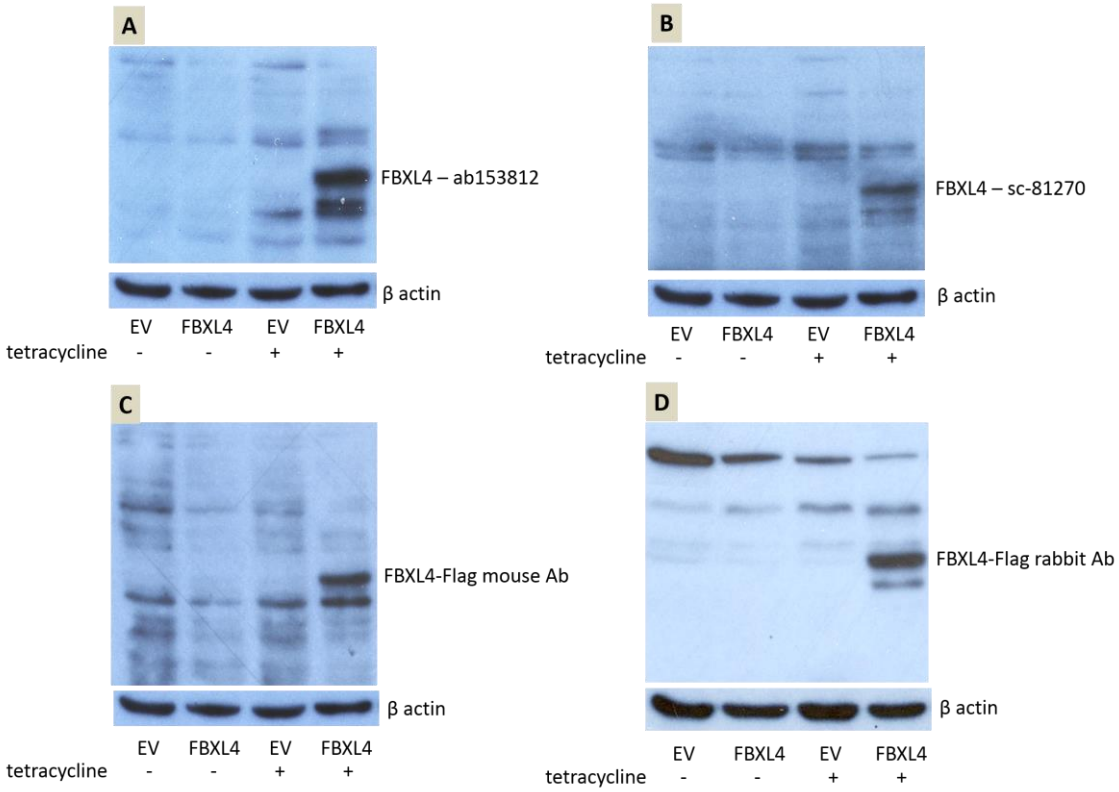

FIGURE 37. ANTI-FBXL4 ANTIBODIES SPECIFICITY IN HEK293 C-FLAG FBXL4 OVEREXPRESSION SYSTEM BY WB. Both anti-FBXL4 antibodies; rabbit ab153812 (A) and mouse sc-81270 (B) produced bands at 70 kDa (size of FBXL4 protein) in protein lysates from FBXL4 overexpressing cells treated with 1µg/ml tetracycline over 48 h. Specificity of supposed FBXL4 bands was confirmed with two anti-Flag antibodies (C) and (D), both producing same bands as anti-FBXL4 antibodies in FBXL4 overexpressing cell lysates. EV, control cells with empty expression vector; FBXL4, HEK293 cells transfected with expression vector containing *FBXL4-Flag*. '-', no tetracycline treatment; '+', 1µg/ml tetracycline treatment. Protein load: 100 µg.

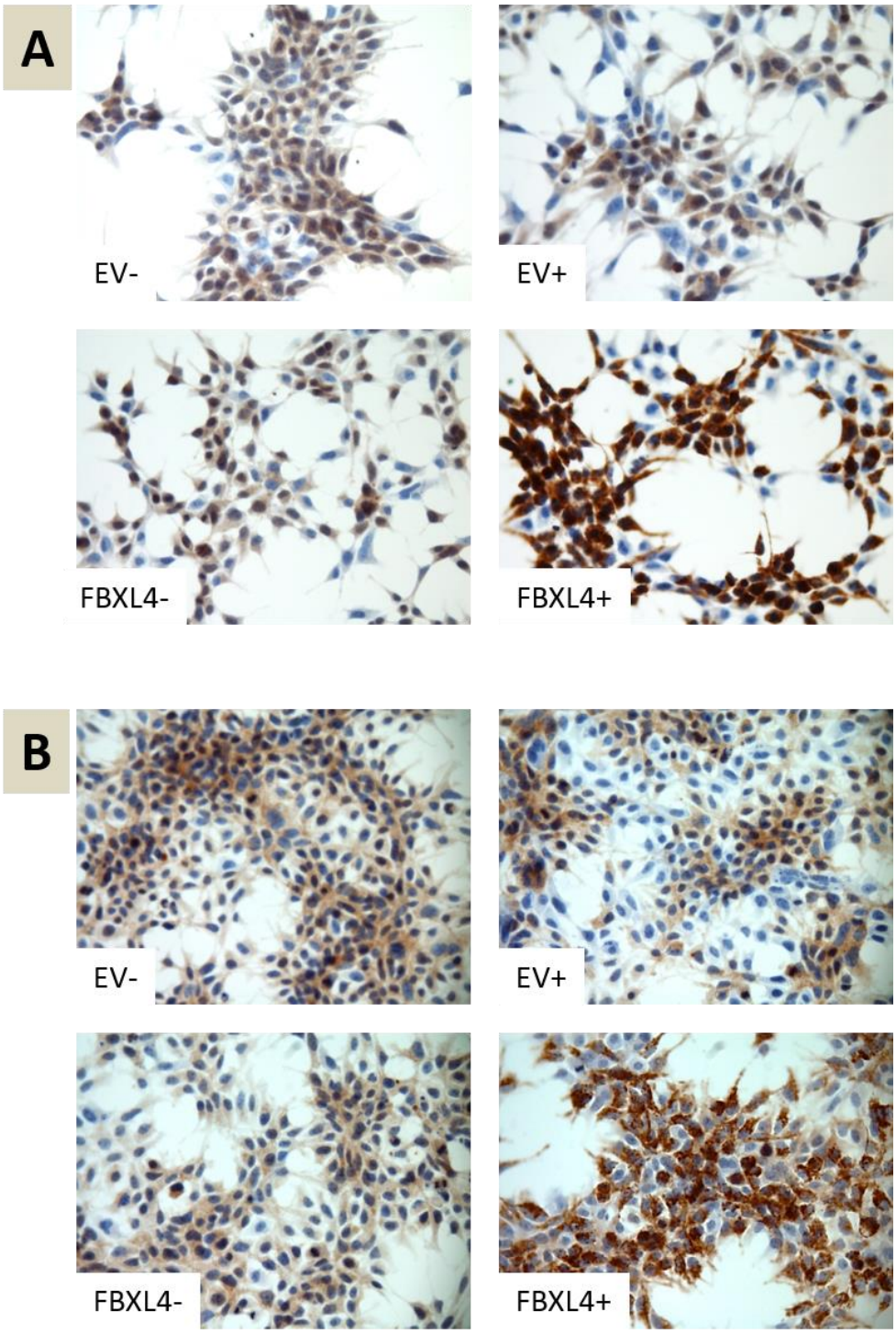

FIGURE 38. CONFIRMATION OF FBXL4 PROTEIN DETECTION BY IHC WITH ANTI-FBXL4 ANTIBODIES IN HEK293 CELLS OVEREXPRESSING FBXL4. FBXL4 protein staining in FBXL4 overexpressing cells shows that mouse anti-FBXL4 sc-81270 antibody (A) produces stronger staining than rabbit ab153812 (B). Both antibodies also seem to detect endogenous levels of FBXL4 in control cells. EV, control cells with empty expression vector; FBXL4, HEK293 cells transfected with expression vector containing *FBXL4-Flag*. '-', no tetracycline treatment; '+', 1µg/ml tetracycline treatment.

5.2.3.2.2 FBXL4 overexpression is lost in PCa cell lines upon selection for stable clones

Stable PCa cell lines transfected with C-flag FBXL4 expression vector were generated upon antibiotic selection for 3 weeks. As DU145 and PC3 cells have FBXL4 loss and express relatively lower FBXL4 RNA levels than cells without FBXL4 copy loss such as 22RV1, we used a constitutive gene expression system to generate stable cells. In case of 22RV1 cells, which already have reasonably high FBXL4 expression we used a tetracycline inducible system to avoid potential toxicity from too high levels of TSG. Initial FBXL4 overexpression was confirmed at RNA levels by qRT-PCR and was very strong 24 h post-transfection/tetracycline treatment. However, it was substantially reduced within the next 48 h, especially in DU145 and 22RV1 cells (Figure 39A). After continuous selection with antibiotics over 3 weeks for stable cell population a substantial decrease in RNA levels of FBXL4 was noticed in all transfected cell lines. PC3 cells on average expressed only five times more FBXL4 RNA than transfection control (Figure 39B). DU145 cells completely lost initial FBXL4 overexpression and returned to FBXL4 levels seen in non-transfected cells (Figure 39C). Inducible expression system used for 22RV1 cells also produced only minor, four-fold increase in FBXL4 levels when compared to transfection control (Figure 39D). About one fold leakage was observed in cells transfected with C-Flag *FBXL4* vector without tetracycline treatment. FBXL4 protein analysis by WB generally showed very weak FBXL4 bands and no increase in FBXL4 band size in FBXL4 overexpressing cells when compared to control cells (Figure 40).

Reduction of FBXL4 expression levels upon continuous antibiotic selection could be explained by the death of the cell population with FBXL4 expression vector and remaining untransfected cells acquiring resistance to antibiotic. Therefore, presence of FBXL4 expression vector was tested by PCR in stable cell populations using a forward primer located within the C-terminus of FBXL4 sequence and a reverse primer located within the vector backbone sequence. All stable cell populations transfected with FBXL4 expression vector still contained the vector, and therefore, capacity to express FBXL4 (Figure 41A).

Unsuccessful attempts to overexpress FBXL4 in three different PCa cell lines led us to test constitutive FBXL4 overexpression over a prolonged period of time in T-Rex-293 cells in order to see if the FBXL4 overexpression would also disappear over time. As T-Rex-293 is a tetracycline-inducible system, we continuously treated the cells with tetracycline over a six week-period, mimicking constitutive FBXL4 expression system

used in PC3 and DU145 cells. In contrary to PCa cells, constant induction of FBXL4 expression in HEK293 cells led to continuous and relatively stable FBXL4 overexpression (Figure 41B). The presence of FBXL4 expression vector in HEK293 over a period of time was confirmed with PCR (Figure 41C).

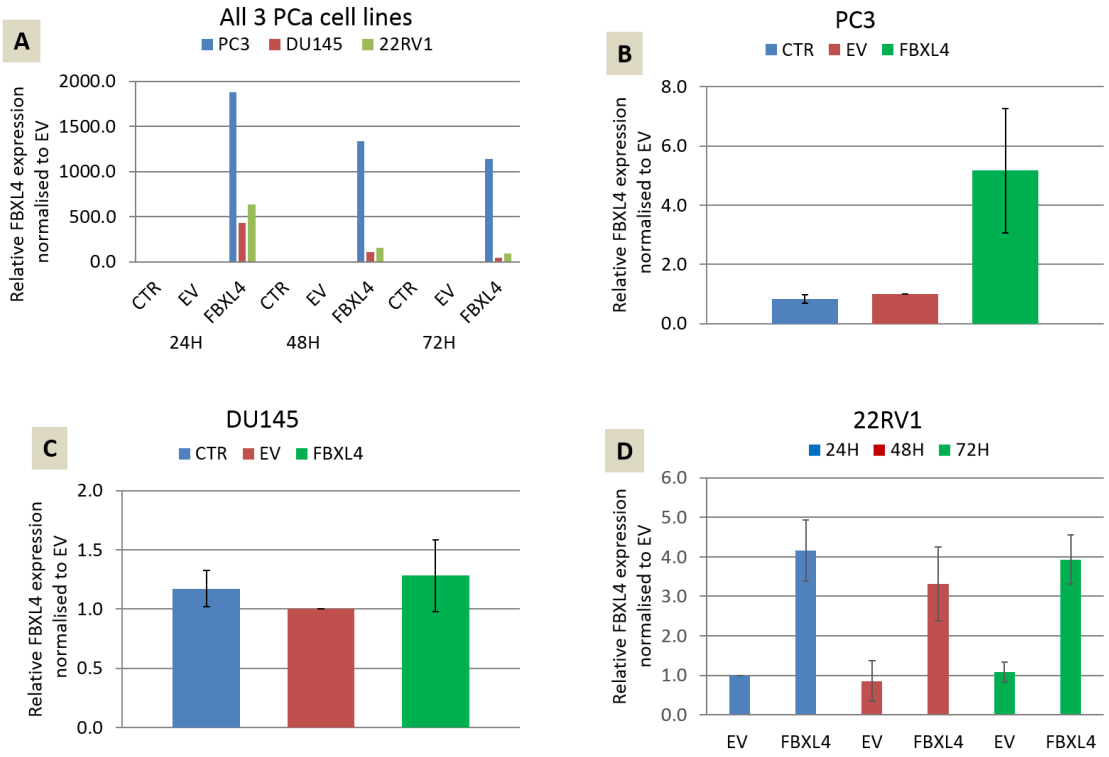

FIGURE 39. PCA CELL LINES FAIL TO STABLY EXPRESS HIGH LEVELS OF FBXL4 PROTEIN. Initial cell transfection with C-flag FBXL4 led to high levels of FBXL4 RNA in all 3 cell lines tested (A). However, upon 2 weeks of antibiotic selection for stable cell population, FBXL4 expression levels dropped dramatically with PC3 cells having FBXL4 expression only 5 times higher than in transfection control (B), and DU145 FBXL4 RNA expression returning to endogenous levels (C). 22RV1 cells showed similar levels of FBXL4 RNA to PC3 cells upon 24, 48 and 72 h of 1µg/ml tetracycline treatment after two weeks of selection (D). CTR, untreated cells; EV, control cells with empty expression vector; FBXL4, cells transfected with expression vector containing C-Flag *FBXL4*. Error bars, SD.

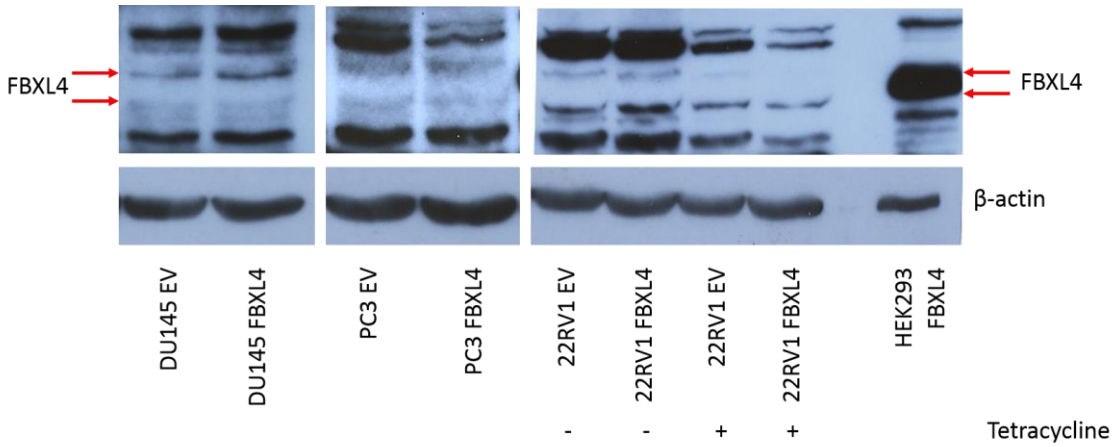

FIGURE 40. LACK OF FBXL4 PROTEIN OVEREXPRESSION IN STABLE PCA CELL LINES. Neither constitutive expression system (DU145 and PC3) nor tetracycline inducible system (22RV1) produced FBXL4 protein overexpression in PCa cell lines. Protein load: 100 µg.

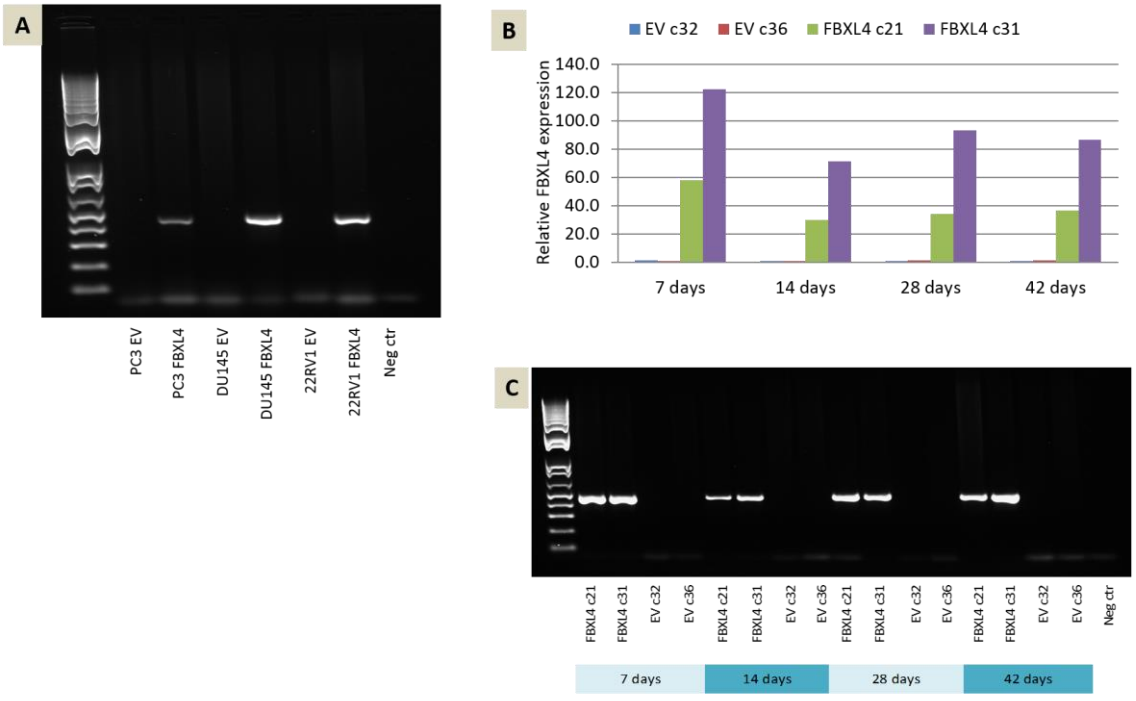

FIGURE 41. STABLE CELL POPULATIONS RETAIN FBXL4 EXPRESSION VECTOR. All PCa stable cell lines were positive for presence of FBXL4 expression vector (A). HEK293 stable clones (two with FBXL4 expression vector and two controls) continuously overexpressed FBXL4 over 42 days of tetracycline treatment (B). Presence of FBXL4 expression vector was confirmed with PCR (C). EV, control cells with empty vector; FBXL4, cells with FBXL4 expression vector.

5.2.3.2.3 Anti-FBXL4 antibody testing using protein downregulation models

FBXL4 knockdown was performed with siRNA and shRNA. Transient *FBXL4* knockdown with siRNA led to 60-70% reduction in *FBXL4* RNA levels in all three cell lines tested (Figure 42A-C). Stable *FBXL4* knockdown performed with shRNA in 22RV1 cells produced the best results for single clone 19 and 26, with *FBXL4* RNA reduction of 60% (Figure 42D).

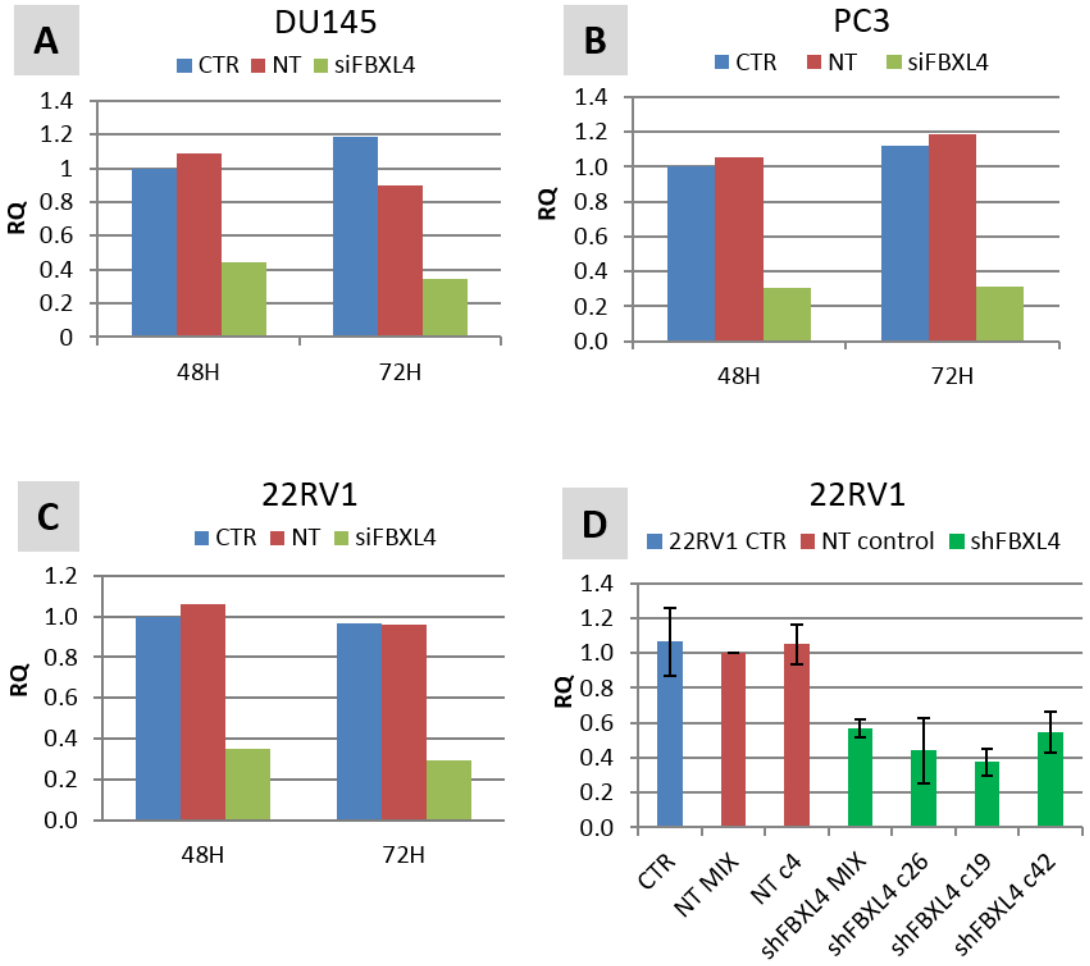

FIGURE 42. FBXL4 KNOCKDOWN IN PCA CELL LINES. *FBXL4* was successfully knockdown by siRNA in DU145 (A), PC3 (B) and 22RV1 (C) cells. NT, cells transfected with non-targeting siRNA smartpool; siFBXL4, cells transfected with anti-*FBXL4* siRNA smartpool. Stable *FBXL4* knockdown in 22RV1 cells with shRNA (D). *FBXL4* RNA levels are normalised to mock-transfectd cells. CTR, mock-transfected cells; NT, cells transfected with non-targetting siRNA/shRNA; siFBXL4/shFBXL4, cells transfected with anti-FBXL4 siRNA/shRNA; c, single clone; MIX, mixed stable cell population. Error bars, SD.

If the observed good FBXL4 knockdown at RNA level translates into downregulation of FBXL4 protein, it should be detectable with anti-FBXL4 antibody by WB. In general,

endogenous FBXL4 protein levels were difficult to detect with tested antibody, as it produced weak FBXL4 bands (Figure 43) and in PC3 cells the bands were hardly visible at all. Longer exposure resulted in background bands becoming so strong that they obscured FBXL4-specific bands. Transient FBXL4 knockdown in 22RV1 and DU145 cell lines was undetectable on WB, with FBXL4 bands size and intensity similar in control and knockdown cells (Figure 43A). Stable FBXL4 knockdown in 22RV1 was tested in protein lysates from uniform single clone cell populations, however the antibody still could not detect differences in FBXL4 expression between FBXL4 knockdown and control clones (Figure 43B), suggesting that anti-FBXL4 antibody was not sensitive/specific enough to detect FBXL4 protein reduction beyond endogenous levels or possibly there was no reduction in FBXL4 protein levels. Testing the IHC-specific anti-FBXL4 antibody in 22RV1 cells with stable (Figure 44A) or transient (Figure 44B) FBXL4 knockdown also produced similar results. IHC staining was reasonably strong with uniform cytoplasmic pattern but no reduction in staining intensity was present in FBXL4 knockdown cells.

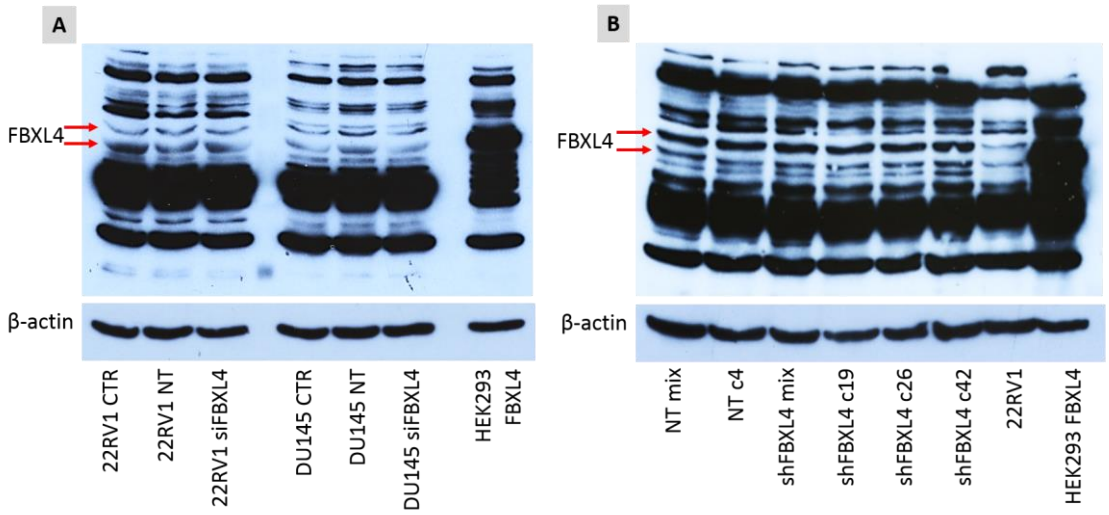

FIGURE 43. FBXL4 KNOCKDOWN IN PCA CELL LINES IS UNDETECTABLE AT PROTEIN LEVELS BY WB. (A) FBXL4 protein levels after knockdown with siRNA in 22RV1 and DU145 cells. (B) FBXL4 protein levels after knockdown with shRNA in 22RV1 cells. CTR, mock-transfected cells; NT, cells transfected with non-targetting siRNA/shRNA; siFBXL4/shFBXL4, cells transfected with anti-FBXL4 siRNA/shRNA; c, single clone; MIX, mixed stable cell population. Protein load: 100 µg.

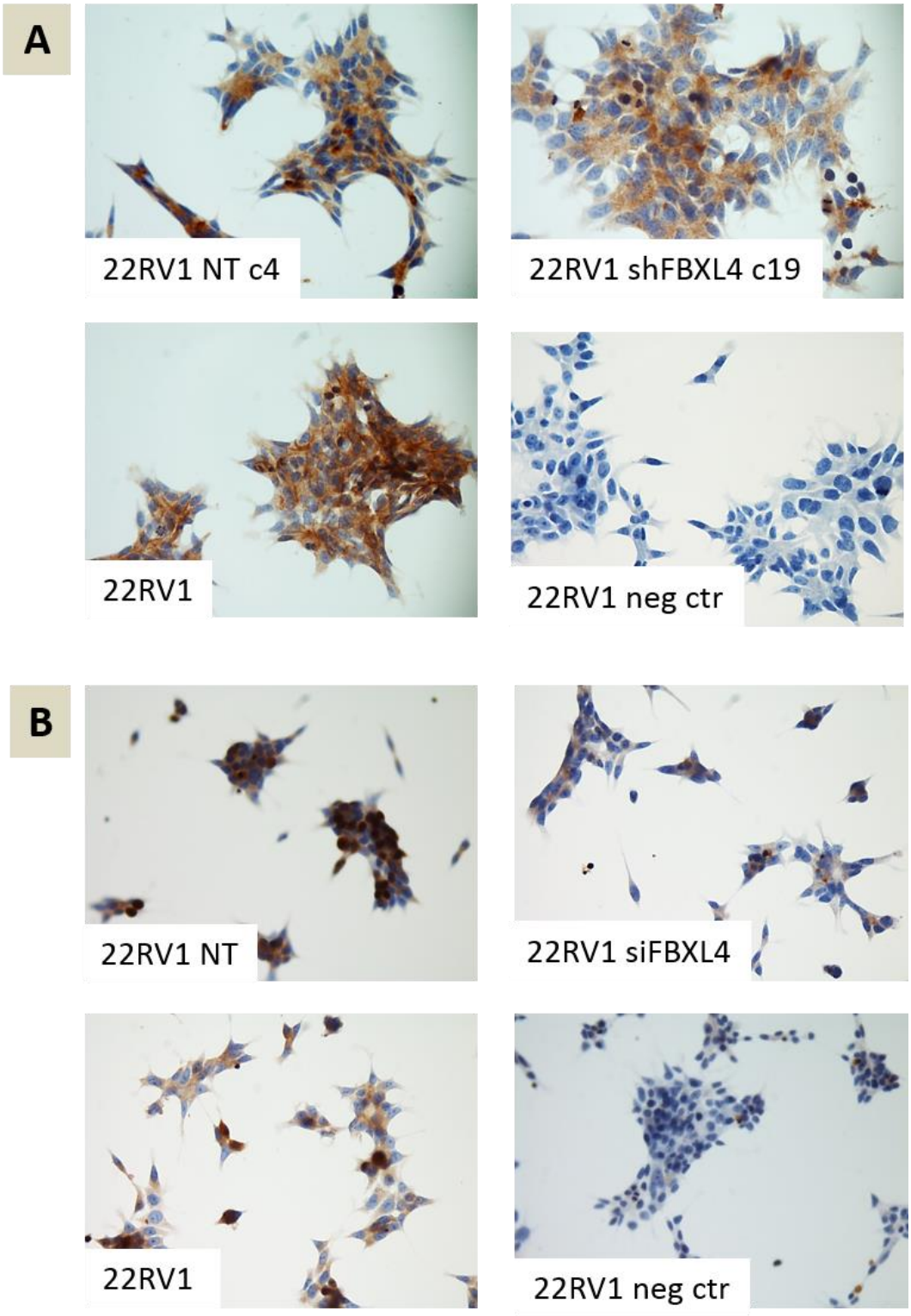

FIGURE 44. ANTI-FBXL4 ANTIBODY FAILS TO DETECT FBXL4 DOWNREDULATION BY IMMUNOHISTOCHEMISTRY IN 22RV1 CELLS. 22RV1 cells show similar staining intensity for FBXL4, regardless of treatment with anti-FBXL4 siRNA (A) or shRNA (B). NT, cells transfected with control non-targeting siRNA/shRNA; siFBXL4/shFBXL4, cells transfected with anti-*FBXL4* siRNA/shRNA.

5.2.3.2.4 FBXL4 protein immunoexpression in FFPE PCa samples

IHC for FBXL4 was successfully performed in 43 bone metastases, 120 primary PCa and 20 BPH non-malignant controls (staining examples shown in Figure 45). FBXL4 staining pattern was cytoplasmic and scored based on staining intensity (score from 0 to 3).

Thirty-five of 43 (81.4%) bone metastases showed various levels of FBXL4 immunoexpression with remaining eight samples (18.6%) negative for FBXL4 staining. Most of the cases positive for FBXL4 were weakly or moderately stained (22/35, 62.9%). Slightly more primary tumours stained for FBXL4 (113/120, 94%) with majority expressing FBXL4 at low or medium levels (100/113, 88.5%). Similar proportion of non-malignant BPH tissues stained for FBXL4 (19/20, 95%), however most cases showed moderate (9/20, 45%) and strong (10/20, 50%) FBXL4 expression (Figure 46A, Table 47). There was a significant difference in FBXL4 staining intensity between those 3 groups ($p=0.0005$, Kruskal-Wallis test, Figure 46B and Table 47). Further group analysis using Mann-Whitney U test (significance levels corrected with Bonferroni correction to $0.05/3=0.017$) showed that a significant difference in FBXL4 expression is present between bone metastases and BPH ($p=0.0097$), and primary PCa and BPH ($p<0.0001$) but not between bone metastases and primary PCa ($p=0.490$).

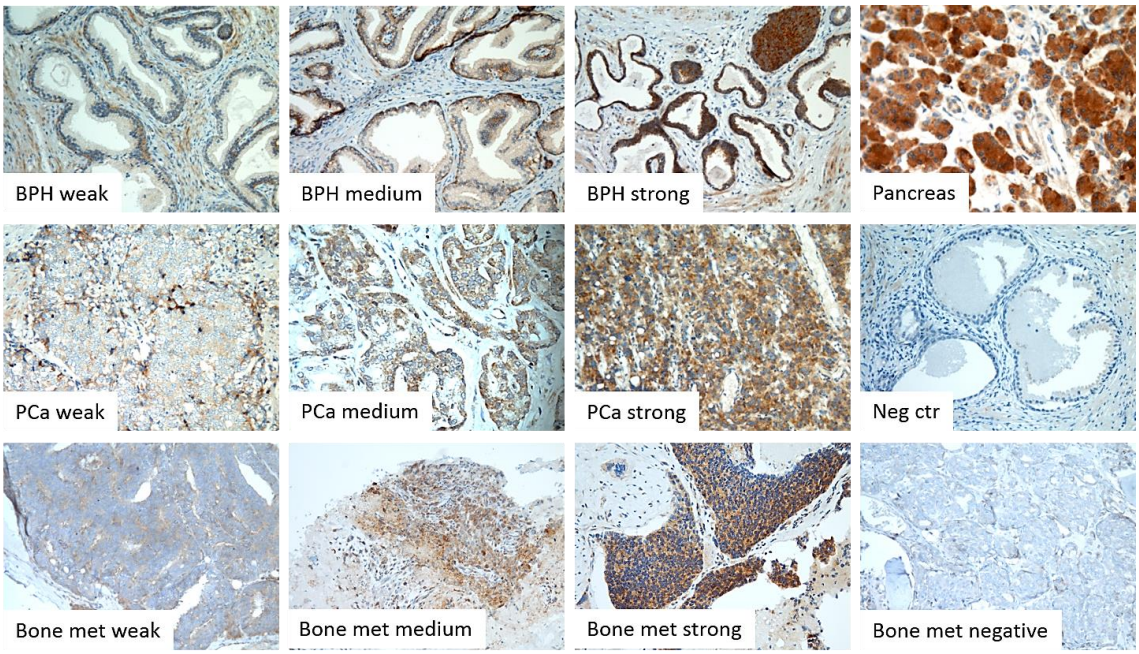

FIGURE 45. EXAMPLES OF FBXL4 IHC IN PROSTATE CLINICAL SAMPLES. Top panel: representative range of FBXL4 staining intensity in BPH samples and strong FBXL4 expression in positive control (pancreas). Middle panel: weak to strong FBXL4 expression in primary PCa and lack of staining in a negative control (no primary antibody). Bottom panel: range of FBXL4 staining intensity in bone metastases samples including no stain in bone negative control.

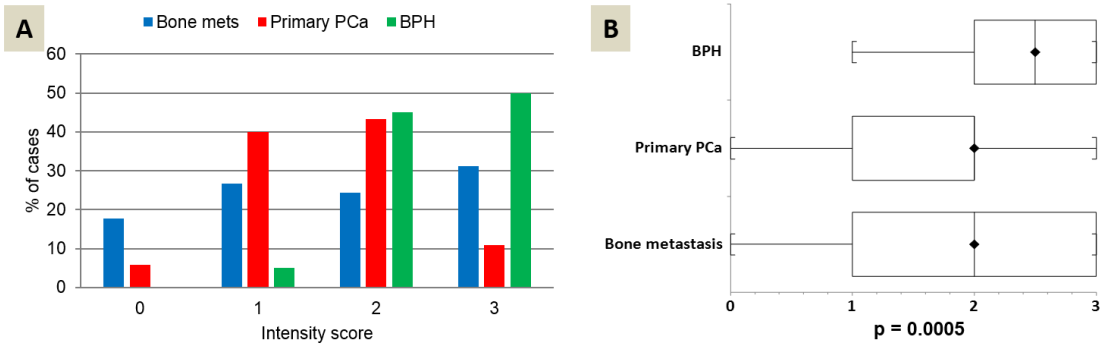

FIGURE 46. COMPARISON OF FBXL4 IMMUNOEXPRESSION IN PRIMARY AND METASTATIC PCA SAMPLES. Bone metastases and primary PCa show lower intensity of FBXL4 expression than BPH samples (A) and the difference in median FBXL4 expression between groups was statistically significant (B).

TABLE 47 MEDIAN AND AVERAGE FBXL4 IMMUNOEXPRESSION IN PROSTATE CLINICAL SAMPLES.

Samples	Median	Mean (SD)
Primary PCa	2	1.7 (1.1)
Bone metastases	2	1.6 (0.8)
BPH	2.5	2.5 (0.6)

FBXL4 expression measured by IHC and 6q16 copy number loss assessed by FISH were both available for 163 cases, which include 23 bone metastases, 120 primary PCa and 20 BPH. Eleven PCa bone metastases and 22 primary tumours were positive for 6q16 copy number loss while all BPH had neutral FBXL4 copy number at 6q16. Three of these 11 (27.3%) bone metastases and 14/22 (63.6%) of primary tumours had no or low FBXL4 expression. Together, half (17/33, 51.5%) of samples with FBXL4 copy number loss had also low or no FBXL4 protein expression while only 43/110 (39.1%) of samples with neutral FBXL4 copy number showed low or absent FBXL4 expression (Figure 47). However, the difference was not statistically significant (p=0.614).

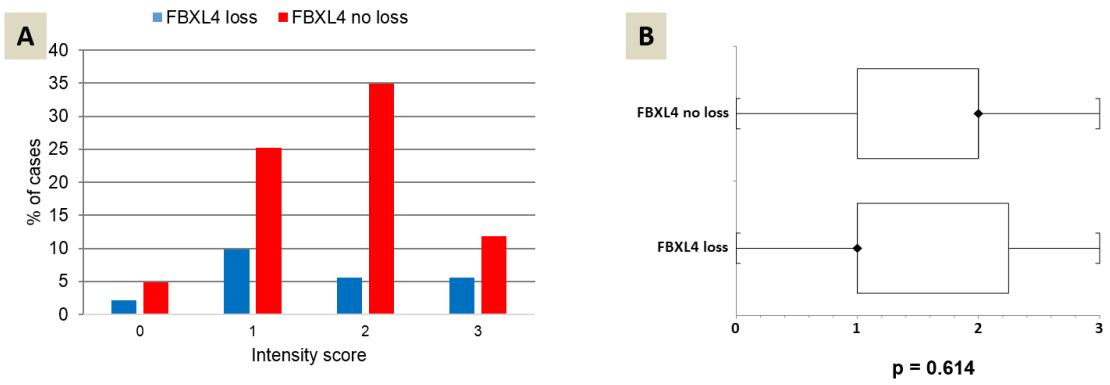

FIGURE 47. NO SIGNIFICANT DIFFERENCE IN FBXL4 IMMUNOEXPRESSION BETWEEN PCAS WITH AND WITHOUT *FBXL4* COPY NUMBER LOSS. (A), staining intensity distribution; (B), no significant difference in median staining intensity.

5.3 Discussion

5.3.1 *FBXL4* loss is more prevalent in metastatic PCa tumours and correlated with cancer progression and poor patient outcome

All PCa bone metastases analysed by DNA microarrays displayed large deletions within the 6q14.1-22.32 region. Copy number loss at 6q14-22 is a common feature of PCa and

is especially enriched in advanced tumours [119, 150, 151]. A recent meta-analysis of PCa somatic copy number alterations from 11 aCGH and SNP microarray publications, which included 546 primary and 116 advanced tumours placed 6q12–q22.33 deletion as the fourth most deleted region in PCa after 8p, 13q and 16q, with a frequency of 46.7% [121]. According to this meta-analysis, the frequency of 6q loss almost doubled in advanced tumours when compared to primary PCa (74.1% versus 40.8%), however, due to large size of the region, the exact drivers for this deletion could not be specified. Our initial focus specifically on PCa bone metastases led us to the detection of a very small region at 6q16 locus, whose loss was shared by all samples. Of the two known genes located within this deletion we concentrated on *FBXL4*, a member of F-box protein family, from which several other members are well known to be involved in cancer [316]. Our further investigation of *FBXL4* copy number status by FISH in a larger cohort of FFPE PCa bone metastases, primary tumours and BPH samples revealed that *FBXL4* loss is indeed commonly present in bone metastases but also found in a small subset of primary tumours (14%). Detection of 6q16 loss in half of the bone metastases correlates well with Holcomb *et al* [151] report of 6q13-q22.31 deletions in 43% (23/54) of their soft tissue metastases retrieved from autopsies of 14 patients who died from PCa. They also found this loss in 37% (4/11) of disseminated tumour cells retrieved from bone marrow aspirates collected from patients with metastatic PCa [150]. Alers *et al* [322] found loss of 6q (with minimal overlapping region at 6q15-q16) specifically enriched in the distant metastases (11/15, 73%) compared to the regional lymph nodes (4/18, 22%). Taylor *et al* [115] performed unsupervised hierarchical clustering of copy-number alterations in 194 PCa, including 37 metastases and found the majority of metastases in clusters 5 and 6, both of which showed substantial CNAs, with cluster 5 tumours having especially many genome-wide alterations, including 6q deletions, and an extremely unfavourable prognosis. Similarly, 6q loss was commonly found in a recent next generation sequencing study of 150 biopsies from distant metastases, including 43 (28.7%) bone metastases [138]. Based on results from all these studies, FBXL4 seems to be generally associated with more advanced disease. In our study we also found reduction of *FBXL4* gene expression at the RNA level in a limited number of fresh frozen primary and bone metastatic tumours when compared to non-malignant BPH samples, which further indicates the downregulation of *FBXL4* in PCa. High frequency of *FBXL4* loss in our metastatic tumours suggests a possible tumour suppressor role for *FBXL4* in PCa. Presence of a cell population with *FBXL4* deletion in limited number of primary tumours could be indicative of *FBXL4* loss being an early event in carcinogenesis and promoting cancer spread and invasiveness. We confirmed this hypothesis when we analysed

FBXL4 loss in in a large cohort of conservatively managed localised PCa diagnosed by TURP [216]. Loss of *FBXL4* in these early cancers positively correlated with all PCa prognostic markers, including high Gleason score, clinical stage, PSA and extent of disease. It also associated with death from PCa, which further implicates the importance of *FBXL4* loss in aggressive disease. Recent comprehensive molecular analysis of 333 primary PCa identified seven distinct subtypes defined by ETS fusions or mutations in SPOP, FOXA1, and IDH1 genes [323]. Interestingly, subtypes with SPOP, FOXA1, and IDH1 mutations and not with ETS fusions were enriched in 6q deletion, similar to 26% of cancers with wide range of genomic alterations, for which no obvious genetic drivers could be found. We did not correlate ETS fusion status with *FBXL4* loss in our cohort of early tumours, but only one of our six bone metastases with *FBXL4* loss had deletion at 21q22.2-22.3, indicative of ERG and TMPRSS2 genes rearrangement. The majority of primary tumours from the above study were locally advanced with limited follow up data (2 years only), rendering the possibility of assessing the association of molecular PCa subtypes with cancer progression by the authors unfeasible. In fact, not many reports looked specifically at 6q loss in very early PCa. Lu *et al* [324] analysed LOH at 6q16–22 in Japanese patients in 53 premalignant lesions of high-grade prostatic intraepithelial neoplasia and 145 primary PCa, including 38 very early tumours (low tumour volume, <100 mm^3; low PSA levels of 0–3.9 ng/ml) detected incidentally in cystoprostatectomy specimens. Similar to our benign samples they did not detect 6q loss in premalignant cases but found it in primary PCa, including the early cases, which led them to conclusion that 6q16–22 deletion is likely involved in the initiation and/or progression of PCa. However, they found no correlation between 6q16–22 loss and PCa progression. Other small studies of 6q loss in primary PCa also found no relation of 6q loss with PCa progression [306, 325]. Interestingly, Strohmeyer *et al* [326] used CGH to analyse 57 primary PCa, including 51 localised tumours and found that loss of 6q, as well as loss of 13q and gain of 7q correlated with cancer progression (biochemical or clinical). The differences between the studies are probably due to a small number of samples analysed. In our cohort loss of *FBXL4* correlated with all PCa progression markers in univariate analysis, however it was not independent prognostic marker in multivariate analysis. Still, *FBXL4* loss detected at the early stage could be indicative of more aggressive tumours, which are likely to progress to a metastatic stage.

5.3.2 Challenges in assessing FBXL4 protein levels

FBXL4 gene is not well studied and despite a range of commercial antibodies offered by different companies, none have been used in published reports. Common copy number

loss of FBXL4 in PCa suggests downregulation of FBXL4 signalling, which can be confirmed at protein levels with anti-FBXL4 antibodies. We tested 5 different antibodies by WB and IHC using inducible C-Flag FBXL4 expression system in HEK293 cells, which provided us with an abundance of FBXL4 protein for easy detection while addition of Flag tag allowed for confirmation of FBXL4-specific band on WB. Similar overexpression systems were previously successfully used for FBXL4 expression analysis of a tagged protein [319-321]. Based on comparison to expression of tagged protein, two tested antibodies produced specific results but with significant background especially visible on WB. Some of the observed multiple bands could still potentially represent FBXL4 protein with different post-translational modification status, breakdown products, or splice variants, however the majority are most likely unspecific [327]. When used for IHC, both antibodies exclusively produced a cytoplasmic staining pattern, which is in agreement with the general function of F-box proteins and with reports of FBXL4 co-localisation with mitochondria [319, 320]. Of the two specific anti-FBXL4 antibodies one performed better in WB while another was more suitable for IHC, which is not surprising considering different protein preparation for these two methods. While WB identifies denatured, linear proteins, IHC stains proteins in their native 3-D structure, therefore epitopes accessible to antibodies on linear peptide may be hidden inside the native protein structure, covered by posttranslational modifications or distorted due to formalin fixation and antigen retrieval prior to IHC [327]. Both antibodies were raised against synthetic peptides, which do not necessarily recapitulate the 3-D structure or post-translational modifications of the native protein, hence their different specificity/sensitivity for different applications. Regardless of the application, both antibodies showed low sensitivity and did not perform well when challenged with more subtle changes in FBXL4 expression as in FBXL4 knockdown cell models. Clearly, there is a need for more specific and sensitive anti-FBXL4 antibody, able to detect endogenous levels of the protein especially in systems with low FBXL4 expression such as PCa cell lines.

Initially we attempted to test the anti-FBXL4 antibodies directly in PCa cell models, however our trials to generate stable PCa cell lines for FBXL4 overexpression failed regardless of the cell line used. We observed an initial strong FBXL4 overexpression in all cells, which then was reduced to insignificant levels under antibiotic selection despite continuous presence of FBXL4 expression vector. It is possible that FBXL4 overexpression led to some unfavourable phenotypic changes within cells such as reduced proliferation or survival. Consequently, within mixed population of transfected cells, cells overexpressing FBXL4 would eventually die off or be outgrown by cells with

lower FBXL4 expression. Changes in proliferation/ survival could potentially explain lack of gene overexpression in PC3 and DU145 cells with constitutive FBXL4 transgene expression but this seems to be a less likely reason for the loss of expression in 22RV1 cells with tetracycline - inducible FBXL4 expression. Nonetheless, the twofold leakage noticed in untreated cells with FBXL4 transgene could also affect cell phenotype. Another explanation for lack of FBXL4 overexpression could be gene repression. Foreign DNA integrated into eukaryotic genomes is often rapidly silenced after a transient state of activity [328, 329]. Rapid silencing of a stably integrated transgene expression is frequently a result of de novo DNA methylation. De novo DNA methylation in mammalian cells gradually spreads across the integrated viral genomes with increasing passage numbers of cells in culture until the genome is strongly methylated [329]. The methylation is especially common when the vector DNA integrates at the region where surrounding endogenous chromatin structure is already repressed [330]. Contrary to PCa cells, we did not encounter any problems when we overexpressed FBXL4 in HEK293 cells, even when we continuously induced FBXL4 expression over 10 weeks. This is probably not surprising as HEK293 cells are commonly used as a model for studying the transforming/oncogenic properties of cancer-associated genes precisely because they are easy to transfect, permitting the expression of a wide range of proteins from many sources [331].

5.3.3 FBXL4 protein expression is reduced in PCa cancer but do not correlate with FBXL4 copy number status.

Being aware of the anti-FBXL4 antibody limitations, we used it to analyse FBXL4 protein expression in our cohort of FFPE clinical samples. Based on RNA expression in fresh frozen samples, tumours seemed to have fairly lower (4-20 times) FBXL4 levels than non-malignant BPH cases, a difference which if reflected in protein levels should be sufficient for detection by IHC. Indeed, we were able to detect significantly lower FBXL4 protein expression in bone metastases and primary tumours than in BPH samples, which is consistent with observed *FBXL4* copy number loss and reduction in RNA expression in tumour samples when compared to BPH. However, despite difference in *FBXL4* copy number loss frequency between bone metastases and primary tumours, no significant difference in FBXL4 protein expression was seen between these two groups, which could be due to the low sensitivity of the antibody. Additionally, antibody performance in bone samples could be further compromised by prolonged tissue decalcification with formic acid, which is known to reduce staining intensity and/or increase background [292]. Apart from general reasons such as antibody specificity/sensitivity and protein quality/epitope

availability after fixation, decalcification and antigen retrieval, lack of correlation between *FBXL4* copy number status and protein expression can be explained by other mechanisms of FBXL4 expression regulation. Other F-box proteins acting as TSGs like FBXW7 are known to be downregulated in cancer at the RNA level by a variety of oncogenic miRNAs [332]. Predicted post-translational modifications for FBXL4 protein, such as phosphorylation, ubiquitination, sumoylation and methylation (http://sumosp.biocuckoo.org, http://cplm.biocuckoo.org, http://bioinfo.ncu.edu.cn, http://www.jci-bioinfo.cn/UbiResultBySegs) can also potentially regulate FBXL4 protein localisation, stability and activity [333]. Therefore, it is possible that in PCa cases without *FBXL4* copy number loss, the protein expression is downregulated by some of these non-genetic mechanisms, similar to other TSGs.

CHAPTER 6

FBXL4 function in PCa

6.1 Introduction

As mentioned in the previous chapter, the *FBXL4* gene product belongs to a large F-box protein family, which are the component of E3 ubiquitin protein ligase complex called the SKP1-CUL1-F-box (SCF) [334]. Within SCF, cullin 1 protein functions as a scaffold with N-terminus occupied by SKP1 adaptor protein and C-terminus bound to a RING finger protein, RBX1. RBX1 recruits ubiquitin-conjugating enzyme E2 and SKP1 is a docking site for substrate-bound F-box proteins. F-box proteins are responsible for substrate recognition and delivery to the core of the ligase. They are the variable component of SCF E3 ligase and bind to SKP1 through their conserved F-box domain. Once the substrate is delivered to the E3 core, it undergoes ubiquitination by ubiquitin charged E2 enzyme (Figure 48) [334, 335]. Consequently, as a part of the ubiquitin proteasome system, E3 ligases together with ubiquitin-activating enzyme E1 and ubiquitin-conjugating enzyme E2 catalyse the ubiquitination of a variety of protein substrates for targeted degradation through the 26S proteasome [336].

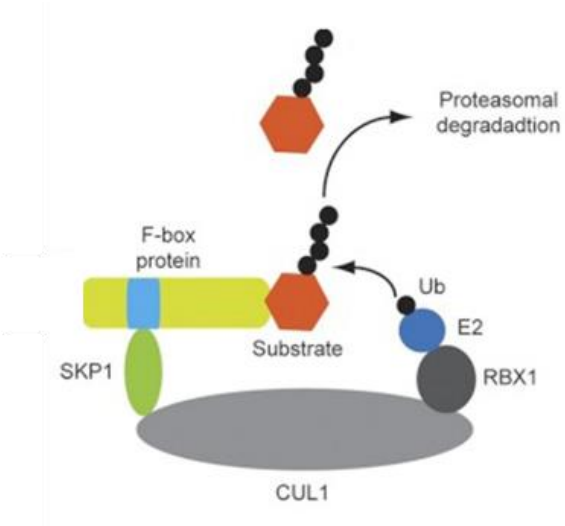

FIGURE 48. THE SKP1-CUL1-F-BOX (SCF) COMPLEX. Adapted from Harper *et al* [335].

F‑box proteins are divided into three families based on substrate binding domain: WD40 domain (FBXW) proteins (12 proteins), Leucine-rich repeat (FBXL) proteins (21 proteins) or other domains (FBXO) proteins (38 members) [315, 334]. In response to various stimuli, F-box proteins selectively bind target proteins based on unique, short degradation peptidic signature (degron) present in their substrates [315, 337]. Through substrate downregulation, F‑box proteins regulate diverse biological pathways that

control cell growth, division, development and differentiation, signalling responses, and cell survival and death [315].

FBXL4 protein belongs to Leucine-rich repeat group of F-box proteins with 9 Leucine-rich repeats present within its target binding domain (Figure 49) [320]. The exact function of FBXL4 is presently unknown. Recent studies found FBXL4 protein to co-localise with mitochondria and linked recessive loss-of-function and splice mutations in this protein with severe respiratory chain deficiency mitochondrial disease [319, 320, 338].

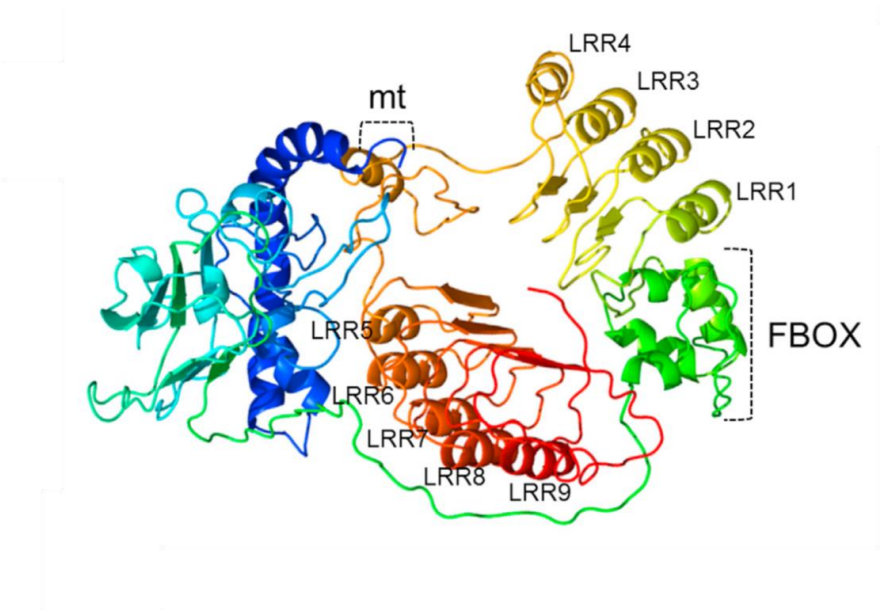

FIGURE 49. THREE-DIMENSIONAL STRUCTURAL MODELLING OF FBXL4 PROTEIN. Bioinformatically determined mitochondrial localisation sequence (mt) is visible at N-terminus, followed by conserved F-box domain and nine leucine-rich repeats located at the C-terminus. Adapted from Bonnen *et al* [320].

Proteomics based approach, aiming at the identification of candidate substrates and stably interacting proteins for a range of F-box family members led to the detection of several proteins potentially interacting with FBXL4 [321], which were mostly located in endoplasmic reticulum (ER) (Endoplasmic Reticulum Lectin 1 - ERLEC1, SEL1L, Calmegin - CLGN, p58) [339-341] and mitochondria (Translocase Of Outer Mitochondrial Membrane 70 Homolog A -TOMM70A, Heat Shock Proteins 90kDa-HSP90AA4P and HSP90AB4P), where they are involved in the unfolded protein response (UPR) during cellular stress [342, 343]. The UPR was first discovered in ER and involves transcriptional induction of molecular chaperones in response to ER stress and is triggered by accumulation of misfolded proteins. As a result, misfolded proteins are

retrotranslocated to the cytoplasm, where they are polyubiquitinated and degraded by the proteasome in a process called ER-associated Protein Degradation (ERAD). ERAD is essential for maintaining ER homeostasis and cell survival under stress, and disruption of ERAD leads to ER stress-induced apoptosis [344]. Increasing evidence suggests the presence of a mitochondria-associated degradation (MAD) pathway that regulates mitochondrial protein quality control, with multiple E3 ubiquitin ligases residing at the outer mitochondrial membrane where misfolded proteins are ubiqitinated and subsequently degraded by proteasomes [345-347]. Additionally, recent evidence shows that ER and mitochondria form physical contacts and collaborate in response to stress [348-351].

Interestingly, ERLEC1 was confirmed as FBXL4 binding target by IP/WB method [321]. ERLEC1, a luminal resident protein of the endoplasmic reticulum, is member of a protein family containing mannose 6-phosphate receptor homology (MRH) domains involved in N-glycan binding [352]. ERLEC1 is a molecular chaperone that plays a role in the recognition of terminally misfolded proteins and the extraction of these proteins to the cytoplasm for proteasomal degradation [353]. Specifically, ERLEC1 binds to misfolded glycoproteins in the ER lumen and delivers them to ER membrane bound HRD1 E3 ligase through binding to transmembrane receptor, SEL1L. Ubiquitinated by HRD1 misfolded proteins are subsequently degraded by the cytosolic ubiquitin–proteasome system [340, 353]. Interestingly, ERLEC1 was identified in lung cancer as a novel cancer invasion and metastasis-related gene controlling the response to hypoxia and ER stress [354]. Ectopic expression of ERLEC1 in lung cancer cells increased their tolerance to hypoxia through reduced degradation and consequently accumulation of a hypoxia-inducible factor, HIF-1α. Stabilisation of HIF-1α activates the transcription of genes involved in cell survival, angiogenesis, dedifferentiation, and invasion [355]. ERLEC1 was also found to activate the UPR pathway and therefore increasing cellular tolerance to ER stress. If ERLEC1 is indeed downregulated by FBXL4, then *FBXL4* loss in PCa would lead to stabilisation of ERLEC1 protein and therefore contribute to tumour progression by protecting cancer cells from apoptosis under hypoxia and ER-stress; conditions which are often encountered by growing tumours [356].

6.2 Results

6.2.1 *FBXL4* knockdown leads to increased PCa cell migration and invasion without affecting cell viability

As mentioned in the previous chapter, *FBXL4* knockdown with siRNA led to a 60-70% reduction in FBXL4 RNA levels in all three PCa cell lines analysed (DU145, 22RV1 and PC3, Figure 50A). *FBXL4* downregulation did not affect cell viability (Figure 50B) but led to significant increase in cell migration and invasion (Figure 51, 52 and Table 48). *FBXL4* knockdown in PC3 (Figure 51A) and DU145 (Figure 51B) cells, which already have heterozygous *FBXL4* DNA copy number loss, led to around a 30% increase in cell migration while in 22RV1 cells exibiting normal *FBXL4* DNA copy number, *FBXL4* knockdown increased their migration by 46% (Figure 51C and Table 48). Stable single clone 22RV1 cells with FBXL4 knockdown showed an even higher two fold increase in cell migration when compared to control (Figure 51D).

The effect of FBXL4 downregulation on cell invasion was tested using basement membrane (Matrigel) and stromal/interstitial type of extracellular matrices (collagen and mixed collagen/Matrigel). Matrigel matrix, a reconstituted basement membrane extracted from the Engelbreth-Holm-Swarm mouse sarcoma containing of 60% laminin, 30% collagen IV, and 8% entactin (https://www.corning.com/) was used to mimic cellular penetration of a basement membrane layer [357-359]. For single cell invasion into stromal/interstitial matrices, which form the majority of the body connective tissue and mainly contain fibrillar collagen I, the solution of 2 mg/ml type I collagen [223, 358-361] and mixed 50:50% collagen/matrigel [224] gels were used. *FBXL4* knockdown significantly increased PCa cells invasion through the Matrigel (Figure 52A and Table 48), with increase ranging from 33% in PC3 cells through to 55% in DU145 to 75% in 22RV1 cells. Further analysis of PCa cells motility/invasion was performed by seeding PCa cells as a single cell suspension on top of collagen gels (2 mg/ml type I collagen) [223, 360, 362]. The invading cells as oppose to non-motile cells, produce cellular protrusions readily visible under the microscope (Figure 52B) and only cells with these protrusions were counted as invading cells. Modest but significant increases in collagen-based cell migration/invasion were seen in cells with *FBXL4* siRNA knockdown compared to cells transfected with non-targeting siRNA in all three cell lines tested (Figure 52B and Table 48). The results were confirmed with stable 22RV1 *FBXL4* knockdown cells seeded as a single cell suspension on collagen/Matrigel gels (1.6 mg/ml collagen, 50% Matrigel) (Figure 53) [224]. These cells also showed 9.2% increase in

motility/invasion when compared to 22RV1 cells transfected with non-targeting shRNA (p=0.01, Figure 53). The above results suggest that *FBXL4* knockdown leads to a modest but consistent increase in cell invasion into collagen.

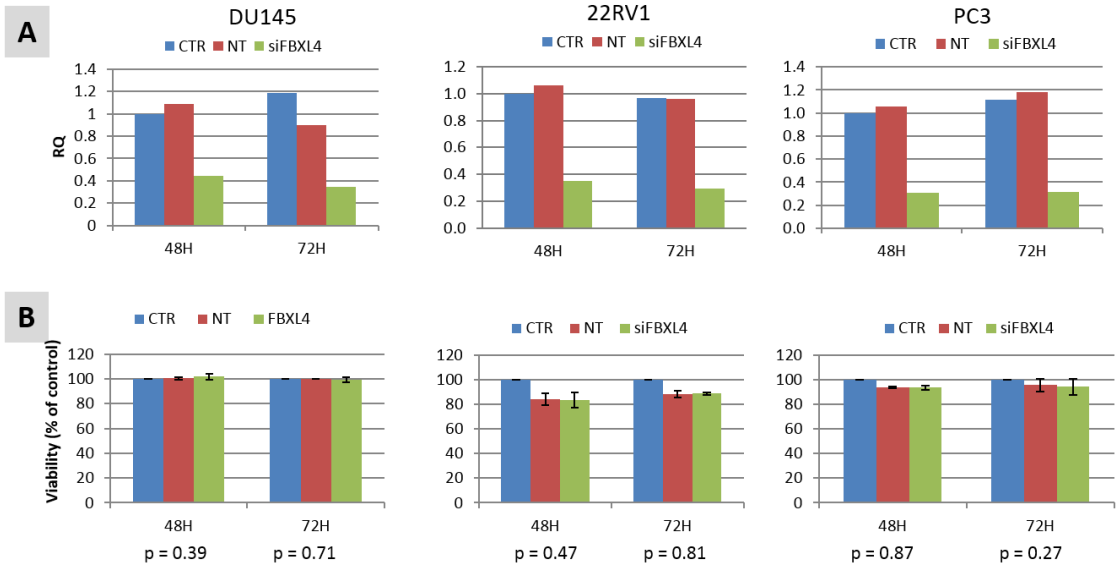

FIGURE 50. THE EFFECT OF *FBXL4* KNOCKDOWN ON PCA CELLS VIABILITY. (A) Confirmation of *FBXL4* knockdown at mRNA level in DU145, 22RV1 and PC3 cells. (B) *FBXL4* knockdown does not affect PCa cell viability in DU145, 22RV1 and PC3 cells compared to non-targeting siRNA. Cell viability was measured by MTS assay at 48 and 72 h post *FBXL4* siRNA transfection. CTR, non-transfected control cells; NT, cells transfected with non-targeting siRNA; siFBXL4, cells transfected with *FBXL4* siRNA. Error bars indicate SD; n = 3.

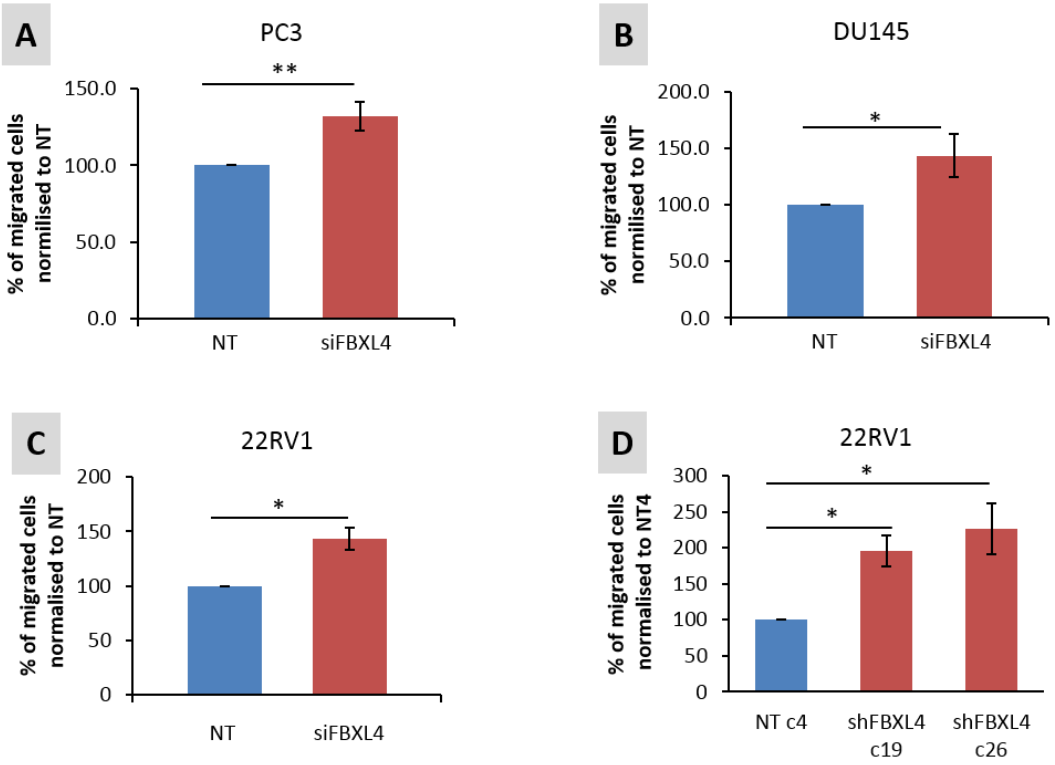

FIGURE 51. FBXL4 KNOCKDOWN INCREASES PCA CELL MIGRATION. *FBXL4* siRNA knockdown increased cell migration by about 30-40% in PC3 (A), DU145 (B), and 22RV1 (C). 22RV1 single clones with stable reduction of FBXL4 showed even higher (two fold) increase in cell migration (D). NT, cells transfected with non-targeting siRNA/shRNA; siFBXL4/shFBXL4, cells transfected with *FBXL4* siRNA/shRNA. Error bars: SD; n=3. *: p<0.05, **: p<0.01.

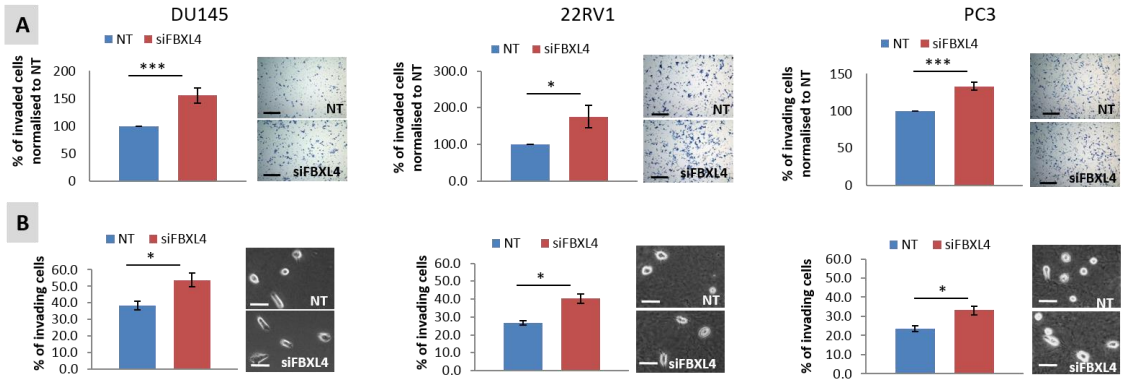

FIGURE 52. *FBXL4* KNOCKDOWN LEADS TO INCREASED PCA CELL INVASION. (A) PCa cell invasion through Matrigel increases from over 30% (PC3) to 70% (22RV1) in *FBXL4* knockdown cells. Scale bar: 300 µm. (B) PCa cell migration/invasion on collagen increases by 10% (PC3) – 15% (DU145) after *FBXL4* knockdown. Single cell suspensions were seeded onto collagen (2mg/ml) and after 24 h cells with cellular protrusions were considered as migrating/invading cells and counted. NT, cells transfected with non-targeting siRNA; siFBXL4, cells transfected with *FBXL4* siRNA. Error bars: SD; n=3. *: p<0.05, **: p<0.01 and *** p<0.001. Scale bar: 50 µm.

TABLE 48. PCA CELL MIGRATION AND INVASION INCREASES AFTER FBXL4 KNOCKDOWN.

PCa cell line	Statistics t-test	Migration %, siFBXL4	Invasion %, Matrigel siFBXL4	Invasion %, Collagen siFBXL4
DU145	**mean**	127.6	155.2	15.3
	SD	10.4	14.3	3.0
	p value	0.04	0.001	0.01
22RV1	**mean**	146.5	175.8	13.5
	SD	10.2	30.4	2.4
	p value	0.02	0.0498	0.01
PC3	**mean**	132.3	133.3	9.8
	SD	9.3	5.1	2.9
	p value	0.03	0.0001	0.03

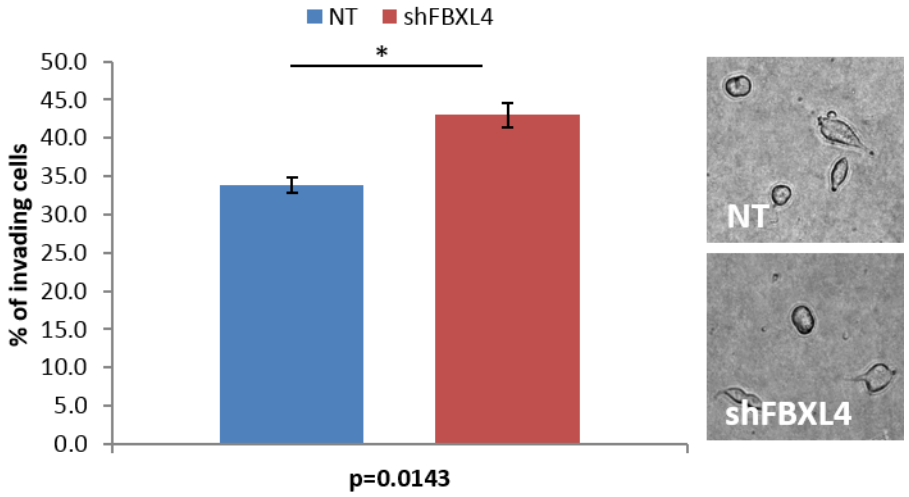

FIGURE 53. FBXL4 KNOCKDOWN INCREASES 22RV1 CELL MIGRATION/INVASION ON COLLAGEN/MATRIGEL 3D CULTURE. 22RV1 single cell suspension was seeded onto gels (1.6 mg/ml collagen, 50% Matrigel) and allowed migration/invasion for 72 h. Cells with cellular protrusions were considered as migrating/invading cells and counted. NT, stable 22RV1 cells transfected with non-targeting shRNA; shFBXL4, stable 22RV1 cells transfected with FBXL4 shRNA. Error bars indicate SD; n = 3.

6.2.2 *FBXL4* overexpression leads to reduced cell migration

To confirm that *FBXL4* expression levels affect cell migration, we used stable HEK293 cells with tetracycline-inducible *FBXL4* expression from the vector. As shown in Chapter 5.2.3.2.1, *FBXL4* overexpression in these cells was confirmed at both, RNA and protein levels (Figure 36, Figure 37, and Figure 38). Overexpression of *FBXL4* had no effect on cell viability (Figure 54A) but as expected led to significant (54.4%) reduction in cell migration when compared to control cells transfected with an empty vector (p=0.00004, Figure 54B).

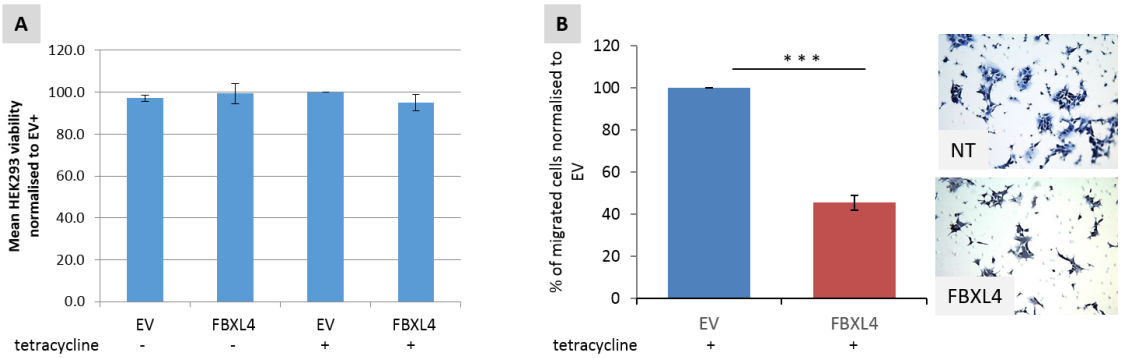

FIGURE 54. *FBXL4* OVEREXPRESSION LEADS TO REDUCED HEK293 CELL MIGRATION WITHOUT AFFECTING CELLS VIABILITY. (A) 72 h induction of FBXL4 overexpression with 1µg/ml tetracycline does not affect HEK293 cell viability when compared to control HEK293 cells containing empty vector. (B) HEK293 cells overexpressing FBXL4 show reduced migration when compared with control HEK293 cells. EV, control cells with empty expression vector; FBXL4, HEK293 cells transfected with expression vector containing FBXL4. '-', no tetracycline treatment; '+', 1µg/ml tetracycline treatment for 72 h. Error bars: SD; n=3.

6.2.3 *FBXL4* co-localises with mitochondria.

Based on previous reports using overexpression systems, FBXL4 protein was found to co-express with mitochondria [319, 320]. Using stable HEK293 cells with induced FBXL4 overexpression and anti-Flag antibody we found by IF that FBXL4 indeed co-localises with mitochondria stained with mitotracker in most of the cells (Figure 55, top panel). HEK293 control cells did not stain for Flag, confirming specificity of the Flag antibody. FBXL4 staining using anti-FBXL4 antibody confirmed co-localisation of FBXL4 with mitochondria but also produced diffused cytoplasmic stain throughout the cells (Figure 55, bottom panel).

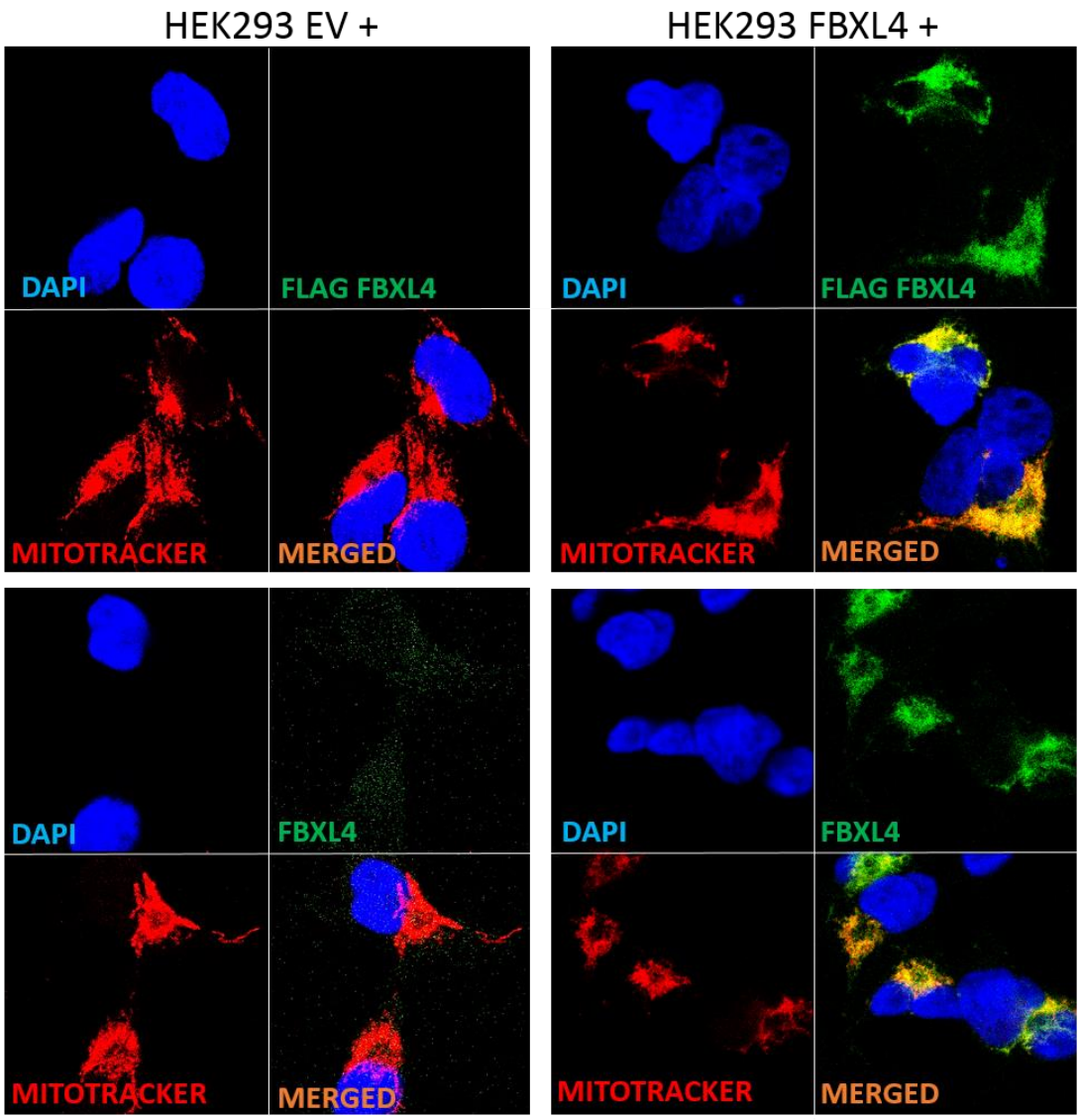

FIGURE 55. FBXL4 PROTEIN CO-LOCALISES WITH MITOCHONDRIA IN HEK293 OVEREXPRESSING FBXL4. FBXL4 protein stained with anti-Flag antibody mainly co-localises with mitochondria (top panel), while IF with anti-FBXL4 antibody gives some additional cytoplasmic staining (bottom panel). FBXL4 overexpression is clearly visible with both antibodies. FBXL4 expression (green) correlates with mitochondria distribution. EV, empty vector control; FBXL4, cells with FBXL4 expression vector; +, tetracycline treatment (1µg/ml, 3 days). Blue, DAPI; green, anti-Flag-FBXL4 or FBXL4 antibody; red, mitotracker.

6.2.4 *FBXL4* does not regulate epithelial to mesenchymal transition (EMT) related proteins

As the acquisition of a motile and invading phenotype is linked to EMT, we investigated the levels of several proteins linked to EMT and cell movement, including mesenchymal markers – vimentin and N-cadherin; epithelial marker E-cadherin as well as F-actin and

focal adhesion kinase (FAK). WB analysis showed no difference in the expression of EMT markers in HEK293 cells overexpressing FBXL4, with all HEK293 cells strongly expressing vimentin and N-cadherin but equally lacking E-cadherin expression (Figure 56A). Similar, no difference in the expression of E- and N-cadherins was found in stable 22RV1 cells with FBXL4 downregulation when compared to control cells (Figure 56B). All 22RV1 cells were negative for vimentin expression. No difference in total and activated, phosphorylated FAK was seen by WB. These results suggest that FBXL4 does not regulate expression of these proteins.

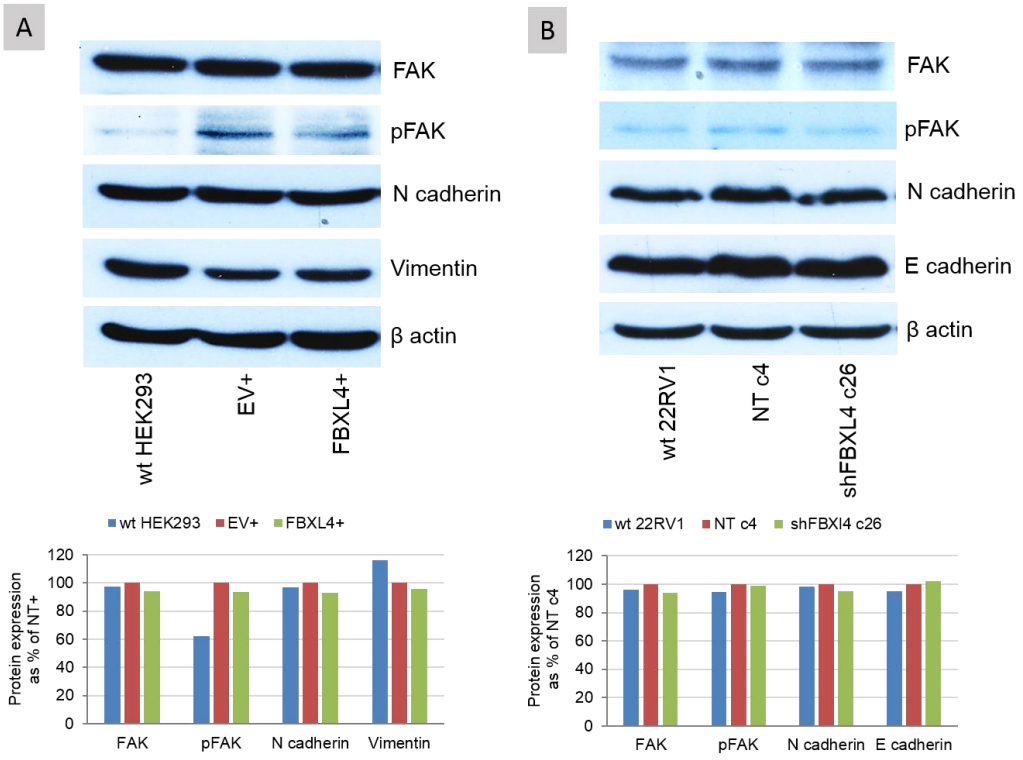

FIGURE 56. FBXL4 DOES NOT REGULATE EMT MARKERS EXPRESSION. (A), all stable HEK293 including cells overexpressing FBXL4 had equally strong expression of mesenchymal N-cadherin and vimentin markers, and low levels of activated FAK. (B), similar lack of difference in EMT markers N- and E-cadherins and very low levels of FAK were visible in all 22RV1 cells, including control cells (NT c4) and cells with FBXL4 downregulation shFBXL4 c26). Protein load, 50µg. wt, wild type, EV, empty vector control; FBXL4 cells with FBXL4 expression plasmid; +, 1 µg/ml tetracycline treatment to induce FBXL4 expression.

6.2.5 ERLEC1 protein as a potential downstream target of FBXL4

6.2.5.1 Anti-ERLEC1 antibody validation

Polyclonal rabbit anti-ERLEC1 antibody (ab102046) was purchased from Abcam, UK and tested by WB, IF and IHC. ERLEC1 knockdown in HEK293 cells with anti-ERLEC1

siRNA produced substantial reduction in ERLEC1 protein expression by WB (Figure 57A), proving antibody suitability for use in WB. However, IF staining of the cells from the same experiment produced mostly nuclear rather than the well documented ER staining [354, 363] with similar intensity in control and knockdown cells, showing lack of specificity of the antibody for use in IF (Figure 57B). Testing the antibody for IHC using PCa bone metastases, primary tumours and BPH also produced mostly nuclear stain (Figure 58) not previously reported for this protein.

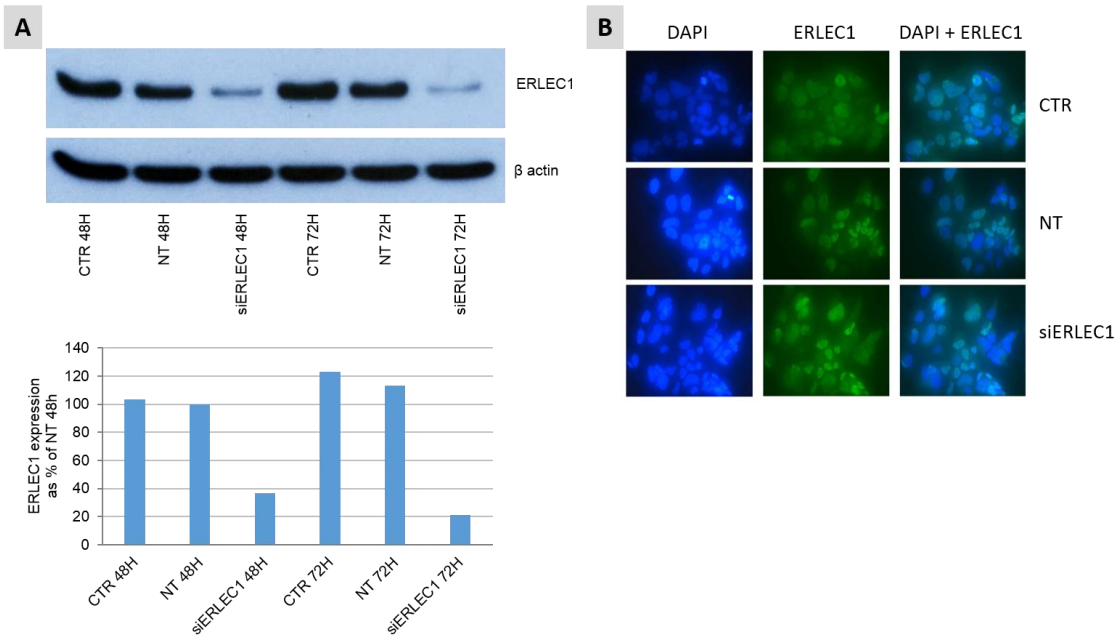

FIGURE 57. ANTI-ERLEC1 ANTIBODY TESTING IN HEK293 CELLS. (A) WB shows ERLEC1 protein reduction by 63.4% (48h) - 78.7% (72h) after knockdown when compared to non-targeting control. (B) There is no difference in IF FBXL4 expression between knockdown and control cells. CTR, control mock-transfected cells; NT, cells transfected with non-targeting siRNA; siERLEC1, cells transfected with anti-ERLEC1 siRNA smartpool.

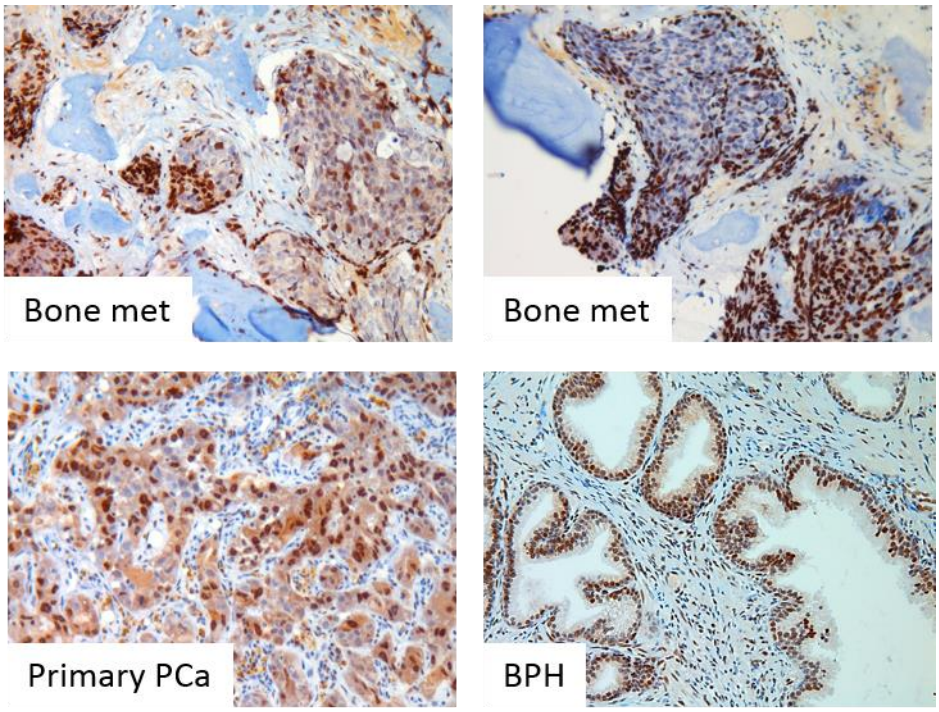

FIGURE 58. ANTI-ERLEC1 ANTIBODY TESTED IN FFPE CLINICAL SAMPLES BY IHC. The anti-ERLEC1 antibody produced mostly nuclear stain.

6.2.5.2 Relation between FBXL4 and ERLEC1 expression levels using *in vitro* cell line models.

The relationship between ERLEC1 and FBXL4 proteins was tested *in vitro* by manipulating FBXL4 expression levels in cell lines. First, endogenous levels of ERLEC1 expression were assessed in prostate cell lines. All PCa cell lines (PC3, DU145, 22RV1 and LnCaP) as well as immortalised normal prostate epithelial cells (PNT1 and PNT2) showed abundant expression of ERLEC1 protein (Figure 59). Transient knockdown of FBXL4 in 22RV1 and DU145 PCa cell lines did not result in a visible change in ERLEC1 protein expression (Figure 60A). However, stable 22RV1 shFBXL4 clones had increased ERLEC1 expression from 24% in shFBXL4 c42 clone through to 57% in shFBXL4 c26 to 95% in shFBXL4 c19 (Figure 60B) when compared to control clone.

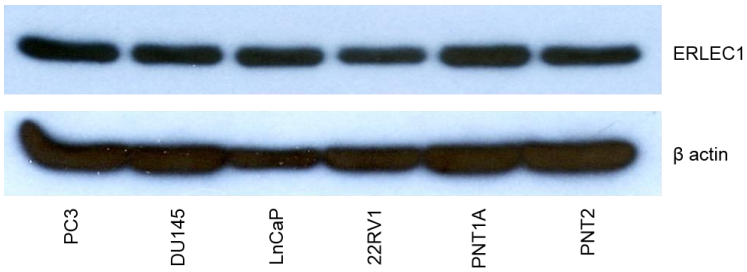

FIGURE 59. ERLEC1 PROTEIN IS COMMONLY EXPRESSED IN PROSTATE CELL LINES.

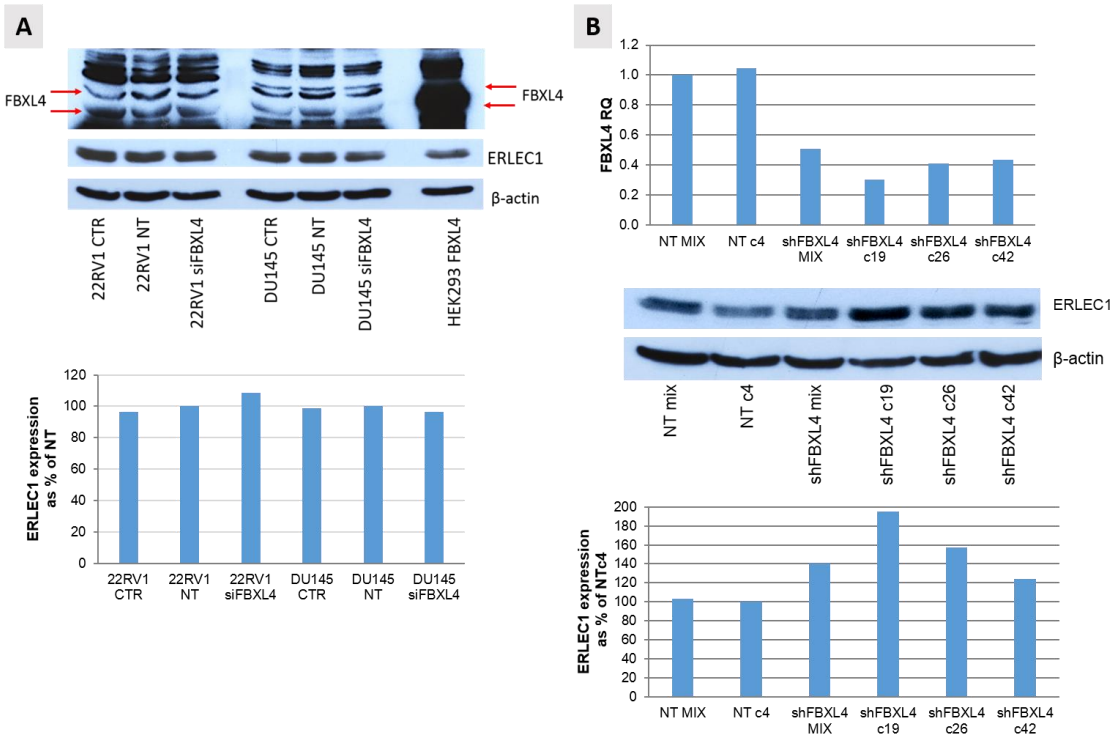

FIGURE 60. ERLEC1 PROTEIN EXPRESSION IN PCA CELL LINES WITH FBXL4 KNOCKDOWN. (A) No visible change in ERLEC1 protein levels after FBXL4 knockdown with siRNA in 22RV1 and DU145 cells. CTR, mock-transfected cells; NT, cells transfected with non-targetting siRNA smartpool; siFBXL4, cells transfected with anti-FBXL4 siRNA smartpool. (B) Increased levels of ERLEC1 protein are detected in stable 22RV1 FBXL4 knockdown clones when compared to 22RV1 transfected with non-targeting shRNA. Top graph – confirmation of FBXL4 downregulation at RNA level. Bottom graph-relative quantification of ERLEC1 protein levels detected on WB. NT, cells transfected with control non-targeting shRNA; shFBXL4, cells transfected with anti-FBXL4 shRNA; c, single clone; MIX, mixed stable cell population. Protein load: 100 µg.

In opposition to FBXL4 downregulation in PCa cells, FBXL4 overexpression in stable HEK293 led to a reduction in ERLEC1 expression (~20%) when measured by WB

(Figure 61A). IHC for ERLEC1, similair to previous results, showed nuclear staining and no visible reduction in ERLEC1 expression was visible in HEK293 cells overexpressing FBXL4 (Figure 61B).

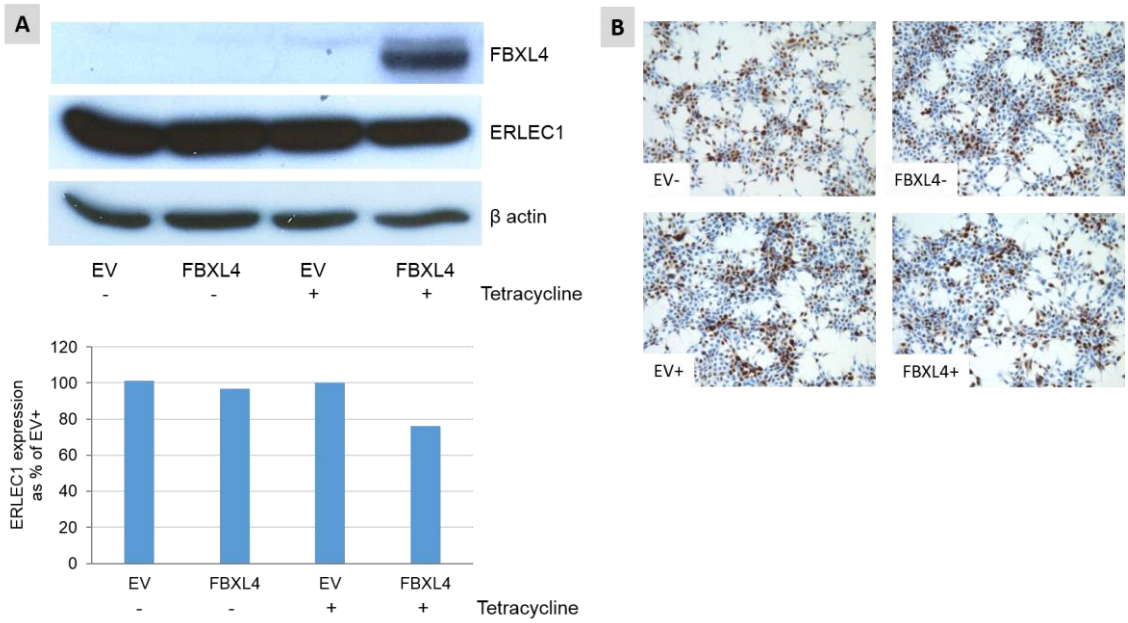

FIGURE 61. ERLEC1 PROTEIN EXPRESSION IN HEK293 CELLS OVEREXPRESSING FBXL4. (A) ERLEC1 protein is downregulated in cells overexpressing FBXL4. ERLEC1 and FBXL4 protein lysates were collected after 48 h treatment with/without 1µg/ml tetracycline. (B) ERLEC1 IHC expression is nuclear and similar in all HEK293 cells, regardless of FBXL4 status. EV, control cells with empty expression vector; FBXL4, HEK293 cells transfected with expression vector. '-', no tetracycline treatment; '+', 1µg/ml tetracycline treatment. Protein load: 100 µg.

6.3 Discussion

6.3.1 FBXL4 regulates cell migration and invasion without affecting proliferation.

The association of *FBXL4* loss with advanced bone metastatic PCa and worse patient survival strongly suggests *FBXL4* role as a TSG. Using *in vitro* experiments, we were able to establish that FBXL4 exerts its possible tumour suppressor function by regulation of cell motility and invasiveness. FBXL4 downregulation led to an increase in PCa cell migration and invasion, which was even more pronounced in 22RV1 cells with normal *FBXL4* DNA copy number status than in PC3 and DU145 cells with heterozygous *FBXL4* loss. Considering that PC3 and DU145 cell lines already had lower FBXL4 RNA expression, additional reduction in FBXL4 levels would have a lesser effect on cell migration and invasion when compared to 22RV1, explaining the observed difference between the cell lines. As expected, overexpression of FBXL4 had the opposite effect on cell migration, confirming the role of FBXL4 in the regulation of cell motility. The

capability for invasion is one of the hallmarks of cancer and enables cancer cells to spread beyond the primary tumour and colonise new sites, where nutrients and space are not limiting [81]. Overexpression of oncogenes or downregulation of tumour suppressors in cancer often results in increased cell proliferation, survival, migration and invasion [364]. Several F-box proteins are known TSGs regulating cell motility and invasion, and similar to FBXL4 are found downregulated in human cancer. The best studied is FBXW7, which exerts its tumour suppressor role by promoting the degradation of various oncoproteins and is often inactivated in cancer by mutations or copy number loss [365, 366]. Like FBXL4, FBXW7 can regulate cell migration and invasion and its inactivation increases cell aggressiveness [367]. *FBXO11* is another F-box TSG regulating cell migration and invasiveness and is deleted or mutated in a subset of human B-cell lymphomas [368]. Interestingly, the deletions/mutations found in *FBXO11* are largely monoallelic, indicating haplo-insufficiency of *FBXO11* TSG, similar to *FBXL4* loss. FBXL5 is one more potential F-box TSG, whose expression is significantly decreased in gastric cancer, especially in metastatic tumours leading to increased cancer invasion and metastasis [369]. Despite similar end effects, these F-box proteins exert their action through downregulation of different targets and currently the targets for FBXL4 are not clear.

Based on observed FBXL4 co-localisation with mitochondria and on recent reports, linking rare recessive loss of function FBXL4 mutants with a form of encephalomyopathic mitochondrial DNA depletion and mitochondrial network fragmentation, it is possible that FBXL4 may play a role in mitochondria maintenance [319, 320, 338, 370]. Mitochondria form in cells dynamic network regulated by fusion and fission (mitochondria fragmentation) events, important for the morphology, function and distribution of mitochondria. Fusion allows the exchange of proteins, DNA, and metabolites between neighbouring mitochondria, rescuing mildly damaged mitochondria. Fission is necessary for efficient mitochondrial transport to the subcellular regions with high energy demands and for separation and removal of damaged mitochondria, therefore maintaining a healthy mitochondrial population [371, 372]. Recent evidence shows that mitochondrial dynamics is involved in migration and invasion of epithelial cells, with fission being necessary for efficient relocation of mitochondria, and upregulation/downregulation of fission/fusion promoting proteins is often observed in invasive cancer cells, including breast and prostate cancer cells [373-375]. Increased mitochondrial network fragmentation was observed in highly invasive metastatic breast cancer cells when compared with non-metastatic cells, and manipulation of mitochondria dynamics by

increasing fusion or fission significantly suppressed or enhanced metastatic abilities of breast cancer cells [373]. Mitochondrial fission also promotes formation of lamellipodia, the leading edge of migrating cells necessary for cancer cell migration and invasion, while mitochondrial fusion suppresses lamellipodia formation in breast cancer cells [373]. Mitochondria localisation in motile cells further affects their migration, with anterior localisation of mitochondria, in between the nucleus and the leading edge correlating with faster migration. Inhibition of the mitochondrial network fragmentation or stimulation of mitochondria fusion significantly reduces the number of cells with anterior localisation of mitochondria and significantly decreases the speed of migrating cells [374].

Based on these reports, we looked at FBXL4 localisation in cells and we confirmed that FBXL4 protein colocalises with mitochondria. However we were not able to assess levels of mitochondrial network fragmentation in cells with overexpression or downregulation of FBXL4 due to too low resolution of our images. To properly study mitochondrial network, laser-scanning confocal microscopy has to be used with high magnification lense (63x or 100x) and multiple image planes acquisition along the Z-axis [376, 377]. Acquired images need to be analysed with image processing program, e.g. ImageJ (U.S. National Institutes of Health, Bethesda, MD, USA) in order to identify and count mitochondrial segments and continuous mitochondrial structures [378, 379]. Such careful examination of mitochondrial network in cells with overexpression or downregulation of FBXL4 is crucial to definitively establish the relationship between FBXL4 levels, mitochondrial network fragmentation and cell migration.

Several F-box proteins with tumour suppressor function such as FBXW7, FBXL5, FBXO45 and FBXL14 are involved in downregulation of the core EMT regulators such as Zeb1/2, Snai1/2 and Twist1 [369, 380-382]. EMT plays a critical role in the development of tumour metastases by enhancing migration and invasion of cancer cells, therefore it could be potentially affected by FBXL4 [383]. The change from an epithelial to a mesenchymal phenotype is characterized by loss of cell apical-basal polarity, cell-cell adhesion, cell adhesion to basement membranes and the acquisition of an invasive, mesenchymal phenotype [383-385]. A critical molecular feature of EMT is a ‘‘cadherin switch’’; a downregulation of epithelial cell adhesion molecule E-cadherin and increased mesenchymal N-cadherin expression, induced by mentioned above transcription factors and resulting in the aggressiveness, de-differentiation and metastasis of many carcinomas [386-388]. Cadherins associate with the cytoskeleton including actin microfilaments and intermediate filaments (e.g. keratin and vimentin) to provide mechanical strength at points of adhesion and scaffolds for proteins involved in cell

signalling [389]. During EMT, intermediate filament composition changes with increase in vimentin filaments expression enabling cell motility, possibly due to the interaction of vimentin with motor proteins [383, 390, 391]. ‘‘Cadherin switch’’ was reported as an independent prognostic factor for PCa progression and cancer-specific death [392] while vimentin overexpression was found to contribute to PCa invasion and metastasis [393].

Our analysis of EMT markers using *in vitro* cell line models showed no changes in their expression upon manipulation of FBXL4 levels suggesting that FBXL4 does not regulate cell migration directly through EMT. No changes in vimentin and N-cadherin protein were seen in HEK293 upon FBXL4 overexpression while E-cadherin levels were undetectable in these cells, which is surprising assuming they are epithelial cells. Low or undetectable E-cadherin expression frequently reported in HEK293 cells [394-396] could be explained by their origin from the adrenal gland rather than the embryonic kidney epithelium, which was suggested in recent detailed study on genetic and expression profiles of HEK293 cells [397]. And indeed, adrenal gland cells do not express E-cadherin at detectable levels [398]. Regardless of HEK293 origin, they still expressed abundance of vimentin and N-cadherin and overexpression of FBXL4 did not lead to the expected decrease in levels of any of these proteins. Similarly, we saw no decrease in expression of E-cadherin or increased N-cadherin expression in 22RV1 cells with stable FBXL4 downregulation, making FBXL4 involvement in EMT regulation unlikely.

The crucial player in cell movement is filamentous actin (F-actin) cytoskeleton, which is responsible for morphological changes and physical forces that occur during migration, such as formation of protruding cellular structures at the front of migrating cells (filopodia and lamellipodia) [399]. F-actin cytoskeleton is linked to focal adhesion complexes, which are the points of adhesion between cell and extracellular matrix (ECM). Turnover of focal adhesions is essential for cell migration and requires coordination between focal adhesion and actin cytoskeleton. A key trigger for adhesion turnover is a non-receptor protein tyrosine kinase, FAK [399-401]. FAK phosphorylation and activation is dependent on its localization to focal contacts, where it promotes integrin-stimulated cell motility through activation of small GTPases RhoA and Rac1 [399], which in turn regulate actin polymerization, and consequently adhesion dynamics and cell movement [399, 402]. FAK-dependent regulation of cycles of focal contact formation and disassembly is required for efficient cell movement [400] and increased FAK expression and activation correlates with tumour progression and metastasis [402]. We analysed F-actin cytoskeleton network and FAK status in our *in vitro* cell models and we did not observe significant changes in expression intensity or distribution of F-actin or FAK proteins upon

manipulation of FBXL4 expression levels, suggesting that FBXL4 regulates cell migration through yet unknown pathways.

6.3.2 ERLEC1 protein levels are regulated by FBXL4

Previous reports studying ERLEC1 expression, including association with FBXL4 [321] were based on tagged protein [352, 353] or custom-made antibodies [363] as there were no available anti-ERLEC1 antibodies. Only more recent reports used, in addition to anti-tag, commercial anti-ERLEC1 antibodies for assessment of endogenous protein by WB [403]. We tested a commercial polyclonal rabbit anti-ERLEC1 antibody (ab102046, Abcam, UK) by WB, IF and IHC. We proved antibody specificity for WB, but not for IF or IHC applications, where instead of well documented ER expression [352-354, 363] we obtained mostly nuclear staining. Using WB we found abundant ERLEC1 expression in all tested prostate cell lines, which seems to be in agreement with a previous report indicating common ERLEC1 RNA expression in a range of human adult tissues, including testis, skeletal muscle, pancreas and prostate [354].

Using proteomics based approach to identify candidate substrates and stably interacting proteins for a range of F-box family members, Tan *et al* [321] found ERLEC1 to interact with FBXL4, which was confirmed by co-immunoprecipitation. In their study, ERLEC1 was enriched in lysates from cells treated with either the proteasome inhibitor Bortezomib or CRL E3 inhibitor MLN4924. These agents increase the abundance of CRL (including SCF E3 ligases) and proteasomal substrates consistent with the assumption that ERLEC1 is a target for ubiquitination and proteasome degradation. Confirming ERLEC1 as a degradation target of FBXL4 proved difficult in cell line models with transient FBXL4 knockdown. This could be due to strong ERLEC1 expression from untransfected cells, which would make it hard to see further increase in ERLEC1 levels from FBXL4 knockdown cells in whole cell lysates. Indeed, when ERLEC1 was tested in monoclonal cell populations with stable FBXL4 knockdown or overexpression, we could confirm that FBXL4 targets ERLEC1 for degradation as cells with reduced FBXL4 had increased levels of ERLEC1 protein while the cells overexpressing FBXL4 showed reduction in ERLEC1 protein expression. ERLEC1 is a luminal ER protein, while FBXL4 mostly co-localises with mitochondria [319, 320], which we confirmed in stable HEK293 cells. It is not clear how these two proteins interact. Based on the study from Tan *et al* [321], FBXL4 targets several ER proteins, with many involved in stress induced unfolded protein response.

Most of ER proteins marked for degradation are dislocated from the ER into the cytoplasm, often with the help of luminal chaperons such as ERLEC1 and OS-9, which deliver them to membrane bound non-SCF E3 ligases, e.g. HRD1. These E3 ligases ubiquitinate misfolded proteins on the cytoplasmic site of the ER membrane, after their dislocation from the ER. Ubiquitinated proteins are then released from the ER membrane and delivered to the proteasome for degradation [340, 404-406]. Mitochondrial proteins are mostly degraded by mitochondrial proteases and only some of them are considered to be degraded by outer mitochondrial membrane-bound non-SCF E3 ligases in a similar way to ER proteins [407].

There is little known about F-box E3 ligases involved in the degradation of ER or mitochondrial proteins. A limited number of cytoplasmic SCF E3 ligases, including these linked to FBXO2, FBXO6, FBXO17, FBXO27, and FBXO44 F-box proteins seem to be capable of recognising and ubiquitinating glycosylated proteins translocated from the ER [408-412]. Even less is known about F-box proteins linked to mitochondrial protein degradation. Global analysis of human proteins for mitochondria targeted sequence predicts mitochondrial association of several components of cytoplasmic ubiquitin proteosome system, including several F-box proteins such as FBXO17, FBXO21, FBXO38, FBXW5, FBXL12 and FBXL4 [407, 413]. FBXL4 capability to bind ER proteins may come from close interactions between ER and mitochondria. Recent evidence shows that ER and mitochondria form physical contacts, which facilitate transfer of metabolites, such as lipids and Ca^{2+}, necessary for the regulation of lipid homeostasis, mitochondrial metabolism and the regulation of apoptotic signalling [348, 349]. Mitochondria sense and respond to ER stress by increasing contact with ER, promoting Ca^{2+} transfer and enhancing metabolism and ATP synthesis, which is then used to mount an adaptive response, protecting cells from stress-induced apoptosis [350, 351]. This stress induced response is regulated by parkin, another E3 ubiquitin ligase involved in mitochondria maintenance [414, 415]. Proximity of these two organelles and their increased contact upon stress would allow mitochondria-bound FBXL4 to interact with both, mitochondrial and ER proteins. This would explain why several of the proposed downstream targets of FBXL4 are involved in response to ER stress [321]. Further studies are necessary to determine where and how exactly FBXL4 interacts with ERLEC1 and leads to its degradation.

CHAPTER 7

Final discussion

7.1 Final discussion

7.1.1 Genomic copy number changes in prostate cancer revealed by genome-wide analysis

Studies of advanced metastatic PCa are hampered by the lack of routine pathological specimen. While there is abundance of primary PCa tissue from radical prostatectomies, no routine biopsies are performed for metastases, due to their skeletal location. Imaging techniques are used instead to confirm presence and excess of metastatic disease [416]. We have a unique set of PCa bone metastases collected from PCa patients, who were treated for pathological bone fractures caused by tumour metastases. Using genome-wide approach, these samples gave us the opportunity to look at the landscape of genomic changes specifically at PCa bone metastatic sites. Until recently the few published studies on genomic changes in metastatic PCa, which included limited number of bone metastases came from autopsies [153, 167, 228, 229], while more recent reports published during the course of our study, specifically consented advanced PCa patients for bone biopsy [138, 230, 231].

Our array-based genome-wide analysis of CNAs in PCa bone metastases found abundance of genomic changes, which is a common feature of advanced PCa [242]. Large losses of 6q, 13q, 16q and 18q as well gains of 8q, 7pq and Xq, which were present in 2-6 (33%-100%) of our six bone metastasis samples are the most frequent genomic changes reported in metastatic PCa and linked to bad prognosis [115, 219, 322, 417]. Many of these CNAs contained well-known PCa associated genes, including TSGs within losses (*PTEN* on 10q23.31, *RB1* on 13q14.2, *TP53* on 17p13.1) and oncogenes in gained regions (*AR* on Xq12, *MYC* on 8q24.21, *NCOA2* on 8q13.3 or *CCND1* on 11q13) [115, 164, 417]. Genetic changes within these genes are much more frequent in metastatic than localised cancers [121] and loss/inactivation of *TP53* and gain/activating mutations of *AR* specifically associate with PCa metastases [138]. We did not detect genomic changes specific in these bone metastasis samples, which is in agreement with current understanding that metastatic PCas display similar genomic changes to primary tumours but with higher frequency [121, 138].

7.1.2 11q13/*CCND1* copy number gain and cyclin D1 expression in PCa

The 11q13-14 gain detected in our 6 bone metastases is one of the most frequent gains in metastatic PCa, with *CCND1* oncogene commonly considered as a potential driver for this alteration [138]. Our genome-wide analysis showed that samples with confirmed *CCND1* copy number gain had also additional genomic changes within common *CCND1/RB/CDKN2A* and *TP53/CDKN1A* pathways controlling cell cycle progression, including losses within *RB*, *CDKN2A* (p16) and *TP53* tumour suppressor genes. These multiple alterations within the same pathway would all result in increased cell proliferation highlighting their importance in PCa progression. Our further analysis of *CCND1* copy number by FISH in larger cohorts of bone metastases as well as primary tumours revealed presence of *CCND1* gain in over half of PCa bone metastases but also in a small number of primary tumours, suggesting that *CCND1* gain can be an early event in PCa progression, which then becomes enriched in advanced tumours [138, 167].

Immunostaining for cyclin D1 protein in these two cohorts showed common presence of a small subset of cells (around 20%) positive for cyclin D1, with stronger staining intensity in tumours with *CCND1* gain and in bone metastases than primary tumours, confirming higher cyclin D1 activation in metastatic PCa [138]. Regardless of common cyclin D1 overexpression and multiple studies confirming its role in tumorigenesis, we found no correlation between cyclin D1 immunoexpression and Gleason score, which is the main prognostic factor for PCa. Our results are in agreement with other studies [299-301] and could possibly be explained by the fact that cyclin D1 often plays a cooperative role in carcinogenesis with other oncogenes, e.g. MYC or Ras [269, 270]. Additionally, cyclin D1 is a known feedback inhibitor of the AR, leading to repression of androgen-dependent proliferation [268, 284, 285, 418]. Considering that PCa is driven by activation of AR pathway, there is now more evidence that cyclin D1b, an alternatively spliced variant of cyclin D1 compromised for AR regulation, is more oncogenic than full size cyclin D1a and associated with PCa progression and poor outcome [282, 419].

We did not observe the same trend in our limited number of fresh-frozen prostate tissues and found low levels of cyclin D1b expressed along cyclin D1a across all samples, including BPHs, primary tumours and bone metastases. Recent *in vivo* study suggests that simply the presence of cyclin D1b can promote tumour formation without need for its elevated levels [419]. Unfortunately proper analysis of cyclin D1b expression in clinical samples is currently hampered by lack of commercially available antibodies.

7.1.3 Role of *FBXL4* loss in PCa

Loss of 6q13-q22 is a common feature of PCa and is especially frequent in advanced mCRPC [119, 150, 151, 236, 306]. However, due to large size of deleted region it is difficult to identify the potential driver of this alteration. Here, using genome-wide approach, we managed to narrow down the location of the driver to a small deletion within 6q16, the only deleted region shared by all six bone metastases analysed and located within, *FBXL4* gene.

FBXL4 is a member of F-box protein family involved in protein ubiquitination and degradation although it hasn't been widely studied and there are no reports linking it to cancer [314]. Here, for the first time we propose for *FBXL4* to be a possible TSG in PCa. We found *FBXL4* copy number loss a common feature of PCa bone metastases, which was also present at low frequency in primary tumours suggesting that *FBXL4* loss is an early event in PCa carcinogenesis. Further analysis of *FBXL4* loss in a large cohort of early stage conservatively managed localised PCas [216] showed that *FBXL4* loss was significantly associated with poor PCa prognostic features and PCa specific death, suggesting its involvement in PCa progression. However, *FBXL4* loss was not independent prognostic factor in multivariate analysis. Analysis of FBXL4 protein expression in clinical samples is currently hindered by lack of good commercial antibodies. We tested several commercial anti-FBXL4 antibodies and only one showed good level of specificity but still was not sensitive to small differences in protein levels based on knockdown *in vitro* experiments. Additionally, to confirm a tumour suppressor role of FBXL4 *in vivo* study is necessary, where mice are injected with PCa cells, e.g. 22RV1 with or without FBXL4 knockdown and size and number of tumours is counted. If FBXL4 is a TSG then mice injected with FBXL4 knockdown cells should have more/bigger tumours than control animals.

Using *in vitro* cell line models we showed that *FBXL4* regulates cell motility and invasion but not proliferation. FBXL4 downregulation in PCa cell lines consistently led to increased PCa cell migration and invasion and this increased cell aggressiveness is in agreement with observed correlation of FBXL4 loss with aggressive metastatic PCa. Currently, it is not known how exactly FBXL4 regulates cells invasiveness but it could be due to regulation of ERLEC1 protein levels. ERLEC1 was previously identified as a FBXL4 binding protein [321]. Using *in vitro* cell line models we confirmed that ERLEC1 is a degradation target of FBXL4 as ERLEC1 protein expression inversely correlated with FBXL4 expression levels. ERLEC1 is an ER chaperone involved in degradation of

misfolded proteins, leading to release of cellular stress [352, 353, 363]. In lung cancer ERLEC1 was identified as a novel cancer invasion and metastasis-related gene involved in increased cells tolerance to stress and protection from apoptosis [354]. Therefore, downregulation of FBXL4 in PCa cells would lead to stabilisation of ERLEC1 allowing malignant cells to efficiently respond to encountered stress such as hypoxia.

Considering that homozygous loss of function mutations in *FBXL4* lead to severe impairment of mitochondrial function including fragmentation of mitochondrial network [319, 320, 338, 370], FBXL4 is probably involved in mitochondria maintenance. We confirmed that FBXL4 associates with mitochondria. Mitochondria are in constant contact with ER and ER is actively involved in their fission [420, 421]. Mitochondria are also responsive to ER stress, adapting their function towards stress attenuation [350, 351]. Therefore, downregulation of ERLEC1 protein levels by FBXL4 could be linked to normal mitochondria-ER dynamics. Moreover, mitochondrial network organisation, specifically its fragmentation levels are important for cell motility, with more fragmented network promoting cell migration and invasion [373, 374]. The relation between FBXL4 and ERLEC1, especially in contest of cellular stress such as hypoxia or ER stress needs to be studied further. Further *in vitro* studies involving manipulation of FBXL4 and ERLEC1 protein levels are necessary to uncover the interplay between these proteins and their impact on mitochondria network integrity, cell invasion abilities and survival under stressful conditions.

7.1.4 Conclusions

In this study, by analysing PCa bone metastases using high-density microarrays, I found many genomic alterations shared by advanced metastatic PCa. Further analysis of two of these regions, 11q13 gain at *CCND1* locus and 6q16 loss at *FBXL4* locus in larger FFPE tissue cohorts of primary PCa and bone metastases, confirmed enrichment of these alterations in metastatic samples. While full length cyclin D1a expression doesn't seem to correlate with Gleason score, studies of the possibly more oncogenic splice variant, cyclin D1b are currently hampered by lack of commercially available antibodies.

The *FBXL4* gene, which until now was never reported to be involved in cancer, seems to be a possible tumour suppressor in PCa, as its loss can be detected in a subset of early stage primary cancers, where it correlates with all poor PCa prognostic features and worse patient survival. My study shows, that the *FBXL4* loss may contribute to PCa progression through increased cancer cells motility and invasion. Impact of FBXL4 on

cell invasiveness could be linked to its role in downregulation of ERLEC1, a protein involved in pro-survival ERAD pathway activated in response to stress. Therfore, loss of *FBXL4* could be one of the mechanisms to increase cancer cells efficiency to respond to stress and to increase their metastatic potential through stabilisation of ERLEC1. Further analysis of FBXL4-ERLEC1 interactions could potentially help to develop novel targeted therapies for aggressive disease harbouring FBXL4 abnormalities. My findings give new insights into PCa progression, raising the potential to develop a novel biomarker to monitor disease progression and novel therapeutic approaches for this subgroup of aggressive PCa.

References

References

1. Kumar, V.L. and P.K. Majumder, *Prostate gland: structure, functions and regulation.* Int Urol Nephrol, 1995. **27**(3): p. 231-43.
2. McNeal, J.E., *The zonal anatomy of the prostate.* Prostate, 1981. **2**(1): p. 35-49.
3. Crawford, E.D., *Understanding the epidemiology, natural history, and key pathways involved in prostate cancer.* Urology, 2009. **73**(5 Suppl): p. S4-10.
4. Miller, G.J. and J.M. Cygan, *Morphology of prostate cancer: the effects of multifocality on histological grade, tumor volume and capsule penetration.* J Urol, 1994. **152**(5 Pt 2): p. 1709-13.
5. Byar, D.P. and F.K. Mostofi, *Carcinoma of the prostate: prognostic evaluation of certain pathologic features in 208 radical prostatectomies. Examined by the step-section technique.* Cancer, 1972. **30**(1): p. 5-13.
6. Shen, M.M. and C. Abate-Shen, *Molecular genetics of prostate cancer: new prospects for old challenges.* Genes & development, 2010. **24**(18): p. 1967-2000.
7. De Marzo, A.M., et al., *Human prostate cancer precursors and pathobiology.* Urology, 2003. **62**(5 Suppl 1): p. 55-62.
8. Brawer, M.K., *Prostatic intraepithelial neoplasia: an overview.* Rev Urol, 2005. **7 Suppl 3**: p. S11-8.
9. Rosenberg, M.T., et al., *Biology and natural history of prostate cancer and the role of chemoprevention.* Int J Clin Pract, 2010. **64**(13): p. 1746-53.
10. Ferlay J, S.I., Ervik M, et al, *Cancer Incidence and Mortality Worldwide.* IARC CancerBase No. 11 [http://globocan.iarc.fr]. Lyon, France: International Agency for Research on Cancer, GLOBOCAN 2012 v1.0.
11. CRUK, *http://www.cancerresearchuk.org/health-professional/cancer-statistics/* , . Accessed [2016].
12. Siegel, R.L., K.D. Miller, and A. Jemal, *Cancer statistics, 2016.* CA Cancer J Clin, 2016. **66**(1): p. 7-30.
13. Kimura, T., *East meets West: ethnic differences in prostate cancer epidemiology between East Asians and Caucasians.* Chin J Cancer, 2012. **31**(9): p. 421-9.
14. Torre, L.A., et al., *Global cancer statistics, 2012.* CA Cancer J Clin, 2015. **65**(2): p. 87-108.
15. Center, M.M., et al., *International variation in prostate cancer incidence and mortality rates.* Eur Urol, 2012. **61**(6): p. 1079-92.
16. Sakr, W.A., et al., *Age and racial distribution of prostatic intraepithelial neoplasia.* Eur Urol, 1996. **30**(2): p. 138-44.
17. CRUK, *CancerStats – Incidence 2008 – UK.* 2011.
18. Selley, S., et al., *Diagnosis, management and screening of early localised prostate cancer.* Health Technol Assess, 1997. **1**(2): p. i, 1-96.
19. Schulz, W.A., M. Burchardt, and M.V. Cronauer, *Molecular biology of prostate cancer.* Mol Hum Reprod, 2003. **9**(8): p. 437-48.
20. Siegel, R., et al., *Cancer statistics, 2011: the impact of eliminating socioeconomic and racial disparities on premature cancer deaths.* CA Cancer J Clin, 2011. **61**(4): p. 212-36.
21. Carter, B.S., et al., *Mendelian inheritance of familial prostate cancer.* Proceedings of the National Academy of Sciences of the United States of America, 1992. **89**(8): p. 3367-71.
22. Johns, L.E. and R.S. Houlston, *A systematic review and meta-analysis of familial prostate cancer risk.* BJU Int, 2003. **91**(9): p. 789-94.
23. Attard, G., et al., *Prostate cancer.* Lancet, 2016. **387**(10013): p. 70-82.
24. Mao, X., et al., *Distinct genomic alterations in prostate cancers in Chinese and Western populations suggest alternative pathways of prostate carcinogenesis.* Cancer Res, 2010. **70**(13): p. 5207-12.

25. Berges, R.R., et al., *Implication of cell kinetic changes during the progression of human prostatic cancer.* Clin Cancer Res, 1995. **1**(5): p. 473-80.
26. Rajan, P., et al., *Next-generation sequencing of advanced prostate cancer treated with androgen-deprivation therapy.* Eur Urol, 2014. **66**(1): p. 32-9.
27. Karantanos, T., et al., *Understanding the mechanisms of androgen deprivation resistance in prostate cancer at the molecular level.* Eur Urol, 2015. **67**(3): p. 470-9.
28. Schweizer, M.T. and E.Y. Yu, *Persistent androgen receptor addiction in castration-resistant prostate cancer.* J Hematol Oncol, 2015. **8**: p. 128.
29. Gjertson, C.K. and P.C. Albertsen, *Use and assessment of PSA in prostate cancer.* The Medical clinics of North America, 2011. **95**(1): p. 191-200.
30. Barry, M.J., *Clinical practice. Prostate-specific-antigen testing for early diagnosis of prostate cancer.* N Engl J Med, 2001. **344**(18): p. 1373-7.
31. Ilic, D., et al., *Screening for prostate cancer.* The Cochrane database of systematic reviews, 2013. **1**: p. CD004720.
32. Schroder, F.H., et al., *Screening and prostate-cancer mortality in a randomized European study.* N Engl J Med, 2009. **360**(13): p. 1320-8.
33. Schroder, F.H., et al., *Screening and prostate cancer mortality: results of the European Randomised Study of Screening for Prostate Cancer (ERSPC) at 13 years of follow-up.* Lancet, 2014. **384**(9959): p. 2027-35.
34. Andriole, G.L., et al., *Mortality results from a randomized prostate-cancer screening trial.* N Engl J Med, 2009. **360**(13): p. 1310-9.
35. Pinsky, P.F., et al., *Assessing contamination and compliance in the prostate component of the Prostate, Lung, Colorectal, and Ovarian (PLCO) Cancer Screening Trial.* Clin Trials, 2010. **7**(4): p. 303-11.
36. Tosoian, J. and S. Loeb, *PSA and beyond: the past, present, and future of investigative biomarkers for prostate cancer.* TheScientificWorldJournal, 2010. **10**: p. 1919-31.
37. Gleason, D.F. and G.T. Mellinger, *Prediction of prognosis for prostatic adenocarcinoma by combined histological grading and clinical staging.* J Urol, 1974. **111**(1): p. 58-64.
38. Humphrey, P.A., *Gleason grading and prognostic factors in carcinoma of the prostate.* Modern pathology : an official journal of the United States and Canadian Academy of Pathology, Inc, 2004. **17**(3): p. 292-306.
39. Epstein, J.I., et al., *The 2005 International Society of Urological Pathology (ISUP) Consensus Conference on Gleason Grading of Prostatic Carcinoma.* The American journal of surgical pathology, 2005. **29**(9): p. 1228-42.
40. Epstein, J.I., *An update of the Gleason grading system.* J Urol, 2010. **183**(2): p. 433-40.
41. Brimo, F., et al., *Contemporary grading for prostate cancer: implications for patient care.* Eur Urol, 2013. **63**(5): p. 892-901.
42. Shah, R.B., *Current perspectives on the Gleason grading of prostate cancer.* Archives of pathology & laboratory medicine, 2009. **133**(11): p. 1810-6.
43. Harnden, P., et al., *Should the Gleason grading system for prostate cancer be modified to account for high-grade tertiary components? A systematic review and meta-analysis.* The lancet oncology, 2007. **8**(5): p. 411-9.
44. Herman, C.M., et al., *Primary Gleason pattern as a predictor of disease progression in gleason score 7 prostate cancer: a multivariate analysis of 823 men treated with radical prostatectomy.* The American journal of surgical pathology, 2001. **25**(5): p. 657-60.
45. Pierorazio, P.M., et al., *Prognostic Gleason grade grouping: data based on the modified Gleason scoring system.* BJU Int, 2013. **111**(5): p. 753-60.
46. Egevad, L., et al., *International Society of Urological Pathology (ISUP) grading of prostate cancer - An ISUP consensus on contemporary grading.* APMIS, 2016. **124**(6): p. 433-5.
47. Spratt, D.E., et al., *Independent Surgical Validation of the New Prostate Cancer Grade Grouping System.* BJU Int, 2016.

48. Humphrey, P.A., et al., *The 2016 WHO Classification of Tumours of the Urinary System and Male Genital Organs-Part B: Prostate and Bladder Tumours.* Eur Urol, 2016.
49. Cohen, M.S., et al., *Comparing the Gleason prostate biopsy and Gleason prostatectomy grading system: the Lahey Clinic Medical Center experience and an international meta-analysis.* Eur Urol, 2008. **54**(2): p. 371-81.
50. Moussa, A.S., et al., *Prostate biopsy clinical and pathological variables that predict significant grading changes in patients with intermediate and high grade prostate cancer.* BJU international, 2009. **103**(1): p. 43-8.
51. Falzarano, S.M. and C. Magi-Galluzzi, *Prostate cancer staging and grading at radical prostatectomy over time.* Advances in anatomic pathology, 2011. **18**(2): p. 159-64.
52. Greene FL, P.D., Fleming ID, et al., *Manual for Staging Cancer*. 6 ed. American Joint Committee on Cancer, ed. Springer. 2002, New York, NY.
53. Kuczyk, M.A., et al., *The prognostic value of p53 for long-term and recurrence-free survival following radical prostatectomy.* European journal of cancer, 1998. **34**(5): p. 679-86.
54. D'Amico, A.V., et al., *Preoperative PSA velocity and the risk of death from prostate cancer after radical prostatectomy.* N Engl J Med, 2004. **351**(2): p. 125-35.
55. Evans, A.J., et al., *Interobserver variability between expert urologic pathologists for extraprostatic extension and surgical margin status in radical prostatectomy specimens.* The American journal of surgical pathology, 2008. **32**(10): p. 1503-12.
56. Kench, J.G., et al., *Prognostic factors in prostate cancer. Key elements in structured histopathology reporting of radical prostatectomy specimens.* Pathology, 2011. **43**(5): p. 410-9.
57. van der Kwast, T.H., et al., *Impact of pathology review of stage and margin status of radical prostatectomy specimens (EORTC trial 22911).* Virchows Archiv : an international journal of pathology, 2006. **449**(4): p. 428-34.
58. Iczkowski, K.A. and M.S. Lucia, *Frequency of positive surgical margin at prostatectomy and its effect on patient outcome.* Prostate cancer, 2011. **2011**: p. 673021.
59. Bangma, C.H., M.J. Roobol, and E.W. Steyerberg, *Predictive models in diagnosing indolent cancer.* Cancer, 2009. **115**(13 Suppl): p. 3100-6.
60. Bangma, C.H., S. Roemeling, and F.H. Schroder, *Overdiagnosis and overtreatment of early detected prostate cancer.* World journal of urology, 2007. **25**(1): p. 3-9.
61. http://www.nice.org.uk/Guidance/CG58.
62. Chung, M.S. and S.H. Lee, *Current status of active surveillance in prostate cancer.* Investig Clin Urol, 2016. **57**(1): p. 14-20.
63. Heidenreich, A., et al., *EAU guidelines on prostate cancer. part 1: screening, diagnosis, and local treatment with curative intent-update 2013.* Eur Urol, 2014. **65**(1): p. 124-37.
64. Tosoian, J.J., et al., *Pathologic Outcomes in Favorable-risk Prostate Cancer: Comparative Analysis of Men Electing Active Surveillance and Immediate Surgery.* Eur Urol, 2016. **69**(4): p. 576-81.
65. Filella, X., J. Alcover, and R. Molina, *Active surveillance in prostate cancer: the need to standardize.* Tumour biology : the journal of the International Society for Oncodevelopmental Biology and Medicine, 2011. **32**(5): p. 839-43.
66. Rosenthal, S.A. and H.M. Sandler, *Treatment strategies for high-risk locally advanced prostate cancer.* Nature reviews. Urology, 2010. **7**(1): p. 31-8.
67. Heinlein, C.A. and C. Chang, *Androgen receptor in prostate cancer.* Endocr Rev, 2004. **25**(2): p. 276-308.
68. Heidenreich, A., et al., *EAU guidelines on prostate cancer.* Eur Urol, 2008. **53**(1): p. 68-80.
69. Chamberlain, J., et al., *The diagnosis, management, treatment and costs of prostate cancer in England and Wales.* Health technology assessment, 1997. **1**(3): p. i-vi, 1-53.
70. Tannock, I.F., et al., *Docetaxel plus prednisone or mitoxantrone plus prednisone for advanced prostate cancer.* N Engl J Med, 2004. **351**(15): p. 1502-12.

71. Vale, C.L., et al., *Addition of docetaxel or bisphosphonates to standard of care in men with localised or metastatic, hormone-sensitive prostate cancer: a systematic review and meta-analyses of aggregate data.* Lancet Oncol, 2016. **17**(2): p. 243-56.
72. Sweeney, C.J., et al., *Chemohormonal Therapy in Metastatic Hormone-Sensitive Prostate Cancer.* N Engl J Med, 2015. **373**(8): p. 737-46.
73. Gravis, G., et al., *Androgen-deprivation therapy alone or with docetaxel in non-castrate metastatic prostate cancer (GETUG-AFU 15): a randomised, open-label, phase 3 trial.* Lancet Oncol, 2013. **14**(2): p. 149-58.
74. James, N.D., et al., *Addition of docetaxel, zoledronic acid, or both to first-line long-term hormone therapy in prostate cancer (STAMPEDE): survival results from an adaptive, multiarm, multistage, platform randomised controlled trial.* Lancet, 2016. **387**(10024): p. 1163-77.
75. Ning, Y.M., et al., *Enzalutamide for treatment of patients with metastatic castration-resistant prostate cancer who have previously received docetaxel: U.S. Food and Drug Administration drug approval summary.* Clin Cancer Res, 2013. **19**(22): p. 6067-73.
76. de Bono, J.S., et al., *Abiraterone and increased survival in metastatic prostate cancer.* N Engl J Med, 2011. **364**(21): p. 1995-2005.
77. de Bono, J.S., et al., *Prednisone plus cabazitaxel or mitoxantrone for metastatic castration-resistant prostate cancer progressing after docetaxel treatment: a randomised open-label trial.* Lancet, 2010. **376**(9747): p. 1147-54.
78. Al Nakouzi, N., et al., *Cabazitaxel Remains Active in Patients Progressing After Docetaxel Followed by Novel Androgen Receptor Pathway Targeted Therapies.* Eur Urol, 2015. **68**(2): p. 228-35.
79. Snoeks, L.L., et al., *New treatment options for patients with metastatic prostate cancer.* The Netherlands journal of medicine, 2013. **71**(6): p. 290-4.
80. Bahl, A., et al., *Second-line treatment options in metastatic castration-resistant prostate cancer: A comparison of key trials with recently approved agents.* Cancer treatment reviews, 2013.
81. Hanahan, D. and R.A. Weinberg, *The hallmarks of cancer.* Cell, 2000. **100**(1): p. 57-70.
82. Hanahan, D. and R.A. Weinberg, *Hallmarks of cancer: the next generation.* Cell, 2011. **144**(5): p. 646-74.
83. Negrini, S., V.G. Gorgoulis, and T.D. Halazonetis, *Genomic instability--an evolving hallmark of cancer.* Nature reviews. Molecular cell biology, 2010. **11**(3): p. 220-8.
84. Lengauer, C., K.W. Kinzler, and B. Vogelstein, *Genetic instabilities in human cancers.* Nature, 1998. **396**(6712): p. 643-9.
85. Ellegren, H., *Microsatellites: simple sequences with complex evolution.* Nat Rev Genet, 2004. **5**(6): p. 435-45.
86. Geiersbach, K.B. and W.S. Samowitz, *Microsatellite instability and colorectal cancer.* Archives of pathology & laboratory medicine, 2011. **135**(10): p. 1269-77.
87. Iacopetta, B., F. Grieu, and B. Amanuel, *Microsatellite instability in colorectal cancer.* Asia-Pacific journal of clinical oncology, 2010. **6**(4): p. 260-9.
88. Hoeijmakers, J.H., *Genome maintenance mechanisms for preventing cancer.* Nature, 2001. **411**(6835): p. 366-74.
89. Lengauer, C., K.W. Kinzler, and B. Vogelstein, *Genetic instability in colorectal cancers.* Nature, 1997. **386**(6625): p. 623-7.
90. Thompson, S.L. and D.A. Compton, *Chromosomes and cancer cells.* Chromosome research : an international journal on the molecular, supramolecular and evolutionary aspects of chromosome biology, 2011. **19**(3): p. 433-44.
91. Carter, B.S., et al., *Hereditary prostate cancer: epidemiologic and clinical features.* J Urol, 1993. **150**(3): p. 797-802.

92. Nwosu, V., et al., *Heterogeneity of genetic alterations in prostate cancer: evidence of the complex nature of the disease.* Human molecular genetics, 2001. **10**(20): p. 2313-8.
93. Kote-Jarai, Z., et al., *Multiple novel prostate cancer predisposition loci confirmed by an international study: the PRACTICAL Consortium.* Cancer epidemiology, biomarkers & prevention : a publication of the American Association for Cancer Research, cosponsored by the American Society of Preventive Oncology, 2008. **17**(8): p. 2052-61.
94. Edwards, S.M., et al., *Two percent of men with early-onset prostate cancer harbor germline mutations in the BRCA2 gene.* American journal of human genetics, 2003. **72**(1): p. 1-12.
95. Ishak, M.B. and V.N. Giri, *A systematic review of replication studies of prostate cancer susceptibility genetic variants in high-risk men originally identified from genome-wide association studies.* Cancer epidemiology, biomarkers & prevention : a publication of the American Association for Cancer Research, cosponsored by the American Society of Preventive Oncology, 2011. **20**(8): p. 1599-610.
96. Schaid, D.J., *The complex genetic epidemiology of prostate cancer.* Human molecular genetics, 2004. **13 Spec No 1**: p. R103-21.
97. Hicks, C., et al., *Comprehensive assessment and network analysis of the emerging genetic susceptibility landscape of prostate cancer.* Cancer informatics, 2013. **12**: p. 175-91.
98. Bambury, R.M. and D.J. Gallagher, *Prostate cancer: germline prediction for a commonly variable malignancy.* BJU international, 2012. **110**(11 Pt C): p. E809-18.
99. Bush, W.S. and J.H. Moore, *Chapter 11: Genome-wide association studies.* PLoS computational biology, 2012. **8**(12): p. e1002822.
100. Wasserman, N.F., I. Aneas, and M.A. Nobrega, *An 8q24 gene desert variant associated with prostate cancer risk confers differential in vivo activity to a MYC enhancer.* Genome research, 2010. **20**(9): p. 1191-7.
101. Han, Y., et al., *Integration of multiethnic fine-mapping and genomic annotation to prioritize candidate functional SNPs at prostate cancer susceptibility regions.* Hum Mol Genet, 2015. **24**(19): p. 5603-18.
102. Chen, H., et al., *Systematic enrichment analysis of potentially functional regions for 103 prostate cancer risk-associated loci.* Prostate, 2015. **75**(12): p. 1264-76.
103. Han, Y., et al., *Generalizability of established prostate cancer risk variants in men of African ancestry.* Int J Cancer, 2015. **136**(5): p. 1210-7.
104. Virlogeux, V., et al., *Replication and heritability of prostate cancer risk variants: impact of population-specific factors.* Cancer Epidemiol Biomarkers Prev, 2015. **24**(6): p. 938-43.
105. Marzec, J., et al., *A genetic study and meta-analysis of the genetic predisposition of prostate cancer in a Chinese population.* Oncotarget, 2016.
106. Whitington, T., et al., *Gene regulatory mechanisms underpinning prostate cancer susceptibility.* Nat Genet, 2016. **48**(4): p. 387-97.
107. Al Olama, A.A., et al., *A meta-analysis of 87,040 individuals identifies 23 new susceptibility loci for prostate cancer.* Nat Genet, 2014. **46**(10): p. 1103-9.
108. Pomerantz, M.M., et al., *The androgen receptor cistrome is extensively reprogrammed in human prostate tumorigenesis.* Nat Genet, 2015. **47**(11): p. 1346-51.
109. Berndt, S.I., et al., *Two susceptibility loci identified for prostate cancer aggressiveness.* Nat Commun, 2015. **6**: p. 6889.
110. Schumacher, F.R., et al., *Genome-wide association study identifies new prostate cancer susceptibility loci.* Hum Mol Genet, 2011. **20**(19): p. 3867-75.
111. Xu, J., et al., *Inherited genetic variant predisposes to aggressive but not indolent prostate cancer.* Proc Natl Acad Sci U S A, 2010. **107**(5): p. 2136-40.
112. Sun, J., et al., *Sequence variants at 22q13 are associated with prostate cancer risk.* Cancer Res, 2009. **69**(1): p. 10-5.
113. Pearson, T.A. and T.A. Manolio, *How to interpret a genome-wide association study.* JAMA, 2008. **299**(11): p. 1335-44.

114. Barbieri, C.E. and S.A. Tomlins, *Reprint of: The prostate cancer genome: Perspectives and potential.* Urol Oncol, 2015. **33**(2): p. 95-102.
115. Taylor, B.S., et al., *Integrative genomic profiling of human prostate cancer.* Cancer cell, 2010. **18**(1): p. 11-22.
116. Barbieri, C.E., et al., *Exome sequencing identifies recurrent SPOP, FOXA1 and MED12 mutations in prostate cancer.* Nat Genet, 2012. **44**(6): p. 685-9.
117. Berger, M.F., et al., *The genomic complexity of primary human prostate cancer.* Nature, 2011. **470**(7333): p. 214-20.
118. Grasso, C.S., et al., *The mutational landscape of lethal castration-resistant prostate cancer.* Nature, 2012. **487**(7406): p. 239-43.
119. Sun, J., et al., *DNA copy number alterations in prostate cancers: a combined analysis of published CGH studies.* Prostate, 2007. **67**(7): p. 692-700.
120. Lapointe, J., et al., *Genomic profiling reveals alternative genetic pathways of prostate tumorigenesis.* Cancer Res, 2007. **67**(18): p. 8504-10.
121. Williams, J.L., P.A. Greer, and J.A. Squire, *Recurrent copy number alterations in prostate cancer: an in silico meta-analysis of publicly available genomic data.* Cancer Genet, 2014. **207**(10-12): p. 474-88.
122. Tomlins, S.A., et al., *Recurrent fusion of TMPRSS2 and ETS transcription factor genes in prostate cancer.* Science, 2005. **310**(5748): p. 644-8.
123. Mosquera, J.M., et al., *Characterization of TMPRSS2-ERG fusion high-grade prostatic intraepithelial neoplasia and potential clinical implications.* Clin Cancer Res, 2008. **14**(11): p. 3380-5.
124. Clark, J., et al., *Complex patterns of ETS gene alteration arise during cancer development in the human prostate.* Oncogene, 2008. **27**(14): p. 1993-2003.
125. Mao, X., et al., *Chromosome rearrangement associated inactivation of tumour suppressor genes in prostate cancer.* American journal of cancer research, 2011. **1**(5): p. 604-17.
126. Clark, J., et al., *Diversity of TMPRSS2-ERG fusion transcripts in the human prostate.* Oncogene, 2007. **26**(18): p. 2667-73.
127. Casey, O.M., et al., *TMPRSS2- driven ERG expression in vivo increases self-renewal and maintains expression in a castration resistant subpopulation.* PloS one, 2012. **7**(7): p. e41668.
128. Demichelis, F., et al., *TMPRSS2:ERG gene fusion associated with lethal prostate cancer in a watchful waiting cohort.* Oncogene, 2007. **26**(31): p. 4596-9.
129. Rajput, A.B., et al., *Frequency of the TMPRSS2:ERG gene fusion is increased in moderate to poorly differentiated prostate cancers.* Journal of clinical pathology, 2007. **60**(11): p. 1238-43.
130. Attard, G., et al., *Duplication of the fusion of TMPRSS2 to ERG sequences identifies fatal human prostate cancer.* Oncogene, 2008. **27**(3): p. 253-63.
131. Saramaki, O.R., et al., *TMPRSS2:ERG fusion identifies a subgroup of prostate cancers with a favorable prognosis.* Clin Cancer Res, 2008. **14**(11): p. 3395-400.
132. Font-Tello, A., et al., *Association of ERG and TMPRSS2-ERG with grade, stage, and prognosis of prostate cancer is dependent on their expression levels.* Prostate, 2015. **75**(11): p. 1216-26.
133. Hagglof, C., et al., *TMPRSS2-ERG expression predicts prostate cancer survival and associates with stromal biomarkers.* PLoS One, 2014. **9**(2): p. e86824.
134. Kim, S.H., et al., *Overexpression of ERG and Wild-Type PTEN Are Associated with Favorable Clinical Prognosis and Low Biochemical Recurrence in Prostate Cancer.* PLoS One, 2015. **10**(4): p. e0122498.
135. Bismar, T.A., et al., *ERG protein expression reflects hormonal treatment response and is associated with Gleason score and prostate cancer specific mortality.* Eur J Cancer, 2012. **48**(4): p. 538-46.

136. Baca, S.C., et al., *Punctuated evolution of prostate cancer genomes.* Cell, 2013. **153**(3): p. 666-77.
137. Rubin, M.A., C.A. Maher, and A.M. Chinnaiyan, *Common gene rearrangements in prostate cancer.* Journal of clinical oncology : official journal of the American Society of Clinical Oncology, 2011. **29**(27): p. 3659-68.
138. Robinson, D., et al., *Integrative clinical genomics of advanced prostate cancer.* Cell, 2015. **161**(5): p. 1215-28.
139. Donovan, M.J. and C. Cordon-Cardo, *Predicting high-risk disease using tissue biomarkers.* Current opinion in urology, 2013. **23**(3): p. 245-51.
140. Beltran, H., et al., *Targeted Next-generation Sequencing of Advanced Prostate Cancer Identifies Potential Therapeutic Targets and Disease Heterogeneity.* Eur Urol, 2012.
141. Tomlins, S.A., M.A. Rubin, and A.M. Chinnaiyan, *Integrative biology of prostate cancer progression.* Annual review of pathology, 2006. **1**: p. 243-71.
142. Tomlins, S.A., et al., *ETS gene fusions in prostate cancer: from discovery to daily clinical practice.* Eur Urol, 2009. **56**(2): p. 275-86.
143. Demichelis, F., et al., *Distinct genomic aberrations associated with ERG rearranged prostate cancer.* Genes, chromosomes & cancer, 2009. **48**(4): p. 366-80.
144. Krohn, A., et al., *Recurrent deletion of 3p13 targets multiple tumour suppressor genes and defines a distinct subgroup of aggressive ERG fusion-positive prostate cancers.* J Pathol, 2013. **231**(1): p. 130-41.
145. Huang, S., et al., *Recurrent deletion of CHD1 in prostate cancer with relevance to cell invasiveness.* Oncogene, 2012. **31**(37): p. 4164-70.
146. Cuzick, J., et al., *Prognostic value of an RNA expression signature derived from cell cycle proliferation genes in patients with prostate cancer: a retrospective study.* Lancet Oncol, 2011. **12**(3): p. 245-55.
147. Cuzick, J., et al., *Prognostic value of a cell cycle progression signature for prostate cancer death in a conservatively managed needle biopsy cohort.* Br J Cancer, 2012. **106**(6): p. 1095-9.
148. Klein, E.A., et al., *A 17-gene assay to predict prostate cancer aggressiveness in the context of Gleason grade heterogeneity, tumor multifocality, and biopsy undersampling.* Eur Urol, 2014. **66**(3): p. 550-60.
149. Erho, N., et al., *Discovery and validation of a prostate cancer genomic classifier that predicts early metastasis following radical prostatectomy.* PLoS One, 2013. **8**(6): p. e66855.
150. Holcomb, I.N., et al., *Genomic alterations indicate tumor origin and varied metastatic potential of disseminated cells from prostate cancer patients.* Cancer Res, 2008. **68**(14): p. 5599-608.
151. Holcomb, I.N., et al., *Comparative analyses of chromosome alterations in soft-tissue metastases within and across patients with castration-resistant prostate cancer.* Cancer Res, 2009. **69**(19): p. 7793-802.
152. Letouze, E., et al., *Analysis of the copy number profiles of several tumor samples from the same patient reveals the successive steps in tumorigenesis.* Genome biology, 2010. **11**(7): p. R76.
153. Robbins, C.M., et al., *Copy number and targeted mutational analysis reveals novel somatic events in metastatic prostate tumors.* Genome research, 2011. **21**(1): p. 47-55.
154. Jarrard, D.F., et al., *Deletional, mutational, and methylation analyses of CDKN2 (p16/MTS1) in primary and metastatic prostate cancer.* Genes, chromosomes & cancer, 1997. **19**(2): p. 90-6.
155. Sircar, K., et al., *PTEN genomic deletion is associated with p-Akt and AR signalling in poorer outcome, hormone refractory prostate cancer.* The Journal of pathology, 2009. **218**(4): p. 505-13.

156. Schmitz, M., et al., *Complete loss of PTEN expression as a possible early prognostic marker for prostate cancer metastasis.* International journal of cancer. Journal international du cancer, 2007. **120**(6): p. 1284-92.
157. Ishkanian, A.S., et al., *Array CGH as a potential predictor of radiocurability in intermediate risk prostate cancer.* Acta oncologica, 2010. **49**(7): p. 888-94.
158. Bookstein, R., et al., *Promoter deletion and loss of retinoblastoma gene expression in human prostate carcinoma.* Proceedings of the National Academy of Sciences of the United States of America, 1990. **87**(19): p. 7762-6.
159. Phillips, S.M., et al., *Loss of the retinoblastoma susceptibility gene (RB1) is a frequent and early event in prostatic tumorigenesis.* British journal of cancer, 1994. **70**(6): p. 1252-7.
160. Kibel, A.S., et al., *Loss of heterozygosity at 12P12-13 in primary and metastatic prostate adenocarcinoma.* J Urol, 2000. **164**(1): p. 192-6.
161. Bethel, C.R., et al., *Decreased NKX3.1 protein expression in focal prostatic atrophy, prostatic intraepithelial neoplasia, and adenocarcinoma: association with gleason score and chromosome 8p deletion.* Cancer Res, 2006. **66**(22): p. 10683-90.
162. Jenkins, R.B., et al., *Detection of c-myc oncogene amplification and chromosomal anomalies in metastatic prostatic carcinoma by fluorescence in situ hybridization.* Cancer Res, 1997. **57**(3): p. 524-31.
163. Reiter, R.E., et al., *Coamplification of prostate stem cell antigen (PSCA) and MYC in locally advanced prostate cancer.* Genes, chromosomes & cancer, 2000. **27**(1): p. 95-103.
164. Silva, M.P., et al., *NCOA2 is a candidate target gene of 8q gain associated with clinically aggressive prostate cancer.* Genes Chromosomes Cancer, 2016. **55**(4): p. 365-74.
165. Visakorpi, T., et al., *In vivo amplification of the androgen receptor gene and progression of human prostate cancer.* Nat Genet, 1995. **9**(4): p. 401-6.
166. Saramaki, O.R., et al., *The gene for polycomb group protein enhancer of zeste homolog 2 (EZH2) is amplified in late-stage prostate cancer.* Genes, chromosomes & cancer, 2006. **45**(7): p. 639-45.
167. Gundem, G., et al., *The evolutionary history of lethal metastatic prostate cancer.* Nature, 2015. **520**(7547): p. 353-7.
168. Tomlins, S.A., et al., *Distinct classes of chromosomal rearrangements create oncogenic ETS gene fusions in prostate cancer.* Nature, 2007. **448**(7153): p. 595-9.
169. Nguyen, D.X. and J. Massague, *Genetic determinants of cancer metastasis.* Nature reviews. Genetics, 2007. **8**(5): p. 341-52.
170. Theriault, R.L., *Biology of bone metastases.* Cancer control : journal of the Moffitt Cancer Center, 2012. **19**(2): p. 92-101.
171. Mundy, G.R., *Metastasis to bone: causes, consequences and therapeutic opportunities.* Nature reviews. Cancer, 2002. **2**(8): p. 584-93.
172. Gupta, P.B., et al., *The evolving portrait of cancer metastasis.* Cold Spring Harbor symposia on quantitative biology, 2005. **70**: p. 291-7.
173. Bernards, R. and R.A. Weinberg, *A progression puzzle.* Nature, 2002. **418**(6900): p. 823.
174. Minn, A.J., et al., *Genes that mediate breast cancer metastasis to lung.* Nature, 2005. **436**(7050): p. 518-24.
175. Kang, Y., et al., *A multigenic program mediating breast cancer metastasis to bone.* Cancer cell, 2003. **3**(6): p. 537-49.
176. Ribatti, D., G. Mangialardi, and A. Vacca, *Stephen Paget and the 'seed and soil' theory of metastatic dissemination.* Clinical and experimental medicine, 2006. **6**(4): p. 145-9.
177. Tantivejkul, K., L.M. Kalikin, and K.J. Pienta, *Dynamic process of prostate cancer metastasis to bone.* Journal of cellular biochemistry, 2004. **91**(4): p. 706-17.
178. Yoneda, T. and T. Hiraga, *Crosstalk between cancer cells and bone microenvironment in bone metastasis.* Biochemical and biophysical research communications, 2005. **328**(3): p. 679-87.

179. Muller, A., et al., *Involvement of chemokine receptors in breast cancer metastasis.* Nature, 2001. **410**(6824): p. 50-6.
180. Teicher, B.A. and S.P. Fricker, *CXCL12 (SDF-1)/CXCR4 pathway in cancer.* Clin Cancer Res, 2010. **16**(11): p. 2927-31.
181. Meads, M.B., L.A. Hazlehurst, and W.S. Dalton, *The bone marrow microenvironment as a tumor sanctuary and contributor to drug resistance.* Clin Cancer Res, 2008. **14**(9): p. 2519-26.
182. Taichman, R.S., et al., *Use of the stromal cell-derived factor-1/CXCR4 pathway in prostate cancer metastasis to bone.* Cancer Res, 2002. **62**(6): p. 1832-7.
183. Sun, Y.X., et al., *Skeletal localization and neutralization of the SDF-1(CXCL12)/CXCR4 axis blocks prostate cancer metastasis and growth in osseous sites in vivo.* Journal of bone and mineral research : the official journal of the American Society for Bone and Mineral Research, 2005. **20**(2): p. 318-29.
184. Wong, D., et al., *Targeting CXCR4 with CTCE-9908 inhibits prostate tumor metastasis.* BMC Urol, 2014. **14**: p. 12.
185. Schneider, J.G., S.R. Amend, and K.N. Weilbaecher, *Integrins and bone metastasis: integrating tumor cell and stromal cell interactions.* Bone, 2011. **48**(1): p. 54-65.
186. Weilbaecher, K.N., T.A. Guise, and L.K. McCauley, *Cancer to bone: a fatal attraction.* Nature reviews. Cancer, 2011. **11**(6): p. 411-25.
187. Kaplan, R.N., S. Rafii, and D. Lyden, *Preparing the "soil": the premetastatic niche.* Cancer Res, 2006. **66**(23): p. 11089-93.
188. Kaplan, R.N., et al., *VEGFR1-positive haematopoietic bone marrow progenitors initiate the pre-metastatic niche.* Nature, 2005. **438**(7069): p. 820-7.
189. Peinado, H., et al., *Melanoma exosomes educate bone marrow progenitor cells toward a pro-metastatic phenotype through MET.* Nat Med, 2012. **18**(6): p. 883-91.
190. Bacac, M. and I. Stamenkovic, *Metastatic cancer cell.* Annual review of pathology, 2008. **3**: p. 221-47.
191. Clezardin, P. and A. Teti, *Bone metastasis: pathogenesis and therapeutic implications.* Clinical & experimental metastasis, 2007. **24**(8): p. 599-608.
192. Chung, L.W., et al., *Molecular insights into prostate cancer progression: the missing link of tumor microenvironment.* J Urol, 2005. **173**(1): p. 10-20.
193. Ye, L., H.G. Kynaston, and W.G. Jiang, *Bone metastasis in prostate cancer: molecular and cellular mechanisms (Review).* International journal of molecular medicine, 2007. **20**(1): p. 103-11.
194. Keller, E.T., et al., *Prostate carcinoma skeletal metastases: cross-talk between tumor and bone.* Cancer metastasis reviews, 2001. **20**(3-4): p. 333-49.
195. Storey, J.A. and F.M. Torti, *Bone metastases in prostate cancer: a targeted approach.* Current opinion in oncology, 2007. **19**(3): p. 254-8.
196. Clarke, B., *Normal bone anatomy and physiology.* Clinical journal of the American Society of Nephrology : CJASN, 2008. **3 Suppl 3**: p. S131-9.
197. Akhtari, M., et al., *Biology of breast cancer bone metastasis.* Cancer biology & therapy, 2008. **7**(1): p. 3-9.
198. Fili, S., M. Karalaki, and B. Schaller, *Mechanism of bone metastasis: the role of osteoprotegerin and of the host-tissue microenvironment-related survival factors.* Cancer letters, 2009. **283**(1): p. 10-9.
199. Azim, H.A., N.S. Kamal, and H.A. Azim, Jr., *Bone metastasis in breast cancer: the story of RANK-ligand.* Journal of the Egyptian National Cancer Institute, 2012. **24**(3): p. 107-14.
200. Chappard, D., et al., *Bone metastasis: histological changes and pathophysiological mechanisms in osteolytic or osteosclerotic localizations. A review.* Morphologie : bulletin de l'Association des anatomistes, 2011. **95**(309): p. 65-75.

201. Guise, T.A., et al., *Basic mechanisms responsible for osteolytic and osteoblastic bone metastases.* Clin Cancer Res, 2006. **12**(20 Pt 2): p. 6213s-6216s.
202. Powell, G.J., et al., *Localization of parathyroid hormone-related protein in breast cancer metastases: increased incidence in bone compared with other sites.* Cancer Res, 1991. **51**(11): p. 3059-61.
203. Buijs, J.T. and G. van der Pluijm, *Osteotropic cancers: from primary tumor to bone.* Cancer letters, 2009. **273**(2): p. 177-93.
204. Kohno, N., et al., *Parathyroid Hormone-related Protein in Breast Cancer Tissues: Relationship between Primary and Metastatic Sites.* Breast cancer, 1994. **1**(1): p. 43-49.
205. Roodman, G.D., *Genes associate with abnormal bone cell activity in bone metastasis.* Cancer metastasis reviews, 2012. **31**(3-4): p. 569-78.
206. Kingsley, L.A., et al., *Molecular biology of bone metastasis.* Molecular cancer therapeutics, 2007. **6**(10): p. 2609-17.
207. Ibrahim, T., et al., *Pathogenesis of osteoblastic bone metastases from prostate cancer.* Cancer, 2010. **116**(6): p. 1406-18.
208. Logothetis, C.J. and S.H. Lin, *Osteoblasts in prostate cancer metastasis to bone.* Nature reviews. Cancer, 2005. **5**(1): p. 21-8.
209. Guise, T.A., J.J. Yin, and K.S. Mohammad, *Role of endothelin-1 in osteoblastic bone metastases.* Cancer, 2003. **97**(3 Suppl): p. 779-84.
210. Nelson, J.B., et al., *Endothelin-1 production and decreased endothelin B receptor expression in advanced prostate cancer.* Cancer Res, 1996. **56**(4): p. 663-8.
211. Tu, S.M. and S.H. Lin, *Current trials using bone-targeting agents in prostate cancer.* Cancer journal, 2008. **14**(1): p. 35-9.
212. Wulfing, P., et al., *Expression of endothelin-1, endothelin-A, and endothelin-B receptor in human breast cancer and correlation with long-term follow-up.* Clin Cancer Res, 2003. **9**(11): p. 4125-31.
213. Bailey, J.M., P.K. Singh, and M.A. Hollingsworth, *Cancer metastasis facilitated by developmental pathways: Sonic hedgehog, Notch, and bone morphogenic proteins.* Journal of cellular biochemistry, 2007. **102**(4): p. 829-39.
214. Loberg, R.D., et al., *Pathogenesis and treatment of prostate cancer bone metastases: targeting the lethal phenotype.* Journal of clinical oncology : official journal of the American Society of Clinical Oncology, 2005. **23**(32): p. 8232-41.
215. Parker, C., et al., *Alpha emitter radium-223 and survival in metastatic prostate cancer.* N Engl J Med, 2013. **369**(3): p. 213-23.
216. Cuzick, J., et al., *Long-term outcome among men with conservatively treated localised prostate cancer.* British journal of cancer, 2006. **95**(9): p. 1186-94.
217. Paulsson, K., et al., *Microdeletions are a general feature of adult and adolescent acute lymphoblastic leukemia: Unexpected similarities with pediatric disease.* Proceedings of the National Academy of Sciences of the United States of America, 2008. **105**(18): p. 6708-13.
218. Mao, X., et al., *Rapid high-resolution karyotyping with precise identification of chromosome breakpoints.* Genes, chromosomes & cancer, 2007. **46**(7): p. 675-83.
219. Boyd, L.K., et al., *High-resolution genome-wide copy-number analysis suggests a monoclonal origin of multifocal prostate cancer.* Genes, chromosomes & cancer, 2012. **51**(6): p. 579-89.
220. Ventura, R.A., et al., *FISH analysis for the detection of lymphoma-associated chromosomal abnormalities in routine paraffin-embedded tissue.* J Mol Diagn, 2006. **8**(2): p. 141-51.
221. Zhang, F., et al., *Immunophenotypic features and t(14;18) (q32;q21) translocation of Chinese follicular lymphomas helps to distinguish subgroups.* Diagn Pathol, 2013. **8**: p. 154.
222. Augello, M.A., et al., *Convergence of oncogenic and hormone receptor pathways promotes metastatic phenotypes.* The Journal of clinical investigation, 2013. **123**(1): p. 493-508.

223. De Wever, O., et al., *Modeling and quantification of cancer cell invasion through collagen type I matrices.* Int J Dev Biol, 2010. **54**(5): p. 887-96.
224. Godinho, S.A., et al., *Oncogene-like induction of cellular invasion from centrosome amplification.* Nature, 2014. **510**(7503): p. 167-71.
225. Saramaki, O. and T. Visakorpi, *Chromosomal aberrations in prostate cancer.* Frontiers in bioscience : a journal and virtual library, 2007. **12**: p. 3287-301.
226. Torring, N., et al., *Genome-wide analysis of allelic imbalance in prostate cancer using the Affymetrix 50K SNP mapping array.* British journal of cancer, 2007. **96**(3): p. 499-506.
227. Fu, W., et al., *Genetic changes in clinically organ-confined prostate cancer by comparative genomic hybridization.* Urology, 2000. **56**(5): p. 880-5.
228. Liu, W., et al., *Copy number analysis indicates monoclonal origin of lethal metastatic prostate cancer.* Nature medicine, 2009. **15**(5): p. 559-65.
229. Dhanasekaran, S.M., et al., *Delineation of prognostic biomarkers in prostate cancer.* Nature, 2001. **412**(6849): p. 822-6.
230. Hong, M.K., et al., *Tracking the origins and drivers of subclonal metastatic expansion in prostate cancer.* Nat Commun, 2015. **6**: p. 6605.
231. Van Allen, E.M., et al., *Successful whole-exome sequencing from a prostate cancer bone metastasis biopsy.* Prostate Cancer Prostatic Dis, 2014. **17**(1): p. 23-7.
232. Deng, X., et al., *Recent advances in bone-targeted therapies of metastatic prostate cancer.* Cancer Treat Rev, 2014. **40**(6): p. 730-8.
233. Hochreiter-Hufford, A. and K.S. Ravichandran, *Clearing the dead: apoptotic cell sensing, recognition, engulfment, and digestion.* Cold Spring Harbor perspectives in biology, 2013. **5**(1): p. a008748.
234. Barker, R.N., et al., *Antigen presentation by macrophages is enhanced by the uptake of necrotic, but not apoptotic, cells.* Clinical and experimental immunology, 2002. **127**(2): p. 220-5.
235. Dai, J., et al., *Vascular endothelial growth factor contributes to the prostate cancer-induced osteoblast differentiation mediated by bone morphogenetic protein.* Cancer Res, 2004. **64**(3): p. 994-9.
236. Dong, J.T., *Chromosomal deletions and tumor suppressor genes in prostate cancer.* Cancer metastasis reviews, 2001. **20**(3-4): p. 173-93.
237. Kraus, J., et al., *High-resolution genomic profiling of occult micrometastatic tumor cells.* Genes, chromosomes & cancer, 2003. **36**(2): p. 159-66.
238. Wu, C., et al., *Integrated genome and transcriptome sequencing identifies a novel form of hybrid and aggressive prostate cancer.* The Journal of pathology, 2012. **227**(1): p. 53-61.
239. Lonigro, R.J., et al., *Detection of somatic copy number alterations in cancer using targeted exome capture sequencing.* Neoplasia, 2011. **13**(11): p. 1019-25.
240. Trotman, L.C., et al., *Pten dose dictates cancer progression in the prostate.* PLoS biology, 2003. **1**(3): p. E59.
241. Ding, Z., et al., *SMAD4-dependent barrier constrains prostate cancer growth and metastatic progression.* Nature, 2011. **470**(7333): p. 269-73.
242. Kim, J.H., et al., *Integrative analysis of genomic aberrations associated with prostate cancer progression.* Cancer Res, 2007. **67**(17): p. 8229-39.
243. Yu, J.T., R.G. Foster, and D.C. Dean, *Transcriptional repression by RB-E2F and regulation of anchorage-independent survival.* Molecular and cellular biology, 2001. **21**(10): p. 3325-35.
244. Palmero, I. and G. Peters, *Perturbation of cell cycle regulators in human cancer.* Cancer surveys, 1996. **27**: p. 351-67.
245. Sherr, C.J. and F. McCormick, *The RB and p53 pathways in cancer.* Cancer cell, 2002. **2**(2): p. 103-12.
246. Shapiro, G.I., et al., *Reciprocal Rb inactivation and p16INK4 expression in primary lung cancers and cell lines.* Cancer Res, 1995. **55**(3): p. 505-9.

247. Cryns, V.L., et al., *Loss of the retinoblastoma tumor-suppressor gene in parathyroid carcinoma.* N Engl J Med, 1994. **330**(11): p. 757-61.
248. Fernandez-Jimenez, N., et al., *Accuracy in copy number calling by qPCR and PRT: a matter of DNA.* PloS one, 2011. **6**(12): p. e28910.
249. Guescini, M., et al., *A new real-time PCR method to overcome significant quantitative inaccuracy due to slight amplification inhibition.* BMC bioinformatics, 2008. **9**: p. 326.
250. D'Haene, B., J. Vandesompele, and J. Hellemans, *Accurate and objective copy number profiling using real-time quantitative PCR.* Methods, 2010. **50**(4): p. 262-70.
251. Armour, J.A., et al., *Accurate, high-throughput typing of copy number variation using paralogue ratios from dispersed repeats.* Nucleic acids research, 2007. **35**(3): p. e19.
252. Knudsen, K.E., et al., *Cyclin D1: polymorphism, aberrant splicing and cancer risk.* Oncogene, 2006. **25**(11): p. 1620-8.
253. Champeme, M.H., et al., *Int-2/FGF3 amplification is a better independent predictor of relapse than c-myc and c-erbB-2/neu amplifications in primary human breast cancer.* Mod Pathol, 1994. **7**(9): p. 900-5.
254. Hughes-Davies, L., et al., *EMSY links the BRCA2 pathway to sporadic breast and ovarian cancer.* Cell, 2003. **115**(5): p. 523-35.
255. Chen, Y. and C. Chen, *DNA copy number variation and loss of heterozygosity in relation to recurrence of and survival from head and neck squamous cell carcinoma: a review.* Head Neck, 2008. **30**(10): p. 1361-83.
256. Schwab, M., *Amplification of oncogenes in human cancer cells.* Bioessays, 1998. **20**(6): p. 473-9.
257. Zaharieva, B.M., et al., *High-throughput tissue microarray analysis of 11q13 gene amplification (CCND1, FGF3, FGF4, EMS1) in urinary bladder cancer.* J Pathol, 2003. **201**(4): p. 603-8.
258. Huang, X., et al., *High-resolution mapping of the 11q13 amplicon and identification of a gene, TAOS1, that is amplified and overexpressed in oral cancer cells.* Proc Natl Acad Sci U S A, 2002. **99**(17): p. 11369-74.
259. Ormandy, C.J., et al., *Cyclin D1, EMS1 and 11q13 amplification in breast cancer.* Breast Cancer Res Treat, 2003. **78**(3): p. 323-35.
260. Wilkerson, P.M., et al., *Functional characterization of EMSY gene amplification in human cancers.* J Pathol, 2011. **225**(1): p. 29-42.
261. Nurminen, R., et al., *Identification of an aggressive prostate cancer predisposing variant at 11q13.* Int J Cancer, 2011. **129**(3): p. 599-606.
262. Nurminen, R., et al., *Fine mapping of 11q13.5 identifies regions associated with prostate cancer and prostate cancer death.* Eur J Cancer, 2013. **49**(15): p. 3335-43.
263. Helsten, T., et al., *The Fgfr Landscape in Cancer: Analysis of 4853 Tumors by Next Generation Sequencing.* Clin Cancer Res, 2015.
264. Parish, A., et al., *Fibroblast growth factor family aberrations in cancers: clinical and molecular characteristics.* Cell Cycle, 2015. **14**(13): p. 2121-8.
265. Latil, A., et al., *Oncogene amplifications in early-stage human prostate carcinomas.* Int J Cancer, 1994. **59**(5): p. 637-8.
266. Fournier, G., et al., *Gene amplifications in advanced-stage human prostate cancer.* Urol Res, 1995. **22**(6): p. 343-7.
267. Muller, W.J., et al., *The int-2 gene product acts as an epithelial growth factor in transgenic mice.* EMBO J, 1990. **9**(3): p. 907-13.
268. Musgrove, E.A., et al., *Cyclin D as a therapeutic target in cancer.* Nat Rev Cancer, 2011. **11**(8): p. 558-72.
269. Li, Z., et al., *Cyclin D1 functions in cell migration.* Cell cycle, 2006. **5**(21): p. 2440-2.
270. Fu, M., et al., *Minireview: Cyclin D1: normal and abnormal functions.* Endocrinology, 2004. **145**(12): p. 5439-47.

271. Dai, M., et al., *Cyclin D1 cooperates with p21 to regulate TGFbeta-mediated breast cancer cell migration and tumor local invasion.* Breast cancer research : BCR, 2013. **15**(3): p. R49.
272. Noel, E.E., et al., *The association of CCND1 overexpression and cisplatin resistance in testicular germ cell tumors and other cancers.* Am J Pathol, 2010. **176**(6): p. 2607-15.
273. Gan, L., et al., *Cyclin D1 promotes anchorage-independent cell survival by inhibiting FOXO-mediated anoikis.* Cell death and differentiation, 2009. **16**(10): p. 1408-17.
274. Malumbres, M. and M. Barbacid, *Cell cycle, CDKs and cancer: a changing paradigm.* Nat Rev Cancer, 2009. **9**(3): p. 153-66.
275. Zhang, Q., K. Sakamoto, and K.U. Wagner, *D-type Cyclins are important downstream effectors of cytokine signaling that regulate the proliferation of normal and neoplastic mammary epithelial cells.* Mol Cell Endocrinol, 2014. **382**(1): p. 583-92.
276. Sherr, C.J., *Mammalian G1 cyclins.* Cell, 1993. **73**(6): p. 1059-65.
277. Sherr, C.J. and J.M. Roberts, *CDK inhibitors: positive and negative regulators of G1-phase progression.* Genes Dev, 1999. **13**(12): p. 1501-12.
278. Tashiro, E., A. Tsuchiya, and M. Imoto, *Functions of cyclin D1 as an oncogene and regulation of cyclin D1 expression.* Cancer science, 2007. **98**(5): p. 629-35.
279. Alao, J.P., *The regulation of cyclin D1 degradation: roles in cancer development and the potential for therapeutic invention.* Molecular cancer, 2007. **6**: p. 24.
280. Knudsen, K.E., et al., *Androgen-mediated Control of the Cyclin D1-RB Axis: Implications for Prostate Cancer*, in *Hormonal Control of Cell Cycle*, S. Melmed, et al., Editors. 2008, Springer Berlin Heidelberg. p. 63-81.
281. Solomon, D.A., et al., *Cyclin D1 splice variants. Differential effects on localization, RB phosphorylation, and cellular transformation.* J Biol Chem, 2003. **278**(32): p. 30339-47.
282. Comstock, C.E., et al., *Cyclin D1 splice variants: polymorphism, risk, and isoform-specific regulation in prostate cancer.* Clin Cancer Res, 2009. **15**(17): p. 5338-49.
283. Knudsen, K.E., K.C. Arden, and W.K. Cavenee, *Multiple G1 regulatory elements control the androgen-dependent proliferation of prostatic carcinoma cells.* The Journal of biological chemistry, 1998. **273**(32): p. 20213-22.
284. Knudsen, K.E., W.K. Cavenee, and K.C. Arden, *D-type cyclins complex with the androgen receptor and inhibit its transcriptional transactivation ability.* Cancer Res, 1999. **59**(10): p. 2297-301.
285. Burd, C.J., et al., *Cyclin D1b variant influences prostate cancer growth through aberrant androgen receptor regulation.* Proceedings of the National Academy of Sciences of the United States of America, 2006. **103**(7): p. 2190-5.
286. Reis-Filho, J.S., et al., *Cyclin D1 protein overexpression and CCND1 amplification in breast carcinomas: an immunohistochemical and chromogenic in situ hybridisation analysis.* Modern pathology : an official journal of the United States and Canadian Academy of Pathology, Inc, 2006. **19**(7): p. 999-1009.
287. Das, K., et al., *Chromosomal changes in prostate cancer: a fluorescence in situ hybridization study.* Clinical genetics, 2005. **68**(1): p. 40-7.
288. Bubendorf, L., et al., *Survey of gene amplifications during prostate cancer progression by high-throughout fluorescence in situ hybridization on tissue microarrays.* Cancer Res, 1999. **59**(4): p. 803-6.
289. Comstock, C.E., et al., *Impact of differential cyclin D1 expression and localisation in prostate cancer.* British journal of cancer, 2007. **96**(6): p. 970-9.
290. Gupta, V., et al., *Role of cyclin D1 immunoreactivity and AgNOR staining in the evaluation of benign and malignant lesions of the prostate.* Prostate Int, 2014. **2**(2): p. 90-6.
291. Torlakovic, E.E., et al., *Call for a European programme in external quality assurance for bone marrow immunohistochemistry; report of a European Bone Marrow Working Group pilot study.* Journal of clinical pathology, 2009. **62**(6): p. 547-51.

292. Frank, J.D., et al., *The effects of three different demineralization agents on osteopontin localization in adult rat bone using immunohistochemistry.* Histochemistry, 1993. **99**(4): p. 295-301.
293. Aaltomaa, S., et al., *Expression of Ki-67, cyclin D1 and apoptosis markers correlated with survival in prostate cancer patients treated by radical prostatectomy.* Anticancer research, 2006. **26**(6C): p. 4873-8.
294. Kallakury, B.V., et al., *The prognostic significance of p34cdc2 and cyclin D1 protein expression in prostate adenocarcinoma.* Cancer, 1997. **80**(4): p. 753-63.
295. Drobnjak, M., et al., *Overexpression of cyclin D1 is associated with metastatic prostate cancer to bone.* Clin Cancer Res, 2000. **6**(5): p. 1891-5.
296. Pereira, R.A., et al., *Cyclin D1 expression in prostate carcinoma.* Braz J Med Biol Res, 2014. **47**(6): p. 515-21.
297. Yasui, M., et al., *Antisense to cyclin D1 inhibits vascular endothelial growth factor-stimulated growth of vascular endothelial cells: implication of tumor vascularization.* Clin Cancer Res, 2006. **12**(15): p. 4720-9.
298. Shiraishi, T., et al., *A clinicopathological study of p53, p21 (WAF1/CIP1) and cyclin D1 expression in human prostate cancers.* Urologia internationalis, 1998. **61**(2): p. 90-4.
299. Vlachostergios, P.J., et al., *p53 and cyclooxygenase-2 expression are directly associated with cyclin D1 expression in radical prostatectomy specimens of patients with hormone-naive prostate cancer.* Pathol Oncol Res, 2012. **18**(2): p. 245-52.
300. Kaukoniemi, K.M., et al., *Epigenetically altered miR-193b targets cyclin D1 in prostate cancer.* Cancer Med, 2015. **4**(9): p. 1417-25.
301. Makarewicz, R., A. Zyromska, and H. Andrusewicz, *Comparative analysis of biological profiles of benign prostate hyperplasia and prostate cancer as potential diagnostic, prognostic and predictive indicators.* Folia Histochem Cytobiol, 2011. **49**(3): p. 452-7.
302. Ju, X., et al., *Identification of a cyclin d1 network in prostate cancer that antagonizes epithelial-mesenchymal restraint.* Cancer Res, 2014. **74**(2): p. 508-19.
303. Witzel, II, L.F. Koh, and N.D. Perkins, *Regulation of cyclin D1 gene expression.* Biochemical Society transactions, 2010. **38**(Pt 1): p. 217-22.
304. Betticher, D.C., et al., *Alternate splicing produces a novel cyclin D1 transcript.* Oncogene, 1995. **11**(5): p. 1005-11.
305. Kluth, M., et al., *Genomic deletion of MAP3K7 at 6q12-22 is associated with early PSA recurrence in prostate cancer and absence of TMPRSS2:ERG fusions.* Mod Pathol, 2013. **26**(7): p. 975-83.
306. Srikantan, V., et al., *Allelic loss on chromosome 6Q in primary prostate cancer.* Int J Cancer, 1999. **84**(3): p. 331-5.
307. He, X., et al., *Expression of a large family of POU-domain regulatory genes in mammalian brain development.* Nature, 1989. **340**(6228): p. 35-41.
308. Dominguez, M.H., A.E. Ayoub, and P. Rakic, *POU-III transcription factors (Brn1, Brn2, and Oct6) influence neurogenesis, molecular identity, and migratory destination of upper-layer cells of the cerebral cortex.* Cereb Cortex, 2013. **23**(11): p. 2632-43.
309. Thomson, J.A., et al., *The brn-2 gene regulates the melanocytic phenotype and tumorigenic potential of human melanoma cells.* Oncogene, 1995. **11**(4): p. 691-700.
310. Goodall, J., et al., *The Brn-2 transcription factor links activated BRAF to melanoma proliferation.* Mol Cell Biol, 2004. **24**(7): p. 2923-31.
311. Kobi, D., et al., *Genome-wide analysis of POU3F2/BRN2 promoter occupancy in human melanoma cells reveals Kitl as a novel regulated target gene.* Pigment Cell Melanoma Res, 2010. **23**(3): p. 404-18.
312. Cook, A.L. and R.A. Sturm, *POU domain transcription factors: BRN2 as a regulator of melanocytic growth and tumourigenesis.* Pigment cell & melanoma research, 2008. **21**(6): p. 611-26.

313. Ishii, J., et al., *POU domain transcription factor BRN2 is crucial for expression of ASCL1, ND1 and neuroendocrine marker molecules and cell growth in small cell lung cancer.* Pathol Int, 2013. **63**(3): p. 158-68.
314. Ho, M.S., P.I. Tsai, and C.T. Chien, *F-box proteins: the key to protein degradation.* Journal of biomedical science, 2006. **13**(2): p. 181-91.
315. Skaar, J.R., J.K. Pagan, and M. Pagano, *Mechanisms and function of substrate recruitment by F-box proteins.* Nat Rev Mol Cell Biol, 2013. **14**(6): p. 369-81.
316. Heo, J., R. Eki, and T. Abbas, *Deregulation of F-box proteins and its consequence on cancer development, progression and metastasis.* Semin Cancer Biol, 2015.
317. Randle, S.J. and H. Laman, *F-box protein interactions with the hallmark pathways in cancer.* Semin Cancer Biol, 2015.
318. Wang, Z., et al., *Roles of F-box proteins in cancer.* Nat Rev Cancer, 2014. **14**(4): p. 233-47.
319. Gai, X., et al., *Mutations in FBXL4, encoding a mitochondrial protein, cause early-onset mitochondrial encephalomyopathy.* American journal of human genetics, 2013. **93**(3): p. 482-95.
320. Bonnen, P.E., et al., *Mutations in FBXL4 cause mitochondrial encephalopathy and a disorder of mitochondrial DNA maintenance.* American journal of human genetics, 2013. **93**(3): p. 471-81.
321. Tan, M.K., et al., *Parallel SCF adaptor capture proteomics reveals a role for SCFFBXL17 in NRF2 activation via BACH1 repressor turnover.* Molecular cell, 2013. **52**(1): p. 9-24.
322. Alers, J.C., et al., *Identification of genetic markers for prostatic cancer progression.* Laboratory investigation; a journal of technical methods and pathology, 2000. **80**(6): p. 931-42.
323. Cancer Genome Atlas Research, N., *The Molecular Taxonomy of Primary Prostate Cancer.* Cell, 2015. **163**(4): p. 1011-25.
324. Lu, T. and H. Hano, *Deletion at chromosome arms 6q16-22 and 10q22.3-23.1 associated with initiation of prostate cancer.* Prostate Cancer Prostatic Dis, 2008. **11**(4): p. 357-61.
325. Cooney, K.A., et al., *Identification and characterization of proximal 6q deletions in prostate cancer.* Cancer Res, 1996. **56**(18): p. 4150-3.
326. Strohmeyer, D.M., et al., *Genetic aberrations in prostate carcinoma detected by comparative genomic hybridization and microsatellite analysis: association with progression and angiogenesis.* Prostate, 2004. **59**(1): p. 43-58.
327. Bordeaux, J., et al., *Antibody validation.* Biotechniques, 2010. **48**(3): p. 197-209.
328. Grandjean, M., et al., *High-level transgene expression by homologous recombination-mediated gene transfer.* Nucleic Acids Res, 2011. **39**(15): p. e104.
329. Orend, G., et al., *The initiation of de novo methylation of foreign DNA integrated into a mammalian genome is not exclusively targeted by nucleotide sequence.* J Virol, 1995. **69**(2): p. 1226-42.
330. Mutskov, V. and G. Felsenfeld, *Silencing of transgene transcription precedes methylation of promoter DNA and histone H3 lysine 9.* EMBO J, 2004. **23**(1): p. 138-49.
331. Thomas, P. and T.G. Smart, *HEK293 cell line: a vehicle for the expression of recombinant proteins.* J Pharmacol Toxicol Methods, 2005. **51**(3): p. 187-200.
332. Wu, Z.H. and L.M. Pfeffer, *MicroRNA regulation of F-box proteins and its role in cancer.* Semin Cancer Biol, 2015.
333. Chan, C.H., et al., *Regulation of Skp2 expression and activity and its role in cancer progression.* ScientificWorldJournal, 2010. **10**: p. 1001-15.
334. Winston, J.T., et al., *A family of mammalian F-box proteins.* Curr Biol, 1999. **9**(20): p. 1180-2.
335. Harper, J.W. and M.K. Tan, *Understanding cullin-RING E3 biology through proteomics-based substrate identification.* Mol Cell Proteomics, 2012. **11**(12): p. 1541-50.

336. Sun, Y., *E3 ubiquitin ligases as cancer targets and biomarkers.* Neoplasia, 2006. **8**(8): p. 645-54.
337. Skaar, J.R., J.K. Pagan, and M. Pagano, *SCF ubiquitin ligase-targeted therapies.* Nat Rev Drug Discov, 2014. **13**(12): p. 889-903.
338. Huemer, M., et al., *Clinical, morphological, biochemical, imaging and outcome parameters in 21 individuals with mitochondrial maintenance defect related to FBXL4 mutations.* J Inherit Metab Dis, 2015. **38**(5): p. 905-14.
339. Ikawa, M., et al., *The putative chaperone calmegin is required for sperm fertility.* Nature, 1997. **387**(6633): p. 607-11.
340. Bernasconi, R., et al., *Stringent requirement for HRD1, SEL1L, and OS-9/XTP3-B for disposal of ERAD-LS substrates.* J Cell Biol, 2010. **188**(2): p. 223-35.
341. Rutkowski, D.T., et al., *The role of p58IPK in protecting the stressed endoplasmic reticulum.* Mol Biol Cell, 2007. **18**(9): p. 3681-91.
342. Siegelin, M.D., et al., *Exploiting the mitochondrial unfolded protein response for cancer therapy in mice and human cells.* J Clin Invest, 2011. **121**(4): p. 1349-60.
343. Haynes, C.M., C.J. Fiorese, and Y.F. Lin, *Evaluating and responding to mitochondrial dysfunction: the mitochondrial unfolded-protein response and beyond.* Trends Cell Biol, 2013. **23**(7): p. 311-8.
344. Ma, Y. and L.M. Hendershot, *The role of the unfolded protein response in tumour development: friend or foe?* Nat Rev Cancer, 2004. **4**(12): p. 966-77.
345. Heo, J.M., et al., *A stress-responsive system for mitochondrial protein degradation.* Mol Cell, 2010. **40**(3): p. 465-80.
346. Taylor, E.B. and J. Rutter, *Mitochondrial quality control by the ubiquitin-proteasome system.* Biochem Soc Trans, 2011. **39**(5): p. 1509-13.
347. Tanaka, A., et al., *Proteasome and p97 mediate mitophagy and degradation of mitofusins induced by Parkin.* J Cell Biol, 2010. **191**(7): p. 1367-80.
348. Friedman, J.R., et al., *ER tubules mark sites of mitochondrial division.* Science, 2011. **334**(6054): p. 358-62.
349. Csordas, G., et al., *Structural and functional features and significance of the physical linkage between ER and mitochondria.* J Cell Biol, 2006. **174**(7): p. 915-21.
350. Bravo, R., et al., *Increased ER-mitochondrial coupling promotes mitochondrial respiration and bioenergetics during early phases of ER stress.* J Cell Sci, 2011. **124**(Pt 13): p. 2143-52.
351. Rainbolt, T.K., J.M. Saunders, and R.L. Wiseman, *Stress-responsive regulation of mitochondria through the ER unfolded protein response.* Trends Endocrinol Metab, 2014. **25**(10): p. 528-37.
352. Cruciat, C.M., C. Hassler, and C. Niehrs, *The MRH protein Erlectin is a member of the endoplasmic reticulum synexpression group and functions in N-glycan recognition.* J Biol Chem, 2006. **281**(18): p. 12986-93.
353. Hosokawa, N., et al., *Human XTP3-B forms an endoplasmic reticulum quality control scaffold with the HRD1-SEL1L ubiquitin ligase complex and BiP.* J Biol Chem, 2008. **283**(30): p. 20914-24.
354. Yanagisawa, K., et al., *Novel metastasis-related gene CIM functions in the regulation of multiple cellular stress-response pathways.* Cancer Res, 2010. **70**(23): p. 9949-58.
355. Brocato, J., Y. Chervona, and M. Costa, *Molecular responses to hypoxia-inducible factor 1alpha and beyond.* Mol Pharmacol, 2014. **85**(5): p. 651-7.
356. Brown, J.M. and W.R. Wilson, *Exploiting tumour hypoxia in cancer treatment.* Nat Rev Cancer, 2004. **4**(6): p. 437-47.
357. Friedl, P. and E.B. Brocker, *The biology of cell locomotion within three-dimensional extracellular matrix.* Cell Mol Life Sci, 2000. **57**(1): p. 41-64.
358. Marshall, J., *Transwell((R)) invasion assays.* Methods Mol Biol, 2011. **769**: p. 97-110.

359. Wolf, K. and P. Friedl, *Extracellular matrix determinants of proteolytic and non-proteolytic cell migration.* Trends Cell Biol, 2011. **21**(12): p. 736-44.
360. Jones, M.L., et al., *Prostate cancer-derived angiogenin stimulates the invasion of prostate fibroblasts.* J Cell Mol Med, 2012. **16**(1): p. 193-201.
361. Bracke, M.E., et al., *Collagen invasion assay.* Methods Mol Med, 2001. **58**: p. 81-9.
362. Sanz, G., et al., *Promotion of cancer cell invasiveness and metastasis emergence caused by olfactory receptor stimulation.* PLoS One, 2014. **9**(1): p. e85110.
363. Christianson, J.C., et al., *OS-9 and GRP94 deliver mutant alpha1-antitrypsin to the Hrd1-SEL1L ubiquitin ligase complex for ERAD.* Nat Cell Biol, 2008. **10**(3): p. 272-82.
364. Sahai, E., *Mechanisms of cancer cell invasion.* Curr Opin Genet Dev, 2005. **15**(1): p. 87-96.
365. Crusio, K.M., et al., *The ubiquitous nature of cancer: the role of the SCF(Fbw7) complex in development and transformation.* Oncogene, 2010. **29**(35): p. 4865-73.
366. Yokobori, T., et al., *Copy number loss of FBXW7 is related to gene expression and poor prognosis in esophageal squamous cell carcinoma.* Int J Oncol, 2012. **41**(1): p. 253-9.
367. Wang, X., et al., *Fbxw7 regulates hepatocellular carcinoma migration and invasion via Notch1 signaling pathway.* Int J Oncol, 2015. **47**(1): p. 231-43.
368. Duan, S., et al., *FBXO11 targets BCL6 for degradation and is inactivated in diffuse large B-cell lymphomas.* Nature, 2012. **481**(7379): p. 90-3.
369. Wu, W., et al., *FBXL5 inhibits metastasis of gastric cancer through suppressing Snail1.* Cell Physiol Biochem, 2015. **35**(5): p. 1764-72.
370. Antoun, G., et al., *Detailed Biochemical and Bioenergetic Characterization of FBXL4-Related Encephalomyopathic Mitochondrial DNA Depletion.* JIMD Rep, 2015.
371. Detmer, S.A. and D.C. Chan, *Functions and dysfunctions of mitochondrial dynamics.* Nat Rev Mol Cell Biol, 2007. **8**(11): p. 870-9.
372. Ranieri, M., et al., *Mitochondrial fusion proteins and human diseases.* Neurol Res Int, 2013. **2013**: p. 293893.
373. Zhao, J., et al., *Mitochondrial dynamics regulates migration and invasion of breast cancer cells.* Oncogene, 2013. **32**(40): p. 4814-24.
374. Desai, S.P., et al., *Mitochondrial localization and the persistent migration of epithelial cancer cells.* Biophys J, 2013. **104**(9): p. 2077-88.
375. Ferreira-da-Silva, A., et al., *Mitochondrial dynamics protein Drp1 is overexpressed in oncocytic thyroid tumors and regulates cancer cell migration.* PLoS One, 2015. **10**(3): p. e0122308.
376. Chevrollier, A., et al., *Standardized mitochondrial analysis gives new insights into mitochondrial dynamics and OPA1 function.* Int J Biochem Cell Biol, 2012. **44**(6): p. 980-8.
377. Mitra, K. and J. Lippincott-Schwartz, *Analysis of mitochondrial dynamics and functions using imaging approaches.* Curr Protoc Cell Biol, 2010. **Chapter 4**: p. Unit 4 25 1-21.
378. Rehman, J., et al., *Inhibition of mitochondrial fission prevents cell cycle progression in lung cancer.* FASEB J, 2012. **26**(5): p. 2175-86.
379. Senyilmaz, D., et al., *Regulation of mitochondrial morphology and function by stearoylation of TFR1.* Nature, 2015. **525**(7567): p. 124-8.
380. Wang, Y., et al., *Rapamycin inhibits FBXW7 loss-induced epithelial-mesenchymal transition and cancer stem cell-like characteristics in colorectal cancer cells.* Biochem Biophys Res Commun, 2013. **434**(2): p. 352-6.
381. Xu, M., et al., *Atypical ubiquitin E3 ligase complex Skp1-Pam-Fbxo45 controls the core epithelial-to-mesenchymal transition-inducing transcription factors.* Oncotarget, 2015. **6**(2): p. 979-94.
382. Lander, R., K. Nordin, and C. LaBonne, *The F-box protein Ppa is a common regulator of core EMT factors Twist, Snail, Slug, and Sip1.* J Cell Biol, 2011. **194**(1): p. 17-25.

383. Mendez, M.G., S. Kojima, and R.D. Goldman, *Vimentin induces changes in cell shape, motility, and adhesion during the epithelial to mesenchymal transition.* FASEB J, 2010. **24**(6): p. 1838-51.
384. Wei, J., et al., *Overexpression of vimentin contributes to prostate cancer invasion and metastasis via src regulation.* Anticancer Res, 2008. **28**(1A): p. 327-34.
385. Polyak, K. and R.A. Weinberg, *Transitions between epithelial and mesenchymal states: acquisition of malignant and stem cell traits.* Nat Rev Cancer, 2009. **9**(4): p. 265-73.
386. Lang, S.H., et al., *Enhanced expression of vimentin in motile prostate cell lines and in poorly differentiated and metastatic prostate carcinoma.* Prostate, 2002. **52**(4): p. 253-63.
387. Thiery, J.P. and J.P. Sleeman, *Complex networks orchestrate epithelial-mesenchymal transitions.* Nat Rev Mol Cell Biol, 2006. **7**(2): p. 131-42.
388. Cavallaro, U., B. Schaffhauser, and G. Christofori, *Cadherins and the tumour progression: is it all in a switch?* Cancer Lett, 2002. **176**(2): p. 123-8.
389. Weber, G.F., M.A. Bjerke, and D.W. DeSimone, *A mechanoresponsive cadherin-keratin complex directs polarized protrusive behavior and collective cell migration.* Dev Cell, 2012. **22**(1): p. 104-15.
390. Lamouille, S., J. Xu, and R. Derynck, *Molecular mechanisms of epithelial-mesenchymal transition.* Nat Rev Mol Cell Biol, 2014. **15**(3): p. 178-96.
391. Windoffer, R., et al., *Cytoskeleton in motion: the dynamics of keratin intermediate filaments in epithelia.* J Cell Biol, 2011. **194**(5): p. 669-78.
392. Gravdal, K., et al., *A switch from E-cadherin to N-cadherin expression indicates epithelial to mesenchymal transition and is of strong and independent importance for the progress of prostate cancer.* Clin Cancer Res, 2007. **13**(23): p. 7003-11.
393. Zhao, Y., et al., *Vimentin affects the mobility and invasiveness of prostate cancer cells.* Cell Biochem Funct, 2008. **26**(5): p. 571-7.
394. Kuang, H.B., et al., *Dickkopf-1 enhances migration of HEK293 cell by beta-catenin/E-cadherin degradation.* Front Biosci (Landmark Ed), 2009. **14**: p. 2212-20.
395. Qian, X., et al., *E-cadherin-mediated adhesion inhibits ligand-dependent activation of diverse receptor tyrosine kinases.* EMBO J, 2004. **23**(8): p. 1739-48.
396. Kim, W.D., et al., *E-cadherin inhibits nuclear accumulation of Nrf2: implications for chemoresistance of cancer cells.* J Cell Sci, 2012. **125**(Pt 5): p. 1284-95.
397. Stepanenko, A.A. and V.V. Dmitrenko, *HEK293 in cell biology and cancer research: phenotype, karyotype, tumorigenicity, and stress-induced genome-phenotype evolution.* Gene, 2015. **569**(2): p. 182-90.
398. Tsuchiya, B., et al., *Differential expression of N-cadherin and E-cadherin in normal human tissues.* Arch Histol Cytol, 2006. **69**(2): p. 135-45.
399. Parsons, J.T., A.R. Horwitz, and M.A. Schwartz, *Cell adhesion: integrating cytoskeletal dynamics and cellular tension.* Nat Rev Mol Cell Biol, 2010. **11**(9): p. 633-43.
400. Schlaepfer, D.D., S.K. Mitra, and D. Ilic, *Control of motile and invasive cell phenotypes by focal adhesion kinase.* Biochim Biophys Acta, 2004. **1692**(2-3): p. 77-102.
401. Gardel, M.L., et al., *Mechanical integration of actin and adhesion dynamics in cell migration.* Annu Rev Cell Dev Biol, 2010. **26**: p. 315-33.
402. Hsia, D.A., et al., *Differential regulation of cell motility and invasion by FAK.* J Cell Biol, 2003. **160**(5): p. 753-67.
403. Fujimori, T., et al., *Endoplasmic reticulum lectin XTP3-B inhibits endoplasmic reticulum-associated degradation of a misfolded alpha1-antitrypsin variant.* FEBS J, 2013. **280**(6): p. 1563-75.
404. Hebert, D.N., R. Bernasconi, and M. Molinari, *ERAD substrates: which way out?* Semin Cell Dev Biol, 2010. **21**(5): p. 526-32.

405. Mehnert, M., T. Sommer, and E. Jarosch, *ERAD ubiquitin ligases: multifunctional tools for protein quality control and waste disposal in the endoplasmic reticulum.* Bioessays, 2010. **32**(10): p. 905-13.
406. Hirsch, C., et al., *The ubiquitylation machinery of the endoplasmic reticulum.* Nature, 2009. **458**(7237): p. 453-60.
407. Lehmann, G., R.G. Udasin, and A. Ciechanover, *On the linkage between the ubiquitin-proteasome system and the mitochondria.* Biochem Biophys Res Commun, 2016. **473**(1): p. 80-6.
408. Glenn, K.A., et al., *Diversity in tissue expression, substrate binding, and SCF complex formation for a lectin family of ubiquitin ligases.* J Biol Chem, 2008. **283**(19): p. 12717-29.
409. Mallinger, A., et al., *Using a ubiquitin ligase as an unfolded protein sensor.* Biochem Biophys Res Commun, 2012. **418**(1): p. 44-8.
410. Lu, A. and S.R. Pfeffer, *A CULLINary ride across the secretory pathway: more than just secretion.* Trends Cell Biol, 2014. **24**(7): p. 389-99.
411. Yoshida, Y., et al., *Glycoprotein-specific ubiquitin ligases recognize N-glycans in unfolded substrates.* EMBO Rep, 2005. **6**(3): p. 239-44.
412. Yoshida, Y. and K. Tanaka, *Lectin-like ERAD players in ER and cytosol.* Biochim Biophys Acta, 2010. **1800**(2): p. 172-80.
413. Kazak, L., et al., *Alternative translation initiation augments the human mitochondrial proteome.* Nucleic Acids Res, 2013. **41**(4): p. 2354-69.
414. Cali, T., et al., *Enhanced parkin levels favor ER-mitochondria crosstalk and guarantee Ca(2+) transfer to sustain cell bioenergetics.* Biochim Biophys Acta, 2013. **1832**(4): p. 495-508.
415. Bouman, L., et al., *Parkin is transcriptionally regulated by ATF4: evidence for an interconnection between mitochondrial stress and ER stress.* Cell Death Differ, 2011. **18**(5): p. 769-82.
416. Carlin, B.I. and G.L. Andriole, *The natural history, skeletal complications, and management of bone metastases in patients with prostate carcinoma.* Cancer, 2000. **88**(12 Suppl): p. 2989-94.
417. Ribeiro, F.R., et al., *Statistical dissection of genetic pathways involved in prostate carcinogenesis.* Genes Chromosomes Cancer, 2006. **45**(2): p. 154-63.
418. Bienvenu, F., et al., *Transcriptional role of cyclin D1 in development revealed by a genetic-proteomic screen.* Nature, 2010. **463**(7279): p. 374-8.
419. Augello, M.A., et al., *Consequence of the tumor-associated conversion to cyclin D1b.* EMBO Mol Med, 2015. **7**(5): p. 628-47.
420. van der Bliek, A.M., Q. Shen, and S. Kawajiri, *Mechanisms of mitochondrial fission and fusion.* Cold Spring Harb Perspect Biol, 2013. **5**(6).
421. Lee, H. and Y. Yoon, *Mitochondrial fission: regulation and ER connection.* Mol Cells, 2014. **37**(2): p. 89-94.